ÉCOLE DE TECHNOLOGIE SUPÉRIEURE
UNIVERSITÉ DU QUÉBEC

THESIS PRESENTED TO
ÉCOLE DE TECHNOLOGIE SUPÉRIEURE

IN PARTIAL FULFILLMENT OF THE REQUIREMENTS FOR
THE DEGREE OF DOCTOR OF PHILOSOPHY
Ph.D.

BY
Mykhaylo SABELKIN

DATA TRANSMISSION ORIENTED ON THE OBJECT, COMMUNICATION MEDIA, APPLICATION, AND STATE OF COMMUNICATION SYSTEMS: TACTICAL COMMUNICATION SYSTEM APPLICATION.

MONTREAL, NOVEMBER 30, 2011

BOARD OF EXAMINERS

THIS THESIS HAS BEEN EVALUATED

BY THE FOLLOWING BOARD OF EXAMINERS:

Mr. François Gagnon, Thesis director
Département de génie électrique à l'école de technologie supérieure

Mr. Stéphane Coulombe, Committee president
Département de génie logiciel et des TI à l'école de technologie supérieure

Mr. Ammar Kouki, Examiner
Département de génie électrique à l'école de technologie supérieure

Mr. Douglas O'Shaughnessy, External independent examiner
INRS EMT

THIS THESIS WAS PRESENTED AND DEFENDED

BEFORE A BOARD OF EXAMINERS AND PUBLIC

ON OCTOBER 19, 2011

AT ÉCOLE DE TECHNOLOGIE SUPÉRIEURE

ACKNOWLEDGEMENTS

The author would like to thank his parents and family, his thesis supervisor Dr François Gagnon, and École de Technologie Supérieure for support and encouragement of the research work.

Also the author would like to thank the Industrial Research Chair of Natural Sciences and Engineering Research Council of Canada (NSERC) and Ultra Electronics Tactical Communication Systems (TCS); and DTMSDR Technologies INC for support of research.

DATA TRANSMISSION ORIENTED ON THE OBJECT, COMMUNICATION MEDIA, APPLICATION, AND STATE OF COMMUNICATION SYSTEMS: TACTICAL COMMUNICATION SYSTEM APPLICATION.

Mykhaylo SABELKIN

ABSTRACT

A proposed communication system architecture is denoted TOMAS, which stands for data Transmission oriented on the Object, communication Media, Application, and state of communication Systems. Given particular tactical communication system scenarios of image transmission over a wireless LOS (Line-of-Sight) channel, a wireless TOMAS system demonstrates superior performance compared to the conventional system, which is a combination of JPEG2000 image compression and OFDM transmission, in restored image quality parameters over a wide range of wireless channel parameters. The wireless TOMAS system provides progressive lossless image transmission under the influence of moderate fading without any kind of channel coding and estimation. The TOMAS system employs a fast proprietary patent pending algorithm Sabelkin (2011), which does not employ any multiplications, and it uses three times less real additions than the algorithm of JPEG2000+OFDM. The TOMAS system exploits a specialized wavelet transform combined for image coding and channel modulation.

Keywords: Tactical Communication System (TCS), Line-of-Sight (LOS), Wavelets, Wavelet Packets, Joint Photographic Experts Group (JPEG), JPEG2000, Quality of Service (QoS), multipath channel, Software Defined Radio (SDR), Error Sensitivity Descriptor (ESD), Orthogonal Frequency Division Multiplexing (OFDM), Wavelet Packet Multiplexing (WPM).

DATA TRANSMISSION ORIENTED ON THE OBJECT, COMMUNICATION MEDIA, APPLICATION, AND STATE OF COMMUNICATION SYSTEMS: TACTICAL COMMUNICATION SYSTEM APPLICATION.

Mykhaylo SABELKIN

RÉSUMÉ

L'architecture du système de communication proposé se nomme TOMAS (Transmission de données orientée sur l'Objet, le Médium de communication, l'Application, et l'état des Systèmes de communications). En fonction de scénarios particuliers de communication tactique de transmission d'image par le canal sans fil en ligne de vue directe, le système TOMAS sans fil obtient une performance supérieure à celle du système combinant le JPEG2000 et la modulation OFDM sur les paramètres de qualité de l'image restaurée et ce, pour une large gamme de paramètres du canal. Sans aucun codage ni estimation du canal, le système TOMAS sans fil fournit une transmission progressive de l'image sans pertes sous l'influence de l'évanouissement modéré du canal. Le système TOMAS sans fil est basé sur l'algorithme propriétaire breveté Sabelkin (2011). Il ne contient pas d'opérations de multiplications, et utilise trois fois moins d'opérations d'additions réelles que celui du système JPEG2000+OFDM. Notre système exploite la transformation en ondelettes specialisée pour un codage de l'image et une modulation du canal.

Mots-clés: Système de communication tactique (TCS), ondelettes, paquets d'ondelettes, JPEG, JPEG2000, qualité de service (QdS), canal aux trajets multiples, radio définie par logiciel (SDR), descripteur de sensibilité aux erreurs (ESD), multiplexage par partition des fréquences orthogonales (OFDM), multiplexage par packets d'ondelettes (WPM).

TABLE OF CONTENTS

Page

INTRODUCTION 1

CHAPTER 1 TACTICAL COMMUNICATION SYSTEMS 11
1.1 Introduction 11
1.2 TCS versus conventional communication systems 11
1.3 Radio frequency interference 14
1.4 Spoofing 15
1.5 Jamming 16
1.6 Anti-jamming and anti-spoofing techniques 17
1.6.1 Frequency hopping 17
1.6.2 Time hopping 18
1.6.3 Time diversity 19
1.6.4 Antenna nulling 19
1.6.5 Forward error correcting code 20
1.7 Conclusion 21

CHAPTER 2 WIRELESS MULTIPATH CHANNEL 23
2.1 Introduction 23
2.2 Multipath fading 23
2.3 Channel characteristic parameters 25
2.3.1 Channel impulse response 25
2.3.2 Time dispersion parameters: delay spread and coherence bandwidth 28
2.3.3 Time variation parameters: Doppler spread and coherence time 31
2.4 Types of multipath fading 32
2.4.1 Multipath signal fading due to time dispersion 32
2.4.2 Multipath signal fading due to frequency dispersion 34
2.4.3 Multipath channel classification 35
2.5 Statistical modeling of multipath channels 36
2.5.1 Ricean Fading 36
2.5.2 Rayleigh Fading 37
2.6 Anti-multipath fading techniques 38
2.7 Conclusion 40

CHAPTER 3 DATA MULTIPLEXING 41
3.1 Introduction 41

3.2 Multiplexing 41
3.2.1 Time Division Multiplexing 42
3.2.2 Frequency Division Multiplexing 43
3.3 Orthogonal Frequency Division Multiplexing 44
3.3.1 Subcarrier Waveform 44
3.3.2 Subcarrier Number 47
3.3.3 OFDM Symbol 48
3.3.4 Cyclic prefix 48
3.4 OFDM System Structure 50
3.5 OFDM Performance 51
3.6 OFDM Advantages and Drawbacks 54
3.7 Literature Review on Wavelet Multiplexing/Modulation 55
3.8 Conclusion 64

CHAPTER 4 WAVELET ANALYSIS 65
4.1 Introduction 65
4.2 History and applications of wavelets 65
4.3 Elementary Wavelet Analysis and Synthesis Cells 67
4.3.1 One-dimensional Cells 67
4.3.2 Two-dimensional Cells 70
4.4 Wavelet Decomposition and Reconstruction 74
4.4.1 One-dimensional Case 74
4.4.2 Two-dimensional Case 76
4.5 Wavelet Tree 82
4.5.1 Wavelet Tree of 1D and 2D Wavelet Decomposition 82
4.5.2 Wavelet Tree Manipulations 84
4.5.3 Best Wavelet Tree 85
4.5.4 Compact Wavelet Tree Representation 87
4.6 Fast Elementary Wavelet Analysis and Synthesis Cells 89
4.6.1 One-dimensional Cells 89
4.6.2 Two-dimensional Cells 94
4.7 Fast Wavelet Decomposition and Reconstruction 100
4.7.1 Fast Wavelet Packet Transform (FWPT) 100
4.7.2 Fast Discrete Wavelet Transform (FDWT) 110
4.8 Conclusion 118

CHAPTER 5 ANALYTICAL EVALUATION OF TOMAS 119
5.1 Introduction 119
5.2 Structure of the still image transmission system 119
5.3 Properties of the transform matrix **W** 125

5.3.1 Property 1. Involution: $\mathbf{W} = \mathbf{W}^{-1}$ 125
5.3.2 Property 2. $\mathbf{W} = \mathbf{W}^{T}$ 126
5.3.3 Property 3. $\mathbf{W} \cdot \mathbf{W} = \mathbf{I}$ 126
5.4 Properties of the thresholding matrix $\mathbf{T}$ 126
5.4.1 Property 1. $\mathbf{T} \cdot \mathbf{T} = \mathbf{T}$ 127
5.4.2 Property 2. $\mathbf{T} = \mathbf{T}^{T}$ 127
5.5 Error between the original and received images 127
5.6 Square error between the original and received images 129
5.7 System performance dilemma 130
5.8 Optimal threshold value 132
5.9 Quasi-optimal hard thresholding 135
5.9.1 Proposal of the quasi-optimal hard thresholding rule 135
5.9.2 Validation of the quasi-optimal hard thresholding rule 137
5.9.3 Quasi-optimal hard thresholding rule 143
5.9.4 Square error in the case of the quasi-optimal hard thresholding 144
5.10 MSE bound for the coefficients transmitted over the AWGN channel 145
5.11 Simulation results for the still image transmission case 151
5.12 Conclusion 154

CHAPTER 6 STILL IMAGE TRANSMISSION USING WIRELESS TOMAS 155
6.1 Introduction 155
6.2 Wireless TOMAS 155
6.3 Data Transmission Scenario 159
6.4 Performance Parameters of Communication System 161
6.4.1 Quality Parameters of Restored Image 162
6.4.2 PSNR and MSE bounds for image transmission based on BPSK 162
6.4.3 Recapitulation 168
6.5 Structure of the Wireless TOMAS for Image Transmission 169
6.6 Structure of the Benchmark Communication System 173
6.7 Performance comparison of wireless TOMAS and JPEG2000 WirelessMAN OFDM communication systems 173
6.8 Conclusion 210

CONCLUSION 215

APPENDIX I INVERSE WAVELET PACKET MATRIX $\mathbb{W}_4^{-1}$ 217

APPENDIX II COMPLEXITY OF ARITHMETIC OPERATIONS 225

BIBLIOGRAPHY 229

LIST OF TABLES

Page

Table 2.1 Types of fading 33

Table 2.2 Classification of channels with both time and frequency dispersion 35

Table 4.1 Input/Output pin assignment of the fast elementary cell 93

Table 4.2 Complexity of $\mathbb{W}_2$, $\mathbb{V}_2$ cells and 2-FFT butterfly 94

Table 4.3 Input/Output pin assignment of the 2D fast elementary cell 96

Table 4.4 Complexity of $\mathbb{W}_4$, $\mathbb{V}_4$ cells in terms of real operations 97

Table 4.5 Bit number of the output of 2D fast elementary cell 99

Table 4.6 Complexity of the N-point FWPT vs. the N-point FFT 110

Table 6.1 Wireless Channel Parameters 161

Table 6.2 Comparison of the PSNR bound and practical values of PSNR 169

Table 6.3 WirelessMAN OFDM PHY Parameters 173

Table 6.4 Algorithm Complexity 212

Table 6.5 Difference in restored image quality between two systems 213

LIST OF FIGURES

Page

Figure 0.1 An example of one-dimensional data. Speech signal and its spectrum 2

Figure 0.2 An example of two-dimensional data. Multichannel satellite imagery..... 3

Figure 0.3 An example of two- and three-dimensional meshes..... 4

Figure 0.4 Data Transmission Oriented on the Object, Communication Media, Application, and State of Communication Systems..... 6

Figure 1.1 Typical scenarios of TCS operation..... 14

Figure 1.2 Typical LOS and NLOS scenarios of TCS operation 15

Figure 1.3 An idea of jammer nulling by an antenna pattern transform..... 20

Figure 2.1 The signal and its two reflections 24

Figure 2.2 Time varying signal fading 24

Figure 2.3 Channel impulse response..... 26

Figure 2.4 Block diagram for the discrete delay channel model..... 28

Figure 2.5 A power delay profile of multipath channel, rms delay spread, mean excess delay and threshold level..... 30

Figure 2.6 Probability density functions of Ricean distributions: K = - ∞ dB (Rayleigh), 0 dB and 6 dB..... 37

Figure 2.7 Rayleigh probability density function 38

Figure 3.1 Time Division Multiplexing (TDM) 42

Figure 3.2 Frequency Division Multiplexing (FDM) 43

Figure 3.3 Orthogonal Frequencies or Subcarriers (N_c = 4) 45

Figure 3.4 OFDM demodulator 46

Figure 3.5 OFDM symbol structure in the frequency domain 49

Figure 3.6 OFDM symbol time structure 49

Figure 3.7 Orthogonal Frequency Multiplexing and Demultiplexing 52

Figure 3.8 Coded OFDM structure 54

Figure 4.1 The elementary one-dimensional analysis and synthesis cells 68

Figure 4.2 The structure of the analysis and synthesis cells for two-dimensional data 71

Figure 4.3 The structure of the one-dimensional Discrete Wavelet Transform (1D DWT) and the one-dimensional Inverse Discrete Wavelet Transform (1D IDWT). The level of decomposition is 3 75

Figure 4.4 The structure of the one-dimensional Wavelet Packet Transform (1D WPT) and the one-dimensional Inverse Wavelet Packet Transform (1D IWPT). The level of decomposition is 3 76

Figure 4.5 The structure of the two-dimensional Discrete Wavelet Transform (2D DWT) and the two-dimensional Inverse Discrete Wavelet Transform (2D IDWT). The level of decomposition is 2 78

Figure 4.6 The structure of the two-dimensional Wavelet Packet Transform (2D WPT) and the two-dimensional Inverse Wavelet Packet Transform (2D IWPT). The level of decomposition is 2 79

Figure 4.7 Wavelet tree representation of the 1D Discrete Wavelet Transform and the 1D Wavelet Packet Transform. The decomposition level is 3 83

Figure 4.8 Wavelet Tree representation of the 2D Discrete Wavelet Transform, and the 2D Wavelet Packet Transform. The decomposition level is 2 84

Figure 4.9 Wavelet Packet Tree: Node Split and Node Merge 85

Figure 4.10 Full wavelet tree and two best wavelet trees 88

Figure 4.11 Reconstruction of the wavelet tree from the set of its terminal nodes 89

Figure 4.12 One-dimensional fast elementary cell..... 93

Figure 4.13 2-FFT butterfly 94

Figure 4.14 Two-dimensional fast elementary cell as a combination of four one-dimensional elementary cells..... 95

Figure 4.15 Two-dimensional fast elementary cell 98

Figure 4.16 The hardware implementations of the one dimensional Fast Wavelet Packet Transform (1D FWPT) and one dimensional Inverse Fast Wavelet Packet Transform (1D IFWPT). Level of decomposition d=3.....103

Figure 4.17 Eight-point Fast Wavelet Packet Transform (8-FWPT) and Inverse Fast Wavelet Packet Transform (8-IFWPT) 104

Figure 4.18 Eight-point decimation-in-time FFT algorithm 109

Figure 4.19 Four-point Fast Discrete Wavelet Transform (4-FDWT) and Inverse Fast Discrete Wavelet Transform (4-IFDWT) 111

Figure 4.20 The hardware implementations of the one dimensional Fast Discrete Wavelet Transform (1D FDWT) and one dimensional Inverse Fast Wavelet Packet Transform (1D IFDWT). Level of decomposition d=3.....113

Figure 4.21 Eight-point Fast Discrete Wavelet Transform (8-FDWT) and Inverse Fast Discrete Wavelet Transform (8-IFDWT) 114

Figure 5.1 The transform-based still image transmission system.....120

Figure 5.2 An element run for conversion of an image matrix into an image vector ...121

Figure 5.3 An element run for conversion of the image vector into the image matrix..124

Figure 5.4 The transform based still image transmission system using TOMAS.....152

Figure 5.5 Quality of a restored image as the function of the hard threshold value 153

Figure 6.1 Wireless TOMAS system structure 156

Figure 6.2 Bit-plan conversion 158

Figure 6.3 Test images from top to bottom and from left to right are Lena128, F16, Mandrill (Baboon), Aerial, Peppers and Aerial2 160

Figure 6.4 Structure of the Wireless TOMAS for Image Transmission 171

Figure 6.5 Structure of the Benchmark Communication System JPEG2000+WirelessMAN OFDM 174

Figure 6.6 Comparison of system performances using the PSNR criterion and the image Lena128. Fading rate = 2 Hz 176

Figure 6.7 Comparison of system performances using the VIF criterion and the image Lena128. Fading rate = 2 Hz 177

Figure 6.8 Comparison of system performances using the PSNR criterion and the image Mandrill. Fading rate = 2 Hz 178

Figure 6.9 Comparison of system performances using the VIF criterion and the image Mandrill. Fading rate = 2 Hz 179

Figure 6.10 Comparison of system performances using the PSNR criterion and the image Peppers. Fading rate = 2 Hz 180

Figure 6.11 Comparison of system performances using the VIF criterion and the image Peppers. Fading rate = 2 Hz 181

Figure 6.12 Comparison of system performances using the PSNR criterion and the image F16. Fading rate = 2 Hz 182

Figure 6.13 Comparison of system performances using the VIF criterion and the image F16. Fading rate = 2 Hz 183

Figure 6.14 Comparison of system performances using the PSNR criterion and the image Aerial. Fading rate = 2 Hz 184

Figure 6.15 Comparison of system performances using the VIF criterion and the image Aerial. Fading rate = 2 Hz 185

Figure 6.16 Comparison of system performances using the PSNR criterion and the image Aerial2. Fading rate = 2 Hz 186

Figure 6.17 Comparison of system performances using the VIF criterion and the image Aerial2. Fading rate = 2 Hz 187

Figure 6.18 Comparison of system performances using the PSNR criterion and the image Lena128. Fading rate = 37 Hz 188

Figure 6.19 Comparison of system performances using the VIF criterion and the image Lena128. Fading rate = 37 Hz 189

Figure 6.20 Comparison of system performances using the PSNR criterion and the image Mandrill. Fading rate = 37 Hz 190

Figure 6.21 Comparison of system performances using the VIF criterion and the image Mandrill. Fading rate = 37 Hz 191

Figure 6.22 Comparison of system performances using the PSNR criterion and the image Peppers. Fading rate = 37 Hz 192

Figure 6.23 Comparison of system performances using the VIF criterion and the image Peppers. Fading rate = 37 Hz 193

Figure 6.24 Comparison of system performances using the PSNR criterion and the image F16. Fading rate = 37 Hz 194

Figure 6.25 Comparison of system performances using the VIF criterion and the image F16. Fading rate = 37 Hz 195

Figure 6.26 Comparison of system performances using the PSNR criterion and the image Aerial. Fading rate = 37 Hz 196

Figure 6.27 Comparison of system performances using the VIF criterion and the image Aerial. Fading rate = 37 Hz 197

Figure 6.28 Comparison of system performances using the PSNR criterion and the image Aerial2. Fading rate = 37 Hz 198

Figure 6.29 Comparison of system performances using the VIF criterion and the image Aerial2. Fading rate = 37 Hz 199

Figure 6.30 Comparison of system performances using the PSNR criterion and the image Lena128. Fading rate = 225 Hz 200

Figure 6.31 Comparison of system performances using the VIF criterion and the image Lena128. Fading rate = 225 Hz.....201

Figure 6.32 Comparison of system performances using the PSNR criterion and the image Mandrill. Fading rate = 225 Hz.....202

Figure 6.33 Comparison of system performances using the VIF criterion and the image Mandrill. Fading rate = 225 Hz.....203

Figure 6.34 Comparison of system performances using the PSNR criterion and the image Peppers. Fading rate = 225 Hz.....204

Figure 6.35 Comparison of system performances using the VIF criterion and the image Peppers. Fading rate = 225 Hz.....205

Figure 6.36 Comparison of system performances using the PSNR criterion and the image F16. Fading rate = 225 Hz 206

Figure 6.37 Comparison of system performances using the VIF criterion and the image F16. Fading rate = 225 Hz 207

Figure 6.38 Comparison of system performances using the PSNR criterion and the image Aerial. Fading rate = 225 Hz 208

Figure 6.39 Comparison of system performances using the VIF criterion and the image Aerial. Fading rate = 225 Hz 209

Figure 6.40 Comparison of system performances using the PSNR criterion and the image Aerial2. Fading rate = 225 Hz 210

Figure 6.41 Comparison of system performances using the VIF criterion and the image Aerial2. Fading rate = 225 Hz 211

LIST OF ABBREVIATIONS

AC, ac	alternating current
ACI	Adjacent Channel Interference
ADC	Analog-to-Digital Converter
AID	Adaptive Iterative Detection
AM	Amplitude Modulation
AWGN	Additive White Gaussian Noise
BER	Bit Error Rate
BICM	Bit-Interleaved Coded Modulation
BI-SFCM	Bit-Interleaved Space-Frequency Coded Modulation
BPSK	Binary Phase Shift Keying
CCI	Co-Channel Interference
CDMA	Code Division Multiple Access
cir	channel impulse response
COFDM	Coded Orthogonal Frequency Division Multiplexing
CP	Cyclic Prefix
CSTBC	Circular Simplex Turbo Block Coded
CWT	Continuous Wavelet Transform

DAC	Digital-to-Analog Converter
DC, dc	direct current
DQPSK	Differential Quadrature Phase Shift Keying
DFT	Discrete Fourier Transform
EEG	electroencephalogram
E_b/N_0	Signal-to-noise ratio normalized by signal bandwidth and bit rate
FEC	Forward Error Correcting
FDM	Frequency Division Multiplexing
FH	Frequency Hopping
FFH	Fast Frequency Hopping
FFT	Fast Fourier Transform
FM	Frequency modulation
FPSK	Filtered Phase Shift Keying
GMSK	Gaussian Minimum Shift Keying
GSM	Global System for Mobile Communications
ICI	Inter Carrier Interference
IDFT	Inverse Discrete Fourier Transform
IFFT	Inverse Fast Fourier Transform
ISI	Inter Symbol Interference

LOS	Line-of-Sight
LSB	Least Significant Bit
LTI	Linear Time-Invariant
MAE	Mean Absolute Error
MAI	Multiple Access Interference
MFSK	M-ary Frequency Shift Keying
MIP	Multipath Intensity Profile
MSB	Most Significant Bit
MSE	Mean Square Error
MWPM	Multi-Wavelet Packet Modulation
NLOS	Non Line-of-Sight
OFDM	Orthogonal Frequency Division Multiplexing
PAPR	Peak-to-Average Power Ratio
PER	Packet Error Rate
PCT	Patent Cooperation Treaty
pdf	probability density function
PHY	Physical layer
PN	Pseudo-random
PSAM	Pilot Symbol Assisted Modulation

PSNR	Peak Signal-to-Noise Ratio
QAM	Quadrature Amplitude Modulation
QMF	Quadrature Mirror Filters
QPSK	Quadrature Phase Shift Keying
QoS	Quality of Service
RF	Radio Frequency (component)
RFI	Radio Frequency Interference
rms	root mean square
SAR	Synthetic Aperture Radar
SC-FD	Single-Carrier with Frequency-Domain processing
SER	Symbol Error Rate
SISO	Soft-Input/Soft-Output
SNR	Signal-to-Noise Ratio
TDM	Time Division Multiplexing
TDMA	Time Division Multiple Access
TCS	Tactical Communication System
WPM	Wavelet Packet Modulation
WPT	Wavelet Packet Transform
WPM	Wavelet Packet Multiplexing

LIST OF SYMBOLS

	Mathematical Definition
$\mathbf{W}, \mathbb{W}$	Matrix
$\overline{C}, C$	Vector
$\mathscr{H}(\cdot)$	Heaviside step function
$\mathbf{u}(\cdot)$	Step function
$\delta(\cdot)$	Delta function
$Q(\cdot)$	Complementary error function
	Arithmetic Operation
$\oplus$	Addition
$\otimes$	Multiplication
$\ominus$	Additive Inverse: $-A$
$\oslash$	Multiplicative Inverse: A^{-1}

INTRODUCTION

Communication has always been an important subject in military domains. Nowadays we are facing growth in requirements to the tactical communication systems in such parameters as data throughput, Quality of Service (QoS) and secrecy. A modern Tactical Communication System (TCS) operates on different kinds of data such as audio and speech (see Figure 0.1); optical, infrared, radar, Synthetic Aperture Radar (SAR) imagery (see Figure 0.2); two or three dimensional (2D/3D) meshes (see Figure 0.3) used in surface mapping; video, etc. The task of a Tactical Communication System becomes much more complicated when it is necessary to transmit a mixture of certain data types simultaneously and at high data rate. There are natural, such as multipath fading, Doppler shift, as well as artificial threats, such as jamming, spoofing, that degrade the TCS performance or even destroy a whole communication session. The Tactical Communication System often operates in a hostile environment, hence high survivability of equipment is very important. TCS has often a limited energy supply, e.g. is battery-operated.

In this context, the objectives of this work may be listed as follows:

1. Analyze specifics of data types the TCS operates on, communication media the TCS operates with, users who operate TCS, hardware the TCS consists of.
2. Propose some measures for evaluation of TCS performance.
3. Propose a structure of TCS which consider specifics of data types, communication media, users and hardware.
4. Using performance measures, evaluate the performance of the proposed system compared to state-of-the-art systems.

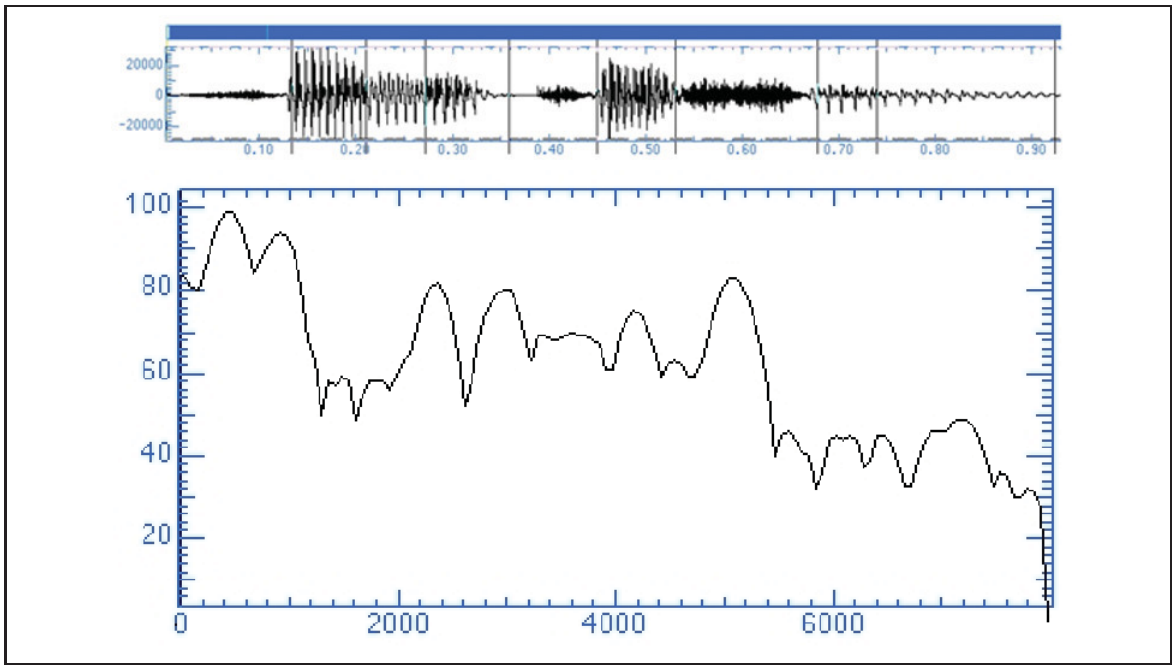

Figure 0.1 An example of one-dimensional data. Speech signal and its spectrum.

Methodology

Our proposed system architecture is called **TOMAS** which is data **T**ransmission oriented on the **O**bject, communication **M**edia, **A**pplication, and state of communication **S**ystems (see Figure 0.4). Efficient data transmission could be provided if communication systems involved in data transmission would take into consideration and monitor constantly the following four aspects:

1. **Object**. Its type, size, nature, etc. It can be either one/two dimensional (1D/2D) signals, a three dimensional (3D) mesh, symbol data alone or any combination of them. For example, audio and video signals or an optical image of surface and its 3D map. Object properties impose certain requirements on processing techniques. For example, the image compression standard JPEG (1994) does not support very large images, since it cannot be used directly for processing such data object;

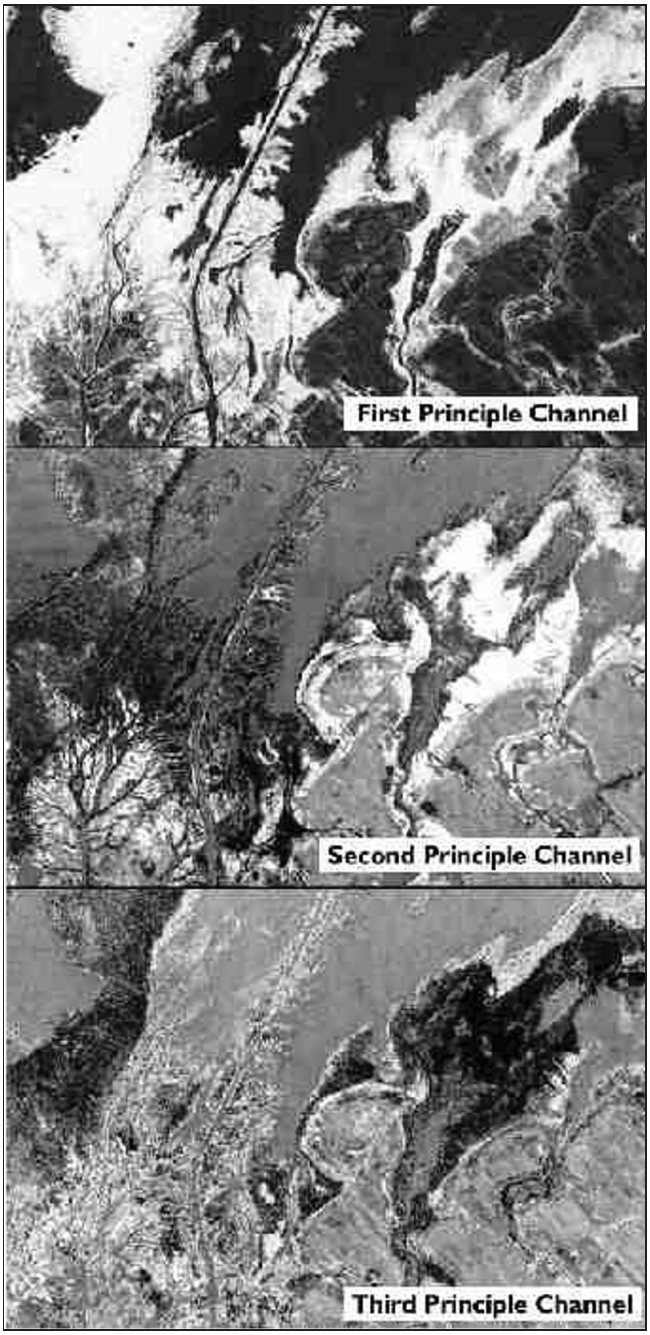

Figure 0.2 An example of two-dimensional data.
Multichannel satellite imagery.

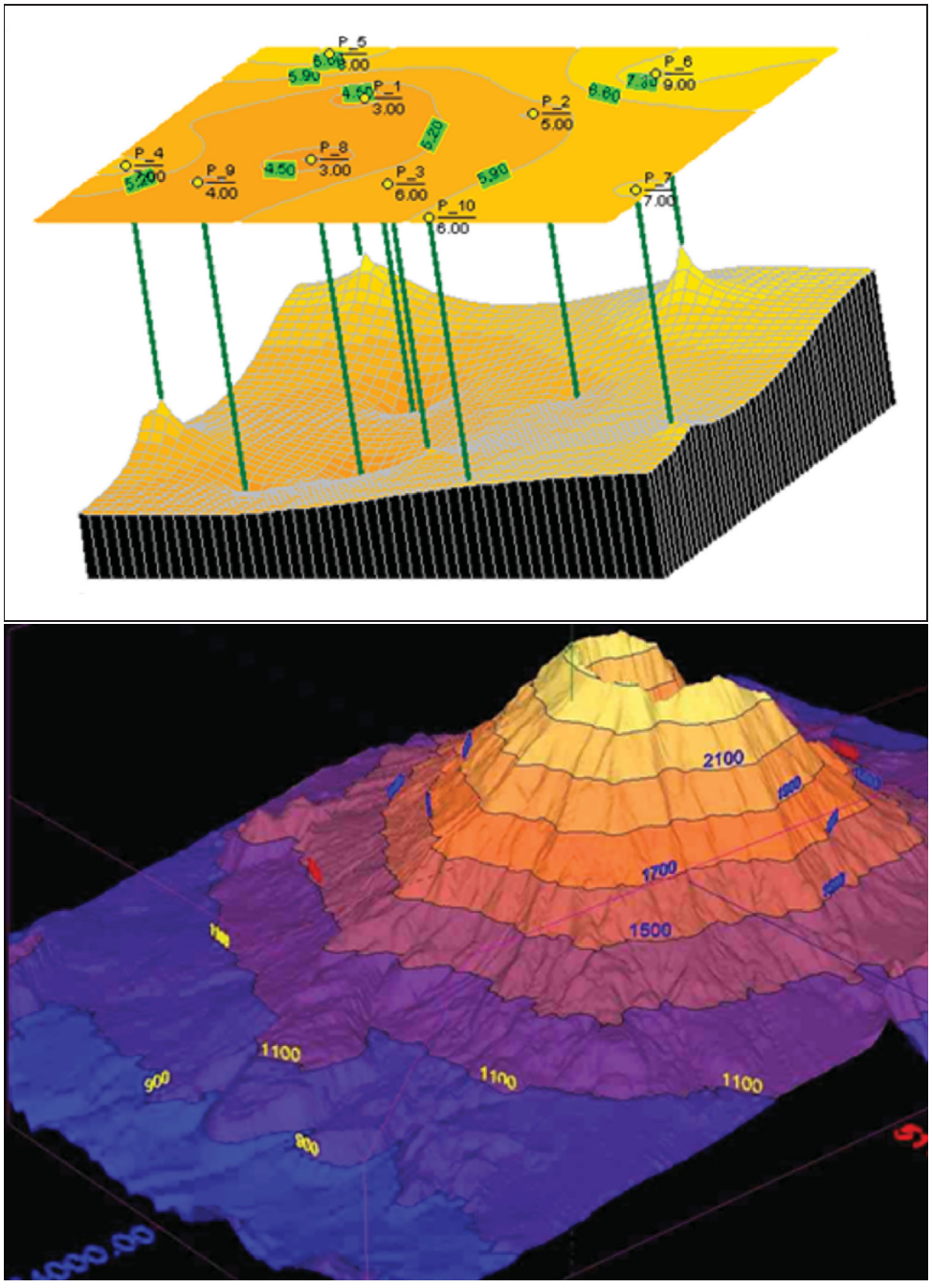

Figure 0.3 An example of two- and three-dimensional meshes.

2. **Communication media**. In the case of a complex communication system, a data object might be transmitted over different communication media such as a wireless, coaxial, fiber optic link, or a waveguide, IEEE (1993). Hence, the total performance of one object transmission will depend on the performance of the weakest link. For example, LOS, fair channel conditions may not require the system to employ a 256 subcarrier OFDM in order to provided required QoS;

3. **Agent and/or Application**. A human user or some application imposes certain requirements on the quality and rapidity of object transmission. For example, if image Region Of Interest (ROI) access is required, JPEG2000 source coding might be preferable, JPEG (2000);

4. **State of communication systems**. Time-varying characteristics of all systems involved in data exchange such as batteries' charge and status of all hardware, firmware and software components have to be monitored constantly. For example, it would not be useful to send a picture on some wireless terminal with a broken screen, or to employ some complex coding technique if the recipient side experiences a problem with the decoder.

Justification

Results of research, presented by Liew et al. (2005), Yu and Bi (2004), You and Ilow (2004a), You and Ilow (2004b), You and Ilow (2004c), Xiaofan et al. (2004), Gao et al. (2004), Fahmy et al. (2004), Ciolino et al. (2004), Okamoto et al. (2003), Kjeldsen et al. (2003), Xingxin et al. (2002), Lee et al. (2002), Daly et al. (2002), Zhang et al. (2001), Zhang and Bi (2001), Weihua et al. (2001), Chang et al. (2001), Van Bouwel et al. (2000), To et al. (2000), Zhang and Dill (1999), Suzuki et al. (1999), Dovis et al. (1999), Newlin (1998), Adhikary and Reddy (1998),

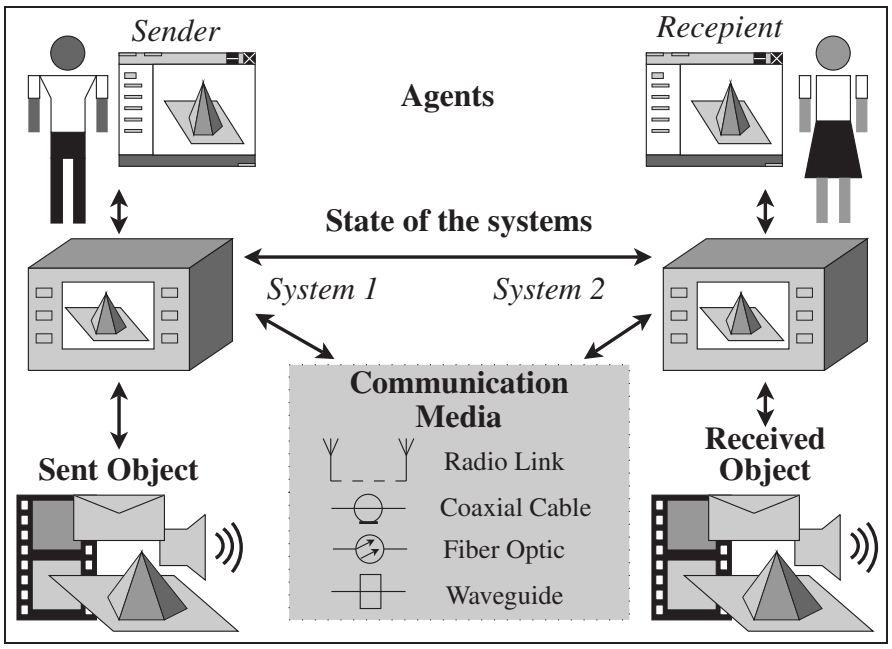

Figure 0.4 Data Transmission Oriented on the Object, Communication Media, Application, and State of Communication Systems.

Yang et al. (1997), Lindsey (1996), Lindsey (1997), Lindsey and Dill (1995), Daneshagaran and Mondin (1994), show certain advantage of using wavelets over harmonic functions, i.e. Wavelet (Packet) Transform over Fourier Transform, for data compression and multiplexing. Wavelet (Packet) Transform (WPT) is known as a multiresolution tool. It can be used for data segmentation. Also, the structure of data decomposed by WPT fits the requirement of rapid access to certain data blocks, for example the regions of interest (ROI) on an image.

The author's own research in the field of data compression: Sabelkin and Piscorzh (1998), Sabelkin and Lukin (1999), Sabelkin (2000), Sabelkin (2001), Sabelkin and Ponomarenko (2001), demonstrates expediency of using the Wavelet Transform.

As for a datastream multiplexing stage, we will consider two candidates. They are Orthogonal Frequency Division Multiplexing (OFDM) and Wavelet Packet Multiplexing (WPM). OFDM

is vulnerable to synchronization errors. Loss of orthogonality to adjacent subcarriers causes an Inter-Carrier Interference (ICI). WPM vulnerability to synchronization errors, in general, depends on the type of basic wavelet function. According to Xiaofan et al. (2004), an appropriate wavelet choice allows to mitigate ICI.

A Cyclic Prefix (CP) in OFDM systems serves to mitigate multipath distortions. In wireless communication standards such as WiFi and WiMAX the duration of CP reaches 1/4 of the symbol duration. It causes a waste of energy and reduces the useful data rate. WPM does not use any CP, and therefore it is more energy efficient, according to Zhang and Bi (2001). Research also shows that, in order to mitigate severe multipath and Doppler shift, the OFDM system requires more complex channel estimation techniques, both in the time and frequency domains, than the WPM system does.

Depending on wavelet types, the system based on WPM has up to 50 dB stopband compared to a 13 dB stopband for the OFDM system. According to You and Ilow (2004b), this allows us to use the spectrum more efficiently by closely packing the subchannels.

Contributions

Our research made the following contributions to knowledge:

- Given a particular scenario of image transmission over a wireless LOS channel, the proposed system provides superior performances compared to the JPEG2000+ OFDM system in restored image quality parameters over a wide range of wireless channel parameters. The JPEG2000+ OFDM system is not able to provide lossless transmission at all.
- Despite a common opinion that channel coding is mandatory in wireless communications, we demonstrated that without any channel coding, the proposed system provides lossless

progressive image transmission under the influence of moderate fading. Channel coding might mitigate effects of severe fading.

- Despite a decrease of interest towards wavelets, they have a high potential in telecommunication. The fast algorithm, derived from wavelets, does not employ any multiplications, and it uses three times fewer real additions than the one of the JPEG2000+ OFDM system.
- Complex telecommunication networks, which operate with multimedia content over mixture of communication media types, could profit from use of TOMAS.

The proposed idea of TOMAS has been validated by presentation of the research results at the 10th Wireless Telecommunications Symposium (WTS 2011) in April 13-15, 2011, in New York City, New York, USA, Sabelkin and Gagnon (2011a). Also the research results have been published in the International Journal of Interdisciplinary Telecommunications and Networking (IJITN), Sabelkin and Gagnon (2011b), and in the Proceedings of the 7th International Conference on Wireless Advanced 2011 (WiAd 2011), June 2011, London, UK, Sabelkin and Gagnon (2011c).

Thesis structure

The thesis is presented as follows: In Chapter 1, we present some details of tactical communication systems that make them different from ordinary communication systems. Hostile operating conditions of TCS are represented by interference, jamming and spoofing. They are described as well as some mitigating techniques called anti-jamming and anti-spoofing.

In Chapter 2, we present parameters that characterize wireless channels with multipath reflections. Statistical models for those channels are proposed. Also, we make the classification of multipath fading. At the end of the chapter, some techniques of multipath fading mitigation are proposed.

In Chapter 3, different types of multiplexing are presented, from the simple Time Division Multiplexing (TDM) to the more complex Orthogonal Frequency Division Multiplexing (OFDM). The functioning principles of OFDM are followed by a description of the structure of an OFDM-based communication system. Also OFDM advantages and drawbacks are highlighted. Literature review on the use of wavelets for data multiplexing demonstrates a high potential of the Wavelet Packet Multiplexing.

Wavelets have been very popular lately. From the history and modern applications to hardware implementation of algorithms and analysis of their complexity, Chapter 4 presents the subject matter. The conception of data compression and denoising using wavelet coefficient thresholding is described. Introducing a wavelet tree structure serves to represent the wavelet analysis/synthesis in a hierarchical form. Application of energy constraints on wavelet coefficients optimizes the wavelet tree, which is called the best wavelet tree. Some interesting properties of orthogonality of wavelet matrices are investigated in this chapter and appendices. High complexity of computation often limits the application of wavelet analysis. We developped fast wavelet algorithms that are being protected by a patent. Proposed fast wavelet analysis algorithms are compared to the conventional Fast Fourier Transform (FFT). A Haar matrix is analyzed as a matrix used in the Fast Discrete Wavelet Transform (FDWT).

In Chapter 5, we propose analytical evaluation of the proposed data Transmission oriented on the Object, communication Media, Application, and State of communication Systems (TOMAS). The transmission Object is a still grayscale image. The communication Media is an Additive White Gaussian Noise (AWGN) channel. The Application uses Mean Square Error (MSE) and Peak Signal-to-Noise Ratio (PSNR) measurements to evaluate the quality of a received image. We show how knowledge of communication media parameters can improve system performance in terms of restored image quality.

In Chapter 6, we propose practical evaluation of the data Transmission oriented on the Object, communication Media, Application, and state of communication Systems for the case of the wireless media (**Wireless TOMAS**). A benchmark system was a system that combines JPEG2000 image compression with Orthogonal Frequency Division Multiplexing (**JPEG2000 + OFDM**). Both the wireless TOMAS and JPEG2000+OFDM systems as well as a wireless channel were simulated in Matlab® environment. A grayscale still image was chosen as a data object. Given a particular scenario of image transmission over a wireless LOS channel, the wireless TOMAS system demonstrates superior performances compared to JPEG2000 + OFDM systems in restored image quality parameters over a wide range of wireless channel parameters. The TOMAS system allows lossless progressive image transmission under the influence of moderate fading. Channel coding might mitigate effects of severe fading in order to provide lossless transmission. The JPEG2000 + OFDM system is not able to provide lossless transmission at all. The TOMAS system algorithm does not employ any multiplications, and it uses three times less real additions than the one of JPEG2000 + OFDM.

In the conclusion, we review the research work that has been done and discuss future work in hardware implementation of the data Transmission oriented on the Object, communication Media, Application, and state of communication Systems. We also discuss the contributions to knowledge of our research.

CHAPTER 1

TACTICAL COMMUNICATION SYSTEMS

1.1 Introduction

In this chapter we will present some details of tactical communication systems that make them different from ordinary communication systems. Hostile operating conditions of TCS are represented by interference, jamming and spoofing. They will be described as well as some mitigating techniques called anti-jamming and anti-spoofing.

1.2 TCS versus conventional communication systems

Tactical communication systems (TCS) are different from conventional systems in various specific requirements:

- **High secrecy**. In order to provide high confidentiality of transmitted information and immunity from eavesdropping, a TCS uses different techniques. Directed antennas with a narrow main lobe and low side/back lobe level in the radiation pattern provide a spatial discrimination. Reduced transmission power helps to reduce a risk of signal detection by an adversary. Coding and cryptography make the transmitted information readable only by allies.
- **Security of usage**. During transmission, a TCS antenna emits energy that makes it a target for radio guided missiles. In order to protect TCS users, it is desirable to separate a TCS antenna mast and a transceiver as shown in Figure 1.1.
- **High Quality of Service (QoS)**. Often, it is much more important to transmit an information correctly than to transmit it rapidly. For example, when somebody needs help in a battlefield,

it is much more important to know his current location coordinates even if it takes a little bit longer (in terms of milliseconds) to get them.

- **Energy saving**. Sometimes, it is impossible to recharge a dead transceiver battery in battlefield conditions, so all TCS components should have minimal possible energy consumption.

- **High mobility**. Civil communication systems often use stationary antennas for base stations, for example, in the case of wireless cellular networks. Unlike them, tactical communication systems must be mobile and they must be deployed fast. In order to provide this, TCS antennas often have a pneumatic or hydraulic deploying mechanism and they base on a truck platform.

- **Easy to use and maintain**. All TCS control buttons and handles must be large enough that a user can operate them in gloves or mittens; all scales must be well-lighted and easy readable in any weather conditions or air contamination. The maintenance must be simple enough even for a low qualified user. All TCS components, for example, a battery, a receiver RF block, must be easy replaceable.

- **Severe operating conditions**. All elements of TCS must be able to operate and preserve their performance in a wide range of temperatures (from -40^oC to $+80^oC$); high humidity (up to 100 %), high level of contamination (dust, sand and smoke). TCS must be designed to tolerate high overloads (up to 100G); high vibration level, especially if it operates onboard of an aircraft. It is desirable to preserve TCS operability in presence of radiation, but in the case of gamma radiation it is often impossible, especially when the TCS components are based on semiconductors.

- **Production cost**. In order to satisfy all of the above mentioned requirements, only carefully selected, high quality electronic components must be used. Also certain blocks or connections must be doubled in order to provide TCS operability in the case when some block or

connection is damaged. It makes the TCS several times more expensive than a similar civil communication system.

Often the tactical communication system operates in such a hostile environment where an ordinary communication system is not even able to survive:

- Low Signal-Noise Ratio (SNR);
- Moving users (see Figure 1.1): Doppler frequency shift, channel parameters change fast, often dramatically;
- Often Non Line-of-Sight (NLOS) conditions (see Figure 1.2);
- Multipath fading channels cause the Inter Symbol Interference (ISI);
- Radio frequency interference (RFI) from other electronic equipment;
- Active jamming and spoofing by adversaries;
- High data rate at narrow frequency bandwidth;

More and more electronic equipment is used in modern warfare for communication, position location etc. Detection of a signal source location can be helpful in controlling their own combat forces or in rescuing missions. However, detection of the signal by an adversary can jeopardize the lives of troops. Therefore, such parameters as low probability of detect (LPD) or low probability of intercept (LPI) become very important in designing tactical communications systems.

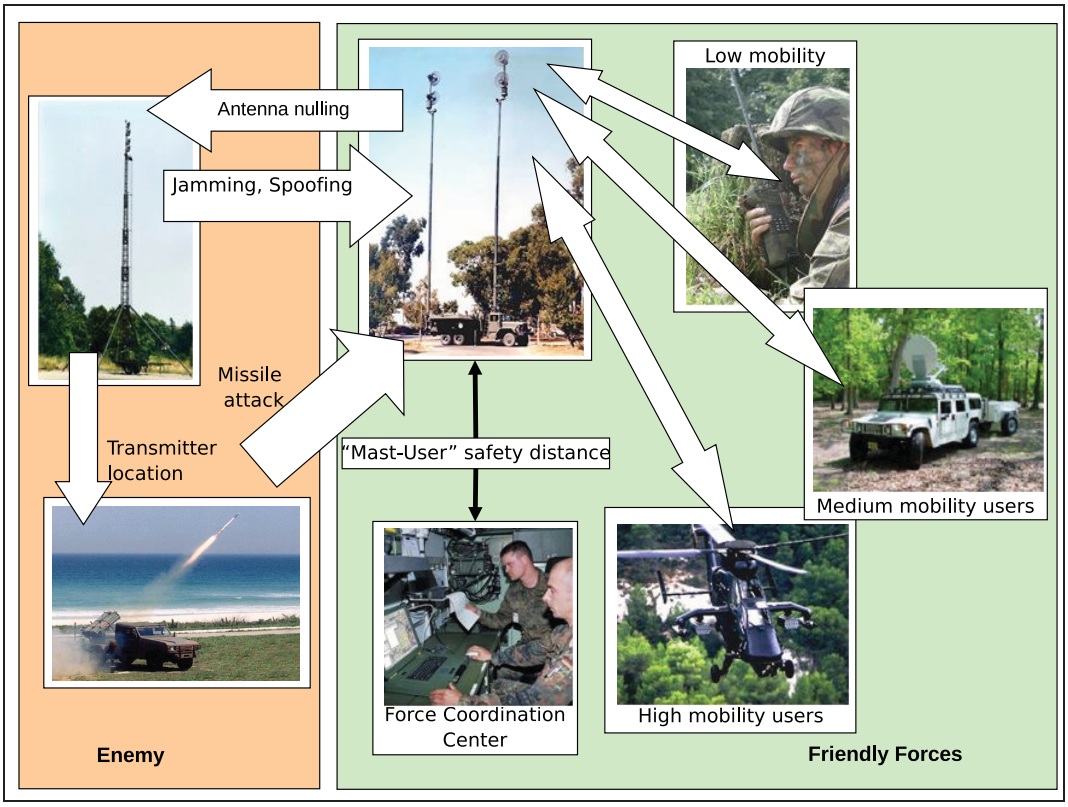

Figure 1.1 Typical scenarios of TCS operation.

Eavesdropping is a technique used to intercept intelligence information from an enemy. This can always change the outcome of a battle or even a war. Unlike detecting an existence of a signal by using a radiometer, eavesdropping requires the right demodulator, decoder, and so on. In order to protect the information from eavesdropping, the TCS uses different spread-spectrum techniques and cryptography, Wang et al. (1999).

1.3 Radio frequency interference

The radio frequency interference (RFI) from other electronic devices penetrates the receiver from the main, side, or back lobes of a receiving antenna, resulting in significant performance degradation. RFI can be located within the intended receiving bandwidth, referred to as the

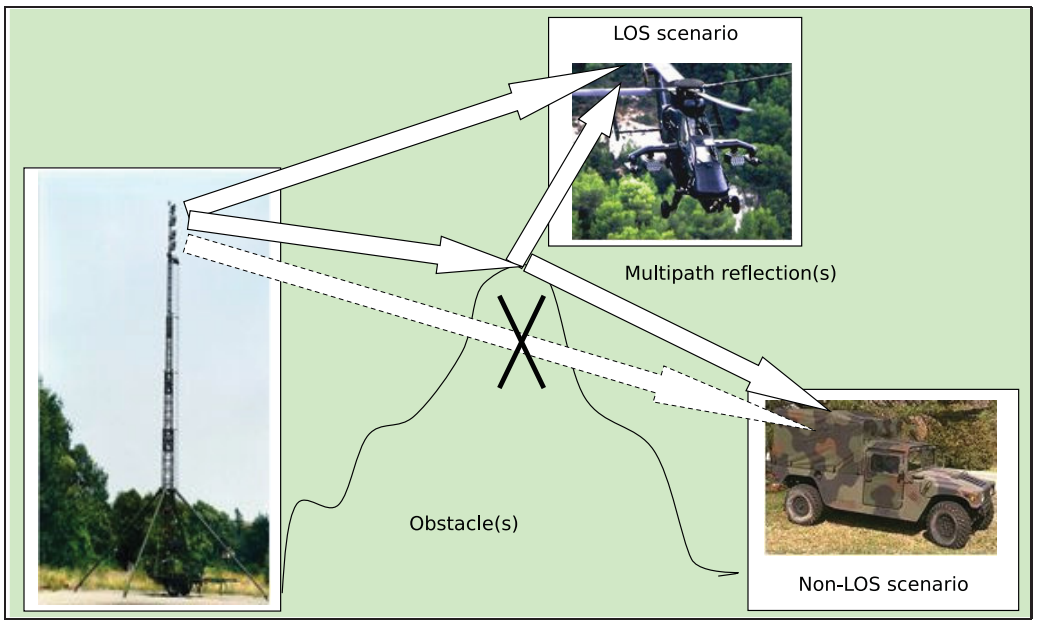

Figure 1.2 Typical LOS and NLOS scenarios of TCS operation.

co-channel interference (CCI), or leaked from the adjacent channels, referred to as the adjacent channel interference (ACI).

Often, an application of channel coding for the desired signal can mitigate the CCI problem. The ACI is caused by leakage of signal power from adjacent channels next to the desired signal bandwidth because of use of a non-ideal brick-wall filter. Thus, the portions of power spectra of adjacent channels overlap each other, resulting in leakage. In addition to the channel coding, the bandwidth-efficient modulation scheme, such as Gaussian minimum shift keying (GMSK) or filtered phase shift keying (FPSK), can mitigate the ACI.

1.4 Spoofing

Using a "look-alike" signal instead of the original by the enemy is called spoofing. It can have a purpose of denial, degradation or misinforming an original external source. Spoofing can cause much more damage than radio frequency interference or jamming. Mistakes made by

troops due to misinformation can have high or even deadly cost. Therefore the TCS uses high level cryptography to protect and authentify the transmitted information.

1.5 Jamming

Intentional sources of interference, called jammers, are devices that seek to nullify a communication system by inserting energy into the target spectrum. By location, jammers can be classified as follows, Lee (1997):

- An air jammer is usually installed on board of an aircraft. It sends a jamming signal via true Line-of-Sight propagation where the signal does not experience any fades, while the reception of the desired signal is under fading circumstances. It allows using the minimal power of a jamming transmitter.
- A ground jammer works in the same multipath fading environment as a TCS. So, for successful jamming it should transmit much more power.

By jamming strategy, jammers can be classified as follows, Lee (1997):

- Single frequency jammer;
- Pulse jammer uses an "on-off" technique in order to maximize peak power in wide bandwidth;
- Broadband noise jammer uses a pseudo-noise signal in a certain bandwidth;
- Partial-band noise jammer applies noise energy to jam certain bandwidth of the original signal spectrum while leaving part of the information intact;
- Multitone jammer uses a set of harmonic signals to cover the jamming band;

- A follow-up or smart jammer detects an original signal waveform and then transmits an appropriate signal that will jam the receiver.

The jammer decreases the SNR, and hence the E_b/N_{total}, in order to raise the bit error rate (BER) of the TCS above acceptable levels:

$$E_b/N_{total} = \frac{E_b}{N_0 + J_0} = \frac{1}{\frac{1}{E_b/N_0} + \frac{1}{E_b/J_0}}, \tag{1.1}$$

where E_b is the signal energy per bit; J_0 is the jamming energy per bit; N_0 is the one-sided power spectral density of the received additive white Gaussian noise (AWGN). The task of a jammer is disruption of communications using minimal resources. In other words, for a given total power it will maximize jamming energy at the detector. Using different techniques the jammer maximizes its effectiveness by reducing the E_b/J_0 relation.

1.6 Anti-jamming and anti-spoofing techniques

Considering an operation of tactical communication system in hostile environments, anti-jamming and anti-spoofing techniques are absolutely necessary. Depending on jammer strategy, different counterattack techniques can be applied. The management of the signal power, frequency, time, and spatial processing are some of them. Often a hybrid system is a reasonable solution to provide several anti-jamming and anti-spoofing techniques. Some of them are presented below.

1.6.1 Frequency hopping

A frequency hopping (FH) system uses a frequency synthesizer controlled by a pseudo-random sequence (PN), Torrieri (2011). The M-ary frequency-shift-keying (MFSK) is commonly used as a modulation technique in the way when the pseudo-random generator chooses carrier fre-

quencies of a MFSK signal. So, the output of the frequency hopper is a continuous sinusoidal waveform that frequency jumps from one value to another. Depending on the hopping rate, the FH system can be categorized into slow frequency hopping (SFH) and fast frequency hopping (FFH).

- **Slow Frequency Hopping**. The hopping rate is slower or equal to the data rate, so there are one or more data bits in each hop.
- **Fast Frequency Hopping**. The hopping rate is faster than the data rate, so there are multiple hops within duration of each data bit.

The conception of frequency discrimination implemented in frequency hopper allows creation the TCS which is robust for a stationary partial-band or multitone jammer. This can be explained by the fact that the signal is jammed for only a small period of time when the hopping frequency falls into the fixed jamming band. The rest of the time, the signal is free of jamming.

1.6.2 Time hopping

The technique of time hopping (TH) is similar to FH in the way that time hopping is also uses a pseudo-noise sequence generated by a PN code generator. But the time hopper uses time stamps for turning on and off the signal transmission in the time domain instead of carrier frequency hopping. Based on the concept of time discrimination, this technique can be effective only for the pulse jammer counterattack. A time hopper can make a jammer to be turned on at all times in order to be effective. But in this case, considering the constraint of fixed energy, the jammer will need to reduce its transmitting power, resulting in less interference, Dixon (1975).

1.6.3 Time diversity

Another technique for counterattack the partial-band or multitone jamming uses time diversity. Before entering the modulator, an information bit is subdivided into several equal spaced sub-bits. This approach is used in the fast frequency hopping system. Robustness of the FFH system increases if the hop duration is equal or less than the sub-bit duration. For example, if one sub-bit is jammed, other sub-bits of the same bit may be hopped to the frequency outside the jamming band.

1.6.4 Antenna nulling

An effective anti-spoofing and anti-jamming technique is based on spatial discrimination, Nitzberg (1991). It is called an antenna nulling or sidelobe cancellation. To be able to create spatial discrimination an array of element antennas, called phased-array antenna, should be used. Phased-array antennas can change the form of their radiation pattern depending on the phase shift and amplitude of the signal from each element of array.

At the first stage of jammer nulling procedure, an antenna system determines the presence of a spoofer or jammer and its azimuth. When the spoofer or jammer is detected, a processor adjusts the phases and attenuation weights of all antenna elements in order to provide a null in the antenna radiation pattern in the jammer direction. So, an interference attack becomes completely ineffective. Figure 1.3 derived from Wang et al. (1999) shows this idea.

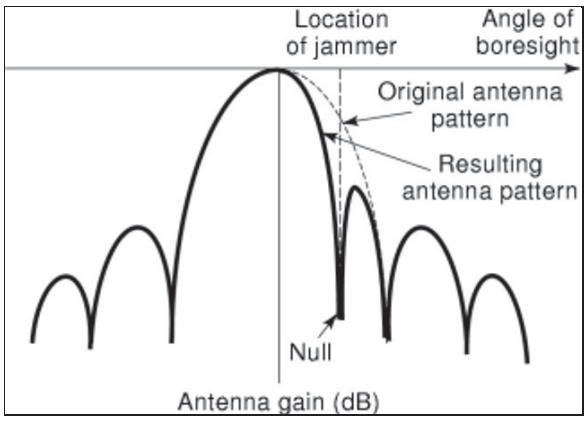

Figure 1.3 An idea of jammer nulling by an antenna pattern transform.
Derived from Wang (1999)

1.6.5 Forward error correcting code

The power efficiency of TCS can be improved using a forward error correcting (FEC). This technique can be also considered as an anti-spoofing or anti-jamming. Among variety of coding schemes preferable techniques are:

- Convolutional code with Viterbi decoding, Viterbi and Omura (1979);
- Reed-Solomon code, Peterson and Weldon (1971);
- Turbo codes and low density parity check codes, Ryan and Lin (2009).

Use of the concatenated code structure with a (7 1/2) convolutional code as the inner code and a Reed-Solomon code as the outer code can provide high anti-corruption communication system performance, Rice (1974). Turbo codes can provide a near-Shannon-limit coding gain, Berrou et al. (1993).

1.7 Conclusion

In this chapter we presented some details of tactical communications systems that make them different from ordinary communications systems. Hostile operating conditions are represented by interference, jamming and spoofing. They have been described as well as some mitigating techniques called anti-jamming and anti-spoofing.

CHAPTER 2

WIRELESS MULTIPATH CHANNEL

2.1 Introduction

Some of the most important factors that have an influence on wireless communication system performance are multipath fading and Doppler spread. Compared to jamming and spoofing (see Chapter 1) that are usually created artificially by an adversary, those factors are passive, i.e., caused by multiple signal reflections, scattering and transceiver movement.

In this chapter we will present parameters that characterize wireless channels with multipath reflections. Statistical models for those channels will be described. Also, we will make the classification of multipath fading. At the end of the chapter some techniques of multipath fading mitigation will be proposed.

2.2 Multipath fading

Often, due to multiple reflections from obstacles the signal from the transmitter arrives at the receiver antenna along with multiple copies as shown in Figure 2.1.

The phase and amplitude of signals arriving on each different path are related to the path length and the conditions of the path. Also, signal reflections arrive at the receiver at slightly different times. Due to the relative movement of the receiver, transmitter and surrounding objects, the path lengths are time-varying. Hence, the received signal from an antenna is the sum of all reflections of the transmitted signal. The received signal has thus considerable and rapid amplitude fluctuations. This phenomenon is called the multipath fading, or simply fading,

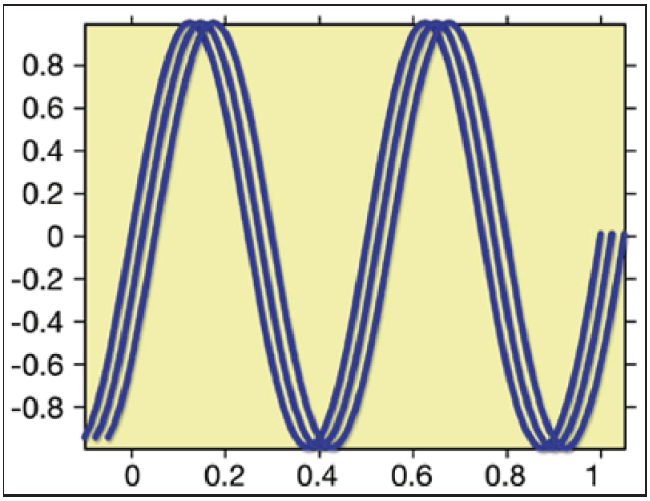

Figure 2.1 The signal and its two reflections.
Derived from the web page "OFDM for Mobile Data Communications"
http://www.iec.org/online/tutorials/ofdm/

and it is shown on Figure 2.2.

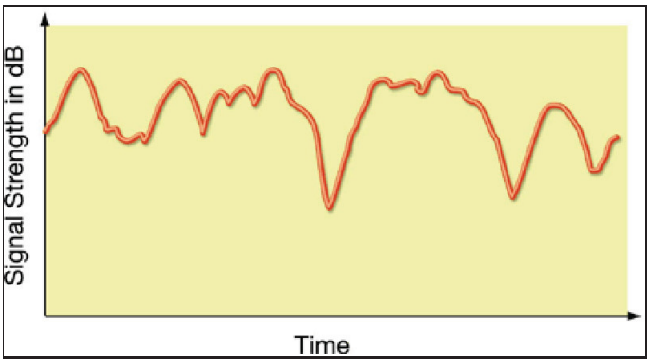

Figure 2.2 Time varying signal fading.
Derived from the web page "OFDM for Mobile Data Communications"
http://www.iec.org/online/tutorials/ofdm/

When there are no obstacles between the transmitter and receiver antenna the communication scenario is called a Line-of-Sight (LOS) transmission, by opposition to a Non Line-of-Sight (NLOS) transmission.

The radio propagation channel of communication system is influenced by the following physical factors:

- **Multipath propagation**. Due to multiple reflections of the transmitted signal from the reflecting objects and an existence of scatterers in the channel, the received signal is subject to fading and/or signal distortion;
- **Mobility of the antennas and/or surrounding objects**. Due to different Doppler shifts on each of the multipath components the received signal is subject to random frequency modulation. Whether the transmitter is moving toward or away from the receiver, Doppler shift could be positive or negative. Moving object effects might dominate the fading effects in the case when they are moving faster than the communication system;
- **Bandwidth of the transmitted signal**. The most important parameter that characterizes the multipath channel is called coherence bandwidth. It is a measure of the maximum frequency difference for which signal fadings are still strongly correlated in amplitude. If the transmitted signal bandwidth is less than the coherence bandwidth, the signal will not be distorted by the channel.

2.3 Channel characteristic parameters.

2.3.1 Channel impulse response

The main characteristic of a communication channel is its impulse response. It is often used to predict and compare the performance of different communication systems for a particular

communication channel. The **channel impulse response** (see Figure 2.3) can be referred to as a wideband channel characterization, because it is the response of the communication channel on a transmitted single pulse, which has an infinite bandwidth.

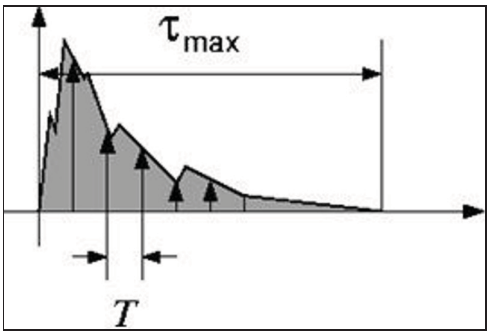

Figure 2.3 Channel impulse response. Derived from the web page "OFDM and the orthogonality principle" http://www.ert.rwth-aachen.de/Projekte/Theo/OFDM/

In Figure 2.3, T stands for the time interval in the transmission and τ_{max} is the delay of the longest path with respect to the earliest path. This is a critical measure concerning the multipath channel.

A communication channel can be modeled as a linear filter. The filtering nature of a communication channel is caused by summation of amplitudes and delays of a signal and its multiple reflections at any instant of time. This filter has a time-varying impulse response, because of relative motion between transmitter and receiver. The channel impulse response $h(t,\tau)$ as a function of both t and τ can completely characterize the communication channel. The variable t represents the time variations of the impulse response due to motion and fixing t, the variable τ represents the channel multipath delay. The received signal $y(t)$ can be obtained by a convolution of the transmitted signal $x(t)$ with the channel impulse response $h(t,\tau)$ as follows,

Rappaport (2002):

$$y(t) = x(t) \circledast h(t,\tau) = \int_{-\infty}^{+\infty} x(t-\tau) \cdot h(t,\tau) d\tau. \tag{2.1}$$

Assuming that the multipath channel is a band-limited band-pass channel, then $h(t,\tau)$ can be equivalently described by a complex baseband impulse response $h_b(t,\tau)$:

$$h(t,\tau) = Re\left\{ h_b(t,\tau) e^{j2\pi f_c t} \right\}, \tag{2.2}$$

where f_c is the central frequency of the channel.

The received signal at the antenna is represented by summation of attenuated, delayed, phase-shifted versions of the transmitted signal. Assume that L replicas of the transmitted signal arrive at the receiver. Hence, the baseband impulse response of a multipath channel can be expressed as

$$h_b(t,\tau) = \sum_{i=1}^{L} a_i(t,\tau) e^{j(2\pi f_c \tau_i(t) + \phi_i(t,\tau))} \delta(\tau - \tau_i(t)), \tag{2.3}$$

where $a_i(t,\tau)$ and $\tau_i(t)$ are the real amplitudes and excess delays of the ith multipath component at time t, respectively. The phase term $j(2\pi f_c \tau_i(t) + \phi_i(t,\tau))$ represents the phase shift due to free space propagation of the ith multipath component, plus any additional phase shifts which are encountered in the multipath channel, Rappaport (2002).

Assuming that the channel impulse response is time invariant or wide-sense stationary over a small time, the expression (2.3) of the composite impulse response can be simplified as follows:

$$h_b(\tau) = \sum_{i=1}^{L} a_i e^{j\phi_i} \delta(\tau - \tau_i), \tag{2.4}$$

where a_i and ϕ_i are the amplitude and phase of the ith path arriving with delay τ_i.

For the simulation of wideband characteristics of the multipath channel the model of discrete delay channel can be used as it is proposed in Choi and Kim (1999). It is reproduced in Figure 2.4.

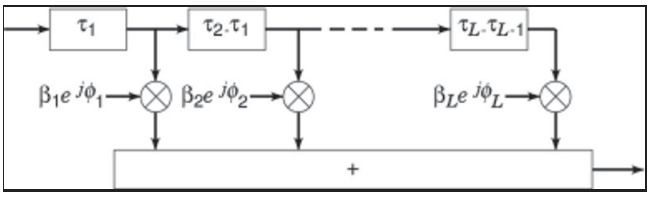

Figure 2.4 Block diagram for the discrete delay channel model.
Derived from Choi (1999)

Taking the spatial average of $|h_b(t,\tau)|^2$ over a local area such useful parameters, as the **power delay profile** $P(\tau)$ (or **multipath intensity profile**, MIP) of the channel, can be obtained. Power delay profiles are generally represented in the form of plots of relative received power as a function of excess delay with respect to a fixed time delay. They can be measured in practice by using channel sounding techniques, Rappaport (2002).

2.3.2 Time dispersion parameters: delay spread and coherence bandwidth

In order to compare different multipath wireless channels, some parameters that grossly quantify the multipath channel are used. They are the **mean excess delay**, the **root-mean-square (rms) delay spread**, the **excess delay spread**. All these parameters are obtained from the power delay profile.

Delay spread

The mean excess delay is the first moment of power delay profile, it is calculated as follows Rappaport (2002):

$$\overline{\tau} = \frac{\sum_k a_k^2 \tau_k}{\sum_k a_k^2} = \frac{\sum_k P(\tau_k)\tau_k}{\sum_k P(\tau_k)}. \tag{2.5}$$

The **root-mean-square delay spread (rms)** τ_{rms} is the square root of the second central moment of a power delay profile and it can be calculated as follows:

$$\tau_{rms} = \sqrt{\overline{\tau^2} - (\overline{\tau})^2}, \tag{2.6}$$

where

$$\overline{\tau^2} = \frac{\sum_k a_k^2 \tau_k^2}{\sum_k a_k^2} = \frac{\sum_k P(\tau_k)\tau_k^2}{\sum_k P(\tau_k)}. \tag{2.7}$$

In practice, values of $\overline{\tau}$ and $\overline{\tau^2}$ depend on the choice of the noise threshold used to calculate equations (2.6) and (2.7). This threshold is supposed to differentiate between a received multipath signal and thermal noise. Setting the low value of the noise threshold leads to processing the noise as a useful multipath signal, thus values of $\overline{\tau}$ and τ_{rms} will be artificially high. An example of a power delay profile, along with the rms delay spread and mean excess delay for a given noise threshold level (-21 dB), are presented in Figure 2.5.

Coherence bandwidth

The delay spread, mentioned above, is caused by multipath propagation of a transmitted signal. Another parameter, which may be used for channel characterization, is called **coherence bandwidth**. It is derived from the *rms* delay and characterizes the channel in the frequency

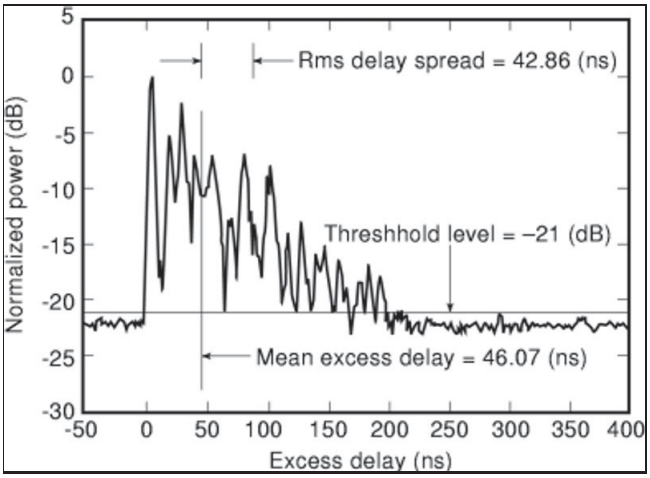

Figure 2.5 A power delay profile of multipath channel, rms delay spread, mean excess delay and threshold level.
Derived from Rappaport (2002, p. 200)

domain. So, the power delay profile and the magnitude frequency response of radio channel are related through the Fourier transform.

Coherence bandwidth B_{coh} is a statistical measure of the range of frequencies over which the channel can be considered "flat". The term "flat" means that all frequency components within the coherence bandwidth of the channel experience approximately equal gain and linear phase throughout the channel. It should be noted that the rms delay spread and coherence bandwidth are inversely proportional to one another, but there is no exact relation between coherence bandwidth and rms delay spread. For the coherence bandwidth, defined as the bandwidth over which the frequency correlation function is above 0.9, it is approximately equal to, Lee (1989):

$$B_{coh} \approx \frac{1}{50\tau_{rms}}. \tag{2.8}$$

And for the case when the frequency correlation function is above 0.5 the coherence bandwidth is approximately equal to, Rappaport (2002):

$$B_{coh} \approx \frac{1}{5\tau_{rms}}. \tag{2.9}$$

2.3.3 Time variation parameters: Doppler spread and coherence time

The delay spread and the coherence bandwidth are used to characterize the time-dispersive nature of the channel due to multipath propagation of a transmitted signal. For characterization of the relative motion between the receiver and transmitter or, in other words, the time-varying nature of the channel, **Doppler spread** and **coherence time** are used.

The relative mobility between the receiver-transmitter pair introduces a **Doppler frequency shift** f_D. Its maximum value can be calculated according to:

$$f_D = \frac{v}{c} f_c, \tag{2.10}$$

where v is the relative speed between the receiver and transmitter (m/s); $c = 3 \cdot 10^8\ m/s$ is the speed of light and f_c is the carrier frequency of the transmitted signal.

Due to Doppler frequency shift, the received signal has a broader spectrum that is called **Doppler spectrum** B_D. For example, if the single harmonic f_c was sent by the transmitter, the received signal spectrum will have components in the range $f_c - f_D$ to $f_c + f_D$.

The **coherence time** T_{coh} is the time-domain characteristic of the channel, the dual of the Doppler spread. It characterizes the time period during which the channel parameters change.

The Doppler spread and the coherence time are inversely proportional to one another:

$$T_{coh} \approx \frac{1}{f_D}. \tag{2.11}$$

For more precise calculation of the channel coherence time the following formula is used, Rappaport (2002):

$$T_{coh} = \sqrt{\frac{9}{16\pi f_D^2}} = \frac{0.423}{f_D}. \tag{2.12}$$

If the symbol duration of the signal is greater than the coherence time of the channel, then the channel will change during the transmission of the baseband signal, thus causing a linear distortion of the signal.

2.4 Types of multipath fading

From the characteristics enumerated above, it can be concluded that the time dispersion due to multipath delay spread and frequency dispersion due to Doppler spread provoke different types of fading. The four types of fading, which depend on the relation between the signal characteristics (bandwidth, symbol period) and the channel characteristics (rms delay spread and Doppler spread), are presented in Table 2.1.

2.4.1 Multipath signal fading due to time dispersion

Flat Fading. The term **"flat fading"** means that the radio channel has a constant gain and linear phase response over a bandwidth that is greater than the bandwidth of the transmitted signal. Hence, the received signal preserves the spectral characteristics of the transmitted signal. But due to multipath the received signal strength varies with time. In that type of fading channel, the symbol period T_{sym} is much larger than the multipath time delay spread τ_{rms} and

Table 2.1 Types of fading
Derived from Rappaport (2002, p.206)

Time dispersion (delay spread)	
Flat fading	**Frequency selective fading**
BW of signal < BW of channel Delay spread < symbol period	BW of signal > BW of channel Delay spread > symbol period
Frequency dispersion (Doppler spread)	
Fast fading	**Slow fading**
High Doppler spread Coherence time < Symbol period Channel variations faster than baseband signal variations	Low Doppler spread Coherence time > Symbol period Channel variations slower than baseband signal variations

the bandwidth of the transmitted signal B_s is much less than the coherence bandwidth of the channel B_{coh}:

$$T_{sym} \gg \tau_{rms},\ B_s \ll B_{coh}. \tag{2.13}$$

Flat fading channels are often referred to as **narrowband channels** because the bandwidth of the transmitted signal is narrower than the bandwidth of the flat fading channel impulse response.

Frequency-Selective Fading. When the bandwidth of the transmitted signal B_s is greater than the coherence bandwidth of the channel B_{coh}, and, correspondingly, the symbol duration of the transmitted signal T_{sym} is smaller than the multipath time delay spread of the channel τ_{rms} :

$$T_{sym} < \tau_{rms},\ B_s > B_{coh}. \tag{2.14}$$

the received signal will undergo frequency-selective fading.

In the time domain, the received signal includes multiple versions of the transmitted signal that are attenuated and delayed in time. It causes the distortion of the received signal. Also, the time dispersion results in **intersymbol interference (ISI)** in the received signal. In the frequency domain, different frequency components of the signal undergo different attenuations through the channel.

Frequency-selective fading channels are often called **wideband channels** because the bandwidth of the transmitted signal is wider than the bandwidth of the channel impulse response.

2.4.2 Multipath signal fading due to frequency dispersion

Fast Fading. When the channel parameters change rapidly within one symbol duration of the signal, this channel is called a **fast-fading** channel. In the time domain, it means that the coherence time of the channel T_{coh} is smaller than the symbol duration T_{sym} of the transmitted signal and, in the frequency domain, that the Doppler spread f_D is greater than the signal bandwidth B_s:

$$T_{sym} > T_{coh},\ B_s < f_D. \tag{2.15}$$

Doppler spreading causes frequency dispersion (or time selective fading), which leads to signal distortion. In practice, fast fading only occurs for communication systems with very low data rates.

Slow Fading. If the rate of channel impulse response (cir) changes is less than the data rate of the transmitted signal, this channel can be referred to as **slow-fading**. It can be assumed that the channel is static over one or several symbol durations. In the frequency domain, this implies that the Doppler spread of the channel f_D is much less than the signal bandwidth B_s:

$$T_{sym} < T_{coh},\ B_s \gg f_D, \tag{2.16}$$

where T_{sym} is the symbol duration of the transmitted signal, and T_{coh} is the coherence time of the channel.

Note that the type of channel fading, slow or fast, depends only on the relative speed between transmitter and receiver.

2.4.3 Multipath channel classification

If both time and frequency dispersion present in a multipath channel, it is useful to introduce a general channel classification as proposed in Table 2.2.

Table 2.2 Classification of channels with both time and frequency dispersion

Flat Fast Fading	**Flat Slow Fading**
Symbol period $>>$ delay spread ($T_{sym} >> \tau_{rms}$) and	
symbol period > coherence time ($T_{sym} > T_{coh}$)	symbol period < coherence time ($T_{sym} > T_{coh}$)
BW of signal $<<$ BW of channel ($B_s << B_{coh}$) and	
BW of signal < Doppler spread of the channel ($B_s < f_D$)	BW of signal > Doppler spread of the channel ($B_s > f_D$)
Frequency-selective Fast Fading	**Frequency-selective Slow fading**
Symbol period < delay spread ($T_{sym} < \tau_{rms}$) and	
symbol period $>>$ coherence time ($T_{sym} >> T_{coh}$)	symbol period $<<$ coherence time ($T_{sym} << T_{coh}$)
BW of signal > BW of channel ($B_s > B_{coh}$) and	
BW of signal $<<$ Doppler spread of the channel ($B_s << f_D$)	BW of signal $>>$ Doppler spread of the channel ($B_s >> f_D$)

2.5 Statistical modeling of multipath channels

2.5.1 Ricean Fading

For the channels with a dominant stationary (non-fading) signal component, or a LOS communication scenario, the multipath fading envelope can be assumed to obey the Ricean distribution. The dominant component appears as a dc component to the random multipath at the output of an envelope detector. Decreasing the dominant component intensity leads to the transformation of a Ricean distribution into a Rayleigh distribution. The Ricean distribution is represented by following expression, Rappaport (2002):

$$f_R(r) = \begin{cases} \frac{r}{\sigma^2} e^{-\frac{r^2+A^2}{2\sigma^2}} I_0\left(\frac{Ar}{\sigma^2}\right),\ A \geq 0,\ r \geq 0 \\ 0,\ r < 0 \end{cases}, \tag{2.17}$$

where A is the peak amplitude of the dominant LOS signal, $I_0(x) = \frac{1}{\pi}\int_0^{\pi} e^{x\cos\theta} d\theta$ is the modified Bessel function of order zero and in terms of Taylor's series it can be represented as follows:

$$I_0(x) = 1 + \frac{x^2}{2^2} + \frac{x^4}{2^2 \cdot 4^2} + \frac{x^6}{2^2 \cdot 4^2 \cdot 6^2} + \cdots. \tag{2.18}$$

The Ricean distribution is often characterized by a parameter K, which defines the ratio between the LOS signal amplitude A and the variance of the multipath reflection signals σ^2. It is known as the **Ricean factor**, and it is calculated according to:

$$K = \frac{A^2}{2\sigma^2},\ or\ K = 10 \cdot log_{10}\left(\frac{A^2}{2\sigma^2}\right),\ dB. \tag{2.19}$$

The Ricean distribution transforms into a Rayleigh distribution as the LOS path decreases in amplitude ($A \to 0, K \to \infty$) that is shown in Figure 2.6 for $\sigma = 1$.

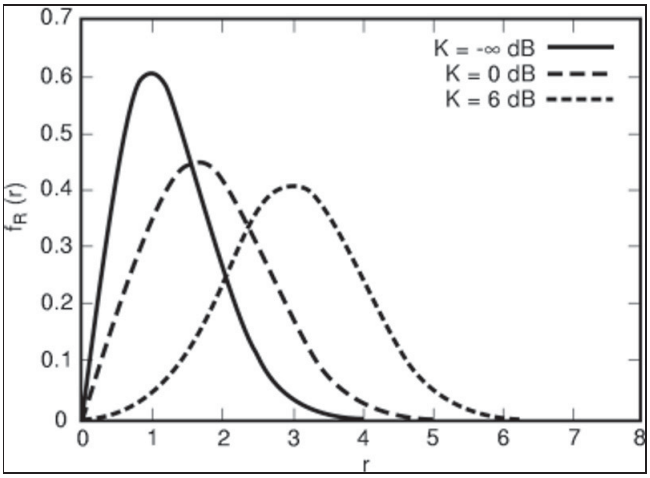

Figure 2.6 Probability density functions of
Ricean distributions: K = - ∞ dB (Rayleigh),
0 dB and 6 dB.
Derived from Rappaport (2002, p. 214)

2.5.2 Rayleigh Fading

In the case of absence of the LOS propagation path, the radio channel can be described by the Rayleigh distribution (see Figure 2.7) to represent the statistical time-varying nature of the received envelope of a flat fading signal or of an individual multipath component. Assume that the number of multipath signal components is sufficiently large. Using the central limit theorem, the received signal can have two quadrature Gaussian noise components. The envelope of the sum of two quadrature Gaussian noise signals follows a Rayleigh distribution represented by the expression:

$$f_R(r) = \begin{cases} \frac{r}{\sigma^2} e^{-\frac{r^2}{2\sigma^2}},\ 0 \le r \le \infty \\ 0,\ r < 0 \end{cases}, \tag{2.20}$$

where σ^2 is the time-average power of the received signal before envelope detection. The mean value m_R of the Rayleigh distribution is given as follows

$$m_R = E\{R\} = \sigma\sqrt{\frac{\pi}{2}} \approx 1.2533\ \sigma. \tag{2.21}$$

The parameter σ_R^2 represents the ac power in the signal envelope and it is determined by the following expression:

$$\sigma_R^2 = E\{R^2\} - E^2\{R\} = \sigma^2\left(2 - \frac{\pi}{2}\right) \approx 0.4292\ \sigma^2. \tag{2.22}$$

The rms value of the envelope is $\sqrt{E\{R^2\}} = \sqrt{2}\ \sigma$.

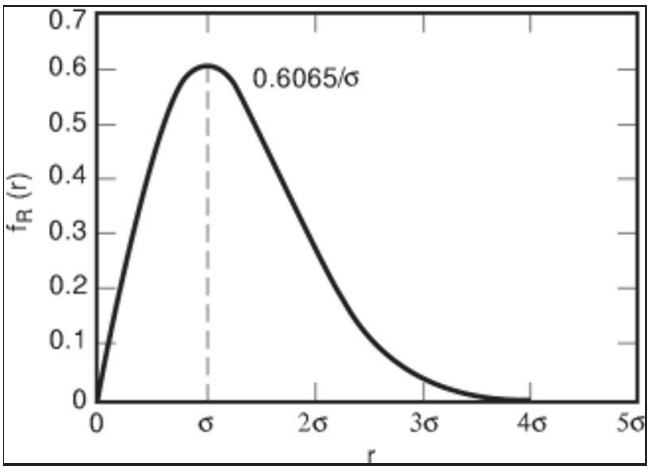

Figure 2.7 Rayleigh probability density function.
Derived from Rappaport (2002, p. 212)

2.6 Anti-multipath fading techniques

Due to multipath fading, the transmitted signal becomes the subject of distortion and, often, severe distortion. There are some techniques that can be used independently or in tandem in order to mitigate a signal distortion. They are equalization, diversity, spread spectrum, and channel coding.

Equalization helps to compensate for the inter-symbol interference (ISI) caused by the frequency-selective fading in communication systems with the signal bandwidth greater than the coher-

ence bandwidth of the channel. Often the channel parameters are time varying and unknown to the receiver, so equalizers should be adaptive, Qureshi (1985).

Diversity is represented by the following types: spatial, antenna polarization diversity, frequency diversity, and time diversity. Those techniques serve to improve the quality of a mobile communication link without increasing the transmitted power or bandwidth. The spatial diversity uses multiple antennas strategically spaced and connected to a common receiving system, Jakes (1974). While one antenna sees a signal null, one of the other antennas may see a signal peak. The receiver is able to select the antenna with the best signal at any time or to combine the signals from the different antennas in a weighted manner to maximize the performance. The time diversity is used in a RAKE receiver, which combines the information obtained from several resolvable multipath components, Price and Green (1958).

Some spectrum spreading and channel coding techniques have already been mentioned in the previous chapter. Here we will make an accent on their anti-multipath fading properties.

Spread spectrum techniques, for example, Code-Division Multiple Access (CDMA) systems, have certain resistance to multipath fading. They use a wideband signal and so, at any time only a small portion of its spectrum undergoes fading. Also, the delayed versions of the transmitted signal will be canceled out in the time domain at the receiver because they are poorly correlated with the original signal, TIA/EIA (1995).

Channel coding techniques are used by the receiver to detect or correct some, or all, if possible, errors introduced by the multipath channel by adding redundant data bits in the transmitted message, Clark Jr. and Cain (1981).

2.7 Conclusion

In this chapter we presented parameters that characterize wireless channels with multipath reflections. Statistical models for those channels have been proposed. Also, the classification of multipath fading has been made, and some techniques of multipath fading mitigation were proposed.

CHAPTER 3

DATA MULTIPLEXING

3.1 Introduction

In most communication systems, wired or wireless, multiple data streams have to be transmitted over a single communication channel. This requires data stream multiplexing. In this chapter different types of multiplexing are presented, from the simple Time Division Multiplexing (TDM) to more complex Orthogonal Frequency Division Multiplexing (OFDM). Development in microelectronics has made possible hardware implementation of complex digital signal processing algorithms. Patented in the 1960s', Orthogonal Frequency Division Multiplexing (OFDM) has been proposed for broadband wireless communications due to its ability for multipath fading mitigation. The principles of functioning of OFDM are followed by a structure of an OFDM based communication system. Also, OFDM advantages and drawbacks are highlighted.

Many researchers use wavelets for data multiplexing. The literature review at the end of this chapter serves to present their findings.

3.2 Multiplexing

The dictionary MSN Encarta® defines **Multiplexing** as "a technique used in communications and input/output operations for transmitting a number of separate signals simultaneously over a single channel or line. To maintain the integrity of each signal on the channel, multiplexing can separate the signals by time, space, or frequency. The device used to combine the signals is a **multiplexer**"(end of citation). The device implementing a reverse operation is often called a **demultiplexer**.

Time Division Multiplexing and **Frequency Division Multiplexing** techniques are often used in communication systems.

3.2.1 Time Division Multiplexing

Time Division Multiplexing (TDM) copies symbols from parallel code streams into different time slots of a serial code stream. An example, shown on Figure 3.1, demonstrates how the K parallel code streams of the symbols duration T are multiplexed into one serial code stream.

One can note that all symbols in the parallel code streams have the same time duration T. Many

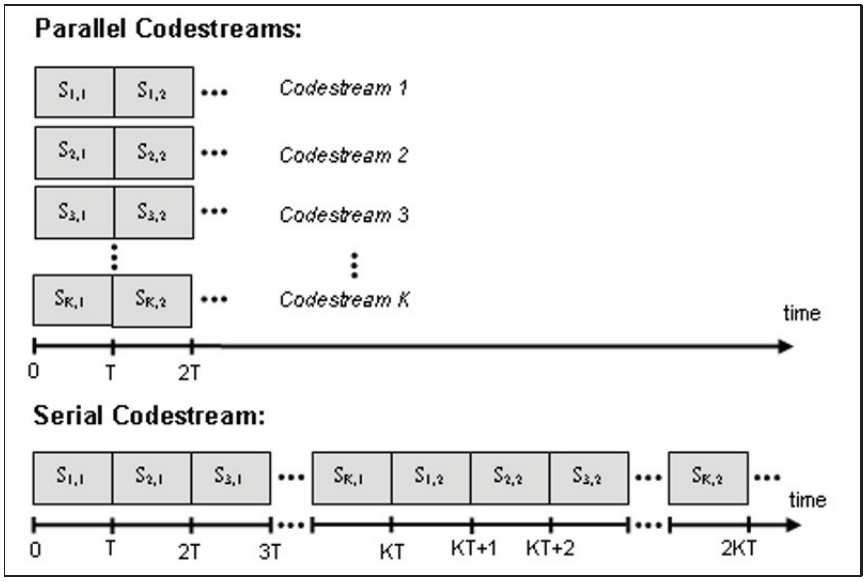

Figure 3.1 Time Division Multiplexing (TDM).

real communication systems deal with unequal symbol rate code streams. In order to use TDM, the system should implement certain symbol rate equalizing techniques before TDM, Proakis and Salehi (2007).

3.2.2 Frequency Division Multiplexing

Frequency Division Multiplexing (FDM) treats symbols from parallel code streams as they were in the frequency domain and assigned to different frequency slots. Then FDM transforms the data into the time domain using certain frequency-time transforms. And the final step is a parallel-to-serial transform of the time-domain data. Figure 3.2 demonstrates the FDM structure. Presented earlier in this section, TDM can be used for parallel-to-serial data transformation.

The fact that FDM operates with the data in the frequency domain makes it an attractive

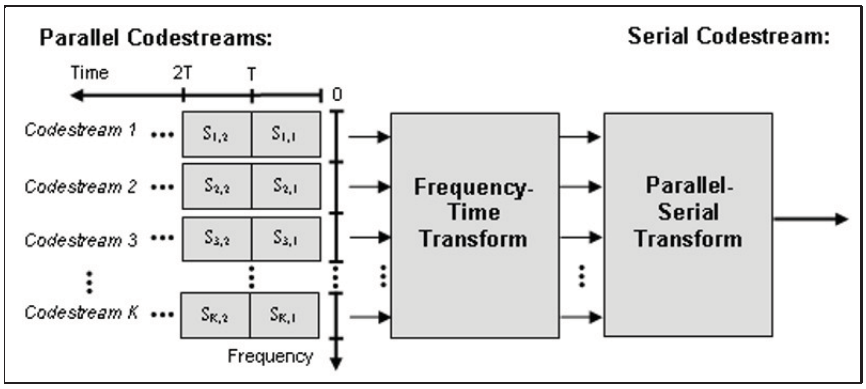

Figure 3.2 Frequency Division Multiplexing (FDM).

technique for pilot-assisted channel estimation. Nowadays, **Orthogonal Frequency Division Multiplexing (OFDM)** and **Wavelet Packet Multiplexing (WPM)** are the most promising techniques representing FDM.

3.3 Orthogonal Frequency Division Multiplexing

The OFDM technique was introduced and patented in the mid 1960's by Chang (1966). In the last decade, thanks to the ability to mitigate the frequency selective fading, OFDM found multiple applications in high data rate wireless communication systems such as:

- Asymmetric Digital Subscriber Line (ADSL);
- Digital Audio Broadcasting (DAB), Digital Video Broadcasting (DVB);
- Wireless Local Area Networks (WLAN): HIPERLAN/2 (Europe), IEEE 802.11a/g (USA), HiSWAN (Japan) - Wi-Fi;
- Wireless Local Loop (WLL): HIPERMAN (Europe), IEEE 802.16 (USA) - WiMAX.

3.3.1 Subcarrier Waveform

It is obvious, from the name of the technique, that OFDM uses a set of orthogonal frequencies called **subcarriers** in order to put each of the parallel code streams in separate frequency slots of allocated bandwidth. A set of N_c harmonic functions is used as subcarriers f_k, Engels (2002):

$$\phi_k(t) = \begin{cases} \frac{1}{\sqrt{T_s}} e^{j2\pi f_k t},\ t = [0, T_s] \\ 0,\ otherwise \end{cases} \quad with\ f_k = f_0 + k \cdot \Delta f;\ k = 0, 1, \ldots, N_c - 1, \tag{3.1}$$

where

f_k is the subcarrier frequency;

f_0 is the lowest frequency used (k=0);

$\Delta f = \frac{BW}{N_c}$ is the spacing between the adjacent subcarriers;

T_s is the symbol duration.

The orthogonality property of subcarriers can be satisfied by having each subcarrier frequency be an integer multiple of the symbol rate of the modulating symbols and each subcarrier separated from its nearest neighbor(s) by the symbol rate, Morais (2004). This is illustrated in Figure 3.3 for the case of four subcarriers.

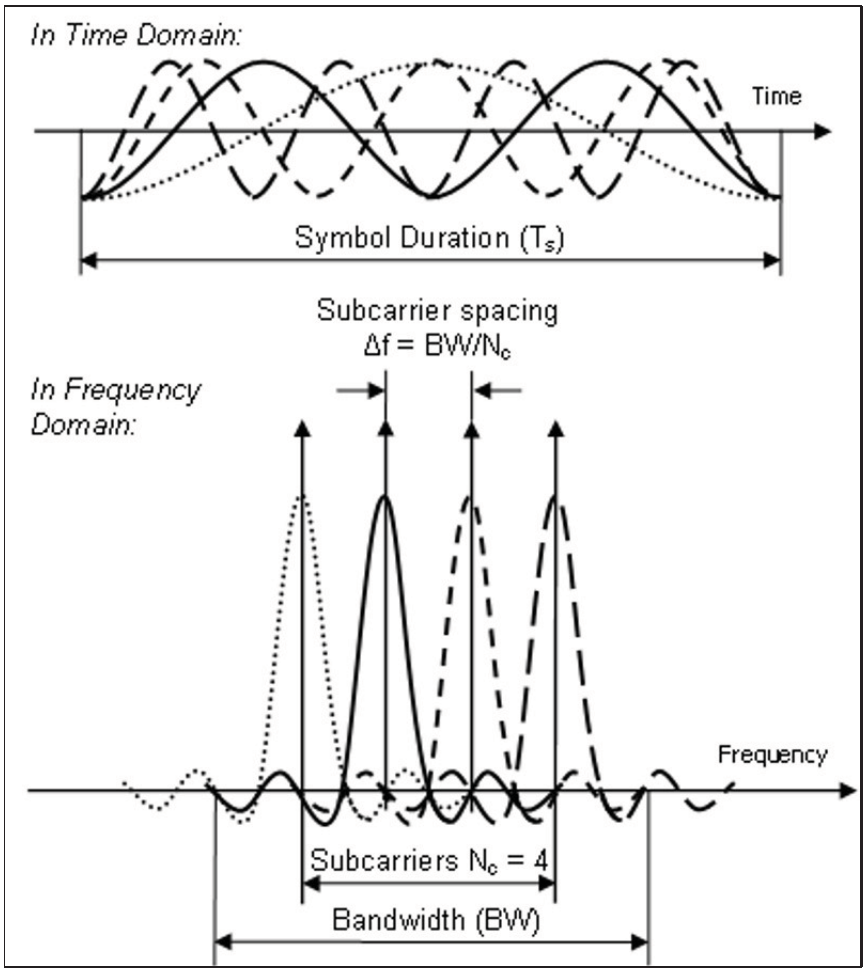

Figure 3.3 Orthogonal Frequencies or Subcarriers ($N_c = 4$) .

Since the waveform $\phi_k(t)$ from Equation 3.1 is restricted to the time window $[0, T_s]$, its spectrum has the following form:

$$\Phi(f_k) = T_s \cdot exp\,(-j2\pi f_k T_s)\,\frac{sin\,(\pi f_k T_s)}{\pi f_k T_s}. \tag{3.2}$$

Figure 3.3 also shows the spectrum of the OFDM signal with four subcarriers, i.e., for $k = 4$ in Equation 3.2. It is obvious that in the frequency domain subcarriers are also orthogonal at frequencies $f = f_k$ $(k = 0, 1, \ldots, N_c - 1)$. So, a demodulation scheme might consist of a bank of N_c matched filters as shown in Figure 3.4.

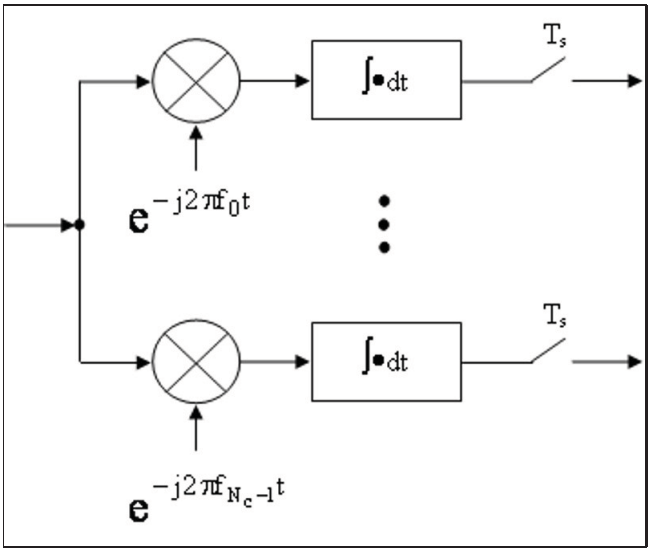

Figure 3.4 OFDM demodulator.
Derived from Engels (2002, p.37)

3.3.2 Subcarrier Number

In order to mitigate frequency selective fading, a sufficient number of subcarriers N_c should be chosen. When the bandwidth of each subchannel becomes less than the coherence bandwidth of the channel B_{coh}, subchannel fading can be considered as flat. Hence, a simple one-tap equalizer can be employed for subchannel equalization. On the other side, an excessive number of subcarriers can lead to a significant increase of the modulation symbol duration T_s. And if the coherence time of the channel τ_{rms} becomes small compared to the symbol period T_s, the channel frequency response changes rapidly during the transmission of one symbol and a reliable detection of the transmitted information becomes impossible. Also, the problem of transmitter-receiver synchronization arises for a large number of subcarriers. Both conditions mentioned above give the rule of thumb for the choice of the subcarrier number N_c:

$$\frac{BW}{B_{coh}} \ll N_c \ll RT_{coh}, \tag{3.3}$$

where

BW is the communication system bandwidth;

R is the transmission symbol rate;

B_{coh}, T_{coh} are the coherence bandwidth and coherence time of the channel.

The left part of Equation 3.3 provides the condition of communication system robustness to channel time dispersion. The right part of Equation 3.3 determines the condition of system robustness to channel frequency dispersion.

In practice, the number of subcarriers can be large. Therefore, the technique employing a bank of N_c modulators and demodulators, as is shown on Figure 3.4, is often unacceptable. The role of such a bank is often played by a pair of Inverse Fast Fourier Transform (IFFT) and Fast

Fourier Transform (FFT) in the majority of the OFDM based communication systems. Since FFT is involved, it usually requires subcarrier number N_c to be a power of two.

3.3.3 OFDM Symbol

In OFDM systems employing FFTs, a notation N-FFT is often defined as the number of subcarriers instead of N_c. In this case, the number of subcarriers is equal to the size of FFT. A set of N-FFT subcarriers is called an OFDM symbol. As it is shown in Figure 3.5, the OFDM symbol is composed of the following subcarriers:

- Data subcarriers (N_{used}) are used for data transmission;
- Pilot subcarriers (P) are used for various estimation purposes;
- Null subcarriers (G_L, G_H, DC) are used for low, high frequency guard bands, and DC (Direct Current) carrier. They do not transmit any information. The purpose of the guard bands is to enable the signal to naturally decay and create the FFT (brick wall) shaping.

3.3.4 Cyclic prefix

A multipath channel destroys orthogonality between subcarriers causing an **intercarrier interference** (ICI). In order to mitigate this problem it was proposed to prolong the OFDM symbol artificially by periodically repeating the tail of the symbol and preceding the symbol with it. This guard time interval T_g is often called a **cyclic prefix** (CP) in the literature. The structure of an OFDM symbol with CP is shown in Figure 3.6.

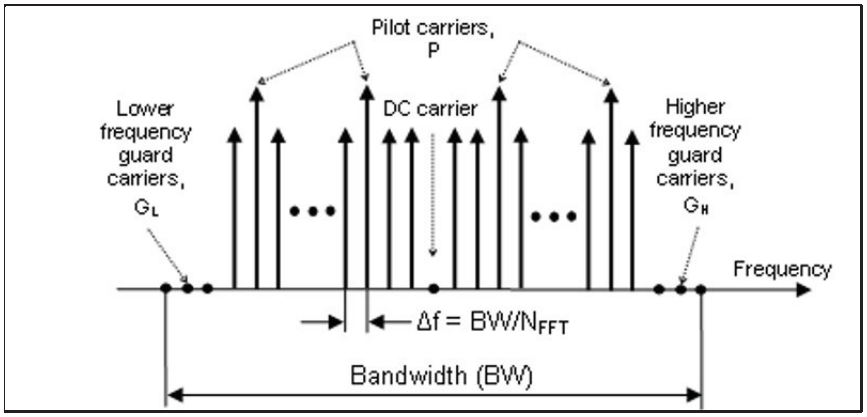

Figure 3.5 OFDM symbol structure in the frequency domain.
Derived from the standard IEEE 802.16 (2004)

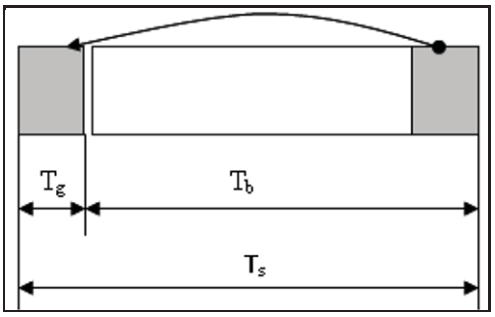

Figure 3.6 OFDM symbol time structure.
Derived from the standard IEEE 802.16 (2004)

where

T_b is the "useful"symbol time ($T_b = 1/\Delta f$);

T_g is the guard time interval or CP time ($Tg = G \cdot T_b$) with a parameter G as the ratio of CP time to "useful "time;

T_s is the OFDM symbol time ($T_s = T_b + T_g$).

An application of CP has two goals. The first one is to add some guard time between successive symbols in order to avoid intersymbol interference (ISI). The second one is to convert the linear convolution with the channel impulse response into a cyclic convolution. It is known that a

cyclic convolution in the time domain translates into a scalar multiplication in the frequency domain, so the subcarriers remain orthogonal and there is no intercarrier interference. Also, it allows applying an Inverse Fast Fourier transform (IFFT) in an OFDM modulator and a Fast Fourier transform (FFT) in an OFDM demodulator.

The choice of the right CP length is a very important task. Adding a guard interval we lose some parts of the signal that cannot be used for transmitting information. It means that if the transmitter energy remains the same, then the receiver energy decreases with the length of CP time. Because the cyclic prefix is discarded in the receiver, there is a loss in SNR:

$$SNR_{loss} = -10 \cdot log_{10}\left(1 - \frac{T_g}{T_b + T_g}\right),\ dB. \tag{3.4}$$

Hence, it is desirable to reduce the cyclic prefix time in order to preserve a high SNR. But on the other side, the cyclic prefix must be long enough to account for the anticipated multipath delay spread experienced by the system. Therefore, the size of the cyclic prefix is always a trade-off between the amount of the channel delay spread and SNR of the system.

Let us note that the SNR loss could be reduced by increasing the FFT size, which would, however, affect the sensitivity of the system to phase noise of the oscillators. Using a cyclic extension, the samples required for performing the FFT at the receiver can be taken anywhere over the length of the extended symbol. This provides multipath immunity as well as a tolerance for symbol time synchronization errors.

3.4 OFDM System Structure

Figure 3.7 shows the classical structure of an OFDM multiplexer and demultiplexer. It operates with a high data rate source of R symbols per second. If the multiplexer employs N_c orthogonal frequencies (subcarriers), then the data stream should be converted into N_c parallel sub-streams

before frequency-time transform. The serial-to-parallel transform reduces the symbol rate of each sub-stream to R/N_c symbols per second each. Hence the bandwidth of each subchannel is effectively decreased by a factor of N_c w.r.t. original data stream.

3.5 OFDM Performance

When the OFDM system operates in an ideal linear time-invariant (LTI) frequency non dispersive AWGN channel, this can be translated into a parallel set of AWGN channels with equal SNR. Hence, the OFDM system performance will be the same as a single carrier system performance, except for the SNR loss due to the cyclic prefix.

Previously, it was mentioned that quadrature amplitude modulation (QAM) is typically employed for subcarrier modulation. So, the symbol error rate (SER) of an OFDM system depends on QAM SER. In general, the SER for M-ary QAM on AWGN channel is given in Nguyen et al. (2004) as follows:

$$\begin{aligned} P_{s\,M-QAM}(\gamma) &= 2\left(1-\frac{1}{\sqrt{M}}\right)Q\left(\sqrt{\frac{3}{M-1}\gamma}\right) - \\ &- \left[\left(1-\frac{1}{\sqrt{M}}\right)Q\left(\sqrt{\frac{3}{M-1}\gamma}\right)\right]^2, \end{aligned} \tag{3.5}$$

where $\gamma = \frac{E_b}{N_0}$ and $Q(x) = \frac{2}{\sqrt{\pi}}\int_x^{+\infty} e^{-u^2}du$ is a complementary error function.

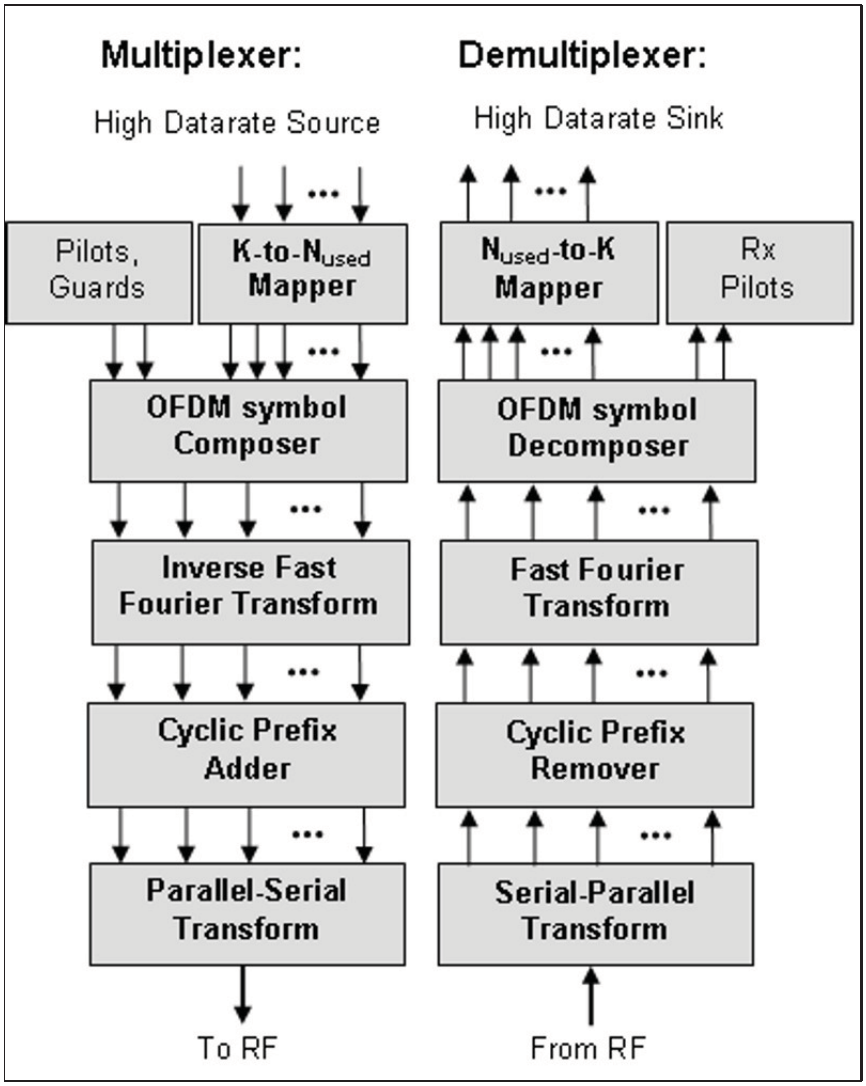

Figure 3.7 Orthogonal Frequency Multiplexing and Demultiplexing.

For the case of modulation QPSK ($M = 4$), Equation 3.5 can be simplified and the probability of symbol error is given by

$$P_{s\ QPSK}(\gamma) = Q(\sqrt{\gamma}) - \frac{1}{4}(Q(\sqrt{\gamma}))^2. \tag{3.6}$$

In order to get the probability of symbol error for the time-varying multipath channel with Rayleigh fading, the symbol error rate must be averaged over the probability density function of SNR γ, as given in Proakis and Salehi (2007):

$$P_{\overline{\gamma}}(\gamma) = \frac{1}{\overline{\gamma}} exp\left(-\frac{\gamma}{\overline{\gamma}}\right). \tag{3.7}$$

The probability of symbol error for the multipath channel with Rayleigh fading can be expressed as in Engels (2002):

$$P_s(\overline{\gamma}) = \int_{\gamma=0}^{\infty} P_s(\gamma) P_{\overline{\gamma}}(\gamma) d\gamma, \tag{3.8}$$

where $\overline{\gamma}$ is the expected SNR given as the following:

$$\overline{\gamma} = \frac{E_b}{\frac{\pi^2 f_D^2}{3\Delta f^2} E_b + N_0}. \tag{3.9}$$

Hence, substituting Equations 3.6 and 3.7 in Equation 3.8 we obtain the formula for the theoretical SER of plain, or uncoded, OFDM which uses QPSK as the subcarrier modulation technique:

$$P_s(\overline{\gamma}) = \frac{3}{4} - \sqrt{\frac{\overline{\gamma}}{1+\overline{\gamma}}}\left(1 - \frac{1}{\pi} tan^{-1}\sqrt{\frac{\overline{\gamma}}{1+\overline{\gamma}}}\right). \tag{3.10}$$

The performance of an OFDM system can degrade seriously in multipath channel conditions because of significant differences in SNR between different carriers. In order to mitigate this problem various Forward Error-Coding (FEC) methods can be applied, like Reed-Solomon, convolutional and turbo codes.

The OFDM system, which uses error coding, is usually called the **coded** OFDM system (COFDM). The following serves to illustrate COFDM performance. Assuming that COFDM employs an (n, k) code, the parameter n stands for the number of total symbols per block and a parameter k is the number of source symbols. The code rate is n/k. If we take the block

size equal to the FFT size, then $n = N_c$ and the probability of symbol error will be equal to, Rappaport (2002):

$$P_{s\ coded\ OFDM}(\overline{\gamma}) = \frac{1}{N_c} \sum_{i=t+1}^{N_c} i \begin{pmatrix} N_c \\ i \end{pmatrix} (1 - P_s(\overline{\gamma}))^{N_c - i} (P_s(\overline{\gamma}))^i, \tag{3.11}$$

where t is the number of errors that can be corrected in a code.

The structure of coded OFDM is shown in Figure 3.8.

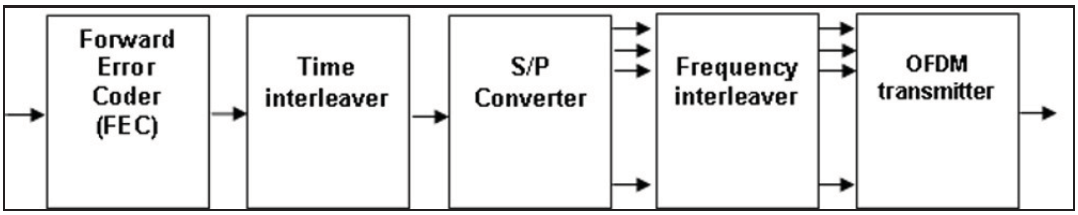

Figure 3.8 Coded OFDM structure.
Derived from Engels (2002, p.49)

A **Frequency Interleaver** puts consecutive bits on uncorrelated subcarriers, such that they experience independent channel attenuation. A **Time Interleaver** separates consecutive bits over different OFDM symbols. Hence, for a fast fading channel these bits also experience different channel attenuation.

3.6 OFDM Advantages and Drawbacks

An OFDM technique has the following **advantages**:

- Resilience to multipath and low intersymbol interference (ISI) due to cyclic prefix adding and time-frequency interleaving;

- Reduced susceptibility to most forms of impulse noise;
- High spectral efficiency;
- The almost rectangular shape of the OFDM spectrum allows for close packing of adjacent OFDM systems;

As well as some **drawbacks**:

- Inter Carrier Interference (ICI) caused by lost of orthogonality between adjacent subcarriers;
- High sensitivity to time and frequency synchronizations. This means that a transmitter and receiver must assume exactly the same modulation frequency and the same time-scale for transmission;
- High Peak-to-Average Power Ratio (PAPR). Some subcarriers have higher magnitude that saturates an RF amplifier causing distortion of the transmitted signal.
- Analog components, part of the transmitter and receiver, must be of very high quality in order to provide a linear amplification at the OFDM signal bandwidth.

3.7 Literature Review on Wavelet Multiplexing/Modulation

The following literature review highlights the research directions in the domain of wavelet and wavelet packet modulation.

The first paper on wavelet modulation of Daneshagaran and Mondin (1994) appeared right after fundamental publications of Ingrid Daubechies: Daubechies (1989), Daubechies (1990); Stefan Mallat: Mallat (1989a), Mallat (1989b), and D. Donoho: Donoho (1995), Donoho and Johnstone (1994) in the late 80's-early 90's of the last century. The authors demonstrated that

use of scaling functions and wavelets as envelope functions for modulation is natural in view of the first Nyquist criterion for ISI removal. Using wavelet packets, the number of dimensions available to the modulator per unit time is increased.

The paper of Newlin (1998) provides an overview of these developments by presenting wavelet implementations of various segments of a general communication system and of proposed wavelet based multiple access communication systems. Promising developments have been made and the potential for future advances seems quite good.

Authors of the paper, Adhikary and Reddy (1998), discuss two approaches for designing complex wavelet packets that can be used as orthogonal carriers for modulations like QAM and PM, and then compare the performance of the wavelet packet based modulation scheme with that of discrete multitone modulation using DFT bases. The results show that the wavelet packet based scheme yields a lower average bit error probability compared to the DFT-based scheme. The improved performance of the wavelet packet-based scheme is obtained because of the spectrally contained nature of the wavelet packet bases, which are under the control of the designer.

Dr Alan R. Lindsey works for the Air Force Research Laboratory (Rome, NY, USA) and applies Wavelet Packet Modulation for tactical communications: Lindsey (1996), Lindsey (1997), Lindsey and Dill (1995), and Kjeldsen et al. (2003). While working on his PhD dissertation at Ohio University, Dr Lindsey et al. introduced multidimensional signaling techniques, Lindsey and Dill (1995), a multirate wavelet based modulation format, which can utilize existing channels designed for conventional QAM. Customizable wavelet packet basis functions were employed as pulse shapes upon which independent QAM data at lower rates were transported. The advantages included dimensionality in both time and frequency for flexible channel exploitation and an efficient all digital filter bank implementation.

In a paper Lindsey (1996), Dr Lindsey highlighted that the most important application of wavelet packet modulation is in direct sequence spread spectrum communications, where the chip symbols determined by the pseudo-noise sequence are constructed with both time and frequency dimensionality. In traditional DSPN, the wide bandwidth of the symbols causes problems in the presence of frequency-domain noise where all chip symbols are corrupted, but the time-frequency dimensionality of spread spectrum wavelet packet modulation (SSWPM) has immediate advantages in mitigating the effects of narrowband jammers and time impulses, where only a fraction of the chip symbols is corrupted.

In a paper Lindsey (1997), Dr Lindsey proposed Wavelet Packet Modulation (WPM) employing the basis functions from an arbitrary pruning of a dyadic tree-structured filter bank as orthogonal pulse shapes for conventional quadrature amplitude modulation (QAM) symbols. This generalized framework enables an entire library of basis sets with increased flexibility in time-frequency (T-F) partitioning. The bandwidth efficiency and power spectral density figures of merit for the general signal are derived and shown to be that of standard QAM.

The paper of Kjeldsen et al. (2003) describes an experimental implementation of an interference avoidance waveform, suitable for mobile or fixed wireless channels, and comprised of orthogonal signaling using wavelet packets in cohesive combination with a multidimensional channel error coding technique. The patent-pending adaptive waveform, known as circular simplex turbo block-coded wavelet packet modulation (CSTBC-WPM), possesses a time-frequency localization and agility capability for avoiding joint narrowband/impulsive interference patterns. Excision of residual interference at the receiver is facilitated by isolation to a sparse number of time-frequency cells and removal using energy thresholding. Moreover, the time dilation of symbols in the WPM subbands is useful in mitigating the adverse effects of multipath-induced, frequency-selective fading. For an even more potent countermeasure to non-Gaussian interference sources and channel propagation anomalies, the patent pending

CSTBC forward error correction component is distinctly mapped onto the orthogonally multiplexed WPM symbols and interleaved to exploit the subband frequency diversity. The shorter block sizes of CSTBC provide a bit error rate performance competitive with turbo product coding's large code blocks, approaching the Shannon limit but with considerably lower latency (up to 20-fold improvement).

A lot of research in the domain of wavelet packet modulation has been done by M. You: You and Ilow (2004a), You and Ilow (2004b), and You and Ilow (2004c). The paper of You and Ilow (2004c) introduces a multiwavelet packet modulation (MWPM), which is a multiband multidimensional modulation scheme with a flexible dyadic time-frequency tiling. The proposed MWPM can be considered as a generalization of orthogonal frequency division multiplexing (OFDM) or wavelet packet multiplexing (WPM). Compared to OFDM, the bandwidth efficiency of MWPM is increased r times for the multiwavelet packets with multiplicity of r. In addition, the effects of frequency-selective wireless channels and high peak-to-average power ratio (PAPR) in OFDM can be mitigated in the new scheme by properly designing the MWPM dyadic structure. To demonstrate MWPM effectiveness in wireless communication systems, the paper investigates the performance of M-ary QAM signaling combined with MWPM in different sub-bands for the additive white Gaussian noise (AWGN) channel, the slow flat Rayleigh fading channel and the Nakagami-m fading channel. With its advantages, the MWPM is a potential candidate for adaptive implementations in time varying and time dispersive fading channels.

In the next paper, You and Ilow (2004b) use a multiwavelet packet modulation (MWPM) scheme because of its bandwidth efficiency and its ability to combat effects of frequency selective channels. The orthogonality in MWP is exploited to guarantee demodulation of the overlapped MWP coded signals in time and frequency domains. A practical implementation of the MWPM transceiver is proposed that employs matrix filter banks. For MWP with multiplicity

r, the bandwidth efficiency is increased r times compared to scalar wavelet packet modulation or the conventional FFT-based OFDM system. Similarly, as these prototype schemes, the MWPM is implementable either as a binary or a multilevel scheme. As a multi-carrier modulation, MWPM can mitigate the time dispersiveness in the channel effectively because the symbol duration can be extended as required by the flexible structure of MWPM. The performance for these MWPM in AWGN and flat Rayleigh fading channels is analyzed and simulated using binary phase shift keying (BPSK) in each subcarrier. The simulation results demonstrate the effectiveness of the proposed MWPM scheme.

In the third paper, You and Ilow (2004a) use the time-frequency (T-F) analysis to model, in wireless channels, the additive interference and noise, which is classified into global and local types. Global noise, such as the additive white Gaussian noise (AWGN), has power distributed at all signaling frequencies for all times, whereas local noise, such as the impulsive noise (IN) and narrow band interferences (NBI), has a localized compact spread in the T-F plane. Within this framework, a general T-F tiling-based block transmission scheme is proposed that implements the modulation to match the channel distortion by avoiding transmission in the corresponding T-F signaling units. Specifically, based on the multiwavelet packet (MWP) theory, a novel multiwavelet packet modulation (MWPM) with a flexible dyadic structure and its adaptive extension are developed. The performance for the adaptive MWPM with GHM MWP and BPSK in each subcarrier is evaluated to show the robustness of the proposed scheme in channels corrupted by the T-F localized interference/noise.

Yu and Bi (2004) propose a novel multicarrier code division multiple access (MC-CDMA) system based on complex wavelet packet and turbo coding. They investigate the system bit error rate (BER) performance in Rayleigh fading channel. The system can overcome the decrease of spectrum efficiency and energy of conventional MC-CDMA due to inserting cyclic prefix (CP); and make full use of the turbo codes' good capacity against a fading channel to improve

the BER performance further. Theoretical analysis and simulation results all show that the proposed system outperforms a conventional MC-CDMA system, and its performance is superior to that of the conventional MC-CDMA with CP. Meanwhile, the application of turbo coding strengthens the system ability to cope with multipath fading and multi-access interference (MAI) significantly.

An orthogonal wavelet division multiplexing (OWDM) has been mentioned firstly in the paper of Yang et al. (1997). The principle of a Wavelet Packet Transform (WPT) and the transceiver structure using WPT were presented. The performance of the system under impulse noise and single tone interference has been analyzed.

The discussion of Multiple Access Orthogonal Wavelet Division Multiplexing (MAOWDM) is continued in the paper of Liew et al. (2005). It presents extensive simulation results from a new modulation technique for use in next generation wireless LANs. MAOWDM is a spread spectrum technique that uses the Discrete Wavelet Packet Transform for modulation. Simulation results from a MA-OWDM simulator in three time varying channels are presented and discussed: AWGN, Rayleigh flat and frequency-selective fading.

The performance advantages of the wavelet packet system over that based on DFT are demonstrated by both analytical and simulation methods in the paper of Xiaofan et al. (2004). The scheme proposed by the authors has good performance in multipath channels because of taking advantages of the properties of wavelet packets. Its performance is investigated for a multipath, slow Rayleigh fading channel.

A multimode transmission method using Wavelet Packet Modulation and Orthogonal Frequency Division Multiplexing is presented in the paper of Okamoto et al. (2003). The WPM keeps data transmission throughput even in tone and impulse interference environments that cannot be achieved with conventional multiplexing methods such as TDM (time division mul-

tiplexing) or OFDM. The authors propose an adaptive transmission in those interference environments using multimode transmission of WPM and OFDM, and evaluate its performance through computer simulations.

The authors of a paper, Xingxin et al. (2002), propose to replace the conventional FFT-based multicarrier modulation with wavelet packets in order to get a more flexible and robust performance. Furthermore, the wavelet packets are optimized in the sense of minimizing the power of intersymbol interference (ISI) and intercarrier interference (ICI). The performance of the optimal wavelet packet-based multicarrier modulation system is simulated and compared with the conventional wavelet and FFT-based multicarrier modulation systems.

A wavelet domain communication system (WDCS) proposed in the paper of Lee et al. (2002) uses transform domain processing and demonstrates enhanced interference avoidance capability under adverse environmental conditions. This work incorporates a wavelet packet-based decomposition technique that permits demonstration of an M-ary orthogonal signaling capability and provides increased adaptability over a larger class of interference signals. Compared to a non-wavelet packet based system, the WDCS provides improved bit error performance in several interference scenarios: single tone, multiple tone, swept tone, and partial band interference. The system was evaluated using an E_b/N_0 of 4.0 dB and interference energy-to-signal energy (I/E) ratios ranging from 0.0 dB to 16.0 dB. For binary, 4-ary, and 8-ary CSK data modulations, the packet based WDCS exhibited average interference suppression capabilities of 6.7, 9.2, and 12.0 dB, respectively.

Authors of the paper, Daly et al. (2002), derive operating conditions for the capacity-optimal tree for a given communication channel and power budget. They present a fast tree-selection algorithm, which achieves this optimum for the case of a finite complexity transceiver. It is found that optimal WPM outperforms conventional multichannel systems of equal complexity for ISI channels.

The paper of Zhang and Bi (2001) presents a class of complex orthogonal wavelet packets through optimization, and proposes a complex wavelet packet-based OFDM system (CWPOFDM). Besides, a serially implemented multistage MLSE/SIC (Successive Interference Cancellation) detector is developed to retrieve the transmitted CWPOFDM symbols. By comparison, it is shown that the performance of CWPOFDM without a cyclic prefix (CP) is close to or superior to that of a DFT-based OFDM with CP, at the price of a little increased computational complexity.

In the paper, Zhang et al. (2001) present a method to model complex time-varying wireless communication channels using wavelet packets as bases. This model has the advantages of flexibility, efficiency, and accuracy. Test results using field measurement data show the effectiveness of the model.

Because of some drawbacks of the OFDM and OWPDM systems, authors of the paper, Weihua et al. (2001), introduce bi-orthogonal wavelets as subcarrier basis functions. The performance of the system is simulated and analyzed on the AWGN and flat Rayleigh channels.

In the paper, Chang et al. (2001) analyze the frequency-selective and the time-varying nature of wireless channels that causes intercarrier interference (ICI) among wavelets. To mitigate the problem, they propose a unitary mapping filter on wavelets to achieve the optimum water-filling solution. Simulations compare the performance of the communication system using the proposed algorithm with the conventional direct sequence code division multiple access (DS-CDMA) system and the wavelet communication system with no unitary mapping filters, and confirm significant advantages of the proposed algorithm.

The paper of Van Bouwel et al. (2000) proposes a discussion on application of wavelet transform versus FFT for signal modulation. The paper studies the implementation of these wavelet packets, and the effects this implementation has on the requirements imposed in the design of

usable wavelets. It is shown that the restrictions imposed by the perfect reconstruction requirement necessitate the use of biorthogonal wavelets. This however influences the performance. Moreover, the frequency behavior of the wavelet packet transform is not straightforward, which limits the practical use of this transform in a multicarrier system.

The paper of To et al. (2000) discusses Wavelet packet division multiplexing (WPDM) as a high-capacity, flexible and robust orthogonal multiplexing scheme in which wavelet packet basis functions are chosen as the coding waveforms. In the paper, characterization of the effects of amplifier nonlinearities over the WPDM signal is performed for a 16-QAM signal constellation. An expression for the symbol error probability in the presence of Gaussian noise and amplifier nonlinearities is derived.

In the paper of Zhang and Dill (1999), a novel wavelet packet-modulated direct sequence spread spectrum system is introduced, and an anti-jamming algorithm is also developed to suppress narrow band jamming signals. According to the time series theory, Fisher's test can detect the hidden sinusoids in an AWGN environment, which give us a clue to detect the jamming signal. Authors generalize this algorithm so that we can detect the hidden wavelet packet components in an AWGN environment. The normalized energy distribution of the wavelet packet transformed signal is derived, a threshold is determined and the jamming signal is excised. Jamming signals with different strength and different bandwidth are investigated. Based on the simulation results, the generalized Fisher's test can effectively suppress interference in wide ranges.

In the paper, Suzuki et al. (1999) propose a maximum likelihood decoding method for WPM without coding before transmitting the signal. The proposed method performs maximum likelihood sequence estimation by utilizing a signal obtained in an intermediate stage of the demultiplexing process. Then, bit error performance under a flat fading channel and a frequency-selective fading channel is evaluated by computer simulation. According to the results, the

proposed method can improve the bit error performance for high relative values of Doppler spread.

3.8 Conclusion

In this chapter different types of multiplexing were presented, from the simple Time Division Multiplexing (TDM) to more complex OFDM. The principles of functioning of OFDM were followed by a structure of an OFDM-based communication system. Also OFDM advantages and drawbacks were highlighted.

A literature review on the use of wavelets for data multiplexing demonstrates a high potential of the wavelet multiplexing.

CHAPTER 4

WAVELET ANALYSIS

4.1 Introduction

From the history and modern applications to hardware implementation of algorithms and analysis of their complexity, this chapter presents a vision on the subject of wavelets. Conception of data compression and denoising using wavelet coefficient thresholding is described. Introducing a wavelet tree structure serves to represent the wavelet analysis/synthesis in a hierarchical form. Application of energy constraints on wavelet coefficients optimizes the wavelet tree, which is called the best wavelet tree. Some interesting properties of orthogonality of wavelet matrices are investigated in this chapter. High complexity of computation often limits the application of wavelet analysis/synthesis. That is why we propose fast wavelet transform algorithms. These fast wavelet analysis algorithms are compared to the conventional Fast Fourier Transform (FFT). A Haar matrix is analyzed as a matrix used in Fast Discrete Wavelet Transform (FDWT).

4.2 History and applications of wavelets

In the late 80's - early 90's of the last century, the fundamental publications on wavelets by Ingrid Daubechies: Daubechies (1989), Daubechies (1990); Stefan Mallat: Mallat (1989a), Mallat (1989b); and D. Donoho, Donoho (1995), arose a wavelet passion among researchers of many different domains.

Scaling aspects of wavelet techniques made them helpful for regularity study in biology, for cell membrane recognition, to distinguish normal from pathological membranes; metallurgy, for

the characterization of rough surfaces; finance, for detecting the properties of quick variation of values; in internet traffic description, for designing the service size.

Time aspects of the wavelet techniques found its application in industrial supervision of gear-wheels, checking undue noises in craned or dented wheels, and more generally in nondestructive control quality processes. Detection of short pathological events as epileptic crises or normal ones has evoked potentials in electroencephalogram EEG (medicine). Synthetic Aperture Radar (SAR) imagery, automatic target recognition, intermittence in physics also employ time aspects of the wavelet techniques.

In telecommunications domain both time and scale aspects of the wavelet techniques are used for signal/image denoising or compression.

In order to deal with continuous signals, a **continuous wavelet transform (CWT)** is employed. It is defined as the sum over all duration of the signal $s(t)$ multiplied by scaled, shifted versions of the wavelet function $\psi(scale, position, t)$:

$$C(scale, position) = \int_{-\infty}^{\infty} s(t) \cdot \psi(scale, position, t) dt. \tag{4.1}$$

Since Digital Signal Processing (DSP) deals with discrete signals, the use of a discrete form of the wavelet transform is appropriate. A Discrete Wavelet Transform (DWT) employs scales and positions based on powers of two, so-called dyadic scales and positions.

An efficient way to implement this scheme using filters was developed in 1988 by Stephan Mallat, Mallat (1989a). The Mallat algorithm is in fact a classical scheme known in the signal processing community as a two-channel subband coder, Strang and Nguyen (1996).

4.3 Elementary Wavelet Analysis and Synthesis Cells

4.3.1 One-dimensional Cells

The Mallat algorithm is a two-channel subband coder that uses conjugate quadrature filters or Quadrature Mirror Filters (QMF). A pair of filters $h(n)$ and $g(n)$ is called the Quadrature Mirror Filters of length L if they satisfy the following property:

$$g_k = (-1)^k \cdot h_{L-1-k}. \tag{4.2}$$

The QMF characteristics are derived from the scaling ϕ (low-pass filter h) and wavelet ψ (high-pass filter g) functions in the following recursive sequence:

$$\begin{aligned} p_{2n}(x) &= \sqrt{2}\sum_{k\in Z} h_k \cdot p_n(2x-k),\ p_0 = \phi(x); \\ p_{2n+1}(x) &= \sqrt{2}\sum_{k\in Z} g_k \cdot p_n(2x-k),\ p_1 = \psi(x). \end{aligned} \tag{4.3}$$

The length of the Quadrature Mirror Filter is equal to twice of the order K of its parent wavelet ψ:

$$L_g = L_h = L = 2K. \tag{4.4}$$

For example, the length of the low-pass and high pass filters, corresponding to the Daubechies' order one wavelet (db1), or Haar wavelet, is equal to 2.

The elementary one-dimensional analysis and synthesis cells that implement the Mallat algorithm are shown on Figure 4.1. An analysis cell splits an input signal into two sub-streams. The first sub-stream is passed through the low-pass filter and downsampled. At the same time, the second sub-stream is passed through the high-pass filter and also downsampled. Hence, the analysis cell outputs the two signals: an approximation signal (A) and a detail one (D).

The approximation signal represents the low-frequency components of the original signal. The symbol of a circle with two diverging arrows inside, shown in Figure 4.1, represents the elementary 1D analysis cell. The detail signal represents the high-frequency components of the original signal. The length of each signal $L_A = L_D$ is calculated as follows:

$$L_A = L_D = \frac{N+L-1}{2} = \frac{N+2K-1}{2} = floor\left(\frac{N-1}{2}\right) + K, \tag{4.5}$$

where, N is the length of the original signal, L is the length of the QMF filter, K is the order of the parent wavelet and the function $floor(x) = max\{m \in \mathbb{Z} | m \leq x\}$.

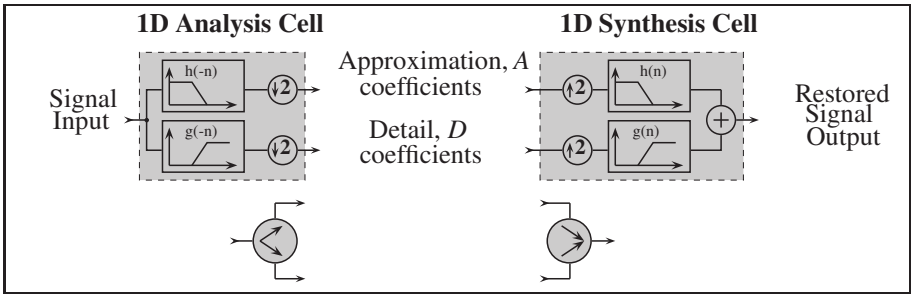

Figure 4.1 The elementary one-dimensional analysis and synthesis cells.

The elementary one-dimensional synthesis cell operates on two input signals: the approximation and detail ones. Each one of the signals is up-sampled first, and then passed through the corresponding filter. The approximation signal is passed through the low-pass filter, and the detail signal passed through the high-pass filter. Then the filter output signals are added. The symbol of a circle with two converging arrows inside, shown in Figure 4.1, represents the elementary 1D synthesis cell.

In theory, the procedure of signal analysis and synthesis using the elementary cells is reversible. It means that a restored signal will be exactly the same as an original one, if the approximation and detail signals are not modified. In real life, it is often not the case. The approximation and detail signals processed by DSP devices are subject to quantization, rounding, fixed-point operations, etc. Therefore the restored signal is not quite the same as the original one.

Complexity of elementary 1D analysis and synthesis cells

In order to obtain the approximation $A[n]$ and detail $D[n]$ signals, the convolution of the original signal x with the pair of Quadrature Mirror Filters $h[n]$, $g[n]$ is performed. This is represented by the following pair of equations:

$$\begin{aligned} A[n] &= \sum_{k=0}^{L-1} h[k]x[n-k], \\ D[n] &= \sum_{k=0}^{L-1} g[k]x[n-k], \end{aligned} \tag{4.6}$$

where $n = 0 \ldots N+L-1$; N is the length of the original signal x; L is the length of each of the QMF.

For this case, the complexity of convolution of the signal x with the pair of QMF filters is the following:

$$\begin{aligned} O(A) &= N \cdot [L \otimes +(L-1) \oplus]; \\ O(D) &= N \cdot [L \otimes +(L-1) \oplus], \end{aligned} \tag{4.7}$$

where $O(A)$ is the complexity of calculation of the approximation signal, $O(D)$ is the complexity of calculation of the detail signal, $\otimes$ is a multiplication operation, and $\oplus$ is an addition operation.

Complexities of the elementary analysis and synthesis cells shown in Figure 4.1 are almost defined by the complexities of convolutions with the QMF filters. Hence

$$O(elem.\ cell) \quad = \quad O(A) + O(D) = 2 \cdot N \cdot [L \otimes + (L-1) \oplus]. \tag{4.8}$$

4.3.2 Two-dimensional Cells

Wavelet decomposition and reconstruction are attractive tools not only for signal processing, but for image processing as well. The case of the one-dimensional wavelet decomposition and reconstruction is usually called the second order decomposition/reconstruction, since the original signal is decomposed into two signals. In case of images, or two-dimensional signals, an original image is decomposed into four sub-arrays. Therefore, the term "decomposition of order four" is usually applied to the wavelet image decomposition. Figure 4.2 shows the structure of the analysis and synthesis cells for two-dimensional data.

In case of the original image size $N \times M$ pixels, the two-dimensional **analysis cell** performs two following steps:

- **Step 1**. The elementary 1D analysis cell (see Figure 4.1) is applied to each row of the original image. This procedure decomposes the original array into two sub-arrays. They are the approximation (A_1) and detail (D_1) coefficients. The size of each sub-array is $N \times m$. The horizontal sub-array size m is calculated as follows:

$$m = floor\left(\frac{M-1}{2}\right) + K, \tag{4.9}$$

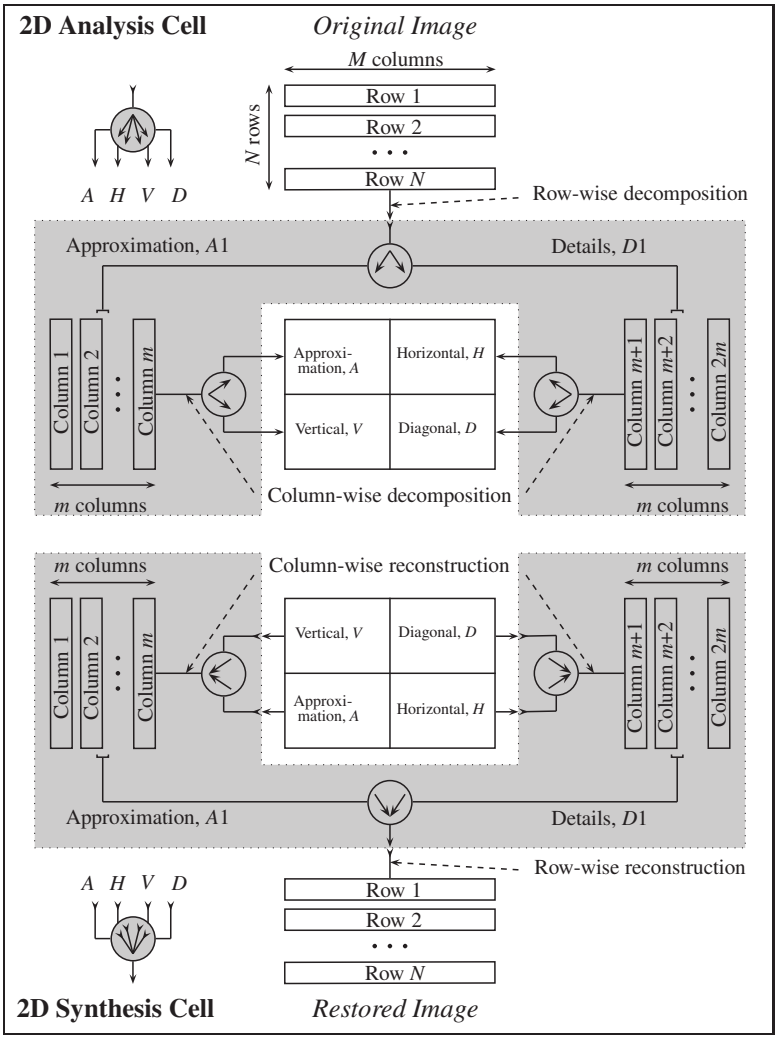

Figure 4.2 The structure of the analysis and synthesis cells for two-dimensional data.

where M is the horizontal image size, and K is the order of the parent wavelet used to create the filter in the elementary analysis cell.

- **Step 2**. The elementary 1D analysis cell is applied to each column of the approximation and detail coefficients calculated in **step 1**. As a result, four sub-arrays are obtained. They are called the Approximation (A), Horizontal (H), Vertical (V), and Diagonal (D) sub-arrays. All

those sub-arrays have the same size $n \times m$ calculated in following manner:

$$n = floor\left(\frac{N-1}{2}\right) + K,$$
$$m = floor\left(\frac{M-1}{2}\right) + K. \tag{4.10}$$

The symbol of a circle with four diverging arrows inside, shown in Figure 4.2, represents the 2D analysis cell.

The two-dimensional **synthesis cell** reverses operations implemented by the 2D analysis cell in the two following steps:

- **Step 1**. The elementary 1D synthesis cell is applied to each column of the Approximation (A), Horizontal (H), Vertical (V), and Diagonal (D) sub-arrays. This procedure reconstructs the two sub-arrays of the Approximation (A_1) and Detail (D_1) coefficients.
- **Step 2**. The elementary 1D synthesis cell is applied to each row of the two sub-arrays of the Approximation (A_1) and Detail (D_1) coefficients. This procedure reconstructs the image.

The symbol of a circle with four converging arrows inside, shown in Figure 4.2, represents the 2D synthesis cell.

Complexity of elementary 2D analysis and synthesis cells

Assume the original image has N rows and M columns of pixels. The two-dimensional elementary analysis and synthesis cells shown in Figure 4.2 employ three one-dimensional elementary analysis and synthesis cells. During wavelet decomposition, the first elementary analysis cell is applied column-wise to each row of the original image. Using the expression for the com-

plexity of an elementary cell (4.8), the complexity of this operation is the following:

$$O(ElemCell_1) = 2NM(L\otimes+(L-1)\oplus). \tag{4.11}$$

The second analysis cell is applied row-wise to the approximation coefficients (A_1). The size of A_1 is $N \times \frac{M+L-1}{2}$. Hence, this operation has the following complexity:

$$\begin{aligned} O(ElemCell_2) &= 2N\frac{M+L-1}{2}(L\otimes+(L-1)\oplus) = \\ &= N(M+L-1)(L\otimes+(L-1)\oplus). \end{aligned} \tag{4.12}$$

The third analysis cell is applied row-wise to the detail coefficients (D_1). The size of D_1 is also $N \times \frac{M+L-1}{2}$. Hence the complexity of this operation is the following:

$$\begin{aligned} O(ElemCell_3) &= 2N\frac{M+L-1}{2}(L\otimes+(L-1)\oplus) = \\ &= N(M+L-1)(L\otimes+(L-1)\oplus). \end{aligned} \tag{4.13}$$

Finally, the complexity of the two-dimensional elementary analysis cell applied to the image $N \times M$ is the following:

$$\begin{aligned} O(2D\ elem.\ cell) &= O(ElemCell_1) + O(ElemCell_2) + O(ElemCell_3) = \\ &= 2NM(L\otimes+(L-1)\oplus) + 2N(M+L-1)(L\otimes+(L-1)\oplus) = \\ &= 2N(2M+L-1)(L\otimes+(L-1)\oplus). \end{aligned} \tag{4.14}$$

4.4 Wavelet Decomposition and Reconstruction

4.4.1 One-dimensional Case

In the previous section we described the structure of the elementary cells used for analysis and synthesis of signals and images. The analysis cell, applied directly to the signal or image, represents one level of wavelet decomposition. Usually, the wavelet decomposition is not stopped after just one level. Depending on a decomposition scheme, the wavelet decomposition is either the Discrete Wavelet Transform (DWT) or the Wavelet Packet Transform (WPT).

The structures of the one-dimensional Discrete Wavelet Transform and one-dimensional Wavelet Packet Transform are shown in Figure 4.3 and Figure 4.4 accordingly. One can note the similarity of the first level of decomposition. In both cases, the original signal is decomposed into two sub-arrays of the approximation (A_1) and detail (D_1) coefficients. The differences show up on the second decomposition level. The Discrete Wavelet Transform decomposes only the approximation coefficients (A). The Wavelet Packet Transform decomposes both the approximation (A) and detail (D) coefficients. Given the original signal of length N, both the DWT and WPT consist of $log_2 N$ decomposition levels at most. The abbreviations used to represent each group of the coefficients shown in Figure 4.3 and Figure 4.4 can be interpreted as follows:

- AAA_3 stands for the third level approximation coefficients of the second level approximation coefficients of the first level approximation coefficients;
- DAA_3 stands for the third level detail coefficients of the second level approximation coefficients of the first level approximation coefficients.

The Wavelet Packet Transform produces more information about a signal structure than the Discrete Wavelet Transform; however, it requires more computations.

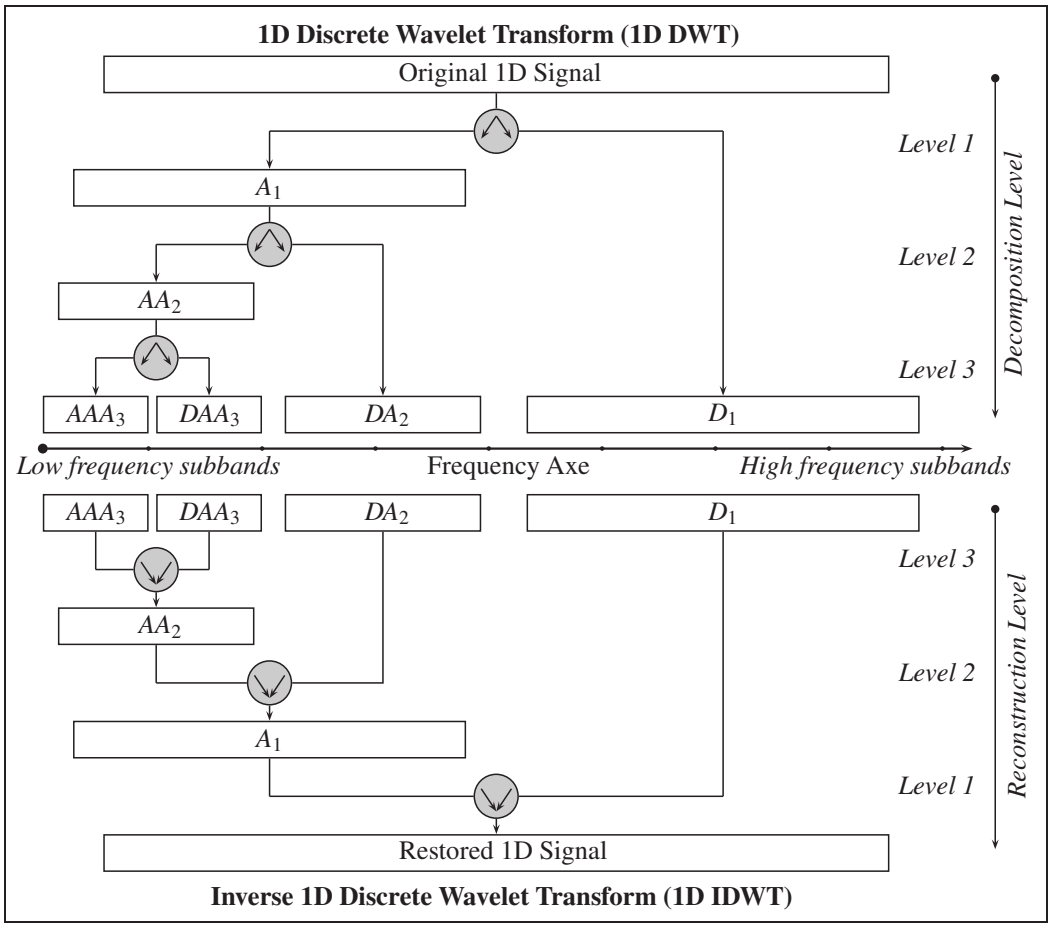

Figure 4.3 The structure of the one-dimensional Discrete Wavelet Transform (1D DWT) and the one-dimensional Inverse Discrete Wavelet Transform (1D IDWT). The level of decomposition is 3.

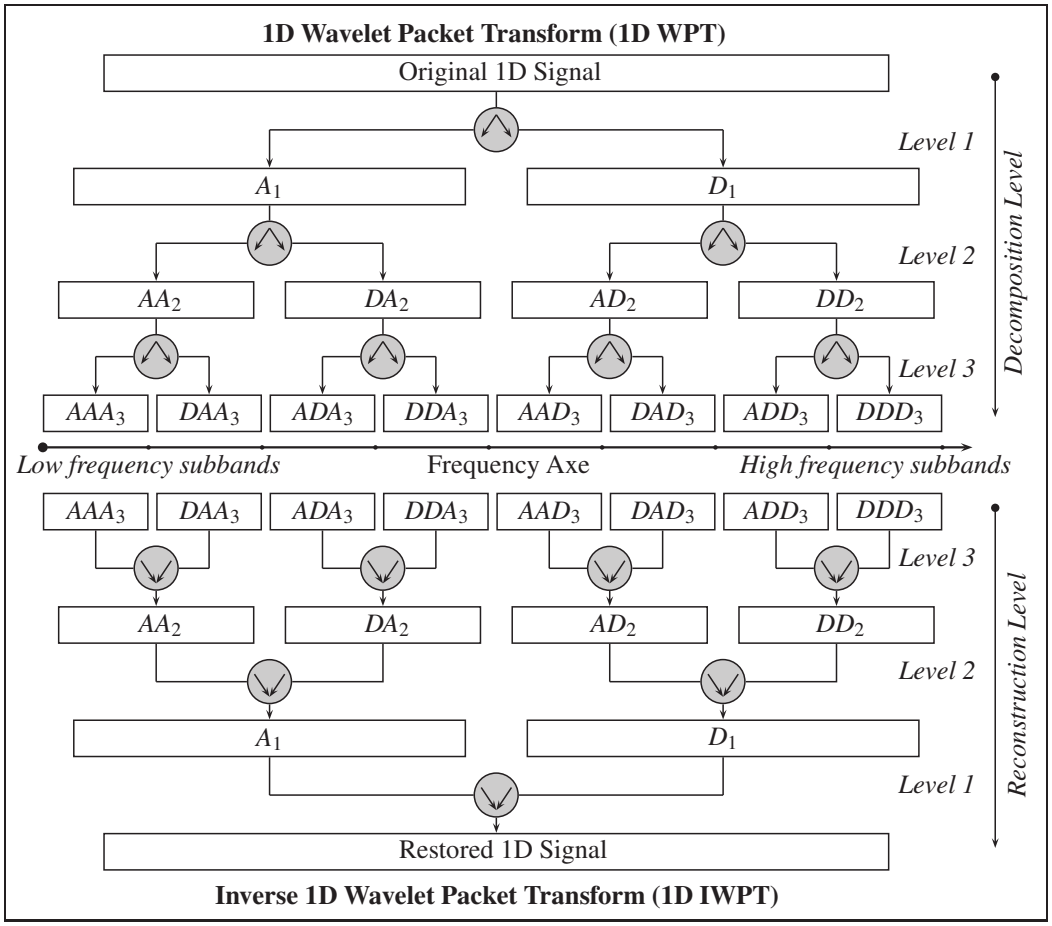

Figure 4.4 The structure of the one-dimensional Wavelet Packet Transform (1D WPT) and the one-dimensional Inverse Wavelet Packet Transform (1D IWPT). The level of decomposition is 3.

4.4.2 Two-dimensional Case

The two-dimensional case of wavelet decomposition is similar to the one-dimensional case. The structures of the two-dimensional Discrete Wavelet Transform (2D DWT) and the two-dimensional Wavelet Packet Transform (2D WPT) are shown in Figure 4.5 and Figure 4.6 accordingly. The similarity between the one- and two-dimensional cases is in the decomposition scheme. Both the 1D DWT and 2D DWT decompose only the approximation coefficients (*A*),

and both the 1D WPT and 2D WPT decompose all coefficients. Given the original image size $N \times M$ $(N < M)$, both the 2D DWT and 2D WPT consist of $log_2 N$ decomposition levels at most.

The only difference between the one- and two-dimensional cases is in the analysis cell used for decompositions. The elementary 1D analysis cell (see Figure 4.1) is used for the one-dimensional wavelet decomposition and the 2D analysis cell (see Figure 4.2) is used for the two-dimensional wavelet decomposition. The abbreviations used to represent each group of the coefficients shown in Figure 4.5 and Figure 4.6 can be interpreted as follows:

- AA_2 stands for the second level approximation coefficients of the first level approximation coefficients;
- DH_2 stands for the second level diagonal coefficients of the first level horizontal coefficients.

Complexity of the 2D DWT and 2D IDWT

The D-level two-dimensional Discrete Wavelet Transform and 2D Inverse Discrete Wavelet Transform apply the two-dimensional elementary analysis and synthesis cells (see Figure 4.2) toward the approximation coefficients D times. Therefore the complexity of the 2D DWT is equal to the sum of 2D elementary cell complexities as follows:

$$O(2D\ DWT) = \sum_{d=1}^{D} O(2D\ elem.\ cell_d). \tag{4.15}$$

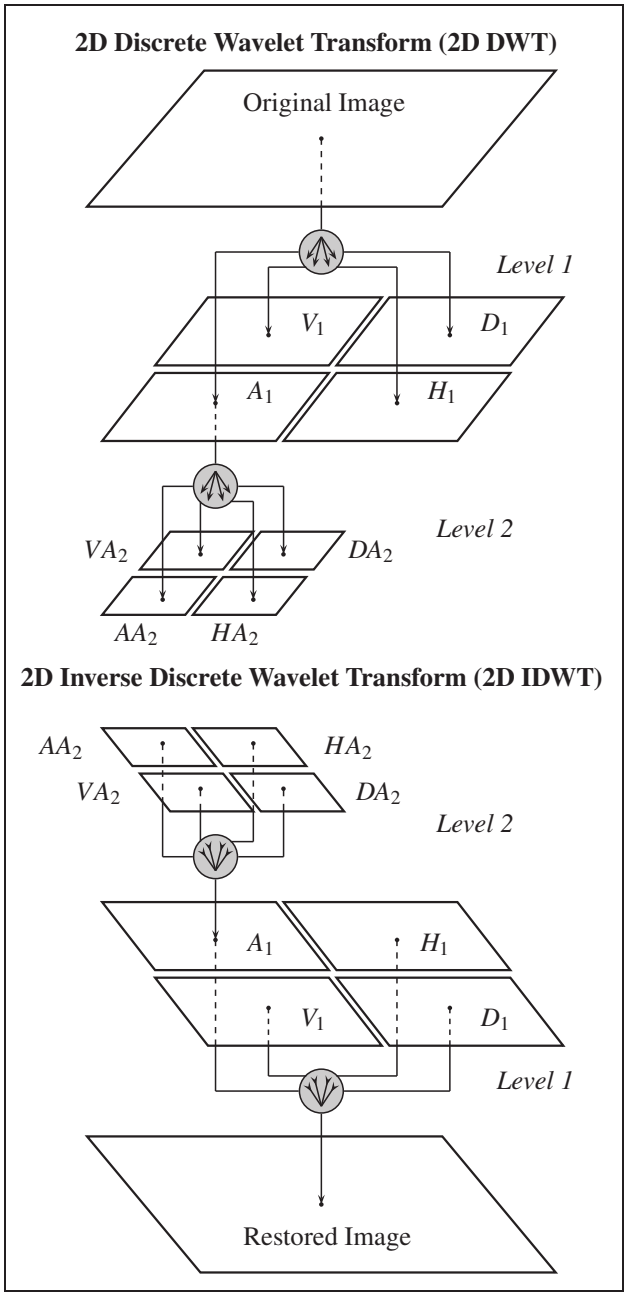

Figure 4.5 The structure of the two-dimensional Discrete Wavelet Transform (2D DWT) and the two-dimensional Inverse Discrete Wavelet Transform (2D IDWT). The level of decomposition is 2.

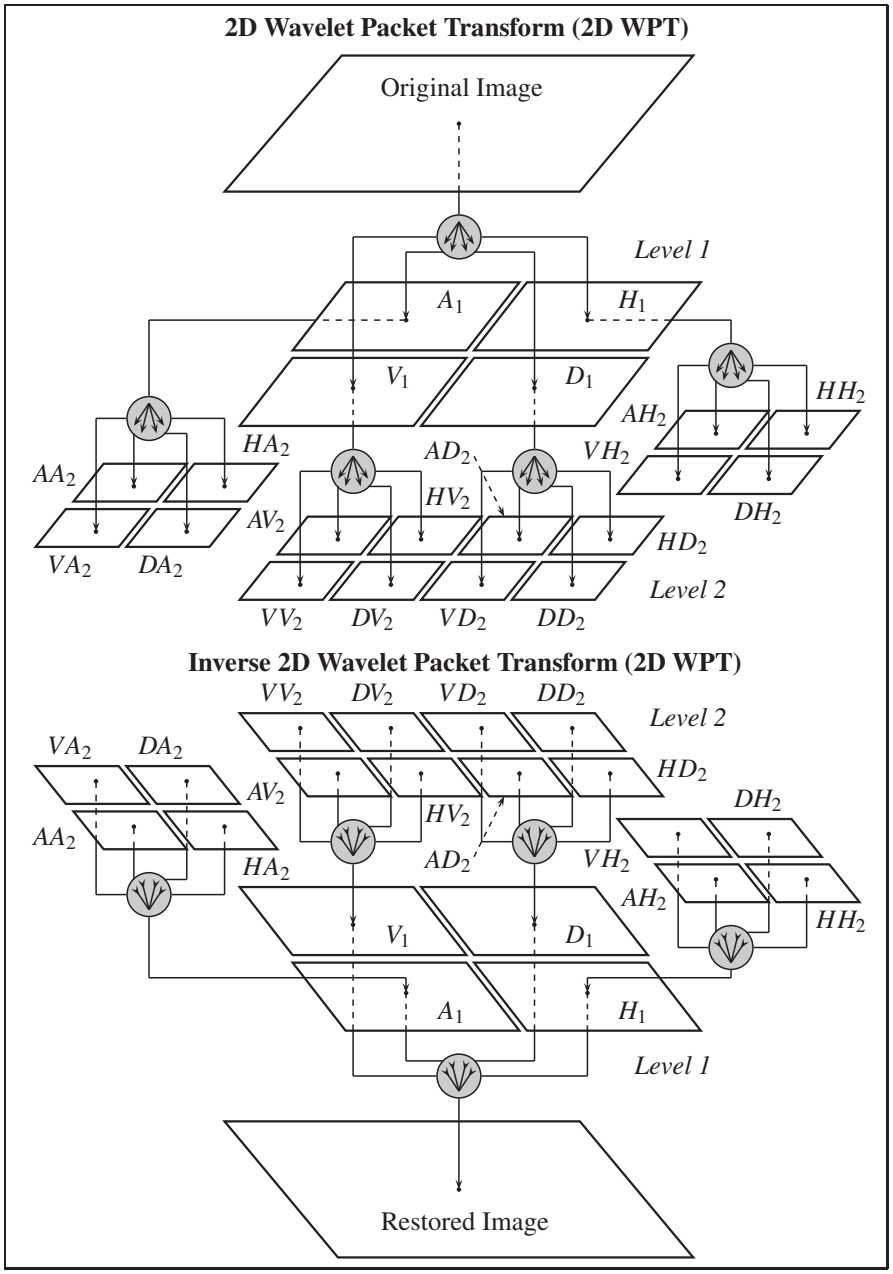

Figure 4.6 The structure of the two-dimensional Wavelet Packet Transform (2D WPT) and the two-dimensional Inverse Wavelet Packet Transform (2D IWPT). The level of decomposition is 2.

The size of the approximation coefficient array at the level d of the 2D DWT is the following:

$$\begin{aligned} N_d &= \frac{1}{2^{d-1}}\left(N+\left(2^{d-1}-1\right)(L-1)\right), \\ M_d &= \frac{1}{2^{d-1}}\left(M+\left(2^{d-1}-1\right)(L-1)\right). \end{aligned} \tag{4.16}$$

Use of Equation 4.14 with parameters $N = N_d,\ M = M_d$ represents Equation 4.15 in the following form:

$$\begin{aligned} &O(2D\,DWT) = \sum_{d=1}^{D} 2N_d(2M_d+L-1)(L\otimes+(L-1)\oplus) = \\ &= (L\otimes+(L-1)\oplus)\left[4\sum_{d=1}^{D} N_dM_d + 2(L-1)\sum_{d=1}^{D} N_d\right]. \end{aligned} \tag{4.17}$$

For simplicity, the derivation of the equation for the complexity of the D-level 2D DWT is accomplished in two stages. At the first stage, the following sum of products N_dM_d is calculated:

$$\begin{aligned} &\sum_{d=1}^{D} N_dM_d = \sum_{d=1}^{D} \frac{1}{2^{d-1}}\left(N+\left(2^{d-1}-1\right)(L-1)\right)\cdot\frac{1}{2^{d-1}}\left(M+\left(2^{d-1}-1\right)(L-1)\right) = \\ &= \sum_{d=1}^{D} 2^{2(1-d)}(NM+(N+M)\left(2^{d-1}-1\right)(L-1)+\left(2^{d-1}-1\right)^2(L-1)^2) = \\ &= NM\sum_{d=1}^{D} 4^{1-d} + (N+M)(L-1)\sum_{d=1}^{D}\left[4^{1-d}\left(2^{d-1}-1\right)\right] + \\ &+(L-1)^2\sum_{d=1}^{D}\left[4^{1-d}\left(2^{d-1}-1\right)^2\right]. \end{aligned} \tag{4.18}$$

Expressions of sums in Equation 4.18 can be simplified in following manner:

$$\begin{aligned}
&\sum_{d=1}^{D} 4^{1-d} = \frac{4}{3}\left(1-4^{-D}\right);\\
&\sum_{d=1}^{D}\left[4^{1-d}\left(2^{d-1}-1\right)\right] = \frac{2}{3}-2^{1-D}+\frac{1}{3}4^{1-D};\\
&\sum_{d=1}^{D}\left[4^{1-d}\left(2^{d-1}-1\right)^{2}\right] = D-\frac{8}{3}+4\cdot 2^{-D}-\frac{1}{3}4^{1-D}.
\end{aligned} \tag{4.19}$$

After replacing the sums in Equation 4.18 with expressions from Equation 4.19:

$$\begin{aligned}
&\sum_{d=1}^{D} N_d M_d = \frac{4}{3}NM\left(1-4^{-D}\right)+(N+M)(L-1)\cdot\\
&\cdot\left(\frac{2}{3}-2^{1-D}+\frac{1}{3}4^{1-D}\right)+(L-1)^2\left(D-\frac{8}{3}+4\cdot 2^{-D}-\frac{1}{3}4^{1-D}\right).
\end{aligned} \tag{4.20}$$

At the second stage, we calculate the following sum:

$$\begin{aligned}
&\sum_{d=1}^{D} N_d = \sum_{d=1}^{D}\frac{1}{2^{d-1}}\left(N+\left(2^{d-1}-1\right)(L-1)\right) =\\
&= N\sum_{d=1}^{D} 2^{1-d}+(L-1)\sum_{d=1}^{D}\left[2^{1-d}\left(2^{d-1}-1\right)\right].
\end{aligned} \tag{4.21}$$

Expressions of sums in Equation 4.21 can be simplified in following manner:

$$\begin{aligned}
&\sum_{d=1}^{D} 2^{1-d} = 2\left(1-2^{-D}\right);\\
&\sum_{d=1}^{D}\left[2^{1-d}\left(2^{d-1}-1\right)\right] = D-2+2^{1-D} = D-2\left(1-2^{-D}\right).
\end{aligned} \tag{4.22}$$

After replacing the sums in Equation 4.21 with expressions from Equation 4.22:

$$\sum_{d=1}^{D} N_d = 2N\left(1-2^{-D}\right)+(L-1)\left(D-2\left(1-2^{-D}\right)\right)= \\ =2(N-L+1)\left(1-2^{-D}\right)+D(L-1). \tag{4.23}$$

After replacing the sums in Equation 4.17 with expressions from Equation 4.20 and Equation 4.23, we obtain the expression for complexity of the D-level 2D Discrete Wavelet Transform of the $N \times M$ image:

$$O(2D\ DWT) = (L\otimes+(L-1)\oplus)\{4[\frac{4}{3}NM\left(1-4^{-D}\right)+(N+M)\cdot \\ \cdot(L-1)\left(\frac{2}{3}-2^{1-D}+\frac{1}{3}4^{1-D}\right)+(L-1)^2\left(D-\frac{8}{3}+4\cdot 2^{-D}-\frac{1}{3}4^{1-D}\right)]+ \\ +2(L-1)\left[2(N-L+1)(1-2^{-D})+D(L-1)\right]\}, \tag{4.24}$$

where L is the length of the wavelet filter.

4.5 Wavelet Tree

As shown in the previous section, the structure of wavelet decomposition is quite complex. A hierarchical tree structure was found helpful in representing of wavelet decomposition. This structure is called a "wavelet tree" by researchers.

4.5.1 Wavelet Tree of 1D and 2D Wavelet Decomposition

Figure 4.3 and Figure 4.4 show 1D DWT and 1D WPT accordingly. Figure 4.7 introduces the wavelet tree representation of each of the cases.

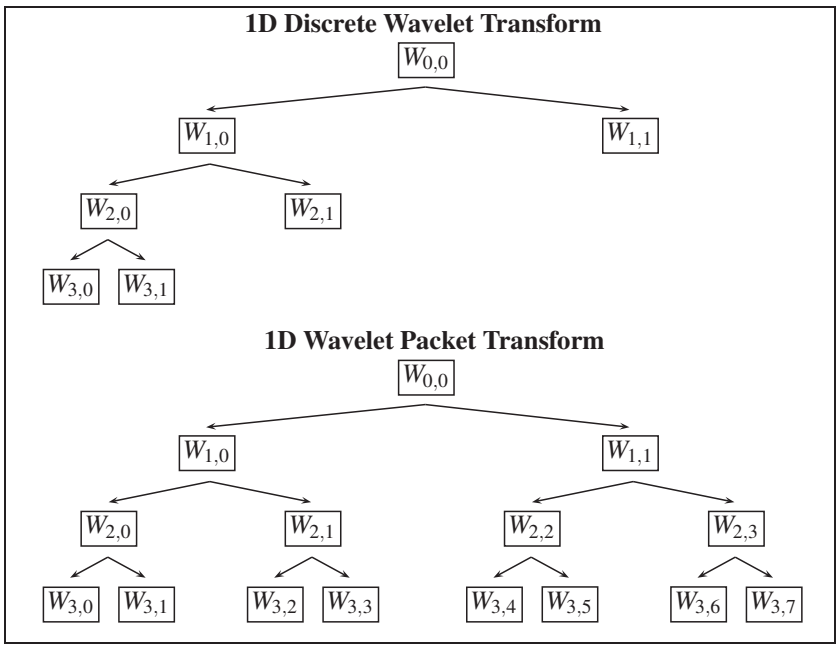

Figure 4.7 Wavelet tree representation of the 1D Discrete Wavelet Transform and the 1D Wavelet Packet Transform. The decomposition level is 3.

As one can see, a bulky notation of coefficients in the form of AAD_n has been replaced by the notation $W_{j,n}$, where j denotes the decomposition level and n the frequency parameter. Sometimes, the term "decomposition depth" is used as a synonym of the decomposition level. In this case, we say that all coefficients are represented by their depth-position wavelet tree label.

Figure 4.8 introduces the wavelet trees of the 2D DWT and the 2D WPT, using this new notation and which were shown earlier in Figure 4.5 and Figure 4.6 accordingly.

Wavelet trees are often classified by their order. The one-dimensional wavelet tree is usually called the second-order tree and the two-dimensional tree is called the fourth-order wavelet tree.

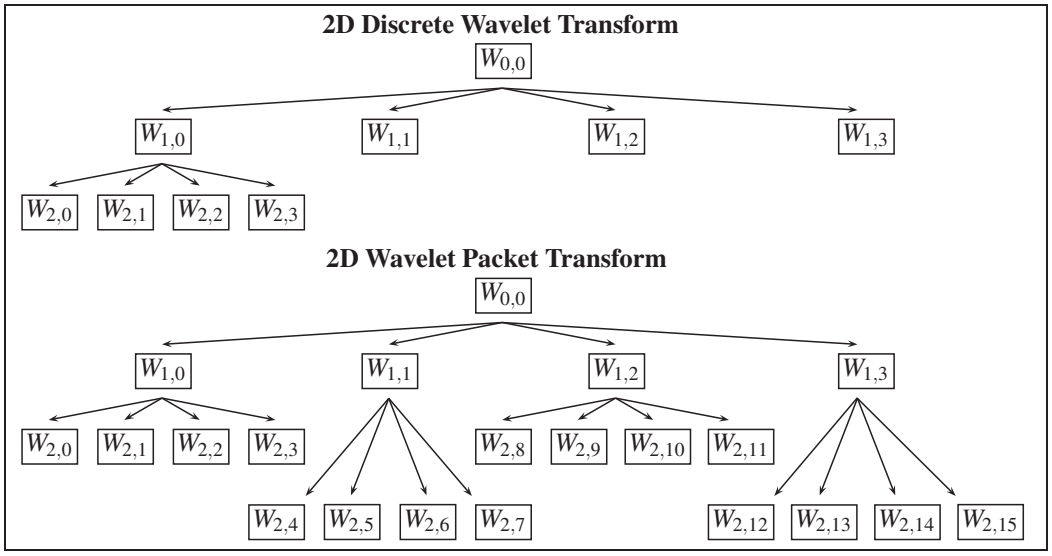

Figure 4.8 Wavelet Tree representation of the 2D Discrete Wavelet Transform, and the 2D Wavelet Packet Transform. The decomposition level is 2.

4.5.2 Wavelet Tree Manipulations

As every complex object, the wavelet tree has to be manipulated in a proper manner. Some terms used while dealing with the wavelet tree are introduced. The first term is a **"node"**. The node defines a group of wavelet coefficients $W_{j,n}$ by its depth j and position n. The wavelet coefficients of the one-dimentional wavelet tree node are represented by a scalar or a vector. The wavelet coefficients of the two-dimentional wavelet tree node are represented by a scalar, a vector or a matrix. The operation of node decomposition is called **node splitting** and the operation of node reconstruction is called **node merging**. The 1D/2D analysis cells are used for node splitting, and the 1D/2D synthesis cells are used for node merging. The operations of node splitting and merging are shown in Figure 4.9.

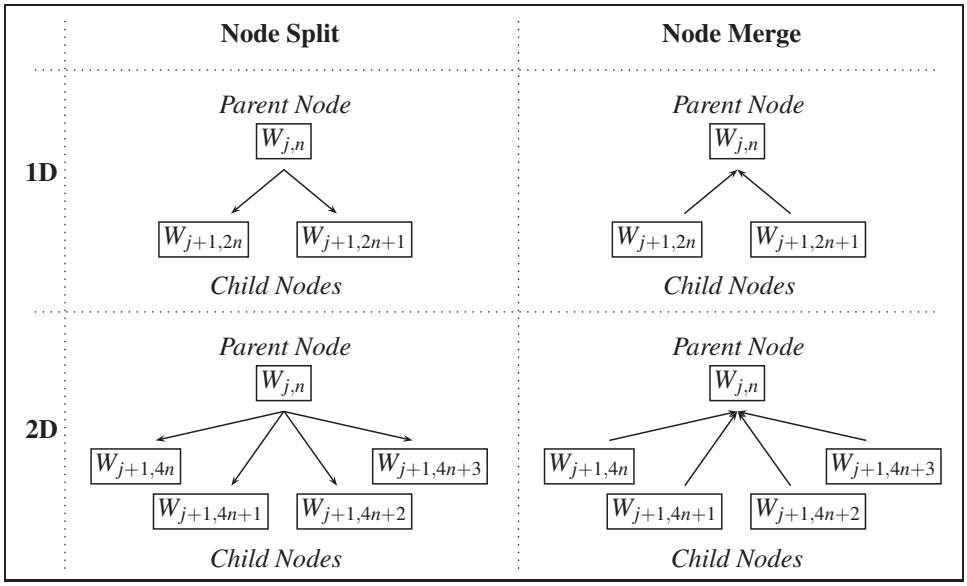

Figure 4.9 Wavelet Packet Tree: Node Split and Node Merge.

The node being split is usually called a **parent node**, and the nodes resulting from a splitting operation are called **child nodes**. The nodes of the second order tree (one-dimensional case) can have two child nodes, and the nodes of the fourth order tree (two-dimensional case) can have four child nodes as shown in Figure 4.9. The original data is assigned to the root node $W_{0,0}$. This node can only be a parent node. The nodes that do not have any children are called **terminal nodes (TN)**. All children and grandchildren of a certain node are called **descendants**. All parents and grandparents of a certain node are called **ascendants**. In this context, the root node has only descendants, and the terminal nodes have only ascendants.

4.5.3 Best Wavelet Tree

Theoretically, the operation of node splitting can be carried on until the node to be split is a scalar in the one-dimensional case or a vector in the two-dimensional case. Often, the node splitting is stopped when a certain criterion is reached. When wavelet decomposition is used for data compression or denoising, the entropy of child nodes can play a role in such a criterion.

For example, a node N is split into two nodes N_1 and N_2 if and only if the sum of the entropy of N_1 and N_2 is lower than the entropy of N. Entropy is often used in signal processing: Coifman and Wickerhauser (1992), Donoho and Johnstone (1994).

There are different entropy criteria. In the following expressions, s is the signal and s_i are the coefficients of s in an orthonormal basis. The entropy E must be an additive cost function such that $E(0) = 0$ and

$$E(s) = \sum_i E(s_i). \tag{4.25}$$

The (non-normalized) **Shannon entropy**:

$$E1(s_i) = s_i^2 \cdot log(s_i^2), \text{ hence } E1(s) = -\sum_i E(s_i^2) log(s_i^2) \tag{4.26}$$

with the convention $0 \cdot log(0) = 0$.

The concentration in $|\ |^p$ **norm entropy** with $1 \leq p$:

$$E2(s_i) = |s_i|^p, \text{ hence } E2(s) = -\sum_i E|s_i|^p = \|s_i\|_p^p. \tag{4.27}$$

The **log energy entropy**:

$$E3(s_i) = log(s_i^2), \text{ hence } E3(s) = -\sum_i log(s_i^2) \tag{4.28}$$

with the convention $0 \cdot log(0) = 0$.

The **threshold entropy**:

$$E4(s_i) = \begin{cases} 1 \text{ if } |s_i| > p \\ 0 \text{ elsewere} \end{cases}, \text{ hence } E4(s) = \#[i \text{ such that } |s_i| > p] \tag{4.29}$$

is the number of time instants when the signal is greater than a threshold p.

Figure 4.10 shows some of the best wavelet trees. The tree of 1D WPT depth 3 is considered as a full wavelet tree. In case we choose to split only approximation coefficients or $W_{j,0}$ nodes, the best wavelet tree will look like the wavelet tree of 1D DWT. In case the Shannon entropy is chosen as a criterion for node splitting, the wavelet tree might look like the third sub-figure of Figure 4.10, depending on values of the node coefficients.

4.5.4 Compact Wavelet Tree Representation

The tree structure makes it easy to imagine and interpret the wavelet decomposition, but it is not a convenient form for data storage and/or transmission. To represent any wavelet tree, the tree order and the set of its terminal node coefficients is enough. An example in Figure 4.11 shows how the wavelet tree represented on the third sub-figure of Figure 4.10 can be reconstructed, if it is defined only by the terminal node coefficients and order.

The set of terminal node coefficients $\left(W_{3,0}, W_{3,1}, W_{3,4}, W_{3,5}, W_{2,1}, W_{2,3}\right)$ has been stored as well as the *best tree order* $= 2$. At the first step of tree reconstruction, the pairs of the deepest nodes $(W_{3,0}, W_{3,1})$ and $\left(W_{3,4}, W_{3,5}\right)$ are merged providing their parent nodes $W_{2,0}$ and $W_{2,2}$. At

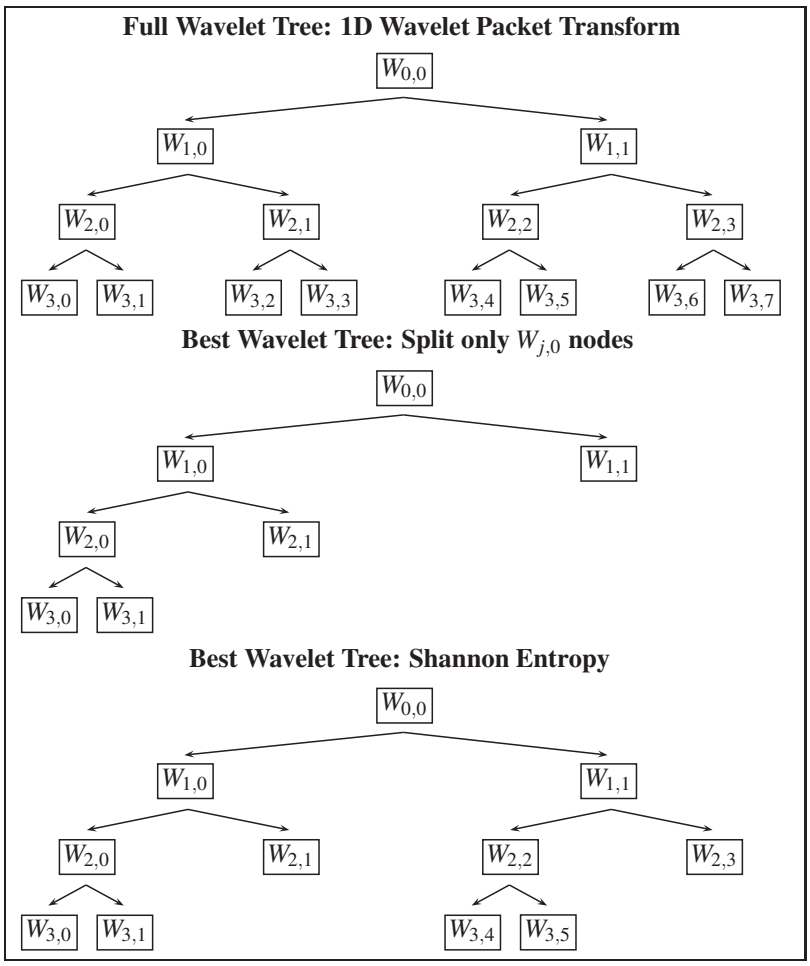

Figure 4.10 Full wavelet tree and two best wavelet trees obtained using different node splitting criteria: split only $W_{j,0}$ nodes and Shannon entropy.

the second step, merging the pairs of nodes $(W_{2,0}, W_{2,1})$ and $(W_{2,2}, W_{2,3})$ provides their parent nodes $W_{1,0}$ and $W_{1,1}$. And finally, at the third step, merging the pairs of nodes $(W_{1,0}, W_{1,1})$ is giving us the root node $W_{0,0}$. The task of best tree restoration is accomplished: having all terminal nodes of a certain tree and knowing its order, we restored the whole tree and the original data.

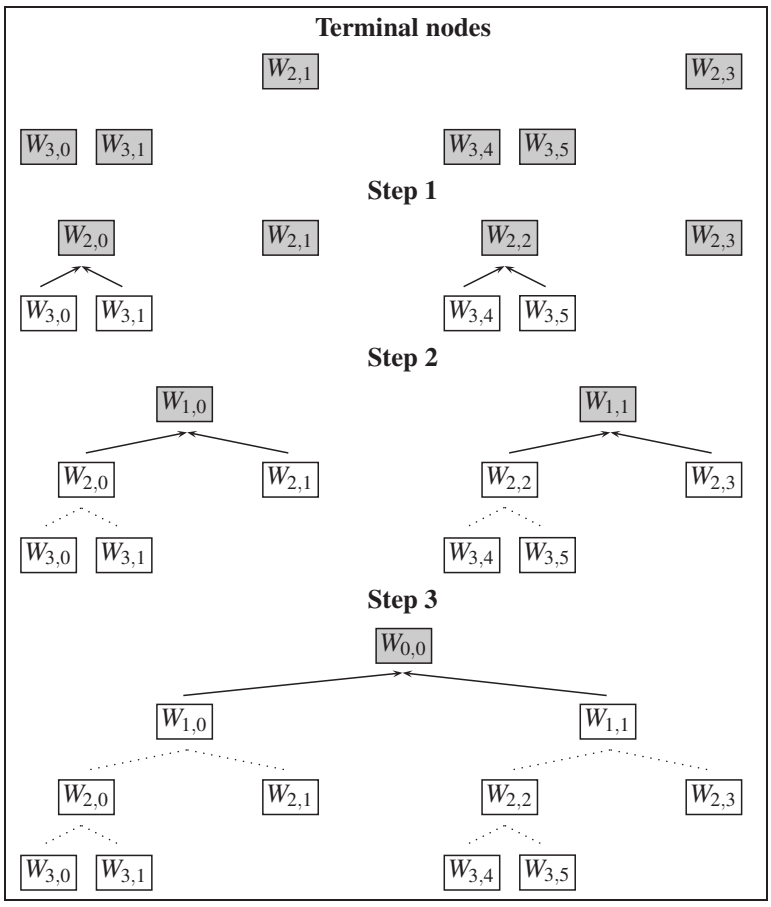

Figure 4.11 Reconstruction of the wavelet tree from the set of its terminal nodes.

4.6 Fast Elementary Wavelet Analysis and Synthesis Cells

4.6.1 One-dimensional Cells

It was mentioned before that the Discrete Wavelet Transform is based on the elementary analysis cell shown on Figure 4.1. In order to obtain the approximation $A[n]$ and detail $D[n]$ signals, the original signal x is passed through the pair of Quadrature Mirror Filters $h[n]$, $g[n]$. This

procedure is called **convolution** and it is represented by the following pair of equations:

$$\begin{aligned} A[n] &= \sum_{k=-\infty}^{\infty} h[k]x[2n-k], \\ D[n] &= \sum_{k=-\infty}^{\infty} g[k]x[2n-k], \end{aligned} \tag{4.30}$$

where n is a discrete time $n = 1 \ldots \frac{N}{2}$; N is the length of the original signal x.

Convolution is a very time-consuming procedure, therefore finding a time-efficient solution is important. Reducing the order of filter is the simplest scheme. A simple pair of Quadrature Mirror Filters $h[n]$, $g[n]$ is based on a Haar wavelet:

$$\begin{aligned} h[0] &= \frac{1}{\sqrt{2}},\ h[1] = \frac{1}{\sqrt{2}}, \\ g[0] &= -\frac{1}{\sqrt{2}},\ g[1] = \frac{1}{\sqrt{2}}. \end{aligned} \tag{4.31}$$

The Quadrature Mirror Filters based on the Haar wavelet are sometimes called **Haar QMF**. Hence the length of Haar QMF is two, the outputs of the elementary analysis cell are represented by the following pair of equations:

$$\begin{aligned} A[n] &= \sum_{k=0}^{1} h[k]x[2n-k] = \frac{1}{\sqrt{2}}(x[2n-1]+x[2n]), \\ D[n] &= \sum_{k=0}^{1} g[k]x[2n-k] = \frac{1}{\sqrt{2}}(x[2n-1]-x[2n]). \end{aligned} \tag{4.32}$$

In a matrix form, the outputs of the elementary analysis cell are the following:

$$\begin{pmatrix} A[n] \\ D[n] \end{pmatrix} = \frac{1}{\sqrt{2}} \begin{pmatrix} 1 & 1 \\ 1 & -1 \end{pmatrix} \begin{pmatrix} x[2n-1] \\ x[2n] \end{pmatrix},$$

$$\overline{C}[n] = \mathbb{W}_2\overline{X}[n] = \frac{1}{\sqrt{2}}\mathbb{V}_2\overline{X}[n], \tag{4.33}$$

where the vector $\overline{C}[n]$ represents a pair of approximation and detail wavelet coefficients $\overline{C}[n] = \begin{pmatrix} A[n] \\ D[n] \end{pmatrix}$;

the vector $\overline{X}[n]$ represents a pair of odd and even signal samples $\overline{X}[n] = \begin{pmatrix} x[2n-1] \\ x[2n] \end{pmatrix}$;

the matrix $\mathbb{V}_2 = \begin{pmatrix} 1 & 1 \\ 1 & -1 \end{pmatrix}$, subscript number 2 reflects the order of the matrix $\mathbb{V}$;

the matrix $\mathbb{W}_2 = \frac{1}{\sqrt{2}}\mathbb{V}_2$.

The algorithm of the fast elementary synthesis cell can be obtained by solving the matrix Equation 4.33 w.r.t. $\overline{X}[n]$:

$$\begin{aligned} \overline{C}[n] &= \mathbb{W}_2\overline{X}[n], \\ \mathbb{W}_2^{-1}\overline{C}[n] &= \mathbb{W}_2^{-1}\mathbb{W}_2\overline{X}[n], \\ \overline{X}[n] &= \mathbb{W}_2^{-1}\overline{C}[n], \end{aligned} \tag{4.34}$$

The fast elementary synthesis cell requires to find the inverse matrix $\mathbb{W}_2^{-1}$.

Suppose

$$\mathbb{W}_2 = \begin{pmatrix} m_{00} = \frac{1}{\sqrt{2}} & m_{01} = \frac{1}{\sqrt{2}} \\ m_{10} = \frac{1}{\sqrt{2}} & m_{11} = -\frac{1}{\sqrt{2}} \end{pmatrix}, \tag{4.35}$$

Then

$$\begin{aligned}
\mathbb{W}_2^{-1} &= \frac{1}{m_{00}m_{11}-m_{01}m_{10}}\begin{pmatrix} m_{11} & -m_{01} \\ -m_{10} & m_{00} \end{pmatrix} = \\
&= \frac{1}{\frac{1}{\sqrt{2}}\cdot\left(-\frac{1}{\sqrt{2}}\right)-\frac{1}{\sqrt{2}}\cdot\frac{1}{\sqrt{2}}}\begin{pmatrix} -\frac{1}{\sqrt{2}} & -\frac{1}{\sqrt{2}} \\ -\frac{1}{\sqrt{2}} & \frac{1}{\sqrt{2}} \end{pmatrix} = \frac{-1}{-\frac{1}{2}-\frac{1}{2}}\begin{pmatrix} \frac{1}{\sqrt{2}} & \frac{1}{\sqrt{2}} \\ \frac{1}{\sqrt{2}} & -\frac{1}{\sqrt{2}} \end{pmatrix} = \\
&= \frac{-1}{-\frac{2}{2}}\begin{pmatrix} \frac{1}{\sqrt{2}} & \frac{1}{\sqrt{2}} \\ \frac{1}{\sqrt{2}} & -\frac{1}{\sqrt{2}} \end{pmatrix} = \begin{pmatrix} \frac{1}{\sqrt{2}} & \frac{1}{\sqrt{2}} \\ \frac{1}{\sqrt{2}} & -\frac{1}{\sqrt{2}} \end{pmatrix} = \mathbb{W}_2. \qquad (4.36)
\end{aligned}$$

Hence the inverse matrix $\mathbb{W}_2^{-1}$ is equal to the direct one $\mathbb{W}_2$. This implies that the same elementary cell can be used in one-dimensional signal decomposition as well as in signal reconstruction. Figure 4.12 shows the scheme of hardware implementation of the fast elementary cell. It has two possible realizations. The first one is based on the matrix $\mathbb{W}_2$ (see Figure 4.12a) and it uses internal multipliers. The second realization (see Figure 4.12b) is based on the matrix $\mathbb{V}_2$ (see Figure 4.12c) and it uses external multipliers. The advantages of the fast elementary cell configuration shown on Figure 4.12b over the configuration shown on Figure 4.12a will be explained below.

The assignments for Input/Output pins are presented in Table 4.1 for both cases of use: the fast elementary cell in signal analysis and synthesis.

Complexity of $\mathbb{W}_2$ and $\mathbb{V}_2$ cells vs. 2-FFT

In this subsection, we compare the complexity of cells for the Haar based wavelet transforms to the usual FFTs. Butterfly computation in the decimation-in-time FFT is shown on Figure 4.13, Proakis and Salehi (2007).

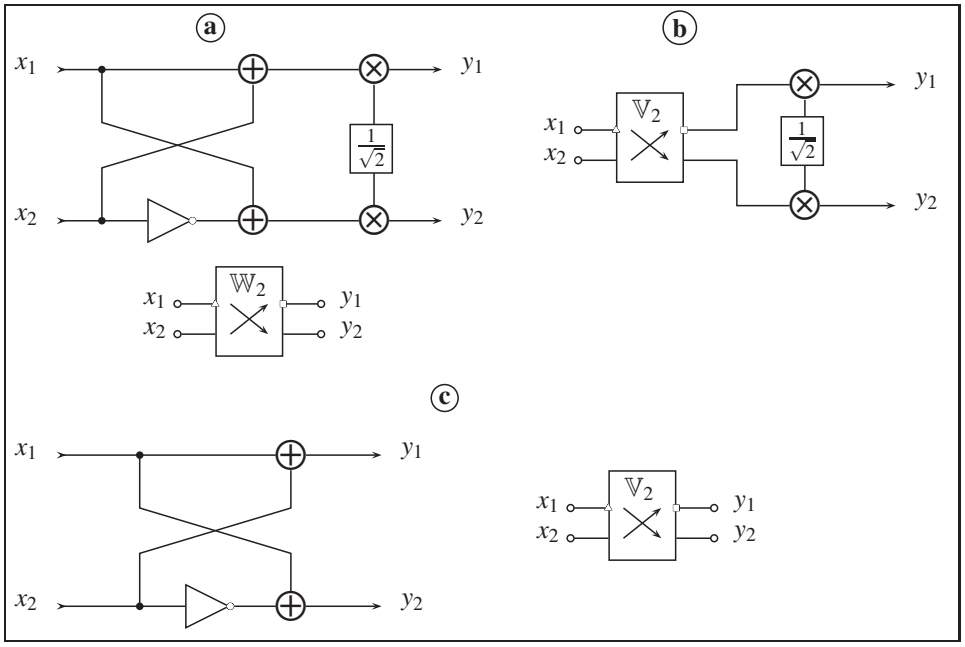

Figure 4.12 One-dimensional fast elementary cell.

Table 4.1 Input/Output pin assignment of the fast elementary cell

Input	**Analysis**	**Synthesis**	**Output**	**Analysis**	**Synthesis**
x_1	x[2n-1]	A[n]	y_1	A[n]	x[2n-1]
x_2	x[2n]	D[n]	y_2	D[n]	x[2n]

Complexity of $\mathbb{W}_2$, $\mathbb{V}_2$ cells and 2-FFT butterfly is calculated using **Appendix II: Complexity of Arithmetic Operations on Complex Numbers**.

The results are presented in Table 4.2. Application of $\mathbb{W}_2$ and $\mathbb{V}_2$ cells does not change the nature of input numbers, i.e., the real input numbers stay real. However, the output of a 2-FFT

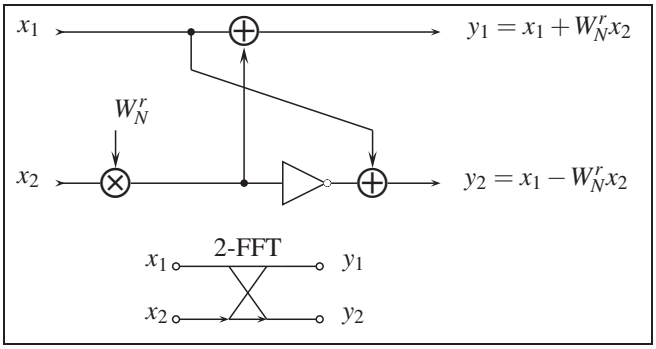

Figure 4.13 2-FFT butterfly.

butterfly is always represented by complex numbers. Since the 2-FFT butterfly is applied more than once, the input of the next stage of 2-FFT operation will be complex, and there is no reason to consider the real input numbers for 2-FFT. Therefore the slot, corresponding to the number of operations on real input numbers, is empty in Table 4.2.

Table 4.2 Complexity of $\mathbb{W}_2$, $\mathbb{V}_2$ cells and 2-FFT butterfly in terms of real operations

Input numbers	$\mathbb{W}_2$	$\mathbb{V}_2$	**2-FFT**
Real	$2\oplus+2\otimes+1\ominus$	$2\oplus+1\ominus$	n/a
Complex	$4\oplus+4\otimes+2\ominus$	$4\oplus+2\ominus$	$6\oplus+4\otimes+3\ominus$

4.6.2 Two-dimensional Cells

In this subsection, we introduce a two-dimensional fast elementary cell, which is shown on Figure 4.14a. The two-dimensional fast elementary cell is a combination of four one-dimensional elementary cells shown on Figure 4.12.

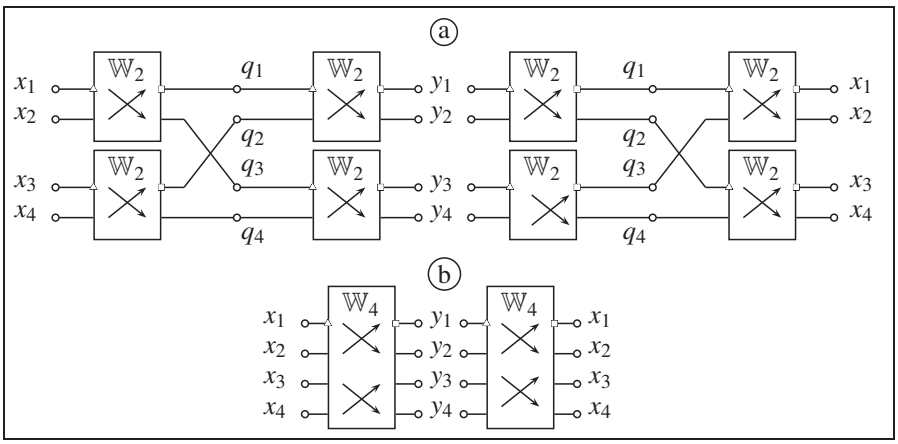

Figure 4.14 Two-dimensional fast elementary cell as a combination of four one-dimensional elementary cells.

During analysis, the 2D fast elementary cell decomposes four elements or pixels of the image $\overline{X}$ into four wavelet packet coefficients $\overline{C}$, where $n = 1 \ldots N$, $m = 1 \ldots M$, $N \times M$ is the image size,

$$\overline{X} = \begin{pmatrix} X[2n-1, 2m-1] \\ X[2n-1, 2m] \\ X[2n, 2m-1] \\ X[2n, 2m] \end{pmatrix}, \overline{C} = \begin{pmatrix} A[n,m] \\ H[n,m] \\ V[n,m] \\ D[n,m] \end{pmatrix}.$$

It will be shown below that the same 2D fast elementary cell can be employed for image analysis as well as for image synthesis. The assignments for Input/Output pins are presented in Table 4.3 for both cases; the 2D fast elementary cell is used in image analysis and synthesis.

Application of the 2D fast elementary cell for image analysis can be presented in a matrix form as follows:

$$\overline{C} = \mathbb{W}_4 \overline{X}. \tag{4.37}$$

Table 4.3 Input/Output pin assignment of the 2D fast elementary cell

Input	**Analysis**	**Synthesis**	**Output**	**Analysis**	**Synthesis**
x_1	X[2n-1,2m-1]	A[n,m]	y_1	A[n,m]	X[2n-1,2m-1]
x_2	X[2n-1,2m]	H[n,m]	y_2	H[n,m]	X[2n-1,2m]
x_3	X[2n,2m-1]	V[n,m]	y_3	V[n,m]	X[2n,2m-1]
x_4	X[2n,2m]	D[n,m]	y_4	D[n,m]	X[2n,2m]

The 2D fast elementary cell is defined by the wavelet packet matrix $\mathbb{W}_4$. Subscript four stands for the order of the matrix. Now we will derive the structure of the wavelet packet matrix $\mathbb{W}_4$ using Figure 4.14:

$$\begin{aligned} y_1 &= \frac{1}{\sqrt{2}}(q_1+q_2) = \frac{1}{2}(x_1+x_2+x_3+x_4); \\ y_2 &= \frac{1}{\sqrt{2}}(q_1-q_2) = \frac{1}{2}(x_1+x_2-x_3-x_4); \\ y_3 &= \frac{1}{\sqrt{2}}(q_3+q_4) = \frac{1}{2}(x_1-x_2+x_3-x_4); \\ y_4 &= \frac{1}{\sqrt{2}}(q_3-q_4) = \frac{1}{2}(x_1-x_2-x_3+x_4). \end{aligned} \tag{4.38}$$

Hence

$$\mathbb{W}_4 = \frac{1}{2}\begin{pmatrix} 1 & 1 & 1 & 1 \\ 1 & 1 & -1 & -1 \\ 1 & -1 & 1 & -1 \\ 1 & -1 & -1 & 1 \end{pmatrix}. \tag{4.39}$$

Calculations proposed in **Appendix I: Inverse Wavelet Packet Matrix** $\mathbb{W}_4^{-1}$ show that the inverse wavelet packet matrix $\mathbb{W}_4^{-1}$ is equal to the direct one $\mathbb{W}_4$. This is basically due to the fact that the elements of the matrix are unitary. This means that the same 2D fast elementary

cell can be employed for image decomposition as well as for image restoration (see Figure 4.14b). Figure 4.15 shows the scheme of hardware implementation of the 2D fast elementary cell. It has two possible realizations. The first one is based on the wavelet packet matrix $\mathbb{W}_4$ (see Figure 4.15a) and it uses internal multipliers. The second realization (see Figure 4.15b) is based on the matrix $\mathbb{V}_4$ (see Figure 4.15c) and it uses external multipliers. The advantage of the fast elementary cell configuration is apparent when comparing Figure 4.15b over the configuration shown on Figure 4.15a.

Complexity of $\mathbb{W}_4$ and $\mathbb{V}_4$ cells

Complexities $\mathbb{W}_4$ and $\mathbb{V}_4$ cells are calculated using Figure 4.15 and **Appendix II: Complexity of Arithmetic Operations on Complex Numbers**.

Table 4.4 Complexity of $\mathbb{W}_4$, $\mathbb{V}_4$ cells in terms of real operations

Input numbers	$\mathbb{W}_4$	$\mathbb{V}_4$
Real	$10\oplus+4\otimes+3\ominus$	$10\oplus+3\ominus$
Complex	$20\oplus+8\otimes+10\ominus$	$20\oplus+6\ominus$

A multiplication operation by $\frac{1}{2}$ can be replaced by the right bit shift operation. In that case, no multiplication operations are required in matrix $\mathbb{W}_4$ calculation.

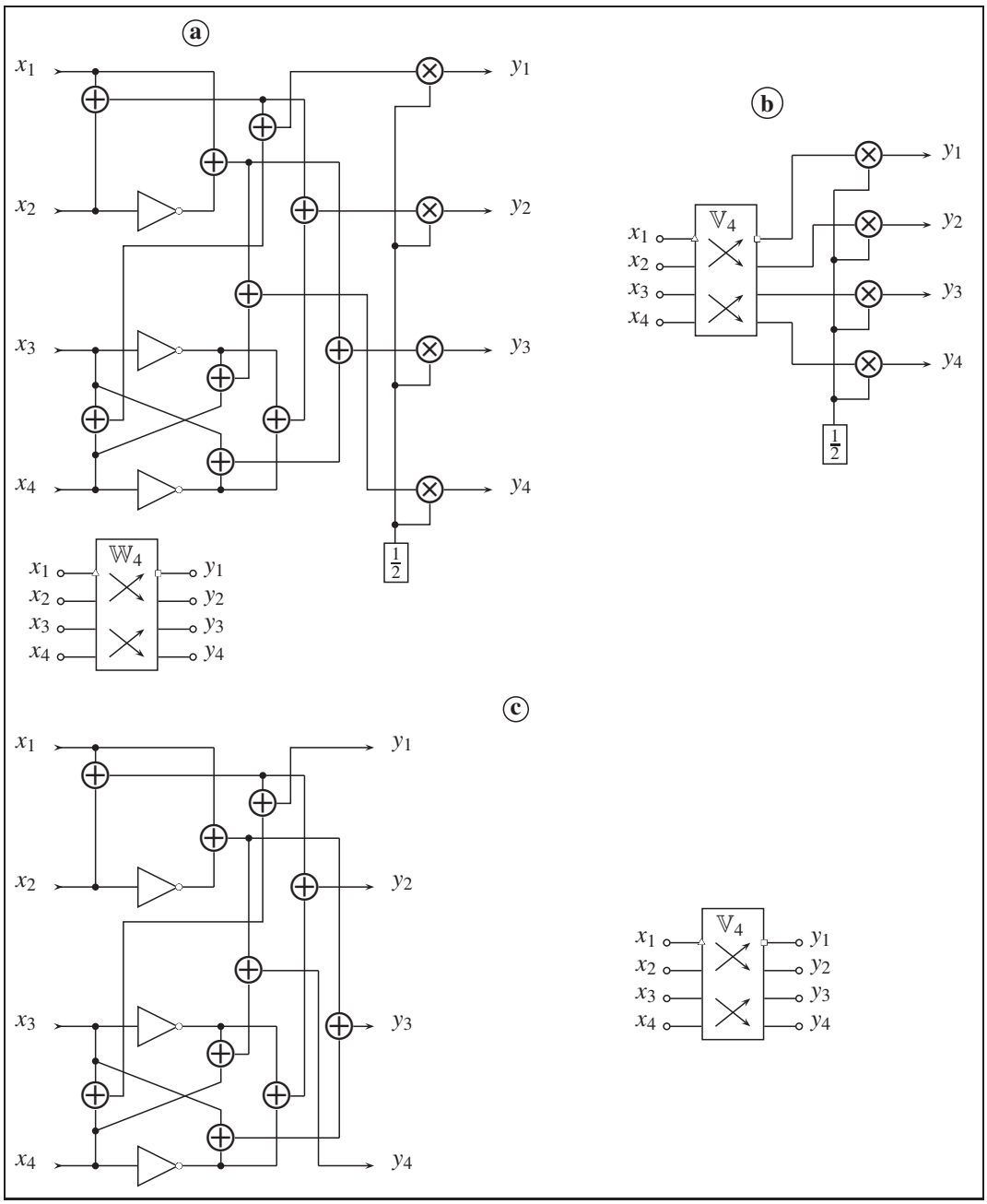

Figure 4.15 Two-dimensional fast elementary cell.

Bit number of the output of 2D fast elementary cell

Application of the 2D fast elementary cell, or the $\mathbb{W}_K$ matrix, adds extra bits to the number of required bits needed for an original coefficient x. In order to calculate one coefficient,

three addition operations and a right bit shift operation are required, according to Equation 4.38. Every addition operation adds one principal bit to an original bit number. The right bit shift operation adds one fractional bit and removes one principal bit. Hence, an output coefficient of $\mathbb{W}_K$ has two principal extra bits and one fractional bit. After d levels of two-dimensional decomposition using $\mathbb{W}_K$, the wavelet packet coefficient will contain $2d$ principal bits and d fractional bits. Table 4.5 shows numbers of principal and fractional bits depending on decomposition depth.

Table 4.5 Bit number of the output of
2D fast elementary cell

Depth	Principal bits	Fractional bits
1	2	1
2	4	2
3	6	3
⋮	⋮	⋮
d	$2d$	d

For example, if every pixel of an image contains 8 bits, then after 3 levels of two-dimensional decomposition ($depth = 3$), the wavelet packet coefficient will contain $8 + 2 \cdot 3 = 14$ principal bits and 3 fractional bits.

4.7 Fast Wavelet Decomposition and Reconstruction

4.7.1 Fast Wavelet Packet Transform (FWPT) of the Full Wavelet Packet Tree

Fast Wavelet Packet Transform (FWPT) of the Full Wavelet Packet Tree can be envisioned as application of the wavelet packet matrix $\mathbb{W}_K$ of order K on the signal vector $\overline{X}$ as follows:

$$\overline{C} = \mathbb{W}_K \overline{X}, \tag{4.40}$$

$$\begin{pmatrix} c_0 \\ c_1 \\ c_2 \\ \vdots \\ c_K \end{pmatrix} = \begin{pmatrix} w_{0,0} & w_{0,1} & w_{0,2} & \cdots & w_{0,K-1} \\ w_{1,0} & w_{1,1} & w_{1,2} & \cdots & w_{1,K-1} \\ w_{2,0} & w_{2,1} & w_{2,2} & \cdots & w_{2,K-1} \\ \vdots & \vdots & \vdots & \ddots & \vdots \\ w_{K-1,0} & w_{K-1,1} & w_{K-1,2} & \cdots & w_{K-1,K-1} \end{pmatrix} \begin{pmatrix} x_0 \\ x_1 \\ x_2 \\ \vdots \\ x_{K-1} \end{pmatrix} \tag{4.41}$$

where the vector $\overline{C}$ represents wavelet packet coefficients and K is a power 2 signal length.

Previously we demonstrated the property of the wavelet packet matrix $\mathbb{W}_K = \mathbb{W}_K^{-1}$ for the cases $K = 2, 4$. Let us assume that this property is valid for $K \in \mathbf{Z}$. In this case the Inverse Fast Wavelet Packet Transform (IFWPT) of the Full Wavelet Packet Tree can be envisioned as an application of the wavelet packet matrix $\mathbb{W}_K$ on the wavelet packet coefficients $\overline{S}$ as follows:

$$\overline{Y} = \mathbb{W}_K \overline{S}, \tag{4.42}$$

$$\begin{pmatrix} y_0 \\ y_1 \\ y_2 \\ \vdots \\ y_{K-1} \end{pmatrix} = \begin{pmatrix} w_{0,0} & w_{0,1} & w_{0,2} & \cdots & w_{0,K-1} \\ w_{1,0} & w_{1,1} & w_{1,2} & \cdots & w_{1,K-1} \\ w_{2,0} & w_{2,1} & w_{2,2} & \cdots & w_{2,K-1} \\ \vdots & \vdots & \vdots & \ddots & \vdots \\ w_{K-1,0} & w_{K-1,1} & w_{K-1,2} & \cdots & w_{K-1,K-1} \end{pmatrix} \begin{pmatrix} s_0 \\ s_1 \\ s_2 \\ \vdots \\ s_K \end{pmatrix} \tag{4.43}$$

where $\overline{Y}$ is the restored signal. In most cases, the restored wavelet packet coefficients $\overline{S}$ are not equal to $\overline{C}$ due to quantization, thresholding and channel noise. Hence, the restored signal $\overline{Y}$ is not the same as the original one, $\overline{X}$.

Denoting

$$\mathbb{W}_K = b\mathbb{V}_K = b \begin{pmatrix} v_{0,0} & v_{0,1} & v_{0,2} & \cdots & v_{0,K-1} \\ v_{1,0} & v_{1,1} & v_{1,2} & \cdots & v_{1,K-1} \\ v_{2,0} & v_{2,1} & v_{2,2} & \cdots & v_{2,K-1} \\ \vdots & \vdots & \vdots & \ddots & \vdots \\ v_{K-1,0} & v_{K-1,1} & v_{K-1,2} & \cdots & v_{K-1,K-1} \end{pmatrix}, \tag{4.44}$$

where the matrix $\mathbb{V}_K$ consists of the elements $v_{i,j} = 1$ *or* -1; the multiplier $b = \left(\frac{1}{\sqrt{2}}\right)^d$; d is a wavelet packet decomposition depth or decomposition level, where $d \leq \log_2(K)$.

Recall the wavelet packet matrix of the fast elementary cell $\mathbb{W}_2$, Equation 4.35:

$$\mathbb{W}_2 = \frac{1}{\sqrt{2}}\mathbb{V}_2, \textit{ where } \mathbb{V}_2 = \begin{pmatrix} 1 & 1 \\ 1 & -1 \end{pmatrix}. \tag{4.45}$$

The fast elementary cell operates with the original signal length $K = 2$ and it implements one level wavelet packet decomposition $d = 1$. Hence, $b = \left(\frac{1}{\sqrt{2}}\right)^d = \left(\frac{1}{\sqrt{2}}\right)^1 = \frac{1}{\sqrt{2}}$, which corresponds to the previous calculations. Therefore, the wavelet packet matrix of the fast elementary cell $\mathbb{W}_2$ represents the specific case of the wavelet packet matrix $\mathbb{W}_K$.

Recall also the wavelet packet matrix of the two-dimensional fast elementary cell $\mathbb{W}_4$, Equation 4.39:

$$\mathbb{W}_4 = \frac{1}{2}\mathbb{V}_4, \textit{ where } \mathbb{V}_4 = \begin{pmatrix} 1 & 1 & 1 & 1 \\ 1 & 1 & -1 & -1 \\ 1 & -1 & 1 & -1 \\ 1 & -1 & -1 & 1 \end{pmatrix}. \tag{4.46}$$

The 2D fast elementary cell can be envisioned as the cell that operates with the original signal length $K = 4$ and implements two levels' wavelet packet decomposition $d = 2$. Hence, $b = \left(\frac{1}{\sqrt{2}}\right)^d = \left(\frac{1}{\sqrt{2}}\right)^2 = \frac{1}{2}$, which corresponds to the previous calculations. Therefore, the wavelet packet matrix of the fast elementary cell $\mathbb{W}_4$ also represents the specific case of the wavelet packet matrix $\mathbb{W}_K$.

Figure 4.16 presents different hardware implementations of the one dimensional Wavelet Packet Transform shown in Figure 4.4. Figure 4.16a employs the fast elementary cells $\mathbb{W}_2$ shown in Figure 4.12. The WPT calculation may be speeded up by applying techniques of parallel computing instead of a serial one. Figure 4.16b illustrates how pairs of the fast elementary cells $\mathbb{W}_2$ can be replaced by the fast 2D elementary cells $\mathbb{W}_4$ shown in Figure 4.15. The fastest version of WPT computing is shown in Figure 4.16c. It implements 8-point WPT based on the wavelet packet matrix $\mathbb{W}_8$ described as follows.

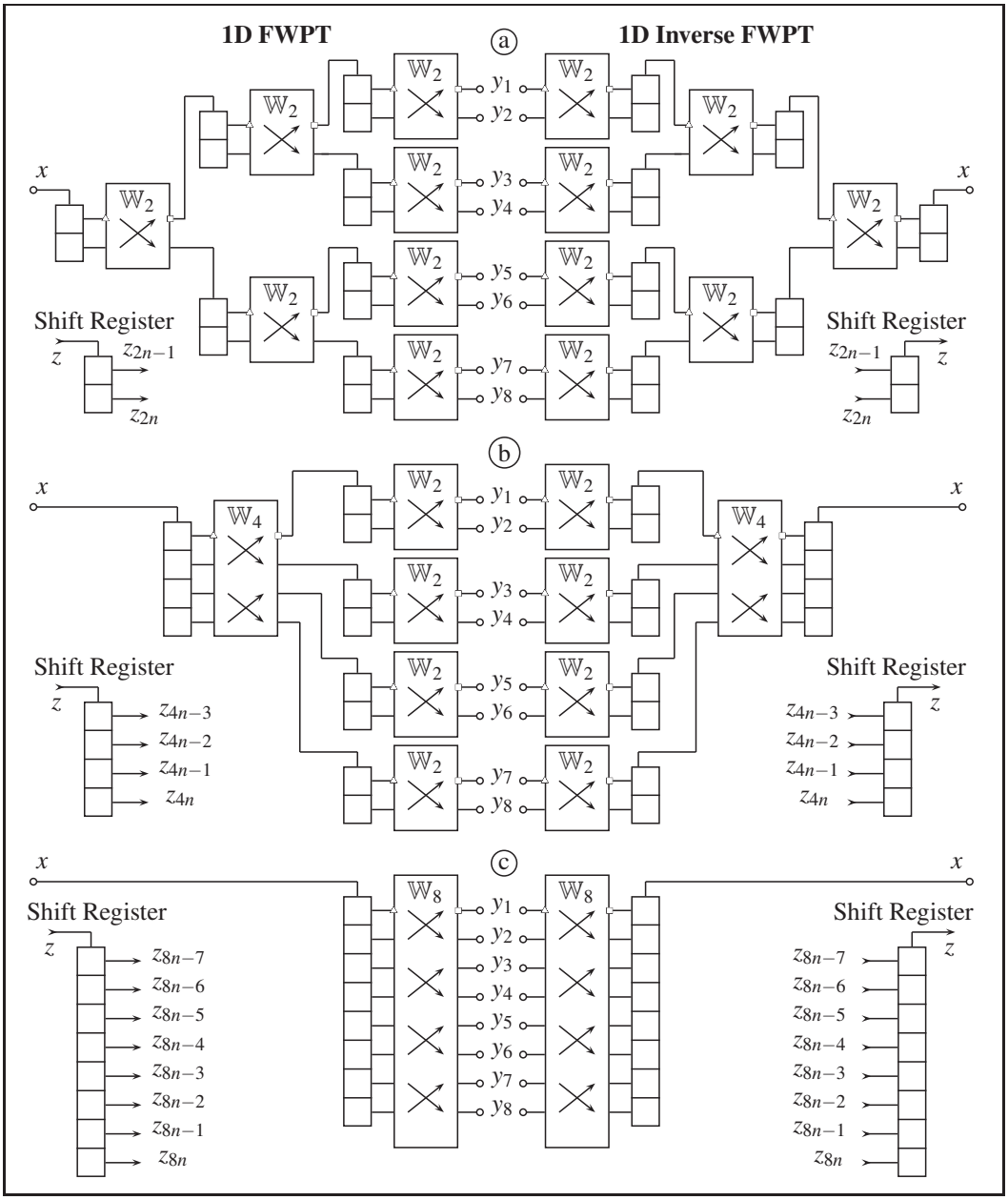

Figure 4.16 The hardware implementations of the one dimensional Fast Wavelet Packet Transform (1D FWPT) and one dimensional Inverse Fast Wavelet Packet Transform (1D IFWPT). Level of decomposition d=3.

Wavelet Packet Matrix $\mathbb{W}_8$

The matrix $\mathbb{W}_8$ is the basis for the 8-point Fast Wavelet Packet Transform (8-FWPT). The hardware implementation is shown on Figure 4.17.

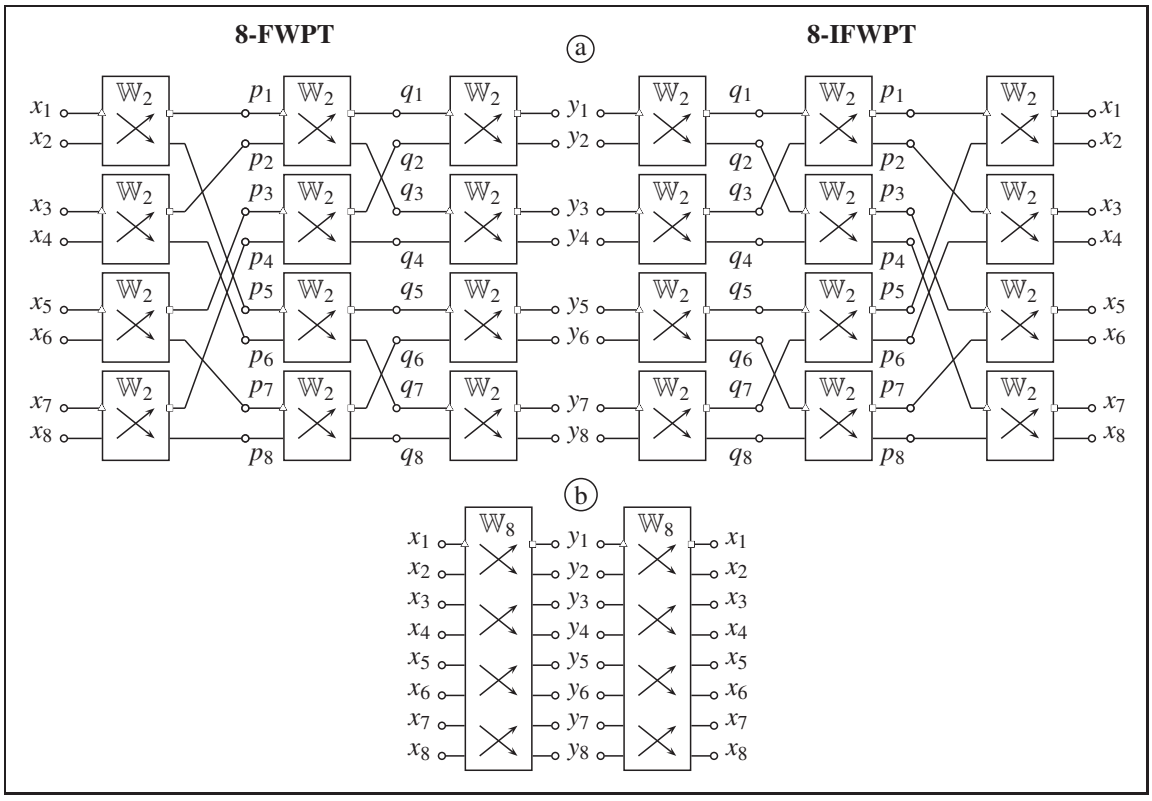

Figure 4.17 Eight-point Fast Wavelet Packet Transform (8-FWPT) and Inverse Fast Wavelet Packet Transform (8-IFWPT).

A set of following equations describes the application of the 8-point Fast Wavelet Packet Transform (8-FWPT):

$$\begin{aligned} y_1 &= \frac{1}{\sqrt{2}}(q_1+q_2) = \frac{1}{2}(p_1+p_2+p_3+p_4) = \\ &= \frac{1}{2\sqrt{2}}(x_1+x_2+x_3+x_4+x_5+x_6+x_7+x_8); \\ y_2 &= \frac{1}{\sqrt{2}}(q_1-q_2) = \frac{1}{2}(p_1+p_2-p_3-p_4) = \\ &= \frac{1}{2\sqrt{2}}(x_1+x_2+x_3+x_4-x_5-x_6-x_7-x_8); \end{aligned}$$

$$
\begin{aligned}
y_3 &= \frac{1}{\sqrt{2}}(q_3+q_4) = \frac{1}{2}(p_1-p_2+p_3-p_4) = \\
&= \frac{1}{2\sqrt{2}}(x_1+x_2-x_3-x_4+x_5+x_6-x_7-x_8); \\
y_4 &= \frac{1}{\sqrt{2}}(q_3-q_4) = \frac{1}{2}(p_1-p_2-p_3+p_4) = \\
&= \frac{1}{2\sqrt{2}}(x_1+x_2-x_3-x_4-x_5-x_6+x_7+x_8); \\
y_5 &= \frac{1}{\sqrt{2}}(q_5+q_6) = \frac{1}{2}(p_5+p_6+p_7+p_8) = \\
&= \frac{1}{2\sqrt{2}}(x_1-x_2+x_3-x_4+x_5-x_6+x_7-x_8); \\
y_6 &= \frac{1}{\sqrt{2}}(q_5-q_6) = \frac{1}{2}(p_5+p_6-p_7-p_8) = \\
&= \frac{1}{2\sqrt{2}}(x_1-x_2+x_3-x_4-x_5+x_6-x_7+x_8); \\
y_7 &= \frac{1}{\sqrt{2}}(q_7+q_8) = \frac{1}{2}(p_5-p_6+p_7-p_8) = \\
&= \frac{1}{2\sqrt{2}}(x_1-x_2-x_3+x_4+x_5-x_6-x_7+x_8); \\
y_8 &= \frac{1}{\sqrt{2}}(q_7-q_8) = \frac{1}{2}(p_5-p_6-p_7+p_8) = \\
&= \frac{1}{2\sqrt{2}}(x_1-x_2-x_3+x_4-x_5+x_6+x_7-x_8). \qquad (4.47)
\end{aligned}
$$

It represents the matrix $\mathbb{W}_8$ as follows:

$$\mathbb{W}_8 = \frac{1}{2\sqrt{2}}\mathbb{V}_8, \textit{ where } \mathbb{V}_4 = \begin{pmatrix} 1 & 1 & 1 & 1 & 1 & 1 & 1 & 1 \\ 1 & 1 & 1 & 1 & -1 & -1 & -1 & -1 \\ 1 & 1 & -1 & -1 & 1 & 1 & -1 & -1 \\ 1 & 1 & -1 & -1 & -1 & -1 & 1 & 1 \\ 1 & -1 & 1 & -1 & 1 & -1 & 1 & -1 \\ 1 & -1 & 1 & -1 & -1 & 1 & -1 & 1 \\ 1 & -1 & -1 & 1 & 1 & -1 & -1 & 1 \\ 1 & -1 & -1 & 1 & -1 & 1 & 1 & -1 \end{pmatrix}. \tag{4.48}$$

A set of following equations describes the application of the 8-point Inverse Fast Wavelet Packet Transform (8-IFWPT):

$$\begin{aligned}
x_1 &= \frac{1}{\sqrt{2}}(p_1 + p_5) = \frac{1}{2\sqrt{2}}(y_1 + y_2 + y_3 + y_4 + y_5 + y_6 + y_7 + y_8); \\
x_2 &= \frac{1}{\sqrt{2}}(p_1 - p_5) = \frac{1}{2\sqrt{2}}(y_1 + y_2 + y_3 + y_4 - y_5 - y_6 - y_7 - y_8); \\
x_3 &= \frac{1}{\sqrt{2}}(p_2 + p_6) = \frac{1}{2\sqrt{2}}(y_1 + y_2 - y_3 - y_4 + y_5 + y_6 - y_7 - y_8); \\
x_4 &= \frac{1}{\sqrt{2}}(p_2 - p_6) = \frac{1}{2\sqrt{2}}(y_1 + y_2 - y_3 - y_4 - y_5 - y_6 + y_7 + y_8); \\
x_5 &= \frac{1}{\sqrt{2}}(p_3 + p_7) = \frac{1}{2\sqrt{2}}(y_1 - y_2 + y_3 - y_4 + y_5 - y_6 + y_7 - y_8); \\
x_6 &= \frac{1}{\sqrt{2}}(p_3 - p_7) = \frac{1}{2\sqrt{2}}(y_1 - y_2 + y_3 - y_4 - y_5 + y_6 - y_7 + y_8); \\
x_7 &= \frac{1}{\sqrt{2}}(p_4 + p_8) = \frac{1}{2\sqrt{2}}(y_1 - y_2 - y_3 + y_4 + y_5 - y_6 - y_7 + y_8); \\
x_8 &= \frac{1}{\sqrt{2}}(p_4 - p_8) = \frac{1}{2\sqrt{2}}(y_1 - y_2 - y_3 + y_4 - y_5 + y_6 + y_7 - y_8).
\end{aligned} \tag{4.49}$$

It represents the inverse matrix $\mathbb{W}_8^{-1}$ as follows:

$$\mathbb{W}_8^{-1} = \mathbb{W}_8 = \frac{1}{2\sqrt{2}}\mathbb{V}_8, \textit{ where } \mathbb{V}_8 = \begin{pmatrix} 1 & 1 & 1 & 1 & 1 & 1 & 1 & 1 \\ 1 & 1 & 1 & 1 & -1 & -1 & -1 & -1 \\ 1 & 1 & -1 & -1 & 1 & 1 & -1 & -1 \\ 1 & 1 & -1 & -1 & -1 & -1 & 1 & 1 \\ 1 & -1 & 1 & -1 & 1 & -1 & 1 & -1 \\ 1 & -1 & 1 & -1 & -1 & 1 & -1 & 1 \\ 1 & -1 & -1 & 1 & 1 & -1 & -1 & 1 \\ 1 & -1 & -1 & 1 & -1 & 1 & 1 & -1 \end{pmatrix}. \quad (4.50)$$

One must note that the inverse matrix $\mathbb{W}_8^{-1}$ is equal to the matrix $\mathbb{W}_8$. It means that the same matrix can be used for the 8-point Fast Wavelet Packet Transform (8-FWPT) and Inverse Fast Wavelet Packet Transform (8-IFWPT).

Complexity of the N-point Fast WPT vs. the N-point FFT

Every stage of the N-point FWPT (see Figure 4.16a) or the N-point FFT (see Figure 4.18) requires $\frac{N}{2}$ applications of the fast elementary cell $\mathbb{W}_2$ or the 2-FFT butterfly accordingly.

Complete processing of N points of data requires $d = log_2 N$ decomposition levels or stages. Hence the total number of required cells or butterflies is $\frac{N}{2} log_2 N$. Complexities of the fast elementary cells $\mathbb{W}_2$, $\mathbb{V}_2$ and the 2-FFT butterfly are presented in Table 4.2.

Recall that the fast elementary cell $\mathbb{W}_2$ can be envisioned as the fast elementary cell $\mathbb{V}_2$ whose output is multiplied by $\frac{1}{\sqrt{2}}$ (see Figure 4.12). Replacement of the fast elementary cells $\mathbb{W}_2$ with

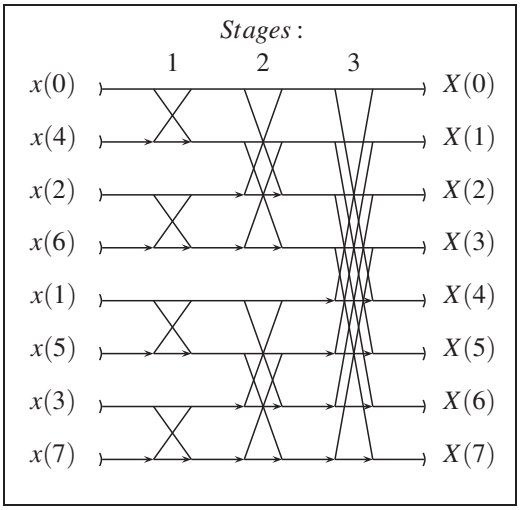

Figure 4.18 Eight-point
decimation-in-time FFT algorithm.

$\mathbb{V}_2$ in $d = log_2 N$ stages FWPT will require multiplication of an output by $\left(\frac{1}{\sqrt{2}}\right)^d = 2^{-\frac{d}{2}}$. In case $d = 2k$ is even, the multiplier $2^{-\frac{d}{2}} = 2^{-k}$ can be replaced by the shift register. In case $d = 2k+1$ is odd, the multiplier can be envisioned as the two multipliers $2^{-\frac{2k+1}{2}} = 2^{-k} \cdot \frac{1}{\sqrt{2}}$. Multiplication by 2^{-k} can be replaced by the shift register, however multiplication by $\frac{1}{\sqrt{2}}$ should be implemented. A total of N multipliers by $\frac{1}{\sqrt{2}}$ are required for the N-point FWPT in case $d = log_2 N$ is odd.

Complexities of the N-point Fast WPT and the N-point FFT are presented in Table 4.6.

Notation in Table 4.6 means that $\frac{N}{2} log_2 N(2 \oplus +1 \ominus) + \beta N \otimes = (2N log_2 N) \oplus +(\frac{N}{2} log_2 N) \ominus +(\beta N) \otimes$.

Table 4.6 Complexity of the N-point FWPT vs. the N-point FFT in terms of real operations

Input numbers	**FWPT**	**FFT**
Real	$\frac{N}{2} log_2 N(2 \oplus +1 \ominus) + \beta N \otimes$	n/a
Complex	$\frac{N}{2} log_2 N(4 \oplus +2 \ominus) + 2\beta N \otimes$	$\frac{N}{2} log_2 N(6 \oplus +4 \otimes +3 \ominus)$
	$where\ \beta = \begin{cases} 0\ if\ d = log_2 N\ is\ even \\ 1\ if\ d = log_2 N\ is\ odd \end{cases}$	

4.7.2 Fast Discrete Wavelet Transform (FDWT)

Fast Discrete Wavelet Transform (FDWT) based on the Haar wavelet is referred sometimes as a Haar Transform. The Haar Transform employs a Haar Matrix $\mathbb{H}_K$ order K, Pratt (1978). Four point Fast Discrete Wavelet Transform (4-FDWT) shown in Figure 4.19 represents the Haar matrix $\mathbb{H}_4$.

Fast Wavelet Packet Transform (FWPT) or Haar Transform can be envisioned as an application of the Haar Matrix $\mathbb{H}_K$ of order K towards the signal vector $\overline{X}$ as follows:

$$\overline{C} = \mathbb{H}_K \overline{X}, \tag{4.51}$$

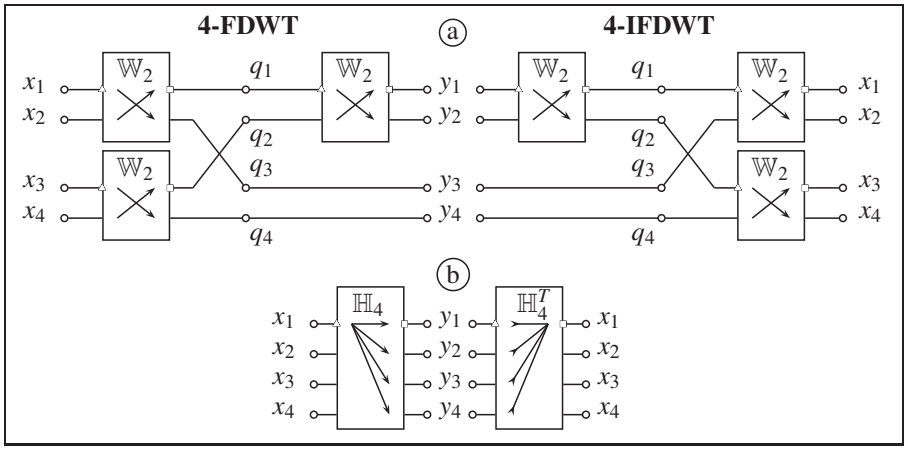

Figure 4.19 Four-point Fast Discrete Wavelet Transform (4-FDWT) and Inverse Fast Discrete Wavelet Transform (4-IFDWT).

For the case $K = 4$, the Haar matrix $\mathbb{H}_4$ can be derived using Figure 4.19:

$$\begin{aligned} y_1 &= \frac{1}{\sqrt{2}}(q_1+q_2) = \frac{1}{2}(x_1+x_2+x_3+x_4); \\ y_2 &= \frac{1}{\sqrt{2}}(q_1-q_2) = \frac{1}{2}(x_1+x_2-x_3-x_4); \\ y_3 &= q_3 = \frac{1}{\sqrt{2}}(x_1-x_2+0\cdot x_3+0\cdot x_4); \\ y_4 &= q_4 = \frac{1}{\sqrt{2}}(0\cdot x_1+0\cdot x_2+x_3-x_4). \end{aligned} \tag{4.52}$$

$$\mathbb{H}_4 = \frac{1}{2}\begin{pmatrix} 1 & 1 & 1 & 1 \\ 1 & 1 & -1 & -1 \\ \sqrt{2} & -\sqrt{2} & 0 & 0 \\ 0 & 0 & \sqrt{2} & -\sqrt{2} \end{pmatrix} \tag{4.53}$$

The Inverse Fast Wavelet Packet Transform (FWPT) or Inverse Haar Transform can be envisioned as application of the Inverse Haar Matrix $\mathbb{H}_K^{-1}$ of order K towards the wavelet coefficients vector $\overline{S}$ as follows:

$$\overline{X} = \mathbb{H}_K^{-1}\overline{S}, \tag{4.54}$$

For the case $K = 4$, the Inverse Haar matrix $\mathbb{H}_4^{-1}$ can be derived using Figure 4.19:

$$\begin{aligned}
x_1 &= \frac{1}{\sqrt{2}}(q_1+q_3) = \frac{1}{\sqrt{2}}\left(\frac{1}{\sqrt{2}}(y_1+y_2)+y_3+0\cdot y_4\right);\\
x_2 &= \frac{1}{\sqrt{2}}(q_1-q_3) = \frac{1}{\sqrt{2}}\left(\frac{1}{\sqrt{2}}(y_1+y_2)-y_3+0\cdot y_4\right);\\
x_3 &= \frac{1}{\sqrt{2}}(q_2+q_4) = \frac{1}{\sqrt{2}}\left(\frac{1}{\sqrt{2}}(y_1-y_2)+0\cdot y_3+y_4\right);\\
x_4 &= \frac{1}{\sqrt{2}}(q_2-q_4) = \frac{1}{\sqrt{2}}\left(\frac{1}{\sqrt{2}}(y_1-y_2)+0\cdot y_3-y_4\right).
\end{aligned} \tag{4.55}$$

$$\mathbb{H}_4^{-1} = \frac{1}{2}\begin{pmatrix} 1 & 1 & \sqrt{2} & 0 \\ 1 & 1 & -\sqrt{2} & 0 \\ 1 & -1 & 0 & \sqrt{2} \\ 1 & -1 & 0 & -\sqrt{2} \end{pmatrix} = \mathbb{H}_4^T. \tag{4.56}$$

Unlike the wavelet packet matrix $\mathbb{W}_4$, the Haar matrix cannot be used for both signal analysis and synthesis. However, the matrix used for the purpose of FDWT synthesis is just a transpose matrix $\mathbb{H}_4^T$.

Figure 4.20 presents different hardware implementations of the one dimensional Discrete Wavelet Transform shown in Figure 4.3. Figure 4.20a employs the fast elementary cells $\mathbb{W}_2$ shown on Figure 4.12. Rapidity of DWT calculation can be augmented by applying techniques of parallel computing instead of serial one. Figure 4.20b illustrates how a pair of the fast elementary cells $\mathbb{W}_2$ can be replaced by the Haar matrix $\mathbb{H}_4$ shown on Figure 4.19. The fastest version of DWT computing is shown in Figure 4.20c. It implements an 8-point DWT based on the Haar matrix $\mathbb{H}_8$.

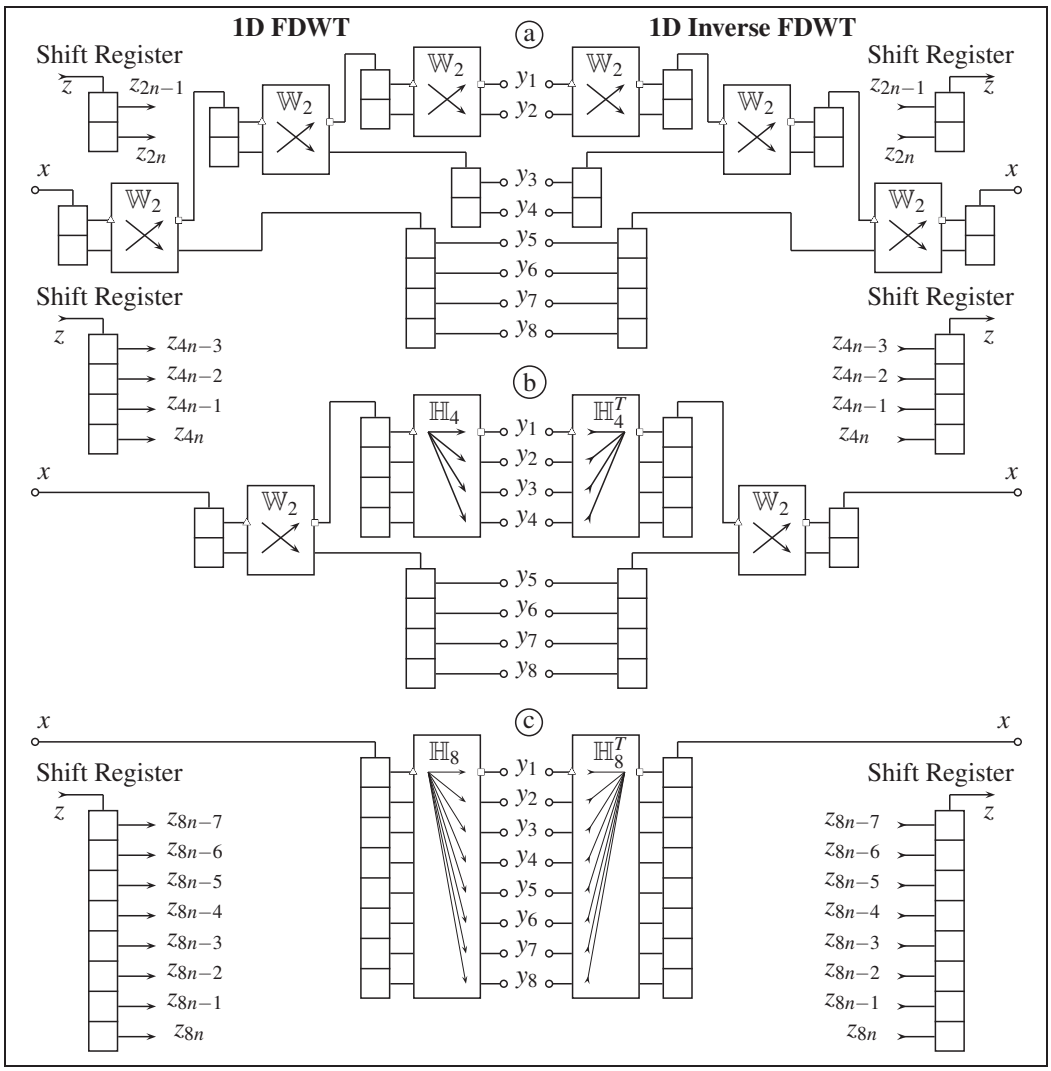

Figure 4.20 The hardware implementations of the one dimensional Fast Discrete Wavelet Transform (1D FDWT) and one dimensional Inverse Fast Wavelet Packet Transform (1D IFDWT). Level of decomposition d=3.

Haar Matrix $\mathbb{H}_8$

The Haar matrix $\mathbb{H}_8$ is the basis for the 8-point DWT. The hardware implementation is shown on Figure 4.21.

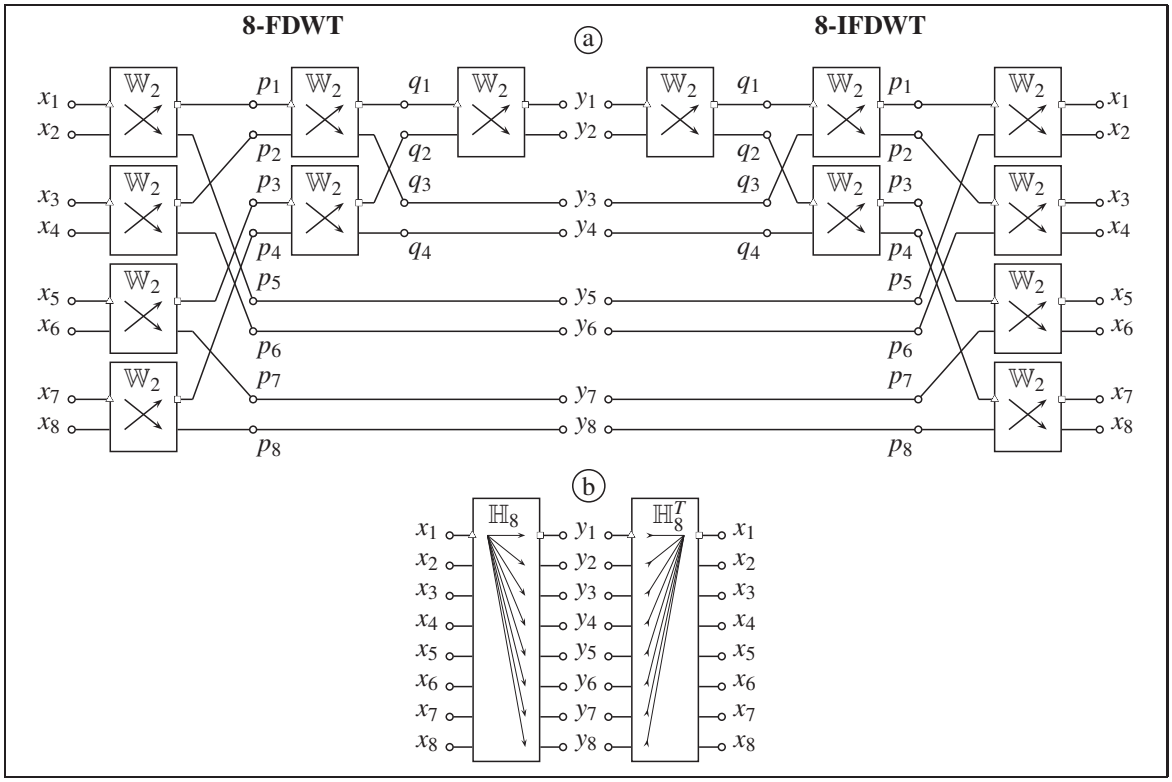

Figure 4.21 Eight-point Fast Discrete Wavelet Transform (8-FDWT) and Inverse Fast Discrete Wavelet Transform (8-IFDWT).

A set of following equations describes the application of the 8-point Fast Discrete Wavelet Transform (8-FDWT):

$$\begin{aligned}
y_1 &= \frac{1}{\sqrt{2}}(q_1+q_2) = \frac{1}{2}(p_1+p_2+p_3+p_4) = \\
&= \frac{1}{2\sqrt{2}}(x_1+x_2+x_3+x_4+x_5+x_6+x_7+x_8); \\
y_2 &= \frac{1}{\sqrt{2}}(q_1-q_2) = \frac{1}{2}(p_1+p_2-p_3-p_4) = \\
&= \frac{1}{2\sqrt{2}}(x_1+x_2+x_3+x_4-x_5-x_6-x_7-x_8); \\
y_3 &= q_3 = \frac{1}{\sqrt{2}}(p_1-p_2) = \\
&= \frac{1}{2}(x_1+x_2-x_3-x_4+0\cdot x_5+0\cdot x_6+0\cdot x_7+0\cdot x_8);
\end{aligned}$$

$$\begin{aligned}
y_4 &= q_4 = \frac{1}{\sqrt{2}}(p_3-p_4) = \\
&= \frac{1}{2}(0\cdot x_1+0\cdot x_2+0\cdot x_3+0\cdot x_4+x_5+x_6-x_7-x_8); \\
y_5 &= p_5 = \frac{1}{\sqrt{2}}(x_1-x_2+0\cdot x_3+0\cdot x_4+0\cdot x_5+0\cdot x_6+0\cdot x_7+0\cdot x_8); \\
y_6 &= p_6 = \frac{1}{\sqrt{2}}(0\cdot x_1+0\cdot x_2+x_3-x_4+0\cdot x_5+0\cdot x_6+0\cdot x_7+0\cdot x_8); \\
y_7 &= p_7 = \frac{1}{\sqrt{2}}(0\cdot x_1+0\cdot x_2+0\cdot x_3+0\cdot x_4+x_5-x_6+0\cdot x_7+0\cdot x_8); \\
y_8 &= p_8 = \frac{1}{\sqrt{2}}(0\cdot x_1+0\cdot x_2+0\cdot x_3+0\cdot x_4+0\cdot x_5+0\cdot x_6+x_7-x_8).
\end{aligned} \tag{4.57}$$

It represents the Haar matrix $\mathbb{H}_8$ as follows:

$$\mathbb{H}_8 = \frac{1}{2\sqrt{2}} \begin{pmatrix} 1 & 1 & 1 & 1 & 1 & 1 & 1 & 1 \\ 1 & 1 & 1 & 1 & -1 & -1 & -1 & -1 \\ \sqrt{2} & \sqrt{2} & -\sqrt{2} & -\sqrt{2} & 0 & 0 & 0 & 0 \\ 0 & 0 & 0 & 0 & \sqrt{2} & \sqrt{2} & -\sqrt{2} & -\sqrt{2} \\ 2 & -2 & 0 & 0 & 0 & 0 & 0 & 0 \\ 0 & 0 & 2 & -2 & 0 & 0 & 0 & 0 \\ 0 & 0 & 0 & 0 & 2 & -2 & 0 & 0 \\ 0 & 0 & 0 & 0 & 0 & 0 & 2 & -2 \end{pmatrix}. \tag{4.58}$$

A set of following equations describes the application of the 8-point Inverse Fast Discrete Wavelet Transform (8-IFDWT):

$$
\begin{aligned}
x_1 &= \frac{1}{\sqrt{2}}(p_1+p_5) = \frac{1}{2}(q_1+q_3+\sqrt{2}\cdot y_5) = \\
&= \frac{1}{2\sqrt{2}}(y_1+y_2+\sqrt{2}\cdot y_3+0\cdot y_4+2\cdot y_5+0\cdot y_6+0\cdot y_7+0\cdot y_8); \\
x_2 &= \frac{1}{\sqrt{2}}(p_1-p_5) = \frac{1}{2}(q_1+q_3-\sqrt{2}\cdot y_5) = \\
&= \frac{1}{2\sqrt{2}}(y_1+y_2+\sqrt{2}\cdot y_3+0\cdot y_4-2\cdot y_5+0\cdot y_6+0\cdot y_7+0\cdot y_8); \\
x_3 &= \frac{1}{\sqrt{2}}(p_2+p_6) = \frac{1}{2}(q_1-q_3+\sqrt{2}\cdot y_6) = \\
&= \frac{1}{2\sqrt{2}}(y_1+y_2-\sqrt{2}\cdot y_3+0\cdot y_4+0\cdot y_5+2\cdot y_6+0\cdot y_7+0\cdot y_8); \\
x_4 &= \frac{1}{\sqrt{2}}(p_2-p_6) = \frac{1}{2}(q_1-q_3-\sqrt{2}\cdot y_6) = \\
&= \frac{1}{2\sqrt{2}}(y_1+y_2-\sqrt{2}\cdot y_3+0\cdot y_4+0\cdot y_5-2\cdot y_6+0\cdot y_7+0\cdot y_8); \\
x_5 &= \frac{1}{\sqrt{2}}(p_3+p_7) = \frac{1}{2}(q_2+q_4+\sqrt{2}\cdot y_7) = \\
&= \frac{1}{2\sqrt{2}}(y_1-y_2+0\cdot y_3+\sqrt{2}\cdot y_4+0\cdot y_5+0\cdot y_6+2\cdot y_7+0\cdot y_8); \\
x_6 &= \frac{1}{\sqrt{2}}(p_3-p_7) = \frac{1}{2}(q_2+q_4-\sqrt{2}\cdot y_7) = \\
&= \frac{1}{2\sqrt{2}}(y_1-y_2+0\cdot y_3+\sqrt{2}\cdot y_4+0\cdot y_5+0\cdot y_6-2\cdot y_7+0\cdot y_8); \\
x_7 &= \frac{1}{\sqrt{2}}(p_4+p_8) = \frac{1}{2}(q_2-q_4+\sqrt{2}\cdot y_8) = \\
&= \frac{1}{2\sqrt{2}}(y_1-y_2+0\cdot y_3-\sqrt{2}\cdot y_4+0\cdot y_5+0\cdot y_6+0\cdot y_7+2\cdot y_8); \\
x_8 &= \frac{1}{\sqrt{2}}(p_4-p_8) = \frac{1}{2}(q_2-q_4-\sqrt{2}\cdot y_8) = \\
&= \frac{1}{2\sqrt{2}}(y_1-y_2+0\cdot y_3-\sqrt{2}\cdot y_4+0\cdot y_5+0\cdot y_6+0\cdot y_7-2\cdot y_8).
\end{aligned}
\tag{4.59}
$$

It represents the inverse Haar matrix $\mathbb{H}_8^{-1}$ as follows:

$$\mathbb{H}_8^{-1} = \mathbb{H}_8^T = \frac{1}{2\sqrt{2}} \begin{pmatrix} 1 & 1 & \sqrt{2} & 0 & 2 & 0 & 0 & 0 \\ 1 & 1 & \sqrt{2} & 0 & -2 & 0 & 0 & 0 \\ 1 & 1 & -\sqrt{2} & 0 & 0 & 2 & 0 & 0 \\ 1 & 1 & -\sqrt{2} & 0 & 0 & -2 & 0 & 0 \\ 1 & -1 & 0 & \sqrt{2} & 0 & 0 & 2 & 0 \\ 1 & -1 & 0 & \sqrt{2} & 0 & 0 & -2 & 0 \\ 1 & -1 & 0 & -\sqrt{2} & 0 & 0 & 0 & 2 \\ 1 & -1 & 0 & -\sqrt{2} & 0 & 0 & 0 & -2 \end{pmatrix}. \tag{4.60}$$

One must note that the inverse Haar matrix $\mathbb{H}_8^{-1}$ is equal to the the transpose Haar matrix $\mathbb{H}_8^T$.

4.8 Conclusion

Conception of data compression and denoising using wavelet coefficient thresholding has been described in this chapter. Introducing a wavelet tree structure has served to represent the wavelet analysis/synthesis in a hierarchical form. Application of energy constraints on wavelet coefficients has optimized the wavelet tree, which is called the best wavelet tree. Some properties of orthogonality of wavelet matrices were investigated in this chapter. High complexity of computation often limits the application of wavelet analysis. We developed the fast wavelet algorithms that are being protected by the patent, Sabelkin (2011). Proposed fast wavelet analysis algorithms were compared to the conventional Fast Fourier Transform (FFT). The Haar matrix was analyzed as the matrix used in Fast Discrete Wavelet Transform (FDWT).

CHAPTER 5

ANALYTICAL EVALUATION OF TOMAS FOR STILL IMAGE TRANSMISSION

5.1 Introduction

In this chapter we propose an analytical evaluation of the data Transmission oriented on the Object, communication Media, Application, and State of communication Systems (TOMAS). The transmission Object is a still grayscale image. The communication Media is an Additive White Gaussian Noise (AWGN) channel. The Application uses Mean Square Error (MSE) to evaluate quality of a received image. The transmission system structure is shown in Figure 5.1. In this chapter we show how knowledge of communication media parameters can improve system performance in terms of received image quality.

5.2 Structure of the still image transmission system

The typical structure of the transform based still image transmission system is shown in Figure 5.1.

A grayscale image is presented by the following matrix:

$$\mathbf{X} = \begin{pmatrix} x_{0,0} & x_{0,1} & x_{0,2} & x_{0,3} & \cdots & x_{0,M-2} & x_{0,M-1} \\ x_{1,0} & x_{1,1} & x_{1,2} & x_{1,3} & \cdots & x_{1,M-2} & x_{1,M-1} \\ x_{2,0} & x_{2,1} & x_{2,2} & x_{2,3} & \cdots & x_{2,M-2} & x_{2,M-1} \\ x_{3,0} & x_{3,1} & x_{3,2} & x_{3,3} & \cdots & x_{3,M-2} & x_{3,M-1} \\ \vdots & \vdots & \vdots & \vdots & \ddots & \vdots & \vdots \\ x_{N-2,0} & x_{N-2,1} & x_{N-2,2} & x_{N-2,3} & \cdots & x_{N-2,M-2} & x_{N-2,M-1} \\ x_{N-1,0} & x_{N-1,1} & x_{N-1,2} & x_{N-1,3} & \cdots & x_{N-1,M-2} & x_{N-1,M-1} \end{pmatrix}, \tag{5.1}$$

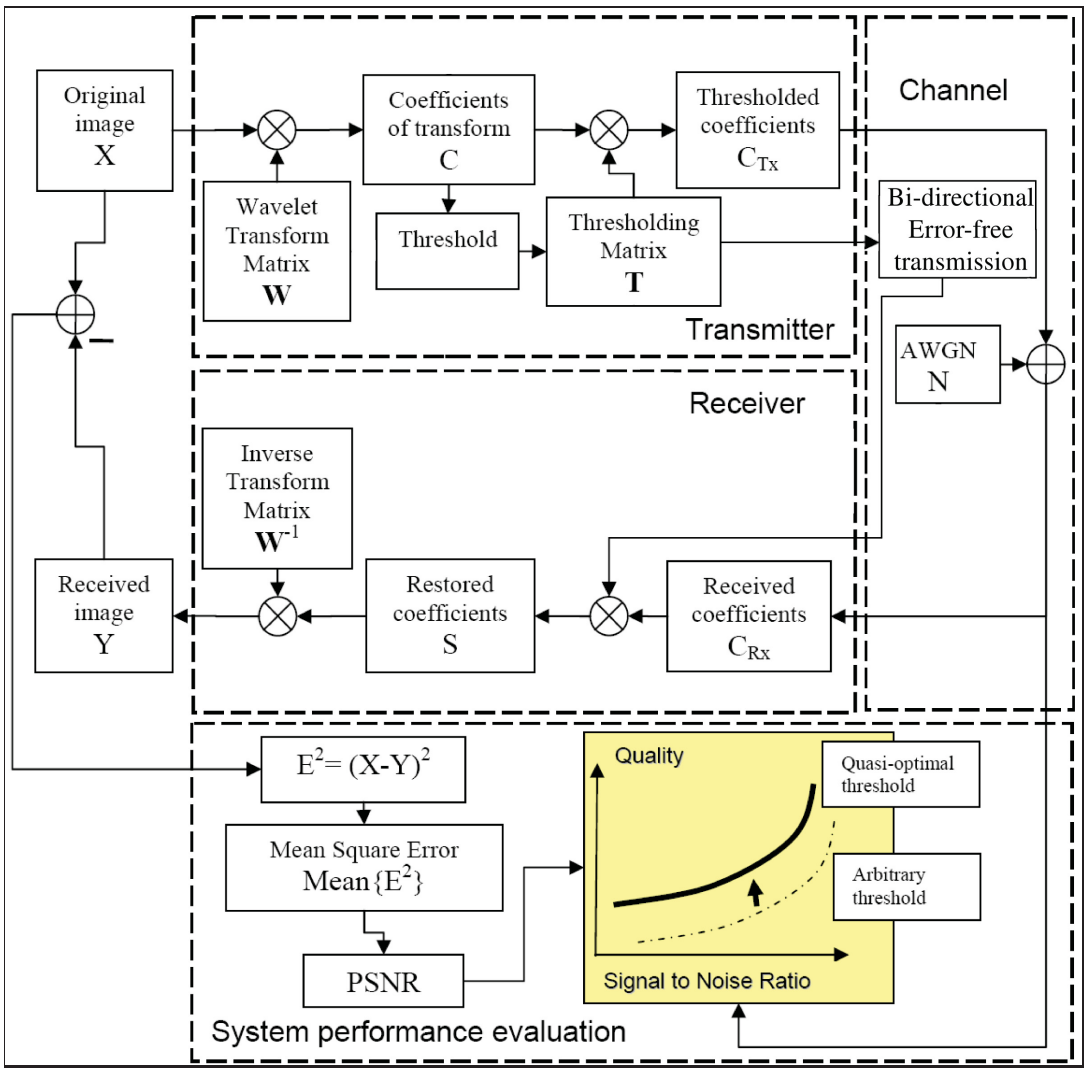

Figure 5.1 The transform-based still image transmission system.

where N is a number of image rows and M is a number of image columns. Elements of the matrix $x_{i,j}$ ($i = 0 \ldots N-1$, $j = 0 \ldots M-1$) represent luminosities of image pixels.

For processing by the image transmission system, the image matrix $\mathbf{X}$ has to be converted into the image vector X as described by following expression:

$$X = \mathscr{R}(\mathbf{X}), \tag{5.2}$$

where the operator $\mathscr{R}$ is a matrix-to-vector conversion operator, which represents an element run shown on Figure 5.2.

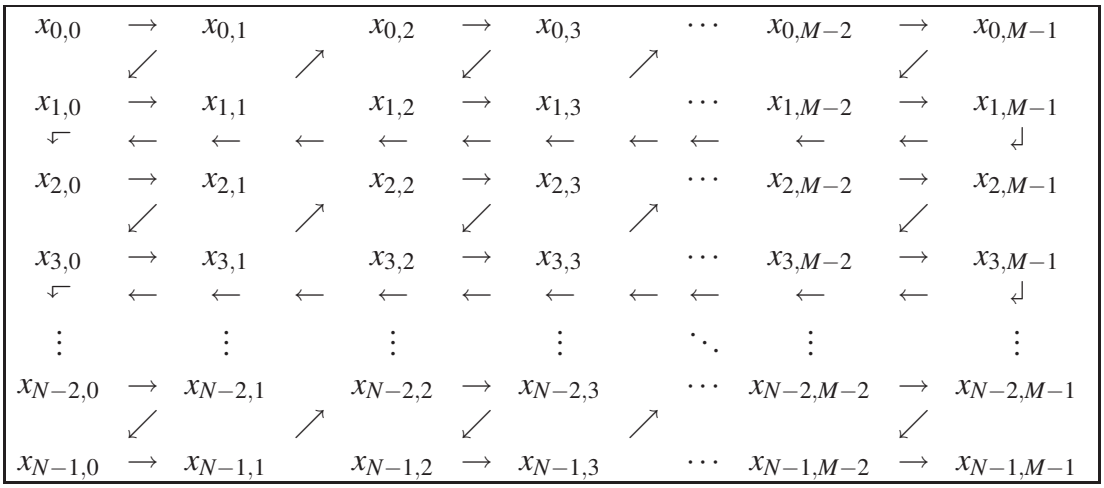

Figure 5.2 An element run for conversion of an image matrix into an image vector.

After matrix-to-vector conversion, the image matrix from Equation 5.1 becomes the image vector X, size $K = N \cdot M$, which has the following look:

$$
\begin{aligned}
X^T = \; (\;\; & x_{0,0}\, x_{0,1}\, x_{1,0}\, x_{1,1}\, x_{0,2}\, x_{0,3}\, x_{1,2}\, x_{1,3} \ldots x_{0,M-2}\, x_{0,M-1}\, x_{1,M-2}\, x_{1,M-1} \\
& x_{2,0}\, x_{2,1}\, x_{3,0}\, x_{3,1}\, x_{2,2}\, x_{2,3}\, x_{3,2}\, x_{3,3} \ldots x_{2,M-2}\, x_{2,M-1}\, x_{2,M-2}\, x_{2,M-1} \\
& x_{N-2,0}\, x_{N-2,1}\, x_{N-1,0}\, x_{N-1,1}\, x_{N-2,2}\, x_{N-2,3}\, x_{N-1,2}\, x_{N-1,3} \cdots \\
& \ldots x_{N-2,M-2}\, x_{N-2,M-1}\, x_{N-1,M-2}\, x_{N-1,M-1} \;).
\end{aligned}
\tag{5.3}
$$

The transform matrix **W** decomposes the original image vector X into the transform coefficient vector C as follows:

$$\begin{pmatrix} c_0 \\ c_1 \\ c_2 \\ \vdots \\ c_K \end{pmatrix} = \begin{pmatrix} w_{0,0} & w_{0,1} & w_{0,2} & \cdots & w_{0,K-1} \\ w_{1,0} & w_{1,1} & w_{1,2} & \cdots & w_{1,K-1} \\ w_{2,0} & w_{2,1} & w_{2,2} & \cdots & w_{2,K-1} \\ \vdots & \vdots & \vdots & \ddots & \vdots \\ w_{K-1,0} & w_{K-1,1} & w_{K-1,2} & \cdots & w_{K-1,K-1} \end{pmatrix} \begin{pmatrix} x_{0,0} \\ x_{0,1} \\ x_{1,0} \\ \vdots \\ x_{N-1,M-1} \end{pmatrix} \tag{5.4}$$

Equation 5.4 in matrix form is:

$$C = \mathbf{W} \cdot X. \tag{5.5}$$

The operation of image decomposition is followed by the operation of coefficient thresholding. Both operations together serve to reduce redundancy of the original image data, and improve spectral efficiency of the still image transmission system.

The operation of coefficient thresholding is represented by multiplication of the thresholding matrix **T** and the transform coefficient vector C as follows:

$$C_{Tx} = \mathbf{T} \cdot C = \mathbf{T} \cdot \mathbf{W} \cdot X; \tag{5.6}$$

The thresholding matrix $\mathbf{T}$ is a linear matrix with diagonal elements that are functions of the transform coefficient vector C and the threshold τ:

$$\mathbf{T} = \begin{pmatrix} t_0 & 0 & 0 & \cdots & 0 \\ 0 & t_1 & 0 & \cdots & 0 \\ 0 & 0 & t_2 & \cdots & 0 \\ \vdots & \vdots & \vdots & \ddots & \vdots \\ 0 & 0 & 0 & \cdots & t_{K-1} \end{pmatrix}, \; where \; t_i = \begin{cases} 0, \; |c_i| \leq \tau \\ 1, \; |c_i| > \tau \end{cases}. \tag{5.7}$$

Assume that the thresholding matrix $\mathbf{T}$ is provided to the transmitter without errors.

The thresholded coefficient vector ${C_{Tx}}^T = \left(c_{Tx_0} \; c_{Tx_1} \ldots c_{Tx_{K-1}}\right)$ is than transmitted over the AWGN channel. Considering the additive nature of the communication channel, the vector of received coefficients ${C_{Rx}}^T = \left(c_{Rx_0} \; c_{Rx_1} \ldots c_{Rx_{K-1}}\right)$ is represented as a summation of the transmitted coefficient vector C_{Tx} and the vector of noise samples $N^T = (n_0 \; n_1 \ldots n_{K-1})$:

$$C_{Rx} = C_{Tx} + N = \mathbf{T} \cdot C + N = \mathbf{T} \cdot \mathbf{W} \cdot X + N; \tag{5.8}$$

Each of noise samples n_0, n_1, $\ldots n_{K-1}$ is represented by a random variable with a Gaussian probability distribution function.

A product of the thresholding matrix $\mathbf{T}$ and the received coefficient vector C_{Rx} represents the vector of restored coefficients $S^T = (s_0 \; s_1 \ldots s_{K-1})$ as follows:

$$S = \mathbf{T} \cdot C_{Rx} = \mathbf{T} \cdot (\mathbf{T} \cdot C + N) = \mathbf{T} \cdot (\mathbf{T} \cdot \mathbf{W} \cdot X + N). \tag{5.9}$$

The vector of received image Y is a product of the inverse transform matrix $\mathbf{W}^{-1}$ and the vector of restored coefficients S as follows:

$$Y = \mathbf{W}^{-1} \cdot S = \mathbf{W}^{-1} \cdot (\mathbf{T} \cdot (\mathbf{T} \cdot C + N)) = \mathbf{W}^{-1} \cdot (\mathbf{T} \cdot (\mathbf{T} \cdot \mathbf{W} \cdot X + N)). \tag{5.10}$$

The received image vector Y is converted into the received image matrix $\mathbf{Y}$ as described by the following expression:

$$\mathbf{X} = \mathscr{R}^{-1}(X), \tag{5.11}$$

where the operator $\mathscr{R}^{-1}$ is a vector-to-matrix conversion operator, which represents an element run shown in Figure 5.3.

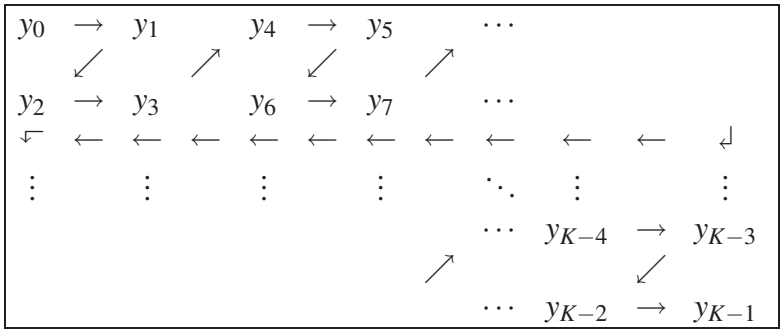

Figure 5.3 An element run for conversion of the image vector into the image matrix.

After vector-to-matrix conversion, the received image vector Y from Equation 5.10 becomes the image matrix $\mathbf{Y}$, size $N \times M$ pixels. The received image matrix $\mathbf{Y}$ has the following look:

$$\mathbf{Y} = \begin{pmatrix} y_0 & y_1 & y_4 & y_5 & \cdots & & \\ y_2 & y_3 & y_6 & y_7 & \cdots & & \\ \vdots & \vdots & \vdots & \vdots & \ddots & \vdots & \vdots \\ & & & & \cdots & y_{K-4} & y_{K-3} \\ & & & & \cdots & y_{K-2} & y_{K-1} \end{pmatrix}. \tag{5.12}$$

5.3 Properties of the transform matrix W

The transform matrix $\mathbf{W}$, which we will use for the still image communication system, has several particular properties described below.

5.3.1 Property 1. Involution: $\mathbf{W} = \mathbf{W}^{-1}$

Consider a scenario when no thresholding and transmission are applied to the original transform coefficients C. The restored transform coefficients S are equal to the original transform coefficients C. This is the case of $S = C = \mathbf{W} \cdot X$. The original transform coefficients C are not corrupted. Hence, the received image vector should be the same as the original one ($Y = X$). From Equation 5.10 we develop the following expression:

$$Y = \mathbf{W}^{-1} \cdot S = \mathbf{W}^{-1} \cdot \mathbf{W} \cdot X; \tag{5.13}$$

$X = \mathbf{W}^{-1} \cdot \mathbf{W} \cdot X$ only if $\mathbf{W}^{-1} \cdot \mathbf{W} = \mathbf{I}$ (identity matrix).

We have the further property that $\mathbf{W} = \mathbf{W}^{-1}$. It was analyzed in Chapter 4 for the case of 2-by-2 ($\mathbf{W_2}$). And the property of the transform matrix 4-by-4 ($\mathbf{W_4}$) is proved in Appendix I.

According to definition, a matrix that is its own inverse, i.e., $\mathbf{A} = \mathbf{A}^{-1}$ and $\mathbf{A}^2 = \mathbf{I}$, is called an **involution**.

5.3.2 Property 2. $\mathbf{W} = \mathbf{W}^T$

The transform matrix $\mathbf{W}$ is symmetric, hence $\mathbf{W} = \mathbf{W}^T$.

5.3.3 Property 3. $\mathbf{W} \cdot \mathbf{W} = \mathbf{I}$

The third property of the transform matrix $\mathbf{W}$ is derived from the first involution property.

$$\mathbf{W} = \mathbf{W}^{-1}, \Rightarrow \mathbf{W} \cdot \mathbf{W} = \mathbf{W}^{-1} \cdot \mathbf{W}, \Rightarrow \mathbf{W} \cdot \mathbf{W} = \mathbf{I}. \tag{5.14}$$

5.4 Properties of the thresholding matrix T

Recall that the thresholding matrix $\mathbf{T}$ is defined in Equation 5.7 in following manner:

$$\mathbf{T} = \begin{pmatrix} t_0 & 0 & 0 & \cdots & 0 \\ 0 & t_1 & 0 & \cdots & 0 \\ 0 & 0 & t_2 & \cdots & 0 \\ \vdots & \vdots & \vdots & \ddots & \vdots \\ 0 & 0 & 0 & \cdots & t_{K-1} \end{pmatrix}, \text{ where } t_i = \begin{cases} 0, & |c_i| \leq \tau \\ 1, & |c_i| > \tau \end{cases}, \tag{5.15}$$

where c_i is the transform coefficient and τ is the threshold value.

The thresholding matrix $\mathbf{T}$ has several properties described below.

5.4.1 Property 1. $\mathbf{T} \cdot \mathbf{T} = \mathbf{T}$

$$\mathbf{T} \cdot \mathbf{T} = \begin{pmatrix} t_0 & 0 & 0 & \cdots & 0 \\ 0 & t_1 & 0 & \cdots & 0 \\ 0 & 0 & t_2 & \cdots & 0 \\ \vdots & \vdots & \vdots & \ddots & \vdots \\ 0 & 0 & 0 & \cdots & t_{K-1} \end{pmatrix} \begin{pmatrix} t_0 & 0 & 0 & \cdots & 0 \\ 0 & t_1 & 0 & \cdots & 0 \\ 0 & 0 & t_2 & \cdots & 0 \\ \vdots & \vdots & \vdots & \ddots & \vdots \\ 0 & 0 & 0 & \cdots & t_{K-1} \end{pmatrix} =$$

$$= \begin{pmatrix} t_0^2 & 0 & 0 & \cdots & 0 \\ 0 & t_1^2 & 0 & \cdots & 0 \\ 0 & 0 & t_2^2 & \cdots & 0 \\ \vdots & \vdots & \vdots & \ddots & \vdots \\ 0 & 0 & 0 & \cdots & t_{K-1}^2 \end{pmatrix}. \tag{5.16}$$

Hence, $t_i^2 = t_i \cdot t_i$ can also accept either value "0" or "1". Therefore, $\mathbf{T} \cdot \mathbf{T} = \mathbf{T}$.

5.4.2 Property 2. $\mathbf{T} = \mathbf{T}^T$

The thresholding matrix T is symmetric, hence $\mathbf{T} = \mathbf{T}^T$.

5.5 Error between the original and received images

The original and received images can be easily converted from the matrix form to the vector one using the operator $\mathscr{R}$, which represents an element run shown in Figure 5.2.

Backward conversion of the original and received images from the vector form to the matrix one can be achieved by the operator $\mathscr{R}^{-1}$, which represents an element run shown in Figure 5.3.

From now on we will operate with the vector forms of the the original and received images.

An error between the original and received images can be calculated as follows:

$$E = X - Y, \tag{5.17}$$

where $E^T = (e_0\ e_1 \ldots e_{K-1})$ is the error vector.

Multiplication of both parts of Equation 5.5 by the inverse matrix $\mathbf{W}^{-1}$ gives:

$$C = \mathbf{W} \cdot X, \Rightarrow\ \mathbf{W}^{-1} \cdot C = \mathbf{W}^{-1} \cdot \mathbf{W} \cdot X, \Rightarrow\ \mathbf{W}^{-1} \cdot C = \mathbf{I} \cdot X. \tag{5.18}$$

The above equation can be developed further using the first property of the transform matrix ($\mathbf{W}^{-1} = \mathbf{W}$):

$$\mathbf{W}^{-1} \cdot C = \mathbf{I} \cdot X, \Rightarrow\ X = \mathbf{W} \cdot C. \tag{5.19}$$

Replace X and Y in Equation 5.17 for the error E with the values from Equation 5.19 and Equation 5.10 accordingly:

$$\begin{aligned} E &= X - Y = \mathbf{W} \cdot C - \mathbf{W}^{-1} \cdot (\mathbf{T} \cdot (\mathbf{T} \cdot C + N)) = \\ &= \mathbf{W} \cdot C - \mathbf{W}^{-1} \cdot \mathbf{T} \cdot \mathbf{T} \cdot C - \mathbf{W}^{-1} \cdot \mathbf{T} \cdot \mathbf{T} \cdot N. \end{aligned} \tag{5.20}$$

Use of the first property of the thresholding matrix ($\mathbf{T} \cdot \mathbf{T} = \mathbf{T}$), and the first property of the transform matrix ($\mathbf{W}^{-1} = \mathbf{W}$) simplifies the equation for the error E:

$$\begin{aligned} E &= X - Y = \mathbf{W} \cdot C - \mathbf{W}^{-1} \cdot \mathbf{T} \cdot \mathbf{T} \cdot C - \mathbf{W}^{-1} \cdot \mathbf{T} \cdot \mathbf{T} \cdot N = \\ &= \mathbf{W} \cdot C - \mathbf{W} \cdot \mathbf{T} \cdot C - \mathbf{W} \cdot \mathbf{T} \cdot N = \mathbf{W} \cdot ((\mathbf{I} - \mathbf{T}) \cdot C - \mathbf{T} \cdot N). \end{aligned} \tag{5.21}$$

5.6 Square error between the original and received images

The square error vector is represented by the following expression:

$$E^2 = (X - Y)^2. \tag{5.22}$$

Using the value for the error vector from the Equation 5.21, we develop the expression for the square error vector as follows:

$$\begin{aligned}
E^2 &= E^T E = \\
&= \{\mathbf{W}\cdot((\mathbf{I}-\mathbf{T})\cdot C - \mathbf{T}\cdot N)\}^T \cdot \{\mathbf{W}\cdot((\mathbf{I}-\mathbf{T})\cdot C - \mathbf{T}\cdot N)\} = \\
&= \{(\mathbf{I}-\mathbf{T})\cdot C - \mathbf{T}\cdot N\}^T \cdot \mathbf{W}^T \cdot \mathbf{W} \cdot \{(\mathbf{I}-\mathbf{T})\cdot C - \mathbf{T}\cdot N\} = \\
&= |\text{using the second property of matrix } \mathbf{W}: \ \mathbf{W}^T\cdot\mathbf{W} = \mathbf{I}\,| = \\
&= \{(\mathbf{I}-\mathbf{T})\cdot C - \mathbf{T}\cdot N\}^T \cdot \{(\mathbf{I}-\mathbf{T})\cdot C - \mathbf{T}\cdot N\} = \\
&= \{((\mathbf{I}-\mathbf{T})\cdot C)^T - (\mathbf{T}\cdot N)^T\} \cdot \{(\mathbf{I}-\mathbf{T})\cdot C - \mathbf{T}\cdot N\} = \\
&= \{C^T\cdot(\mathbf{I}-\mathbf{T})^T - N^T\cdot\mathbf{T}^T\} \cdot \{(\mathbf{I}-\mathbf{T})\cdot C - \mathbf{T}\cdot N\} = \\
&= C^T\cdot(\mathbf{I}-\mathbf{T})^T\cdot(\mathbf{I}-\mathbf{T})\cdot C - C^T\cdot(\mathbf{I}-\mathbf{T})^T\cdot\mathbf{T}\cdot N - \\
&- N^T\cdot\mathbf{T}^T\cdot(\mathbf{I}-\mathbf{T})\cdot C + N^T\cdot\mathbf{T}^T\cdot\mathbf{T}\cdot N = \\
&= |\, C^T\cdot(\mathbf{I}-\mathbf{T})^T\cdot\mathbf{T}\cdot N = C^T\cdot(\mathbf{I}^T-\mathbf{T}^T)\cdot\mathbf{T}\cdot N = \\
&= C^T\cdot(\mathbf{I}^T\cdot\mathbf{T}\cdot N - \mathbf{T}^T\cdot\mathbf{T}\cdot N) = C^T\cdot(\mathbf{T}\cdot N - \mathbf{T}\cdot N) = \mathbf{0} \text{ (zero matrix) }, \\
&\quad N^T\cdot\mathbf{T}^T\cdot(\mathbf{I}-\mathbf{T})\cdot C = (C^T\cdot(\mathbf{I}-\mathbf{T})^T\cdot\mathbf{T}\cdot N)^T = \mathbf{0}\,| \\
&= C^T\cdot(\mathbf{I}-\mathbf{T})^T\cdot(\mathbf{I}-\mathbf{T})\cdot C - \mathbf{0} - \mathbf{0} + N^T\cdot\mathbf{T}^T\cdot\mathbf{T}\cdot N = \\
&= |\text{using the properties of the thresholding matrix } \mathbf{T}, \text{it is easy to show that} \\
&\quad \mathbf{T}^T\cdot\mathbf{T} = \mathbf{T} \text{ and } (\mathbf{I}-\mathbf{T})^T\cdot(\mathbf{I}-\mathbf{T}) = (\mathbf{I}-\mathbf{T})| = \\
&= C^T\cdot(\mathbf{I}-\mathbf{T})\cdot C + N^T\cdot\mathbf{T}\cdot N.
\end{aligned} \tag{5.23}$$

Finally, the square error vector between the original and received images is equal to the following:

$$E^2 = (X-Y)^2 = C^T \cdot (\mathbf{I}-\mathbf{T}) \cdot C + N^T \cdot \mathbf{T} \cdot N. \tag{5.24}$$

5.7 System performance dilemma

In order to simplify an interpretation of the square error between the original and received images, the matrix representation of Equation (5.24) is replaced with the element representation:

$$\begin{aligned} E^2 &= C^T \cdot (\mathbf{I}-\mathbf{T}) \cdot C + N^T \cdot \mathbf{T} \cdot N, \\ e_i^2 &= c_i \cdot (1-t_i) \cdot c_i + n_i \cdot t_i \cdot n_i = c_i^2 \cdot (1-t_i) + n_i^2 \cdot t_i. \end{aligned} \tag{5.25}$$

Recall that $t_i = \begin{cases} 0, & |c_i| \le \tau \\ 1, & |c_i| > \tau \end{cases}$. t_i can accept either value "0" or "1", hence we rewrite an expression for e_i^2 from Equation 5.25 in the following manner:

$$e_i^2 = \begin{cases} c_i^2 \cdot (1-0) + n_i^2 \cdot 0, \text{in case } t_i = 0 \\ c_i^2 \cdot (1-1) + n_i^2 \cdot 1, \text{in case } t_i = 1 \end{cases} = \begin{cases} c_i^2, \text{in case } t_i = 0 \\ n_i^2, \text{in case } t_i = 1 \end{cases}. \tag{5.26}$$

According to the definition of t_i, the case $t_i = 0$ is possible when $|c_i| \le \tau$, and the case $t_i = 1$ is possible when $|c_i| > \tau$, where τ is the threshold value. Hence Equation 5.26 can be represented in the following form:

$$e_i^2 = \begin{cases} c_i^2, \text{in case } t_i = 0 \\ n_i^2, \text{in case } t_i = 1 \end{cases} = \begin{cases} c_i^2, \text{in case } |c_i| \le \tau \\ n_i^2, \text{in case } |c_i| > \tau \end{cases}. \tag{5.27}$$

From Equation 5.27 it becomes obvious that the quality of received image Y, expressed in terms of square error E^2, depends on the threshold value τ:

$$e_i^2 = \text{func}(\tau). \tag{5.28}$$

In case $|c_i| \leq \tau$, the transform coefficient c_i is discarded from transmission sequence. This discarded coefficient is not bringing the additive noise sample n_i into a receiver. Discarding of coefficients increases spectral efficiency of the transmission. The negative aspect of coefficient discarding is an increase of the square error, because $e_i^2 = c_i^2$. It leads to degradation of system performance in terms of restored image quality. Such degradation can be considered as degradation due to an internal factor.

In case $|c_i| > \tau$, the transform coefficient c_i is left for the transmission stage. It brings the additive noise sample n_i into the receiver. The spectral efficiency of the system stays unchanged, but the presence of additive noise causes the square error $e_i^2 = n_i^2$. It leads to degradation of the system performance in terms of restored image quality. Such degradation can be considered as degradation due to an external factor.

It is obvious that the system performance depends on the threshold value τ. Given fixed AWGN SNR, received image quality suffers from the high threshold value τ, whatever spectral efficiency benefits. From the other side, spectral efficiency suffers from the low threshold value τ, whatever received image quality benefits.

The system performance dilemma is a choice of spectral efficiency over received image quality or vice versa by choosing the threshold value τ.

5.8 Optimal threshold value

Recall Equation 5.24, that in order to evaluate the performance of communication system in terms of received image quality, we chose the square error vector between the original and received images:

$$E^2 = (X-Y)^2 = C^T \cdot (\mathbf{I}-\mathbf{T}) \cdot C + N^T \cdot \mathbf{T} \cdot N. \tag{5.29}$$

Given the fixed Signal-to Noise Ratio of the Additive White Gaussian Noise channel ($N = const$), we assume that, according to Equation 5.29, the quality of the received image completely depends on the thresholding matrix $\mathbf{T}$:

$$E^2 = (X-Y)^2 = E(\mathbf{T})^2. \tag{5.30}$$

The optimal thresholding matrix $\mathbf{T_{opt}}$ should minimize the square error vector between the original and received images, which is represented in Equation 5.29. The following equation expresses the above statement in mathematical terms:

$$\mathbf{T}_{opt} = \arg_{\mathbf{T}} \min \left((X-Y)^2\right) = \arg_{\mathbf{T}} \min E(\mathbf{T})^2, \tag{5.31}$$

The optimal thresholding matrix $\mathbf{T}_{opt}$ is a solution to the following equation:

$$\nabla_{\mathbf{T}} E(\mathbf{T})^2 = \mathbf{0}, \tag{5.32}$$

where $\nabla_{\mathbf{T}} = \frac{d}{d\mathbf{T}}$ is a differentiation operator with respect to the thresholding matrix $\mathbf{T}$.

Finding the solution for Equation 5.32 requires development of the following expression for $\nabla_{\mathbf{T}} E(\mathbf{T})^2$:

$$\nabla_{\mathbf{T}} \{E(\mathbf{T})^2\} = 2 \cdot E(\mathbf{T}) \cdot \nabla_{\mathbf{T}} \{E(\mathbf{T})\}. \tag{5.33}$$

Use of the error between the the original and received images $E(\mathbf{T})$ from Equation 5.21 in Equation 5.33 gives:

$$\begin{aligned}
\nabla_{\mathbf{T}}\{E(\mathbf{T})^2\} &= 2\cdot\mathbf{W}\cdot(C-\mathbf{T}\cdot C-\mathbf{T}\cdot N)\cdot\nabla_{\mathbf{T}}\{\mathbf{W}\cdot(C-\mathbf{T}\cdot C-\mathbf{T}\cdot N)\} \\
&= 2\cdot\mathbf{W}\cdot(C-\mathbf{T}\cdot(C+N))\cdot\mathbf{W}\cdot\nabla_{\mathbf{T}}\{C-\mathbf{T}\cdot C-\mathbf{T}\cdot N\} = \\
&= 2\cdot\mathbf{W}\cdot(C-\mathbf{T}\cdot(C+N))\cdot\mathbf{W}\cdot\{\nabla_{\mathbf{T}}C-\nabla_{\mathbf{T}}(\mathbf{T}\cdot C)- \\
&- \nabla_{\mathbf{T}}(\mathbf{T}\cdot N)\} = \\
&= 2\cdot\mathbf{W}\cdot(C-\mathbf{T}\cdot(C+N))\cdot\mathbf{W}\cdot\{-C-N\} = \\
&= (-2)\cdot\mathbf{W}\cdot(C-\mathbf{T}\cdot(C+N))\cdot\mathbf{W}\cdot(C+N). \qquad (5.34)
\end{aligned}$$

Find the solution for Equation 5.32 using results of development from Equation 5.34. Recall that $\mathbf{0}$ is a zero matrix:

$$\begin{aligned}
\nabla_{\mathbf{T}}\{E(\mathbf{T})^2\} &= \mathbf{0}; \\
(-2)\cdot\mathbf{W}\cdot(C-\mathbf{T}\cdot(C+N))\cdot\mathbf{W}\cdot(C+N) &= \mathbf{0}; \\
(C-\mathbf{T}\cdot(C+N))\cdot\mathbf{W}\cdot(C+N) &= \mathbf{0}; \\
C-\mathbf{T}\cdot(C+N) &= \mathbf{0}. \qquad (5.35)
\end{aligned}$$

Finally, the optimal thresholding matrix $\mathbf{T}_{opt}$ that minimizes square error between the original and received images $E(\mathbf{T})^2$ is calculated as following:

$$\begin{aligned}
\mathbf{T}_{opt} &= C\cdot(C+N)^{-1}; \\
t_{i_{opt}} &= \frac{c_i}{c_i+n_i}. \qquad (5.36)
\end{aligned}$$

The expression for t_i in case of $t_{i_{opt}} = \begin{cases} 0, \ |c_i| \leq \tau_{opt} \\ 1, \ |c_i| > \tau_{opt} \end{cases}$. t_i can accept either value "0" or "1"; hence we rewrite an expression for $t_{i_{opt}}$ from Equation 5.36 in the following manner:

$$t_{i_{opt}} = \begin{cases} \frac{c_i}{c_i+n_i} = 0 \text{ in case } c_i = 0, \ \forall n_i \\ \frac{c_i}{c_i+n_i} = 1 \text{ in case } n_i = 0, \ \forall c_i \end{cases} . \tag{5.37}$$

According to the definition of $t_{i_{opt}}$, the case $t_{i_{opt}} = 0$ is possible when $|c_i| \leq \tau_{opt}$. In case $|c_i| = 0$, the inequality $|c_i| \leq \tau_{opt}$ can be true only if the threshold value $\tau_{opt} = 0$. In this case the value of the noise sample n_i does not play any role. The case $t_{i_{opt}} = 1$ is possible when the inequality $|c_i| > \tau_{opt}$ is true. Previously we determined that the threshold value $\tau_{opt} = 0$; hence the inequality $|c_i| > \tau_{opt}$ is true for any non-zero value of the transform coefficient c_i.

In case of $\tau_{opt} = 0$, Equation 5.27 for the square error between a received and original image pixel will have the following look:

$$\begin{aligned} e_i^2 &= \begin{cases} c_i^2, \text{ in case } t_i = 0 \\ n_i^2, \text{ in case } t_i = 1 \end{cases} = \begin{cases} c_i^2, \text{ in case } |c_i| \leq \tau_{opt} \\ n_i^2, \text{ in case } |c_i| > \tau_{opt} \end{cases} = \\ &= \begin{cases} c_i^2, \text{ in case } |c_i| \leq 0 \\ n_i^2, \text{ in case } |c_i| > 0 \end{cases} = \begin{cases} 0, \text{ in case } c_i = 0 \\ n_i^2, \ \forall c_i \end{cases} . \end{aligned} \tag{5.38}$$

Equation 5.38 allows making the following conclusion. The optimal threshold value ($\tau_{opt} = 0$) provides the zero square error vector ($E(\tau_{opt})^2 = 0$) between the original and received images in absence of the additive white Gaussian noise ($N = 0$). In this case the communication system operates in a lossless mode.

In presence of AWGN the quality of the received image is totally affected by the channel noise (N). Use of the optimal threshold value ($\tau_{opt} = 0$) provides minimal spectral efficiency

of the communication system, since only zero transform coefficients are excluded from the transmission.

5.9 Quasi-optimal hard thresholding

5.9.1 Proposal of the quasi-optimal hard thresholding rule

The proposal of the quasi-optimal hard thresholding rule is inspired by the research of Sabelkin and Ponomarenko (2001), Ponomarenko et al. (2006). Those works on image compression apply hard thresholding on transform coefficients of a noise corrupted image. The authors use a similar restored image quality measure - Peak Signal-to-Noise Ratio - to estimate performance of their algorithms. Research shows that certain hard threshold values are able to improve the quality of a restored image.

In our case we also have the image with transform coefficients corrupted by AWGN. We propose to choose the threshold value (τ) somehow depending on noise. This threshold value is called the quasi-optimal threshold value (τ_{qo}). The following quasi-optimal hard thresholding rule can be applied: "discard not only zero coefficients but also all coefficients whose magnitudes are less than the magnitude of the noise sample". The assumption makes sense because those coefficients will be severely corrupted by the noise anyway. It is the case when the external degradation factor of system performance dominates the internal one.

The element of the quasi-optimal thresholding matrix $\mathbf{T}_{qo}$ will be represented by the following expression:

$$t_{i_{qo}} = \begin{cases} 0, \; if \; |c_i| < |n_i| \\ ?, \; if \; |c_i| = |n_i| \\ 1, \; if \; |c_i| > |n_i| \end{cases}, \tag{5.39}$$

where the noise sample magnitude $|n_i|$ is a subject of further discussion.

Note that the case when the coefficient magnitude is equal to one of the noise is not defined yet.

In order to present the element $t_{i_{qo}}$ of the quasi-optimal thresholding matrix in more compact form, we introduce the **Heaviside step** function often simply called the **step** function:

$$\mathscr{H}(x) = \begin{cases} 0, & x < 0 \\ \frac{1}{2}, & x = 0 \\ 1, & x > 0 \end{cases} . \tag{5.40}$$

Often, it is assumed that $\mathscr{H}(0) = 1$. It is more common in the Digital Signal Processing (DSP) domain to use the step function $\mathbf{u}(x)$ instead of the Heaviside function $\mathscr{H}(x)$:

$$\mathbf{u}(x) = \begin{cases} 0, & x < 0 \\ 1, & x \geq 0 \end{cases} . \tag{5.41}$$

The derivative of the step function is called the **delta** function $\delta(x)$:

$$\begin{aligned} \delta(x) &= \frac{\mathbf{d}}{\mathbf{dx}}\mathbf{u}(x), \\ \delta(x) &= \begin{cases} 1, & x = 0 \\ 0, & \text{otherwise} \end{cases} . \end{aligned} \tag{5.42}$$

Use of the step function $\mathbf{u}(x)$ in Equation 5.39 simplifies the expression for the element $t_{i_{qo}}$ of the quasi-optimal thresholding matrix:

$$t_{i_{qo}} = \mathbf{u}(|c_i| - |n_i|). \tag{5.43}$$

5.9.2 Validation of the quasi-optimal hard thresholding rule

In a previous section the intuitively chosen element $t_{i_{qo}}$ of the quasi-optimal thresholding matrix is as follows (5.43):

$$t_{i_{qo}} = \mathbf{u}(|c_i| - |n_i|). \tag{5.44}$$

In order to validate our assumption with the element $t_{i_{qo}}$ of the quasi-optimal thresholding matrix, we solve the problem of minimization of the square error between the original and received images again. This time we solve the problem with respect to the transform coefficient vector C. The task can be formulated as follows: "What is the value of transform coefficient vector C_{opt} that minimizes the square error between original and received images $E(C)^2$?"

$$C_{opt} = \arg_C \min E(C)^2. \tag{5.45}$$

The optimal coefficient vector C_{opt} is a solution to the following equation:

$$\nabla_C E(C)^2 = 0, \tag{5.46}$$

where $\nabla_C = \frac{d}{dC}$ is a differentiation operator with respect to the transform coefficient vector C, and 0 is a zero vector.

Before finding the solution for the above equation, we need to develop an expression for $\nabla_C E(C)^2$:

$$\nabla_C \{E(C)^2\} = 2 \cdot E(C) \cdot \nabla_C \{E(C)\}. \tag{5.47}$$

Use of the error between the original and received images $E(\mathbf{C})$ from Equation 5.21 in Equation 5.47 gives:

$$\begin{aligned}
\nabla_C E(C)^2 &= 2\cdot\mathbf{W}\cdot(C-\mathbf{T}\cdot C-\mathbf{T}\cdot N)\cdot\nabla_{\mathbf{C}}\{\mathbf{W}\cdot(C-\mathbf{T}\cdot C-\mathbf{T}\cdot N)\} \\
&= 2\cdot\mathbf{W}\cdot(C-\mathbf{T}\cdot(C+N))\cdot\mathbf{W}\cdot\nabla_{\mathbf{C}}\{C-\mathbf{T}\cdot C-\mathbf{T}\cdot N\} = \\
&= 2\cdot\mathbf{W}\cdot(C-\mathbf{T}\cdot(C+N))\cdot\mathbf{W}\cdot\{\nabla_{\mathbf{C}}C-\nabla_{\mathbf{C}}(\mathbf{T}\cdot C)- \\
&- \nabla_{\mathbf{C}}(\mathbf{T}\cdot N)\} = \\
&= 2\cdot\mathbf{W}\cdot(C-\mathbf{T}\cdot(C+N))\cdot \\
&\cdot \mathbf{W}\cdot\{\mathbf{I}-[\mathbf{T}+(\nabla_{\mathbf{C}}\mathbf{T})\cdot C]-(\nabla_{\mathbf{C}}\mathbf{T})\cdot N\} = \\
&= 2\cdot\mathbf{W}\cdot(C-\mathbf{T}\cdot(C+N))\cdot \\
&\cdot \mathbf{W}\cdot\{\mathbf{I}-\mathbf{T}-(\nabla_{\mathbf{C}}\mathbf{T})\cdot(C+N)\}. \qquad (5.48)
\end{aligned}$$

Find the solution for Equation 5.46 using results of development from Equation 5.48. Recall that 0 is a zero vector:

$$\begin{aligned}
\nabla_C E(C)^2 = 0; \\
2\cdot\mathbf{W}\cdot(C-\mathbf{T}\cdot(C+N))\cdot\mathbf{W}\cdot\{\mathbf{I}-\mathbf{T}-(\nabla_{\mathbf{C}}\mathbf{T})\cdot(C+N)\} = 0; \\
(C-\mathbf{T}\cdot(C+N))\cdot\{\mathbf{I}-\mathbf{T}-(\nabla_{\mathbf{C}}\mathbf{T})\cdot(C+N)\} = 0. \qquad (5.49)
\end{aligned}$$

In order to simplify development and interpretation, Equation 5.49 is represented in its element form instead of the matrix one:

$$\begin{aligned}
\frac{\mathbf{d}}{\mathbf{dc_i}} e_i(c_i) = 0; \\
(c_i - t_i \cdot (c_i + n_i)) \cdot \left(1 - ti - \left(\frac{\mathbf{d}}{\mathbf{dc_i}} t_i\right) \cdot (c_i + n_i)\right) = 0; \\
|\text{recall that } t_i = \mathbf{u}(|c_i| - |n_i|)| \\
(c_i - \mathbf{u}(|c_i| - |n_i|) \cdot (c_i + n_i)) \cdot \\
\cdot \left(1 - \mathbf{u}(|c_i| - |n_i|) - \frac{\mathbf{d}}{\mathbf{dc_i}} (\mathbf{u}(|ci| - |ni|)) \cdot (ci + ni)\right) = 0.
\end{aligned} \tag{5.50}$$

A derivative from the step function is calculated as follows:

$$\frac{\mathbf{d}}{\mathbf{dc_i}} (\mathbf{u}(|c_i| - |n_i|)) = \delta(|c_i| - |n_i|) \cdot \frac{\mathbf{d}}{\mathbf{dc_i}} |c_i|. \tag{5.51}$$

Substitute the derivative from the step function in Equation 5.50 with an expression from Equation 5.51:

$$\begin{aligned}
(c_i - \mathbf{u}(|c_i| - |n_i|) \cdot (c_i + n_i)) \cdot \\
\cdot \left(1 - \mathbf{u}(|c_i| - |n_i|) - \delta(|c_i| - |n_i|) \cdot \left(\frac{\mathbf{d}}{\mathbf{dc_i}} |c_i|\right) \cdot (ci + ni)\right) = 0.
\end{aligned} \tag{5.52}$$

Solutions of Equation 5.52 are found for the following intervals and cases:

1. $0 < |c_i| < |n_i|$;

2. $|c_i| = |n_i|$;

3. $|c_i| > |n_i|$.

Solution for the interval $0 < |c_i| < |n_i|$

In the interval $0 < |c_i| < |n_i|$, the functions, involved in Equation 5.52, accept the following values:

$$\begin{aligned}
\mathbf{u}(|c_i| - |n_i|) &= \begin{cases} 0, \ (|c_i| - |n_i|) < 0 \\ 1, \ (|c_i| - |n_i|) \geq 0 \end{cases} = 0; \\
\delta(|c_i| - |n_i|) &= \begin{cases} 1, \ (|c_i| - |n_i|) = 0 \\ 0, \text{ otherwise} \end{cases} = 0; \\
\frac{\mathbf{d}}{\mathbf{dc_i}}|c_i| &= \begin{cases} -1, \ c_i < 0 \\ 1, \ c_i > 0 \\ \text{undefined}, \ c_i = 0 \end{cases} . \qquad (5.53)
\end{aligned}$$

Using the values of the functions from Equations 5.53 we obtain the solution of Equation 5.52 for the interval $0 < |c_i| < |n_i|$:

$$\begin{aligned}
&(c_i - \mathbf{u}(|c_i| - |n_i|) \cdot (c_i + n_i)) \cdot \\
&\cdot \left(1 - \mathbf{u}(|c_i| - |n_i|) - \delta(|c_i| - |n_i|) \cdot \left(\frac{\mathbf{d}}{\mathbf{dc_i}}|c_i|\right) \cdot (c_i + n_i)\right) = 0; \\
&(c_i - 0 \cdot (c_i + n_i)) \cdot \left(1 - 0 - 0 \cdot \left(\frac{\mathbf{d}}{\mathbf{dc_i}}|c_i|\right) \cdot (c_i + n_i)\right) = 0; \\
&c_i = 0. \qquad (5.54)
\end{aligned}$$

The explication of the obtained solution is following. In order to minimize the square error between the original and received images transmitted over the AWGN channel, a transform coefficient whose magnitude is inferior to the one of the noise ($0 < |c_i| < |n_i|$) must be eliminated from the processing ($c_i = 0$). The elimination procedure is considered as the quasi-optimal thresholding described by the step function $\mathbf{u}(|c_i| - |n_i|)$.

Solution for the case $|c_i| = |n_i|$

In case $|c_i| = |n_i|$, the functions involved in Equation 5.52 accept the following values:

$$\begin{aligned} \mathbf{u}(|c_i| - |n_i|) &= \begin{cases} 0, \ (|c_i| - |n_i|) < 0 \\ 1, \ (|c_i| - |n_i|) \geq 0 \end{cases} = 1; \\ \delta(|c_i| - |n_i|) &= \begin{cases} 1, \ (|c_i| - |n_i|) = 0 \\ 0, \text{ otherwise} \end{cases} = 1. \end{aligned} \tag{5.55}$$

Using the values of functions from Equations 5.55 we simplify Equation 5.52 for the case $|c_i| = |n_i|$:

$$\begin{aligned} (c_i - \mathbf{u}(|c_i| - |n_i|) \cdot (c_i + n_i)) \cdot \\ \cdot \left(1 - \mathbf{u}(|c_i| - |n_i|) - \delta(|c_i| - |n_i|) \cdot \left(\frac{\mathbf{d}}{\mathbf{dc_i}}|c_i|\right) \cdot (c_i + n_i)\right) = 0; \\ (c_i - 1 \cdot (c_i + n_i)) \cdot \left(1 - 1 - 1 \cdot \left(\frac{\mathbf{d}}{\mathbf{dc_i}}|c_i|\right) \cdot (c_i + n_i)\right) = 0; \\ (c_i - c_i - n_i) \cdot \left(0 - 1 \cdot \left(\frac{\mathbf{d}}{\mathbf{dc_i}}|c_i|\right) \cdot (c_i + n_i)\right) = 0; \\ -n_i \cdot \left(0 - \left(\frac{\mathbf{d}}{\mathbf{dc_i}}|c_i|\right) \cdot (c_i + n_i)\right) = 0; \\ n_i \cdot (c_i + n_i) \cdot \left(\frac{\mathbf{d}}{\mathbf{dc_i}}|c_i|\right) = 0. \end{aligned} \tag{5.56}$$

Consider that a derivative from $|c_i|$ is equal to the following:

$$\frac{\mathbf{d}}{\mathbf{dc_i}}|c_i| = \begin{cases} -1, \ c_i < 0 \\ 1, \ c_i > 0 \\ \text{undefined}, \ c_i = 0 \end{cases}. \tag{5.57}$$

The cases $c_i < 0$, $c_i > 0$ do not influence the solution of Equation 5.56. Only the case $c_i = 0$ constrains the solution:

$$\begin{aligned} n_i \cdot (c_i + n_i) \cdot \left(\frac{\mathbf{d}}{\mathbf{dc_i}} |c_i| \right) &= 0; \\ n_i \cdot (c_i + n_i) &= 0,\ c_i \neq 0; \\ n_i \cdot c_i + n_i^2 &= 0,\ c_i \neq 0; \\ n_i \cdot c_i &= -n_i^2,\ c_i \neq 0; \\ c_i &= -n_i,\ c_i \neq 0. \end{aligned} \tag{5.58}$$

The particular case when the transform coefficient magnitude is equal to the one of the noise ($|c_i| = |n_i|$) proposes the following solution. In order to minimize the square error between the original and received images transmitted over AWGN channel only the transform coefficient with the sign opposite to the one of the noise sample ($c_i = -n_i$) should be processed, otherwise it should be discarded.

Solution for the interval $|c_i| > |n_i|$

In the interval $|c_i| > |n_i|$, the functions, involved in Equation 5.52, accept the following values:

$$\begin{aligned} \mathbf{u}(|c_i| - |n_i|) &= \begin{cases} 0,\ (|c_i| - |n_i|) < 0 \\ 1,\ (|c_i| - |n_i|) \geq 0 \end{cases} = 1; \\ \delta(|c_i| - |n_i|) &= \begin{cases} 1,\ (|c_i| - |n_i|) = 0 \\ 0,\ \text{otherwise} \end{cases} = 0; \\ \frac{\mathbf{d}}{\mathbf{dc_i}} |c_i| &= \begin{cases} -1,\ c_i < 0 \\ 1,\ c_i > 0 \\ \text{undefined},\ c_i = 0 \end{cases}. \end{aligned} \tag{5.59}$$

Using the values of the functions from Equations 5.59 we obtain the solution of Equation 5.52 for the interval $|c_i| > |n_i|$:

$$\begin{aligned}
(c_i - \mathbf{u}(|c_i| - |n_i|) \cdot (c_i + n_i)) \cdot \\
\cdot \left(1 - \mathbf{u}(|c_i| - |n_i|) - \delta(|c_i| - |n_i|) \cdot \left(\frac{\mathbf{d}}{\mathbf{dc_i}}|c_i|\right) \cdot (c_i + n_i)\right) = 0; \\
(c_i - 1 \cdot (c_i + n_i)) \cdot \left(1 - 1 - 0 \cdot \left(\frac{\mathbf{d}}{\mathbf{dc_i}}|c_i|\right) \cdot (c_i + n_i)\right) = 0; \\
(c_i - c_i - n_i) \cdot (0 - 0 \cdot (c_i + n_i)) = 0; \\
-n_i \cdot 0 = 0; \\
0 = 0. \qquad (5.60)
\end{aligned}$$

The solution of Equation 5.60 does not depend on the value of the transform coefficient c_i. Hence, in order to minimize the square error between the original and received images transmitted over AWGN channel, any transform coefficient whose magnitude is superior to the one of the noise ($|c_i| > |n_i|$) must be processed. The procedure is considered as the quasi-optimal thresholding described by the step function $\mathbf{u}(|c_i| - |n_i|)$.

5.9.3 Quasi-optimal hard thresholding rule

In the previous section, we solved the problem of minimization of the square error $e_i(c_i)^2$ between the original and received images:

$$c_i = \arg_{c_i} \min e_i(c_i)^2. \qquad (5.61)$$

We found the values of the transform coefficients c_i that minimize the square error $e_i(c_i)^2$:

$$c_i = \begin{cases} 0,\ 0 < |c_i| < |n_i| \\ -n_i,\ |c_i| = |n_i| \\ c_i,\ |c_i| > |n_i| \end{cases} . \tag{5.62}$$

In order to minimize the square error between the original and received images in the presence of AWGN, the element of the quasi-optimal thresholding matrix should be the following:

$$t_i = \begin{cases} 0,\ 0 < |c_i| < |n_i| \\ 0,\ c_i = n_i \\ 1,\ c_i = -n_i \\ 1,\ |c_i| > |n_i| \end{cases} . \tag{5.63}$$

5.9.4 Square error in the case of the quasi-optimal hard thresholding

The square error between the original and received images in the presence of AWGN is calculated according to Equation 5.25. Use of the element of the quasi-optimal thresholding matrix

from Equation 5.63 leads to the following square error:

$$e_i^2 = c_i^2 \cdot (1-t_i) + n_i^2 \cdot t_i = \begin{cases} c_i^2 \cdot (1-0) + n_i^2 \cdot 0, \ 0 < |c_i| < |n_i| \\ c_i^2 \cdot (1-0) + n_i^2 \cdot 0, \ c_i = n_i \\ c_i^2 \cdot (1-1) + n_i^2 \cdot 1, \ c_i = -n_i \\ c_i^2 \cdot (1-1) + n_i^2 \cdot 1, \ |c_i| > |n_i| \end{cases} ;$$

$$e_i^2 = \begin{cases} c_i^2, \ 0 < |c_i| < |n_i| \\ c_i^2, \ c_i = n_i \\ n_i^2, \ c_i = -n_i \\ n_i^2, \ |c_i| > |n_i| \end{cases} . \tag{5.64}$$

5.10 MSE bound for the coefficients transmitted over the AWGN channel

Application of the quasi-optimal thresholding, according to Equation 5.63, requires a knowledge of the noise vector N.

The noise vector N is a random vector, and its value is not defined in a deterministic way. However it is possible to estimate statistically an impact of AWGN on data transmitted over the channel. In our case it is the impact on transmitted image coefficients.

Recall that the Mean Square Error of coefficients transmitted over the AWGN channel represents the normalized squared difference between the values of the received coefficients C_{Rx_i} and the transmitted ones C_{Tx_i}:

$$MSE = \frac{1}{L} \sum_{i=1}^{L} (C_{Rx_i} - C_{Tx_i})^2 , \tag{5.65}$$

where L is the size of coefficient vector C_{Rx} and C_{Tx}.

Using Equation 5.8, the MSE of transmitted coefficients C_{Tx} can be interpreted as a mean square of an additive white Gaussian noise as follows:

$$MSE = \frac{1}{L}\sum_{i=1}^{L}(C_{Rx_i} - C_{Tx_i})^2 = \frac{1}{L}\sum_{i=1}^{L}N_i^2. \tag{5.66}$$

The coefficients C_{Tx_i} and C_{Rx_i} are in a binary form. An arbitrary modulation technique is chosen to convert the coefficient vector C_{Tx} from the binary stream form into a symbol stream form. The coefficient symbol stream is transmitted over the AWGN channel. An error probability per bit p for the arbitrary modulation technique is the function of a Signal-to-Noise Ratio per bit E_b/N_0:

$$p = \mathbf{f}\left(\frac{E_b}{N_0}\right). \tag{5.67}$$

Each of coefficients C_{Tx_i} and C_{Rx_i} is represented by ψ bits. Hence, the total bit number Θ, for the coefficient vector C_{Tx} or C_{Rx}, consists of the following:

$$\Theta = \psi \cdot L. \tag{5.68}$$

The coefficient vector C_{Tx} bits become the subject of corruption, while propagating over the AWGN channel. The total number of corrupted coefficient vector bits κ_{total} is the following:

$$\kappa_{total} = p \cdot \Theta = p \cdot \psi \cdot L, \tag{5.69}$$

where p is the bit error probability and Θ is the total number of coefficient vector bits calculated in Equations 5.67 and 5.68 accordingly.

While propagating over the AWGN channel, any bit representing the coefficient C_{Tx_i} could be corrupted. It is obvious that corruption of the Most Significant Bit (MSB) of the coefficient C_{Tx_i} affects the MSE (Equation 5.65) more than corruption of the Least Significant Bit (LSB). In

general, the total number of corrupted coefficient vector C_{Tx} bits κ_{total} consists of the number of corrupted MSB, corrupted LSB and all corrupted bits between them. Assume that a bit $(\psi-1)$ is MSB and a bit 0 is LSB. In that case, the total number of corrupted coefficient vector C_{Tx} bits κ_{total} is the following:

$$\kappa_{total} = \kappa_{\psi-1} + \kappa_{\psi-2} + \kappa_{\psi-3} + \ldots + \kappa_1 + \kappa_0 = \sum_{b=0}^{\psi-1} \kappa_b, \tag{5.70}$$

where $\kappa_{\psi-1}$ is the overall number of corrupted $(\psi-1)$th bits (MSB), κ_0 is the overall number of corrupted 0th bits (LSB), and κ_b is the overall number of corrupted bth bits in the coefficient vector C_{Tx}.

Consider a case of one transmitted coefficient C_{Tx_i}. The difference between the received C_{Rx_i} and transmitted C_{Tx_i} coefficients is a noise component N_i which can be represented by the following expression:

$$N_i = C_{Rx_i} - C_{Tx_i} = \sum_{b=0}^{\psi-1} C_i^b \cdot w_b, \tag{5.71}$$

where C_i^b is the **coefficient bit corruption operator**. $C_i^b = 1$ if bth bit of the transmitted coefficient C_{Tx_i} is corrupted during transmission, and $C_i^b = 0$ if bth bit of the transmitted coefficient C_{Tx_i} is preserved.

Using Equation 5.71, Equation 5.66 for the Mean Square Error can be transformed in the following form:

$$\begin{aligned} MSE &= \frac{1}{L}\sum_{i=1}^{L}(C_{Rx_i} - C_{Tx_i})^2 = \frac{1}{L}\sum_{i=1}^{L} N_i^2 = \\ &= \frac{1}{L}\sum_{i=1}^{L}\left(\sum_{b=0}^{\psi-1} C_i^b \cdot w_b\right)^2. \end{aligned} \tag{5.72}$$

Now we can present MSE of transmitted coefficients C_{Tx_i} as a function of the coefficient bit corruption operator C_i^b. The coefficient bit corruption operator C_i^b is often difficult to determine, because it is impossible to predict theoretically which bit in which coefficient will be corrupted due to signal propagation over the AWGN channel. Hence, Equation 5.72 in its actual form is not very useful. Let us make some changes. At first, we thus replace the deterministic pixel bit corruption operator C_i^b with the expected value of discrete random variable $\overline{C_i^b}$, which is the random pixel bit corruption operator of the bth bit in the transmitted coefficient C_{Tx_i} as follows:

$$\begin{aligned} \overline{C_i^b} \quad &= C_{1_i}^b \cdot Pr\left(\overline{b}|b\right)_i + C_{0_i}^b \cdot Pr\left(b|b\right)_i = \\ &= 1 \cdot Pr\left(\overline{b}|b\right)_i + 0 \cdot Pr\left(b|b\right)_i = Pr\left(\overline{b}|b\right)_i . \end{aligned} \tag{5.73}$$

After substitution of the coefficient bit corruption operator C_i^b from Equation 5.73 into Equation 5.72, an expression for MSE will have a new stochastic look:

$$MSE = \frac{1}{L} \sum_{i=1}^{L} \left(\sum_{b=0}^{\psi-1} \Pr\left(\overline{b}|b\right)_i \cdot w_b \right)^2 . \tag{5.74}$$

Any transmitted coefficient C_{Tx_i} that contains one or more corrupted bits is considered as a **corrupted coefficient**. Only corrupted coefficients influence MSE:

$$MSE = \frac{1}{L} \sum_{corrupted\ \ coefficients} \left(\sum_{b=0}^{\psi-1} \Pr\left(\overline{b}|b\right)_i \cdot w_b \right)^2 . \tag{5.75}$$

For further development of the expression for MSE we need to determine the number of corrupted coefficients. Assume that a telecommunication system performs so badly (may be due to low E_b/N_0) that every transmitted coefficient C_{Tx_i} contains a corrupted bit, hence the total

number of corrupted bits is equal to the total number of transmitted coefficients C_{Tx_i}:

$$\kappa_{total} = L. \tag{5.76}$$

This assumption allows us to use the value of κ_{total} from Equation 5.69 in Equation 5.76 or vice versa:

$$\begin{aligned} \kappa_{total} = L \text{ and } \kappa_{total} = p \cdot \psi \cdot L, \\ \text{hence } L = p \cdot \psi \cdot L => \ 1 = p \cdot \psi \ => \ p = \frac{1}{\psi}. \end{aligned} \tag{5.77}$$

Having in mind the real values of bits per coefficient, we can conclude that if every transmitted coefficient C_{Tx_i} contains a corrupted bit, the system provides the following bit error rates:

$$\begin{aligned} \text{for } \psi &= 8 \text{ bits BER } p = \frac{1}{\psi} \ => \ p = \frac{1}{8} = 0.125; \\ \text{for } \psi &= 12 \text{ bits BER } p = \frac{1}{\psi} \ => \ p = \frac{1}{12} = 0.0833. \end{aligned} \tag{5.78}$$

Those values of BER from Equation 5.78 are far away from the reality. Usually, the telecommunication system performs much better providing BER $p_{real} = 10^{-3} \ldots 10^{-6}$. Hence, for the real system not every coefficient of a received image contains a corrupted bit and the following inequality makes sense:

$$p_{real} \leq \frac{1}{\psi}. \tag{5.79}$$

Suppose that the corrupted transmitted coefficient C_{Tx_i}, or received coefficient C_{Rx_i} contains only one corrupted bit. In that case the total number of corrupted coefficients is equal to the total number of corrupted bits as follows:

$$\text{total corrupted coefficients} = \kappa_{total} = p \cdot \psi \cdot L. \tag{5.80}$$

A substitution of the total number of corrupted coefficients from Equation 5.80 into Equation 6.15 gives the following MSE expression:

$$\begin{aligned} MSE &= \frac{1}{L}(p \cdot \psi \cdot L)\left(\sum_{b=0}^{\psi-1} \Pr\left(\overline{b}|b\right)_i \cdot w_b\right)^2 = \\ &= (p \cdot \psi)\left(\sum_{b=0}^{\psi-1} \Pr\left(\overline{b}|b\right)_i \cdot w_b\right)^2. \end{aligned} \tag{5.81}$$

Assume that any bit in the coefficient has an equal probability of error, and the probability of bit error does not depend on which coefficient is considered. It can be represented by the following:

$$\Pr\left(\overline{b}|b\right)_i = Pr\left(\overline{b}|b\right) = \frac{1}{\psi}. \tag{5.82}$$

Further development of Equation 5.81 using Equation 5.82 gives the following:

$$\begin{aligned} MSE &= (p \cdot \psi)\left(\sum_{b=0}^{\psi-1} \Pr\left(\overline{b}|b\right)_i \cdot w_b\right)^2 = (p \cdot \psi)\left(\sum_{b=0}^{\psi-1} \frac{1}{\psi} \cdot w_b\right)^2 \\ &= \frac{p \cdot \psi}{\psi^2}\left(\sum_{b=0}^{\psi-1} w_b\right)^2 = \frac{p}{\psi}\left(\sum_{b=0}^{\psi-1} w_b\right)^2. \end{aligned} \tag{5.83}$$

The summation $\sum_{b=0}^{\psi-1} w_b = w_\psi$, hence MSE in Equation 6.22 can be represented by the following equation:

$$MSE = \frac{p}{\psi}\left(\sum_{b=0}^{\psi-1} w_b\right)^2 = \frac{p}{\psi} w_\psi^2. \tag{5.84}$$

Use of Equation 5.67 for error probability per bit p for the arbitrary modulation technique, and Equation 5.66 gives:

$$MSE = \frac{1}{L}\sum_{i=1}^{L} N_i^2 = \mathbf{E}\{N_i^2\} = \frac{w_\psi^2}{\psi} \cdot p = \frac{w_\psi^2}{\psi} \cdot \mathbf{f}\left(\frac{E_b}{N_0}\right), \tag{5.85}$$

where

N_i is the additive white Gaussian noise sample;

E_b/N_0 is the Signal-to-Noise Ratio per bit for the AWGN channel;

w_ψ is the weight of the ψ-th bit, the most significant bit (MSB) in the transmitted coefficient C_{Tx_i};

ψ is the total number of bits that represents the transmitted coefficient C_{Tx_i}.

5.11 Simulation results for the still image transmission case

We simulate the still image transmission system shown on Figure 5.4. Basically, it is the still image transmission system shown in Figure 5.1 with an added AWGN estimation block. Knowledge of an AWGN level and a modulation type allows calculating a probability of bit error used in Equation 5.85.

We conduct experiments with a grayscale image; every pixel contains 8 bits. The wavelet transform has three levels of two-dimensional decomposition ($depth = 3$). After such decomposition a wavelet packet coefficient will contain $8 + 3 \cdot 2 = 14$ principal bits and 3 fractional bits, according to Table 4.5. In our calculations, we will consider only the principal bits of the wavelet packet coefficient, hence the most significant bit (MSB) of the coefficient is the 14th bit, $\psi = 14$. The coefficient is in a binary form; hence the weight of the ψ-th bit is $w_\psi = 2^\psi$.

Afterwards hard thresholding is applied towards the coefficients. We run experiments several times for the different threshold values. Figure 5.5 presents a PSNR curve, which characterizes the quality of a restored image as a function of a hard threshold value. One can see a peak on the quality curve, corresponding to some optimal threshold value. The hard threshold value, which is less than that optimal value, improves the quality of the restored image. It is explained by a

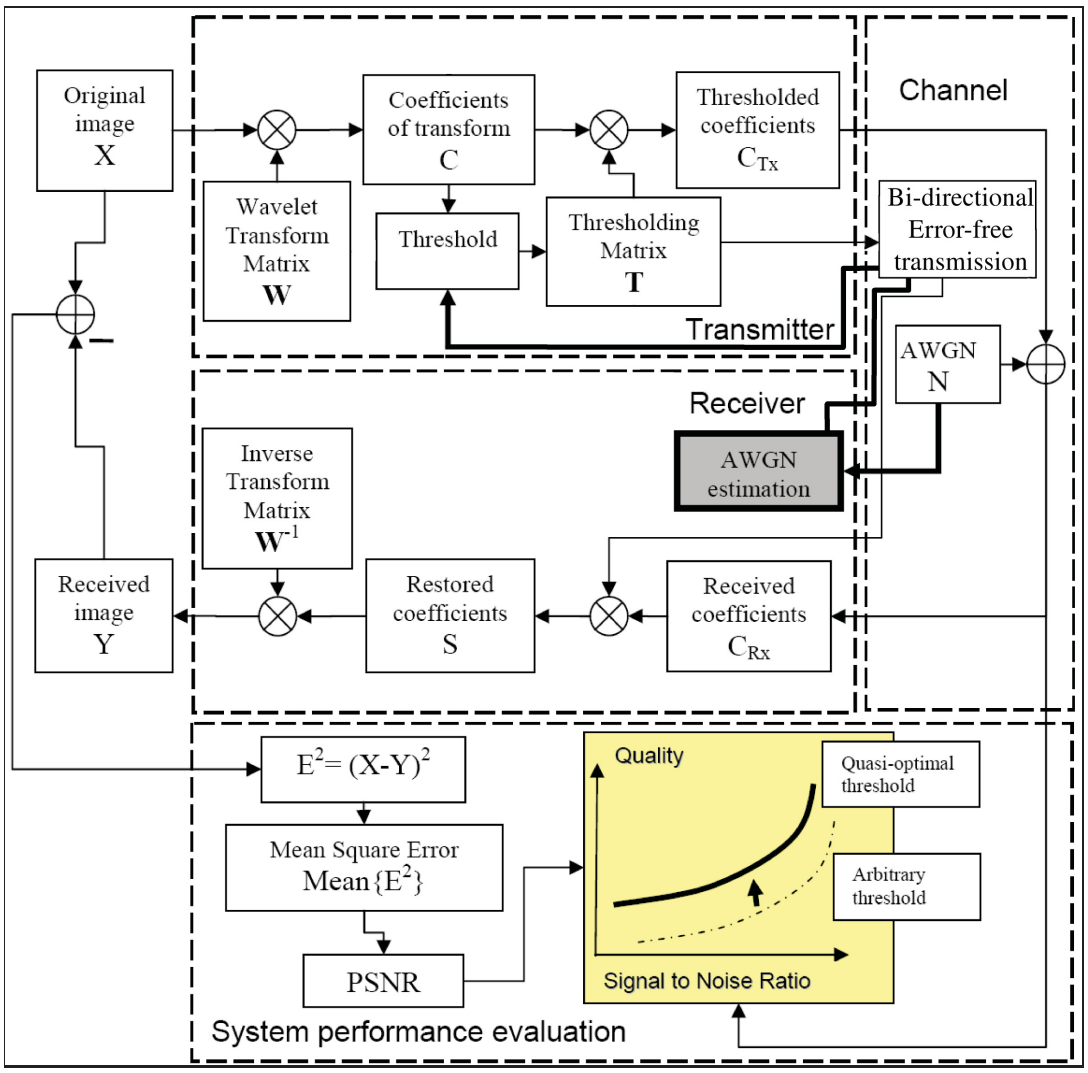

Figure 5.4 The transform based still image transmission system using TOMAS.

denoising property of the wavelet transform: Donoho (1995), Donoho and Johnstone (1994).

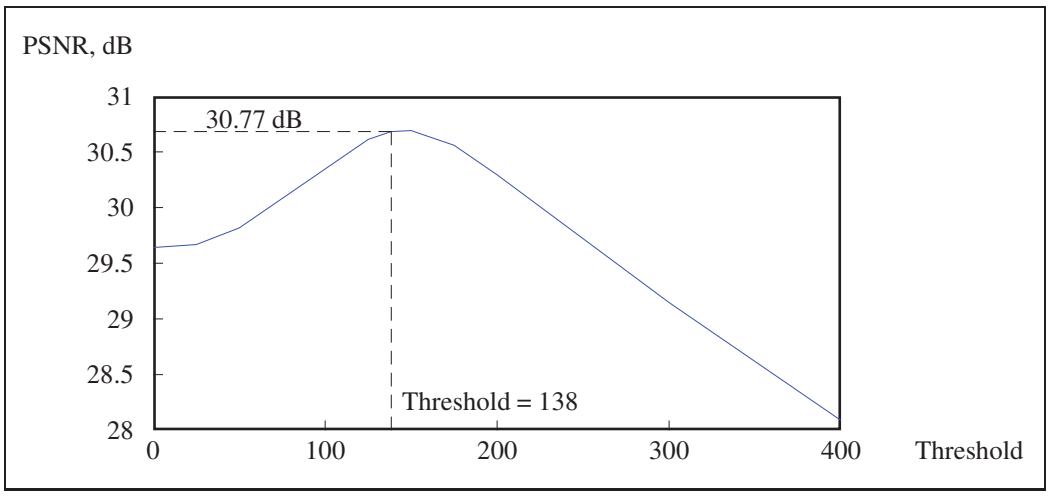

Figure 5.5 Quality of a restored image as the function of the hard threshold value.

In our experiments, we have chosen the probability of error $p = 0.001$. When p is substituted in Equation 5.85,

$$MSE = \frac{w_\psi^2}{\psi} \cdot p = \left| \psi = 14,\ w_\psi = 2^{14} \right| = \frac{2^{2 \cdot 14}}{14} \cdot 0.001 \approx 19173.96;$$
$$\text{Mean Error} = \sqrt{MSE} = \sqrt{19173.96} \approx 138.47. \tag{5.86}$$

We put the value of the Mean Error (ME) of wavelet packet coefficients from Equation 5.86 on the performance curve shown on Figure 5.5. One can see that use of the ME as the threshold provides almost the best quality of restored image. Hence, the value of ME of wavelet packet coefficients can be considered as the value for the quasi-optimal hard thresholding.

Being unable to determine the noise vector N for the quasi-optimal thresholding, we however derived instead a bound for the Mean Error of wavelet packet coefficients caused by the channel noise. This ME value can be used for the quasi-optimal hard thresholding.

5.12 Conclusion

This chapter has represented an analytical approach that validates the idea of TOMAS. It is demonstrated that the quality of an image, transmitted over an AWGN channel, can be improved, if the channel parameters, such as a Signal-to-Noise ratio of the channel, are taken into consideration during hard thresholding of wavelet packet coefficients.

CHAPTER 6

STILL IMAGE TRANSMISSION USING WIRELESS TOMAS

6.1 Introduction

In this chapter, the data Transmission oriented on the Object, communication Media, Application, and state of communication Systems is evaluated for the case of a wireless line-of-sight channel (**Wireless TOMAS**). The benchmark system for comparison is a system that combines JPEG2000 image compression with Orthogonal Frequency Division Multiplexing. Further this system is referred to as a **JPEG2000+OFDM** system. Both the wireless TOMAS and JPEG2000+OFDM systems as well as a wireless channel are simulated in a Matlab® environment. A grayscale still image is chosen as a data object. The physical layer (PHY) of wireless TOMAS is represented by a **Transmitter** and **Receiver**, while a **Control Block** represents a Media Access Control (MAC) layer in terms of an Open Systems Interconnection Basic Reference Model (OSI), ISO/IEC (1994).

6.2 Wireless TOMAS

While the idea of TOMAS can be applied to any type of communication media, we concentrate our attention on a radio link or wireless communications. Figure 6.1 proposes an architecture for **Wireless TOMAS**.

At the **Data Object Analysis** stage, features of a data object are extracted. Any appropriate technique may be used for this procedure. For example, Mel-Frequency Cepstral Coefficients (MFCC) efficiently represent features of a voice signal, O'Shaughnessy (1999). Or a two dimensional image might be represented by a set of its Discrete Cosine Transform (DCT)

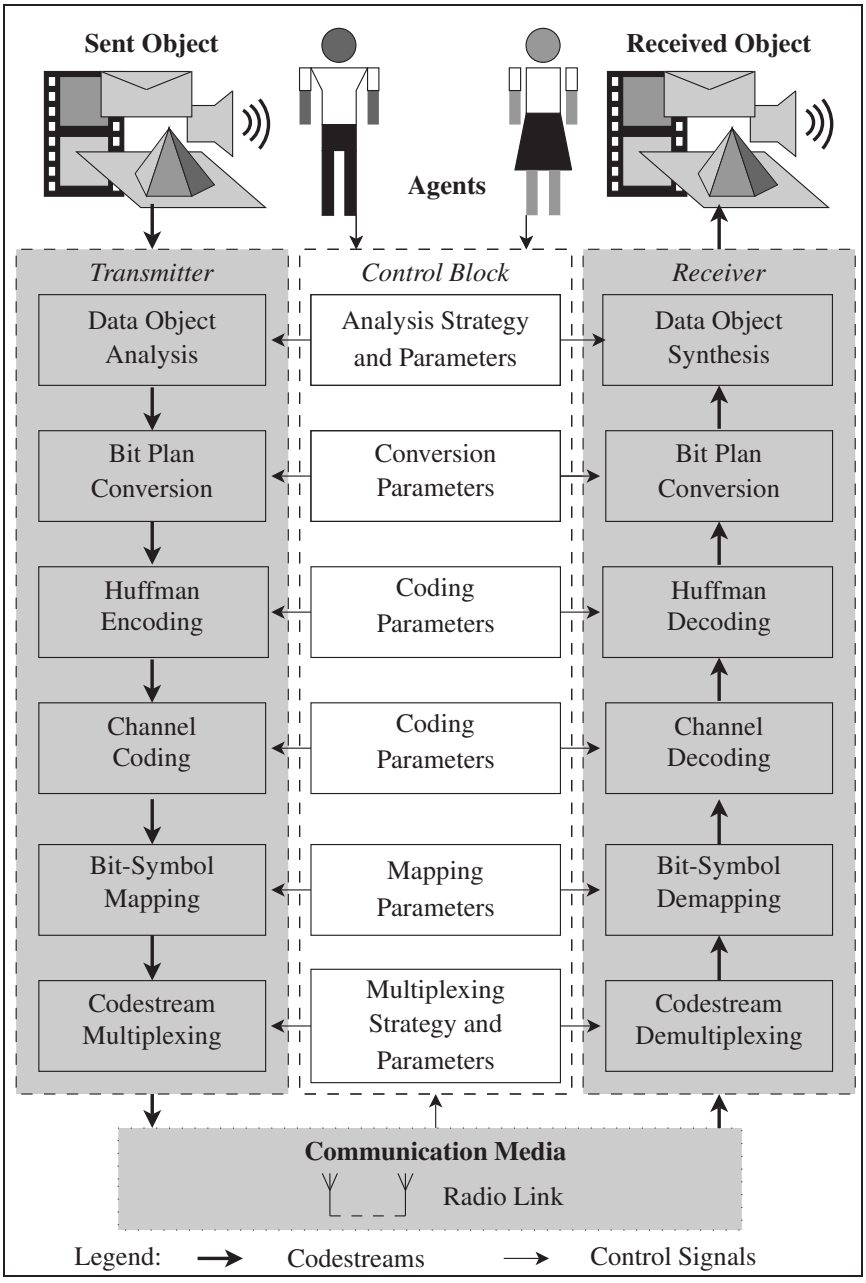

Figure 6.1 Wireless TOMAS system structure.

coefficients. The right Data Object Analysis tool should be able to decompose the data object into data segments of unequal importance. The right **Data Object Synthesis** tool should be

able to restore the data object from the data segments with minimal loss, Pratt (1978). An appropriate quality criterion of a restored data object should be used. Additionally, an Error Sensitivity Descriptor (ESD) might be introduced. ESD reflects the importance of the data segments. A data segment is considered to be more sensitive than a second one if corruption of the first segment causes more damage to the restored data object than corruption of the second segment. The output of the Data Object Analysis block is the set of data segments ranked in descending order according to their importance. The Control Block obtains the list that contains the order of the data segments from the Transmitter and provides it to the Receiver.

The Data Object Analysis often employs floating-point transformations such as DCT or wavelet transform. Therefore the data segments at the output of Data Object Analysis are represented by floating-point numbers. The **Bit-plan Conversion** stage transforms the data segments into a fixed-point representation. Truncation or rounding of floating-point numbers might cause a degradation of quality of a restored data object. A bit-plan conversion stage is the second stage of decomposition of the data object into data segments of unequal importance. The bit-plans of a data segment are formed by grouping corresponding bits of the coefficients as is shown in Figure 6.2. The bit-plan of the data segment that consists of the Most Significant Bits (MSB) of coefficients is considered to be the most important. The bit-plan of the data segment that consists of the Least Significant Bits (LSB) is considered to be the least important. The bits of each bit-plan are grouped into words. A word length can differ from one bit-plan to another as well as from one data segment to another.

The **Huffman Encoding** serves to reduce a redundancy of the bit-plan data. First of all, a histogram of the whole bit-plan data is created. From these results a Huffman code is generated, and finally, the bit-plan data is encoded. The Control Block obtains the histogram from the

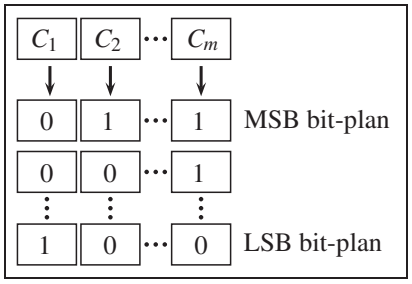

Figure 6.2 Bit-plan conversion.

Transmitter and provides it to the Receiver. An output of the Huffman Encoder is represented by multiple binary code streams.

The Huffman code is very sensitive to the noise, therefore the **Channel Coding** can be useful for some communication environments.

A **Symbol Mapping** stage serves to improve spectral efficiency by mapping a group of bits into a complex symbol. Any appropriate type of Quadrature Amplitude Mapping or Modulation could be employed at this stage, for example, BPSK, QPSK, or in general form, M-QAM.

Multiple code streams of complex symbols should be multiplexed in order to be sent over a serial radio link. Promising techniques such as Orthogonal Frequency Division Multiplexing (OFDM): Engels (2002), Burr (2001), and Wavelet Packet Multiplexing (WPM): Lindsey (1996), Lindsey (1997), Lindsey and Dill (1995), might be used at this stage.

A task of the **Control Block** is to look for a compromise between an application's demands on object transmission and communication media/communication system abilities. In order to fulfill this task, the Control Block could either assign appropriate parameters to the PHY blocks or reconfigure inter-connections between blocks from the PHY layer toolbox.

A technique called Unequal Error Protection (UEP) has been known for a while. Recent works of Wang et al. (2006), Soyjaudah and Fowdur (2006), Ramzan and Izquierdo (2006), Boeglen

and Chatellier (2006), and Thomos et al. (2005) demonstrate some potential of such a technique. A common observation is that most researchers are concentrated on improving some parameters while leaving other parameters unmonitored. For example, they modify their algorithms in order to improve the quality of the transmitted image. Often this leads to degradation of the spectral efficiency of the system.

6.3 Data Transmission Scenario

The following scenario is used to validate the proposed wireless TOMAS technique:

1. **Objects** are grayscale images (8 bits per pixel) from the image database of the Signal and Image Processing Institute, University of Southern California, USC-SIPI (2006). The first image, Lena128, has size 128×128 pixels. It is derived from the image Lena (Girl or Lenna, 4.2.04). Other images have size 512×512 pixels. They are Mandrill or Baboon (4.2.03), Peppers (4.2.07), F16 (4.2.05), Aerial (5.2.09) and Aerial2 (2.1.01). See Figure 6.3;

2. **Communication media** is a band-pass wireless LOS channel, Kjeldsen et al. (2003), with parameters presented in Table 6.1. Additive White Gaussian Noise (AWGN) is present in the channel. The Symbol Rate is 10 MBaud, in other words 10 Msymbols per second;

3. **Application** requires progressive lossless transmission. In other words, transmit the image progressively and without losses in restored image quality;

4. **State of communication systems**. Communication systems employ neither channel coding nor channel estimation.

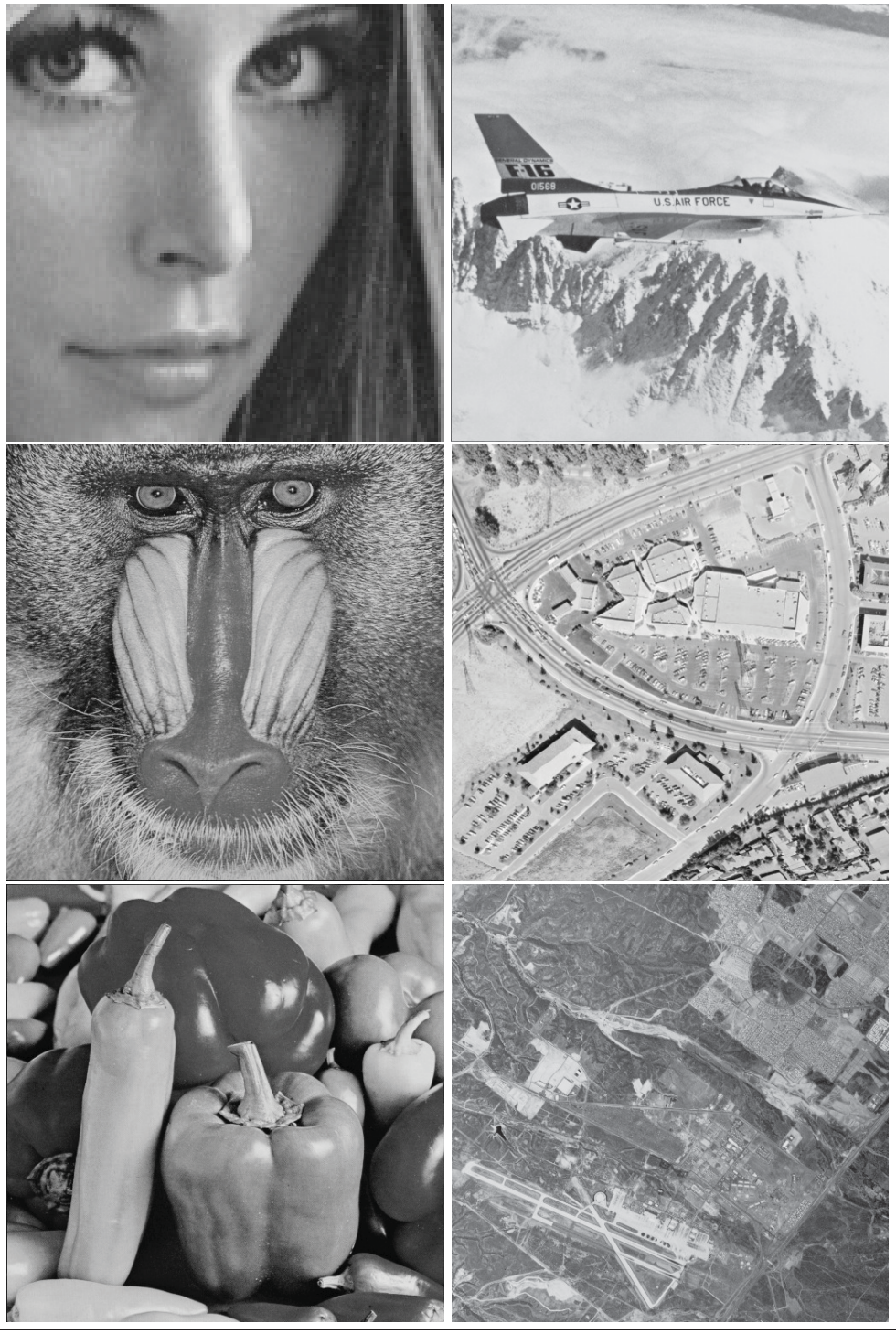

Figure 6.3 Test images from top to bottom and from left to right are Lena128, F16, Mandrill (Baboon), Aerial, Peppers and Aerial2.

Table 6.1 Wireless Channel Parameters

Path	**Type**	**Delay, μs**	**Fade Rate, Hz**	**Loss, dB**
Direct	Ricean	0	2, 37, 225	0
Second	Rayleigh	0.9	2, 37, 225	-3
Third	Rayleigh	5.1	2, 37, 225	-9

6.4 Performance Parameters of Communication System

In order to evaluate performance of a communication system, the following parameters are used:

$$\text{Spectral Efficiency} = \frac{\text{Total Object Bits}}{\text{Transmitted Symbols}}, \tag{6.1}$$

$$\text{Algorithm Complexity} = \frac{\text{Total Processing Operations}}{\text{Total Object Bits}}, \tag{6.2}$$

where

$$\text{Total Object Bits} = 512 * 512 * 8 = 2,097,152 \tag{6.3}$$

for the particular data object described above.

In our case, the **Spectral Efficiency** mentioned in Equation 6.1 is measured in **bits-per-symbol**. It depends on the number of transmitted symbols. The goal of the communication system is to represent the Data Object by a minimal number of symbols. Let us note that, in the case of fixed symbol mapping parameters, any kind of channel coding employed by the system will decrease the spectral efficiency.

The complexity of the communication system is measured by the **Algorithm Complexity** parameter mentioned in Equation 6.2. It reflects how many operations of real addition and multiplication are required in order to process one bit of the transmitted data object.

6.4.1 Quality Parameters of Restored Image

Historically, researchers working in the domain of image processing use **Mean Square Error (MSE)** and **Peak Signal-to-Noise Ratio (PSNR)** as measures of restored image quality. MSE represents a normalized squared difference between pixel values of an original image X and a restored one Y:

$$MSE = \frac{1}{N \cdot M} \sum_{i=1}^{N} \sum_{j=1}^{M} (X_{i,j} - Y_{i,j})^2, \tag{6.4}$$

where $N \times M$ is the image size. PSNR measured in dB, of the 8 bit grayscale image is calculated according to:

$$PSNR = 20 \log_{10} \frac{255}{\sqrt{MSE}}. \tag{6.5}$$

Despite obvious simplicity in calculation and interpretation, the integral image quality parameters, such as MSE and PSNR, are not always reliable image quality measures. Often, the value of PSNR is equal up to 20 dB, even for the case when the restored image is totally destroyed. In the case of lossless transmission, MSE equals to zero, and that leads the value of PSNR to infinity. Therefore the **Visual Information Fidelity measure (VIF)**, Sheikh and Bovik (2006), has also been measured. It is a natural measure of restored image quality. VIF usually lies in the interval [0,1]. VIF = 0 indicates that all sent image data has been lost in the distortion channel. VIF = 1 shows that the image is not distorted at all. The case VIF>1 indicates that received image is better than the sent one.

6.4.2 PSNR and MSE bounds for image transmission based on BPSK

Making experiments, it is always important to have some benchmark data to evaluate the performance of a simulated system. In our case it would be theoretically calculated PSNR and MSE bounds for image transmission based on a BPSK modulation in the AWGN channel.

In a general form, PSNR can be represented by the following expression:

$$PSNR_{dB} = 20\log_{10}\frac{w_\psi - 1}{\sqrt{MSE}}, \tag{6.6}$$

where w_ψ is the weight of the ψ-th bit, the most significant bit (MSB) in an image pixel, and ψ is a total number of bits that represents the image pixel, also known as a **bits-per-pixel** (bpp) parameter.

The MSE parameter tends to decrease and the PSNR parameter tends to increase, when values of the received image pixels approach ones of the transmitted image pixels. Let us assume an ideal image transmission system, and the only source of received image corruption is a propagation channel. Suppose we deal with the AWGN channel. The further assumption is that we transmit our image line-by-line using a **Binary Phase Shift Keying** (BPSK). It is known that the error probability per bit p for such a technique is the following:

$$p = Q\left(\sqrt{\frac{2E_b}{N_0}}\right), \tag{6.7}$$

where, E_b/N_0 is a Signal-to-Noise Ratio of the AWGN channel per bit. It is often expressed in decibels:

$$(E_b/N_0)_{dB} = 10 \cdot log_{10}(E_b/N_0). \tag{6.8}$$

Assume that we transmit a grayscale image, size $N \times M$ pixels. The luminosity of each image pixel is represented by ψ bits. Hence, the total bit number Θ the image consists of is the following:

$$\Theta = \psi \cdot N \cdot M. \tag{6.9}$$

The image bits become the subject of corruption, while propagating over the AWGN channel. The total number of corrupted image bits κ_{total} is the following:

$$\kappa_{total} = p \cdot \Theta = p \cdot \psi \cdot N \cdot M, \tag{6.10}$$

where p is the bit error probability and Θ is the total image bits calculated in Equations 6.7 and 6.9 accordingly.

Any bit representing the image pixel could be corrupted, while propagating over the AWGN channel. It is obvious that corruption of the Most Significant Bit (MSB) of the image pixel affects the restored image quality more than corruption of the Least Significant Bit (LSB). In general, the total number of corrupted image bits κ_{total} consists of the number of corrupted MSB, corrupted LSB and all corrupted bits between them. Assume that the bit $(\psi - 1)$ is MSB and the bit 0 is LSB. In that case, the total number of corrupted image bits κ_{total} is the following:

$$\kappa_{total} = \kappa_{\psi-1} + \kappa_{\psi-2} + \kappa_{\psi-3} + \ldots + \kappa_1 + \kappa_0 = \sum_{b=0}^{\psi-1} \kappa_b, \tag{6.11}$$

where $\kappa_{\psi-1}$ is the overall number of corrupted $(\psi - 1)$th bits (MSB), κ_0 is the overall number of corrupted 0th bits (LSB), and κ_b is the overall number of corrupted bth bits in the image pixels.

The MSE parameter represents the square difference between the sent $X_{i,j}$ and received $Y_{i,j}$ pixels accumulated over the whole image and normalized. Consider the one pixel case. The absolute difference between the sent and received pixel intensity, $d_{i,j}$, can be represented by the following expression:

$$d_{i,j} = |X_{i,j} - Y_{i,j}| = \sum_{b=0}^{\psi-1} C_{i,j}^{b} \cdot w_b, \tag{6.12}$$

where $C^b_{i,j}$ is the **pixel bit corruption operator**. $C^b_{i,j} = 1$ if the bth bit of the image pixel (i, j) is corrupted during transmission, and $C^b_{i,j} = 0$ if the bth bit of the image pixel (i, j) is preserved.

Equation 6.4 for the Mean Square Error (MSE) can be transformed into the following form using Equation 6.12:

$$\begin{aligned} MSE &= \frac{1}{N \cdot M} \sum_{i=1}^{N} \sum_{j=1}^{M} (|X_{i,j} - Y_{i,j}|)^2 = \frac{1}{N \cdot M} \sum_{i=1}^{N} \sum_{j=1}^{M} d^2_{i,j} = \\ &= \frac{1}{N \cdot M} \sum_{i=1}^{N} \sum_{j=1}^{M} \left(\sum_{b=0}^{\psi-1} C^b_{i,j} \cdot w_b \right)^2 . \end{aligned} \tag{6.13}$$

Now we can present the received image quality parameter PSNR as a function of the pixel bit corruption operator C. The pixel bit corruption operator C is often difficult to determine, because it is impossible to predict theoretically which bit in which pixel will be corrupted due to signal propagation over the AWGN channel. Hence, Equation 6.13 in its actual form is not very helpful. At first, we thus replace the deterministic pixel bit corruption operator C with the expected value of discrete random variable $\overline{C}$ which is the random pixel bit corruption operator of the bth bit in the (i, j) pixel as follows:

$$\begin{aligned} \overline{C^b_{i,j}} &= C^b_{1_{i,j}} \cdot Pr\left(\overline{b}|b\right)_{i,j} + C^b_{0_{i,j}} \cdot Pr\left(b|b\right)_{i,j} = \\ &= 1 \cdot Pr\left(\overline{b}|b\right)_{i,j} + 0 \cdot Pr\left(b|b\right)_{i,j} = Pr\left(\overline{b}|b\right)_{i,j} . \end{aligned} \tag{6.14}$$

After substitution of the pixel bit corruption operator C in Equation 6.13 with the expected value of the random pixel bit corruption operator $\overline{C}$ from Equation 6.14, an expression for MSE will have a new stochastic look:

$$MSE \frac{1}{N \cdot M} \sum_{i=1}^{N} \sum_{j=1}^{M} \left(\sum_{b=0}^{\psi-1} Pr\left(\overline{b}|b\right)_{i,j} \cdot w_b \right)^2 .$$

A pixel that contains one or more corrupted bits is considered the **corrupted pixel**. Only corrupted pixels influence the quality of the received image:

$$MSE = \frac{1}{N \cdot M} \sum_{corrupted\ \ pixels} \left(\sum_{b=0}^{\psi-1} Pr\left(\overline{b}|b\right)_{i,j} \cdot w_b \right)^2. \tag{6.15}$$

For further development of the expression for MSE we need to define the number of corrupted pixels. Assume that a telecommunication system performs so badly (due to low E_b/N_0) that every pixel of the received image contains a corrupted bit, hence the total number of corrupted bits is equal to the total number of image pixels:

$$\kappa_{total} = N \cdot M. \tag{6.16}$$

This assumption allows us to use the value of κ_{total} from Equation 6.10 in Equation 6.16 or vice versa:

$$\begin{gathered} \kappa_{total} = N \cdot M \text{ and } \kappa_{total} = p \cdot \psi \cdot N \cdot M, \\ \text{hence } N \cdot M = p \cdot \psi \cdot N \cdot M \ => \ 1 = p \cdot \psi \ => \ p = \frac{1}{\psi}. \end{gathered} \tag{6.17}$$

Having in mind the real values of bits-per-pixel (bpp), we can conclude that if every pixel of the received image contains a corrupted bit, the system provides the following bit error rates:

$$\begin{aligned} \text{for } \psi &= 8 \text{ bits BER } p = \frac{1}{\psi} \ => \ p = \frac{1}{8} = 0.125; \\ \text{for } \psi &= 12 \text{ bits BER } p = \frac{1}{\psi} \ => \ p = \frac{1}{12} = 0.0833. \end{aligned} \tag{6.18}$$

Those values of BER from Equation 6.18 are far away from the reality. Usually, the telecommunication system performs much better, providing BER $p_{real} = 10^{-3} \ldots 10^{-6}$. Hence, for the real system not every pixel of the received image contains a corrupted bit and the following

inequality makes sense:

$$p_{real} \leq \frac{1}{\psi}. \tag{6.19}$$

Suppose that the corrupted pixel contains only one corrupted bit. In that case the total number of corrupted pixels is equal to the total number of corrupted bits as follows:

$$Total\ corrupted\ pixels = \kappa_{total} = p \cdot \psi \cdot N \cdot M. \tag{6.20}$$

Substitution of Equation 6.20 into Equation 6.15 gives:

$$\begin{aligned} MSE &= \frac{1}{N \cdot M}(p \cdot \psi \cdot N \cdot M) \cdot \left(\sum_{b=0}^{\psi-1} Pr\left(\overline{b}|b\right)_{i,j} \cdot w_b \right)^2 = \\ &= p \cdot \psi \cdot \left(\sum_{b=0}^{\psi-1} Pr\left(\overline{b}|b\right)_{i,j} \cdot w_b \right)^2. \end{aligned}$$

Assume that any bit in the image pixel has an equal probability of error. And the probability of bit error does not depend on which pixel is considered. It can be represented by the following:

$$Pr\left(\overline{b}|b\right)_{i,j} = Pr\left(\overline{b}|b\right) = \frac{1}{\psi}. \tag{6.21}$$

Further development of Equation 6.21 using Equation 6.21 gives the following:

$$\begin{aligned} MSE &= p \cdot \psi \cdot \left(\sum_{b=0}^{\psi-1} Pr\left(\overline{b}|b\right)_{i,j} \cdot w_b \right)^2 = p \cdot \psi \cdot \frac{1}{\psi} \cdot \sum_{b=0}^{\psi-1} w_b^2 = \\ &= p \cdot \sum_{b=0}^{\psi-1} w_b^2. \end{aligned} \tag{6.22}$$

Consider the following geometric serie:

$$S = a + ar + ar^2 + ar^3 + \ldots + ar^{n-1} = \sum_{k=0}^{n-1} ar^k = a\frac{1-r^n}{1-r}, \tag{6.23}$$

hence the summation:

$$\sum_{b=0}^{\psi-1} w_b^2 = \sum_{b=0}^{\psi-1} 2^2 b = \sum_{b=0}^{\psi-1} 4^b - \frac{1-4^{\psi}}{1-4} = \frac{4^{\psi}-1}{4-1} = \frac{4^{\psi}-1}{3}. \tag{6.24}$$

Equation 6.22 can be presented as follows:

$$MSE = p \cdot \sum_{b=0}^{\psi-1} w_b^2 = p \cdot \frac{4^{\psi}-1}{3}. \tag{6.25}$$

In the case $w^{\psi} = 2^{\psi}$, use of Equation 6.25 in Equation 6.6 gives the following result:

$$PSNR_{dB} = 20 \cdot \log_{10} \frac{w_{\psi}-1}{\sqrt{MSE}} = 20 \log_{10} \frac{2^{\psi}-1}{\sqrt{p \cdot \frac{4^{\psi}-1}{3}}}, \tag{6.26}$$

6.4.3 Recapitulation

In order to evaluate performance of the BPSK-based single-carrier transmission system used for the still image transmission over the AWGN channel, the bounds of Peak Signal-to-Noise Ratio and Mean Square Error of the received image can be calculated according to:

$$\begin{aligned} MSE &= p \cdot \frac{4^{\psi}-1}{3}; \\ PSNR_{dB} &= 20 \cdot \log_{10} \frac{2^{\psi}-1}{\sqrt{p \cdot \frac{4^{\psi}-1}{3}}}. \end{aligned} \tag{6.27}$$

where

E_b/N_0 is the Signal-to-Noise Ratio of the AWGN channel per bit;

ψ is a total number of bits that represents the image pixel, bits-per-pixel (bpp). In case of

grayscale image transmission:

$$\begin{aligned} MSE &= p \cdot \frac{4^8 - 1}{3} = 21845 \cdot p; \\ PSNR_{dB} &= 20 \cdot \log_{10} \frac{2^8 - 1}{\sqrt{21845 \cdot p}} = 20 \cdot \log_{10} \frac{255}{\sqrt{21845 \cdot p}}. \end{aligned} \tag{6.28}$$

Table 6.2 shows how the theoretically obtained PSNR bound is close to the simulated values of PSNR.

Table 6.2 Comparison of the PSNR bound and practical values of PSNR

AWGN E_b/N_0, dB	**BER, p**	**PSNR, dB**	
		Theory	Practice
4.5	10^{-2}	24.74	24.7
6.5	10^{-3}	34.74	34.7

The MSE and PSNR bounds obtained theoretically, for the case of grayscale image transmission over the AWGN channel using BPSK modulation, could serve as the benchmark values for more complex cases of data communication, for example, a still image transmission over a multipath AWGN channel, as it is described in the following section.

6.5 Structure of the Wireless TOMAS for Image Transmission

A communication system under investigation operates with two-dimensional images. Now-a-days the most popular technique to deal with such data is a Discrete Cosine Transform (DCT). It is employed by several standards: JPEG (1994) for still image compression, and MPEG-1,2,4 for video compression. These standards are well developed and may be employed at the

Data Object Analysis stage of the wireless TOMAS algorithm. However the data compression technique based on the block DCT has a drawback that makes it unsuitable for our scenario. It does not support a progressive transmission which is important for our wireless communication scenario. This type of data transmission operates in the following manner: a low resolution, low quality thumbnail of the original image is sent in the first place, and refinement data is sent later. **Progressive transmission** allows a recipient to have the whole image even if transmission is not completed. The quality of restored images will depend on transmission duration before it is cut. Longer transmission time provides better quality. Ideally, progressive transmission should be lossless if no interruption occurs. Progressive transmission provides also a flexible tool for a spectral efficiency manipulation. Arbitrary spectral efficiency could be obtained simply by stopping data transmission after a certain number of symbols have been transmitted (see Equation 6.1). Techniques that decompose the data object into segments suitable for the progressive transmission typically use wavelet or wavelet packet decomposition.

Figure 6.4 shows the structure of a communication system that satisfies the required scenario. A two-dimensional wavelet packet decomposition has been employed for the Data Object Analysis. Wavelet packet decomposition is chosen over wavelet decomposition, employed in the JPEG 2000 algorithm, JPEG (2000), because it provides far finer data segmentation. Losing a large data segment while transmitting data in a harsh channel leads to more damage than losing a small segment. However this choice increases algorithm complexity. The depth of image decomposition is selected to be equal to three. This choice is motivated by the compromise between data segment size and algorithm complexity.

The part of the wireless TOMAS system most vulnerable to channel noise is the Huffman encoding. Long Huffman codes are more vulnerable than short ones. Since our experimental data transmission system does not employ any channel coding, the transmitted data will be

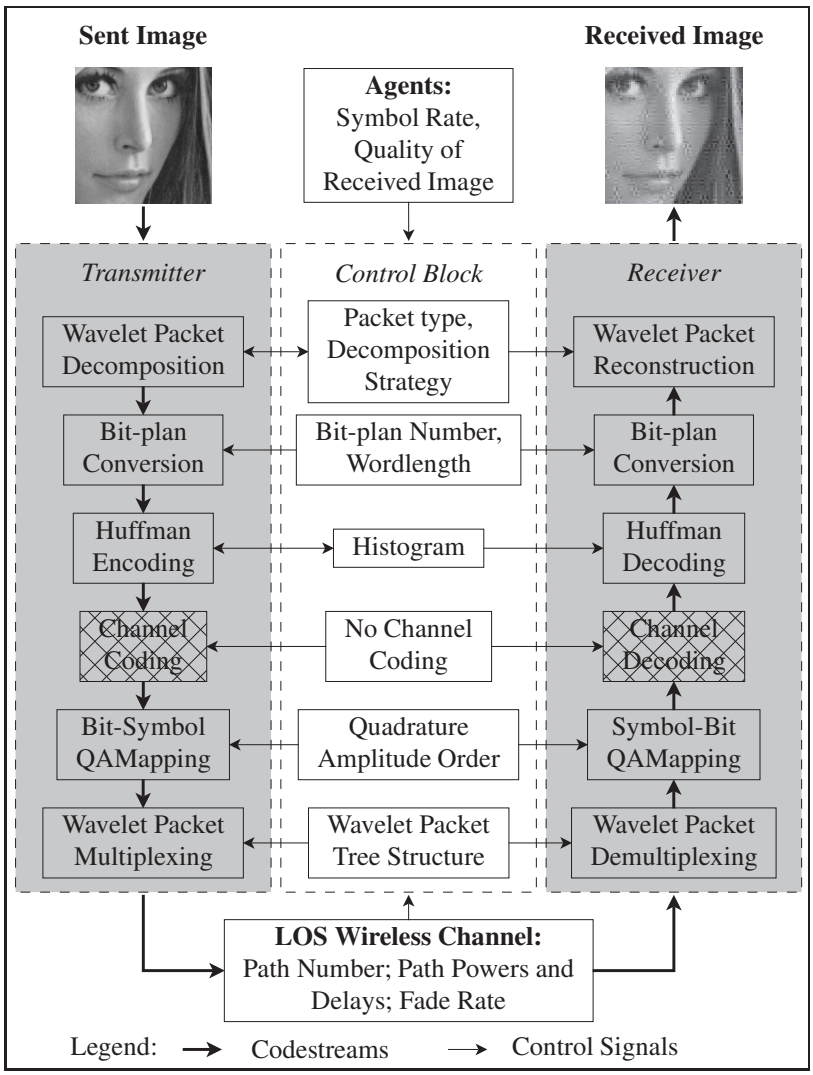

Figure 6.4 Structure of the Wireless TOMAS for Image Transmission.

affected seriously by harsh channel conditions. Therefore the *word length* $= 2$ bits is chosen as a bit-plan conversion parameter. It means that in every bit-plan two bits are grouped into one symbol. A two-bit symbol may take $2^2 = 4$ different values. The histogram of such a source has only 4 bins. This makes a Huffman map very short and less vulnerable to noise. However a short Huffman code reduces spectral efficiency of the system.

In order to convert the code stream bits into complex symbols, Quadrature Amplitude Mapping is employed. QAM $order = 2$ provides high robustness to the channel noise, but reduces the spectral efficiency of the system.

Two alternatives were considered for the Code stream Multiplexing. They are Orthogonal Frequency Division Multiplexing (OFDM) and Wavelet Packet Multiplexing (WPM). Harmonics employed by OFDM are orthogonal in the frequency domain only. Wavelet Packets are orthogonal to each other both in the time and frequency domains. Papers of Yang et al. (1997), Newlin (1998), Suzuki et al. (1999) show that WPM mitigates multipath channel interference better than OFDM does. Relatively high complexity of the wavelet packet transformation algorithms used in the mentioned above papers might be the reason WPM did not gain as much popularity as OFDM did. We developed the fast wavelet packet algorithm, which allowed us to employ WPM for the wireless TOMAS at the Code stream Multiplexing stage. Results of Wang et al. (2006) show that increasing the order of a wavelet does not bring significant improvement in performance, but dramatically increases algorithm complexity.

In order to preserve orthogonality between wavelet packets, one frame WPM should consist of the following number of wavelet packets, called subbands in the literature:

$$Subband\ Number = 2 \cdot 2^{ceil(\log_2 \frac{\tau_{max}}{T_s})}, \tag{6.29}$$

where τ_{max} is the maximum path delay and T_s is the symbol duration. In the case of our particular data transmission scenario, shown in Table 6.1, WPM operates with the following number of subbands:

$$Subband\ Number = 2 \cdot 2^{ceil(\log_2 \frac{5.1 \cdot 10^{-6}}{10^{-7}})} = 128. \tag{6.30}$$

6.6 Structure of the Benchmark Communication System

The performance of data transmission using wireless TOMAS has been compared to the results of the benchmark communication system. The benchmark system uses the JPEG2000 algorithm for the Data Object Analysis and the WirelessMAN OFDM, IEEE (2004), for the code stream multiplexing, as shown in Figure 6.5.

JPEG2000 employs wavelet decomposition based on the wavelet **jpeg9.7**. The decomposition depth is equal to four. The word length is equal to two, as the bit-plan conversion parameter, and the QAM order is equal to two, as the bit-symbol mapping parameter. The WirelessMAN OFDM parameters are presented in Table 6.3.

Table 6.3 WirelessMAN
OFDM PHY Parameters

FFT size	Nfft = 256
Guard Number	Ng = 55
Pilot Number	P = 8
Cyclic Prefix Ratio	CP = 1/2

6.7 Performance comparison of wireless TOMAS and JPEG2000 WirelessMAN OFDM communication systems

Performances of the two communication systems are evaluated and compared for the cases of low (fade rate = 2 Hz), moderate (fade rate = 37 Hz) and high (fade rate = 225 Hz) relative mobility between the transmitter and receiver antennas. The influence of AWGN was estimated

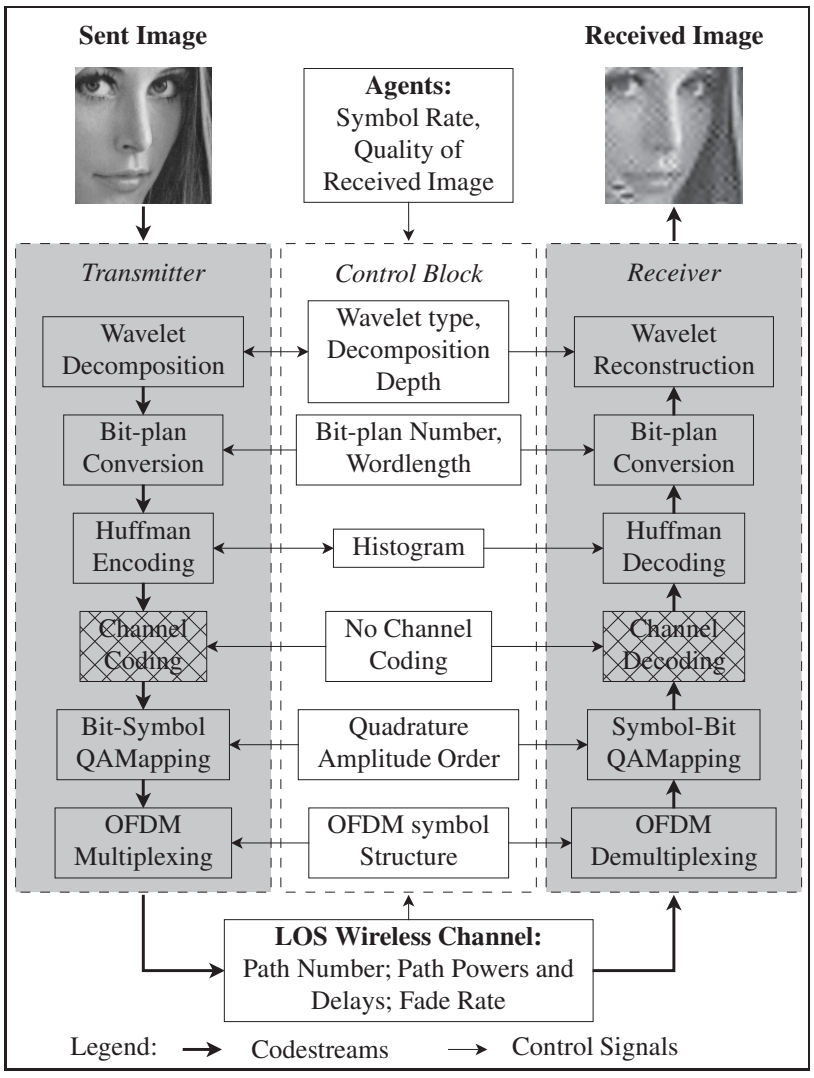

Figure 6.5 Structure of the Benchmark Communication System JPEG2000+WirelessMAN OFDM.

for the following values of SNR: 6, 8, 10, 17, 25, 35, 40 and 45 dB. Figures 6.6-6.17 present performances of the two systems and the difference between them for the case of low (fade rate = 2 Hz) relative mobility between the transmitter and receiver antennas. Let us recall that the lossless transmission case drives PSNR towards infinity. We assumed that PSNR = 80 dB corresponds to the **lossless case**. Figures 6.18-6.29 present performances of the two systems

and the difference between them for the case of moderate (fade rate = 37 Hz) relative mobility between the transmitter and receiver antennas. Figures 6.30-6.41 present performances of the two systems and the difference between them using the PSNR criterion for the case of high (fade rate = 225 Hz) relative mobility between the transmitter and receiver antennas.

The wireless TOMAS provides lossless image transmission in low and moderate fading rates. For spectral efficiencies of 2 bit/symbol and 10 bit/symbol, the two systems have a similar performance in low and moderate fading environments according to the PSNR criterion. However, according to the VIF criterion, the wireless TOMAS performs better than its competitor. Low spectral efficiency of 0.8 bit/symbol results demonstrate the advantage of wavelet packet decomposition employed by the wireless TOMAS over wavelet decomposition employed by JPEG2000. As was mentioned above, wavelet packet decomposition provides finer data segmentation than wavelet decomposition. In a fading channel environment a larger data segment is transmitted longer, hence it is more affected by fading than the short data segment. In the case of fast fading rates (fading rate = 225 Hz), the wireless TOMAS also outperforms JPEG2000+OFDM by providing up to 7 dB more in PSNR and up to 35 percent in VIF.

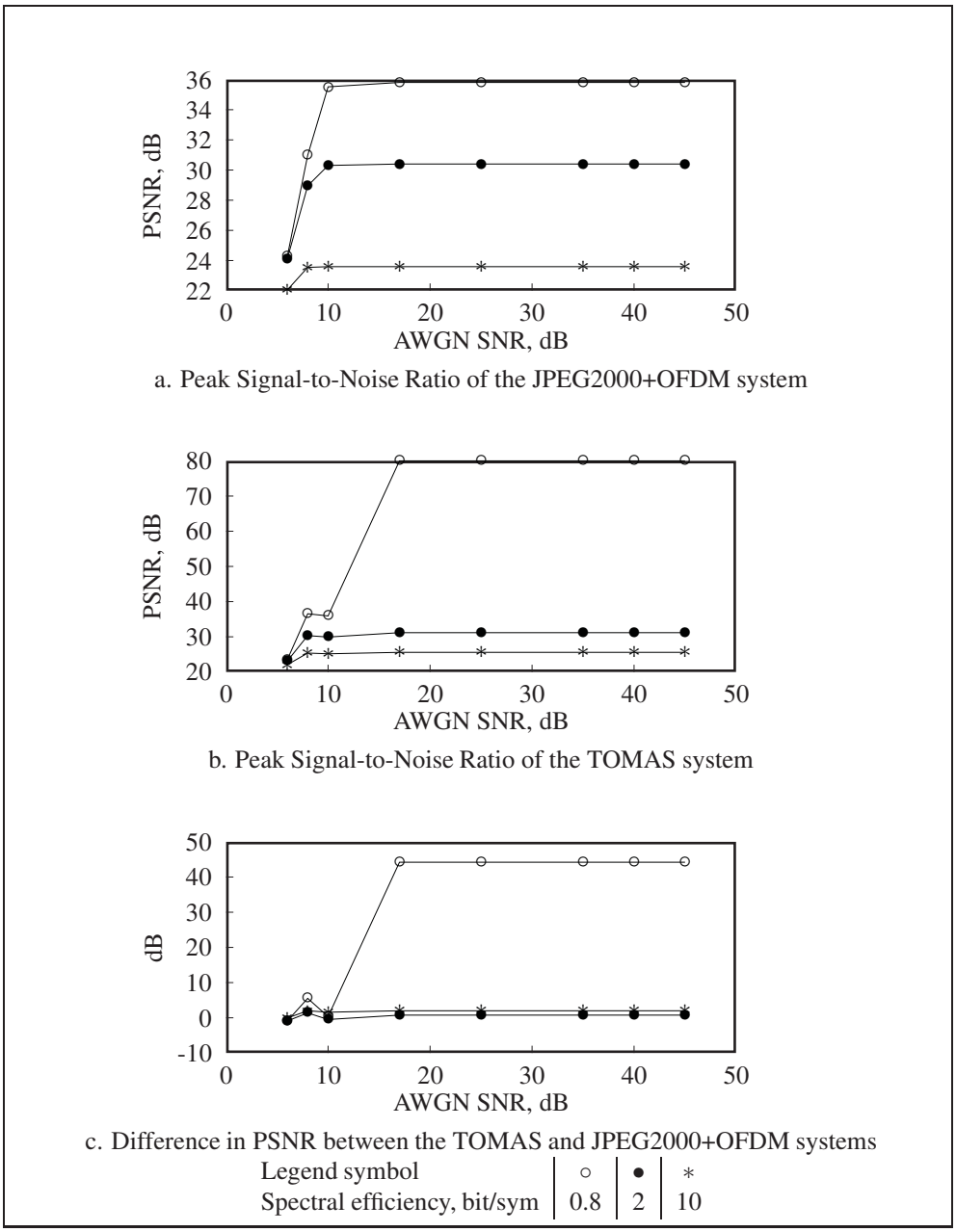

Figure 6.6 Comparison of system performances using the PSNR criterion and the image Lena128. Fading rate = 2 Hz.

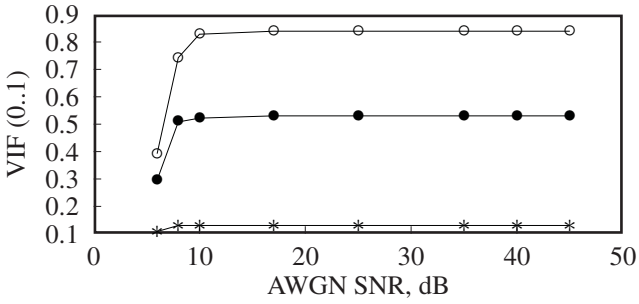

a. Visual Information Fidelity Measure of the JPEG2000+OFDM system

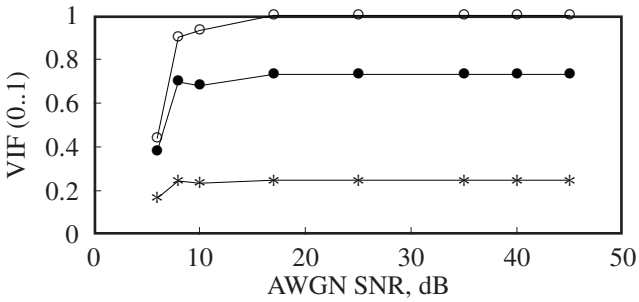

b. Visual Information Fidelity Measure of the TOMAS system

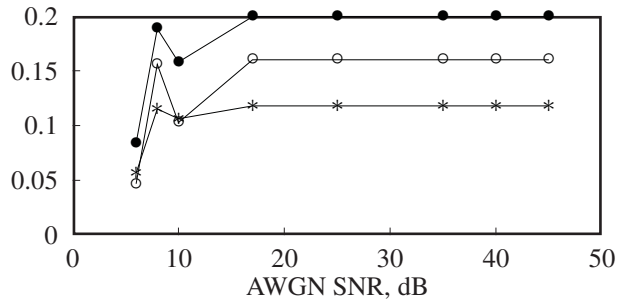

c. Difference in VIF between the TOMAS and JPEG2000+OFDM systems

Legend symbol	○	●	∗
Spectral efficiency, bit/sym	0.8	2	10

Figure 6.7 Comparison of system performances using the VIF criterion and the image Lena128. Fading rate = 2 Hz.

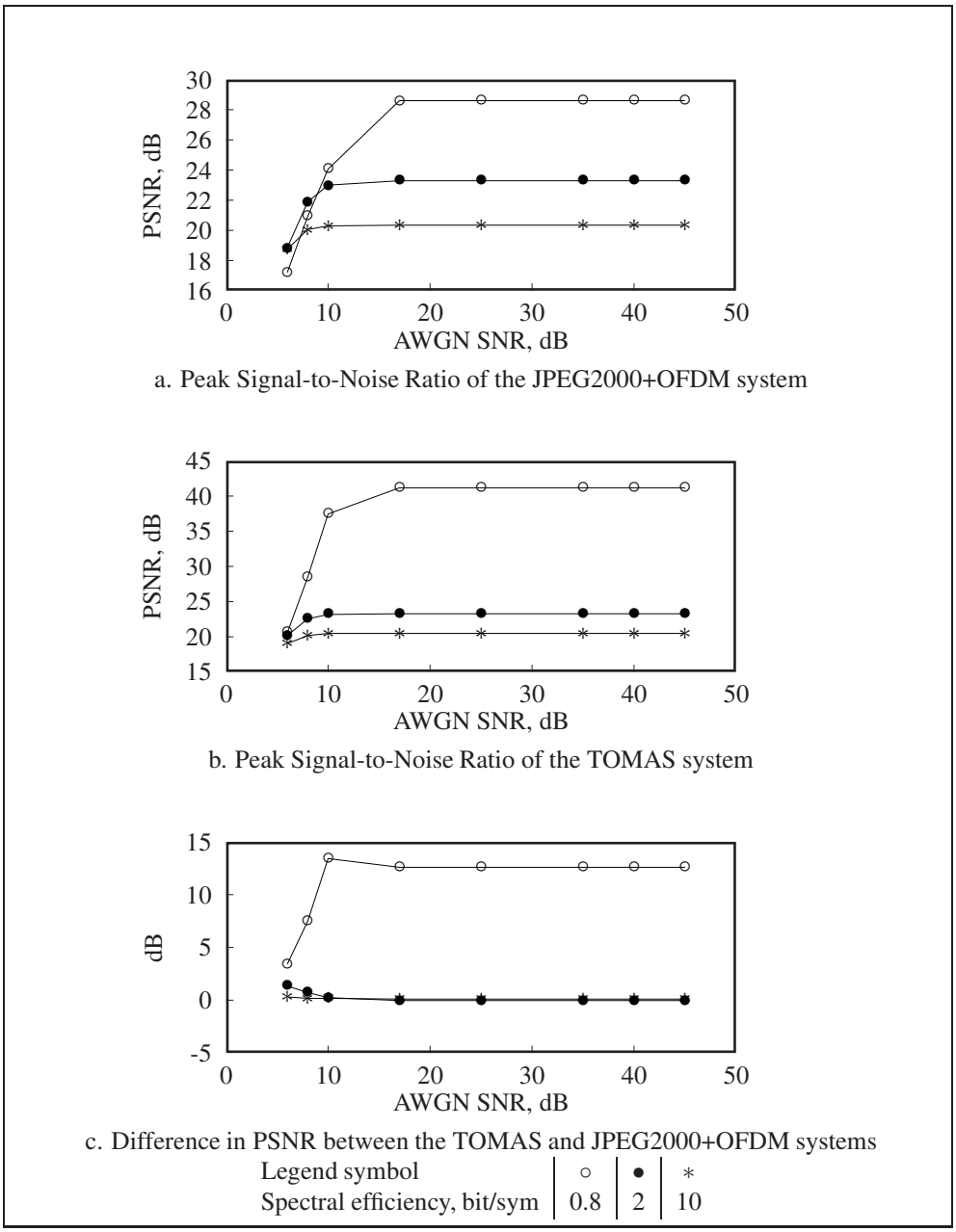

Figure 6.8 Comparison of system performances using the PSNR criterion and the image Mandrill. Fading rate = 2 Hz.

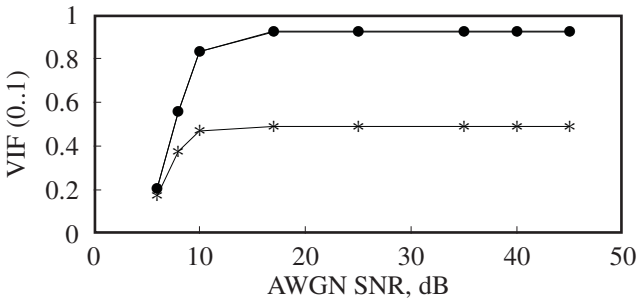

a. Visual Information Fidelity Measure of the JPEG2000+OFDM system

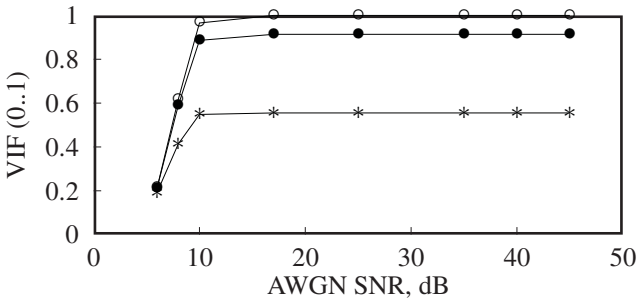

b. Visual Information Fidelity Measure of the TOMAS system

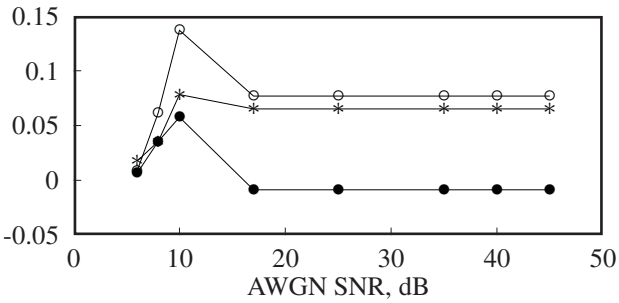

c. Difference in VIF between the TOMAS and JPEG2000+OFDM systems

Legend symbol	○	●	∗
Spectral efficiency, bit/sym	0.8	2	10

Figure 6.9 Comparison of system performances using the VIF criterion and the image Mandrill. Fading rate = 2 Hz.

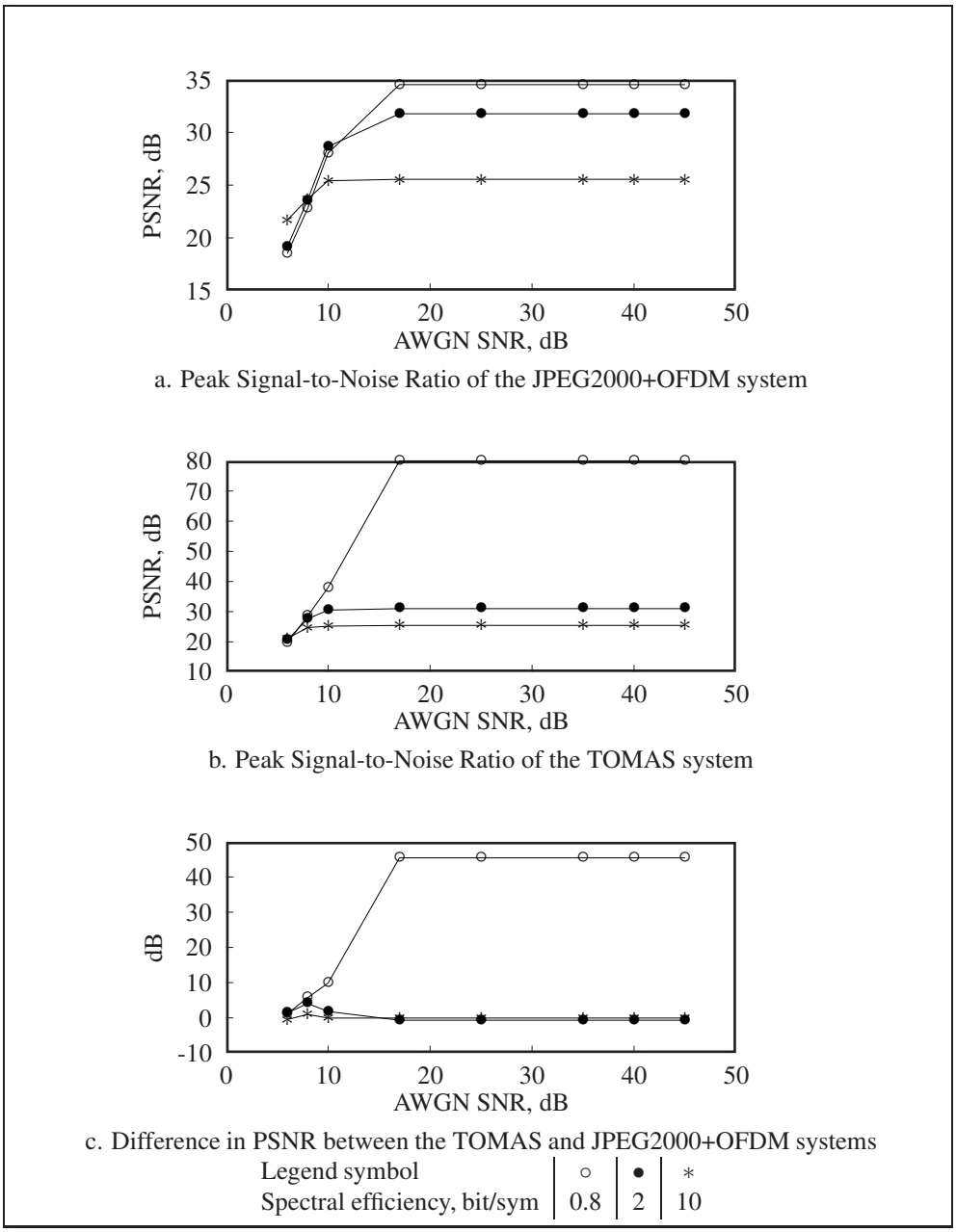

Figure 6.10 Comparison of system performances using the PSNR criterion and the image Peppers. Fading rate = 2 Hz.

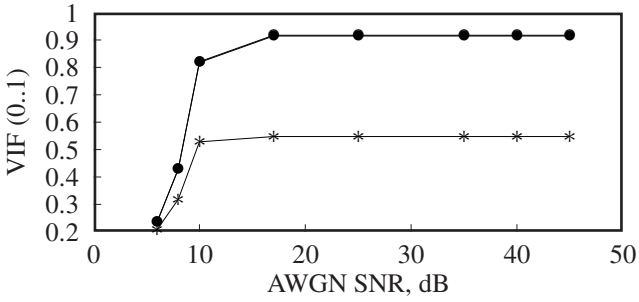

a. Visual Information Fidelity Measure of the JPEG2000+OFDM system

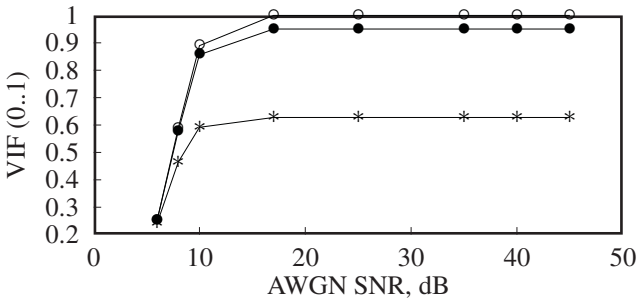

b. Visual Information Fidelity Measure of the TOMAS system

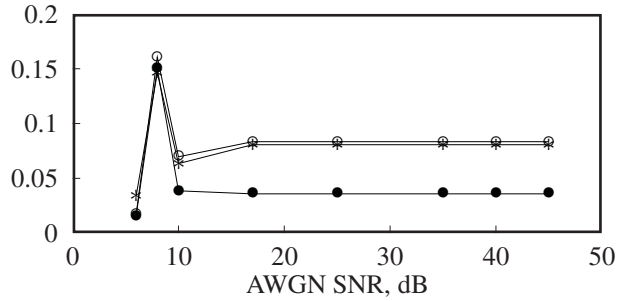

c. Difference in VIF between the TOMAS and JPEG2000+OFDM systems

Legend symbol	○	●	∗
Spectral efficiency, bit/sym	0.8	2	10

Figure 6.11 Comparison of system performances using the VIF criterion and the image Peppers. Fading rate = 2 Hz.

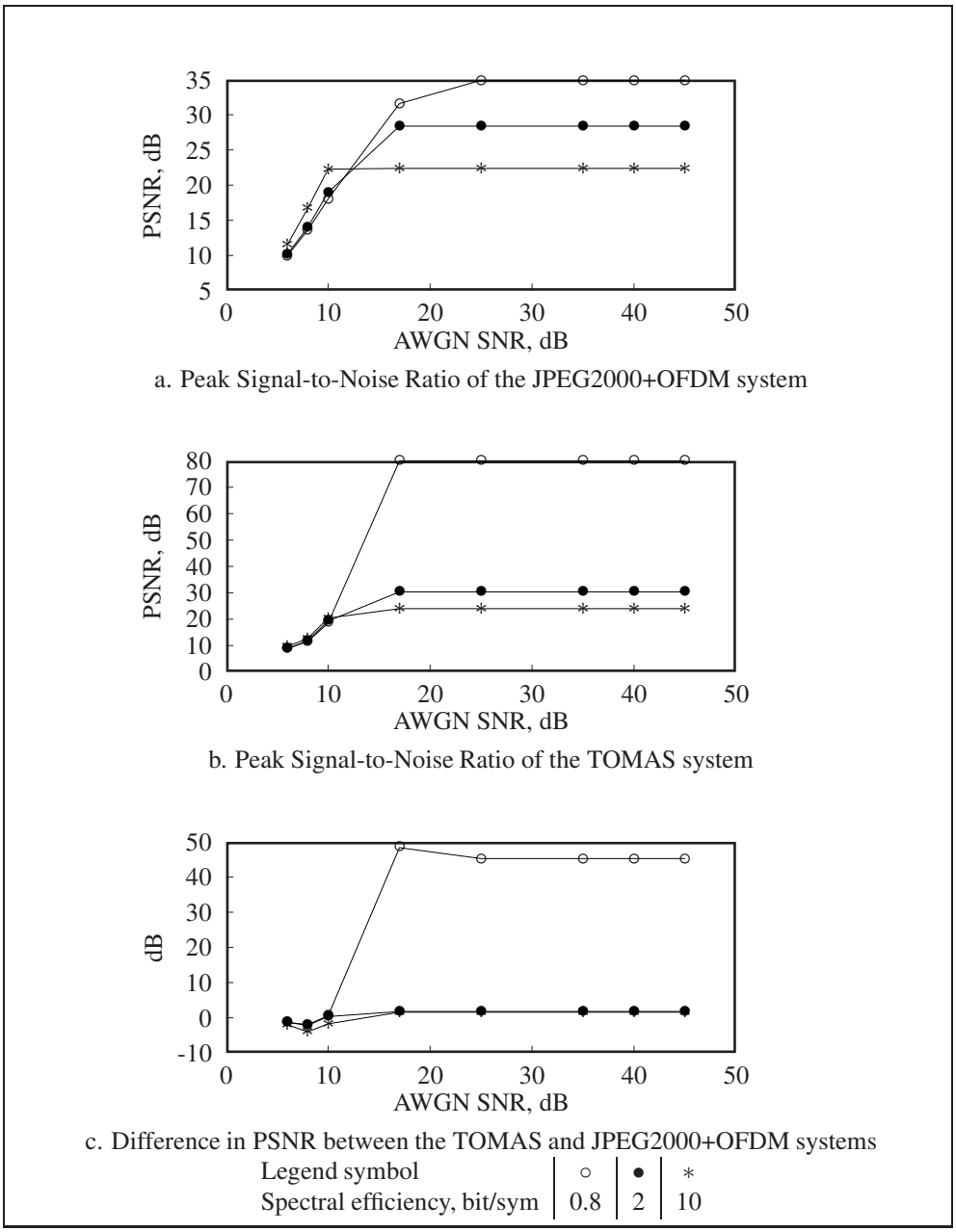

Figure 6.12 Comparison of system performances using the PSNR criterion and the image F16. Fading rate = 2 Hz.

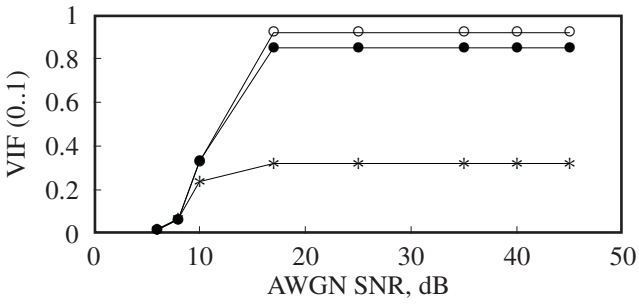

a. Visual Information Fidelity Measure of the JPEG2000+OFDM system

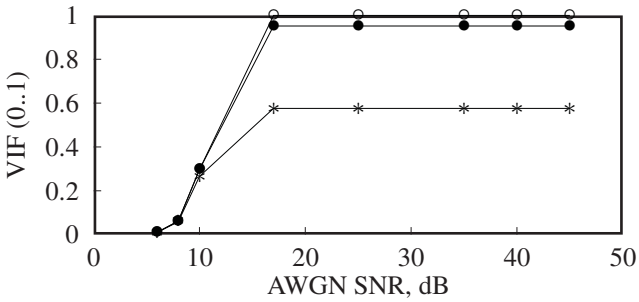

b. Visual Information Fidelity Measure of the TOMAS system

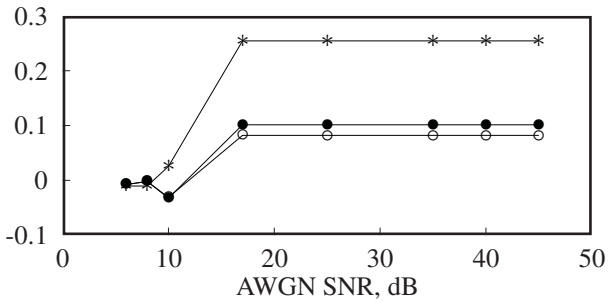

c. Difference in VIF between the TOMAS and JPEG2000+OFDM systems

Legend symbol	○	●	∗
Spectral efficiency, bit/sym	0.8	2	10

Figure 6.13 Comparison of system performances using the VIF criterion and the image F16. Fading rate = 2 Hz.

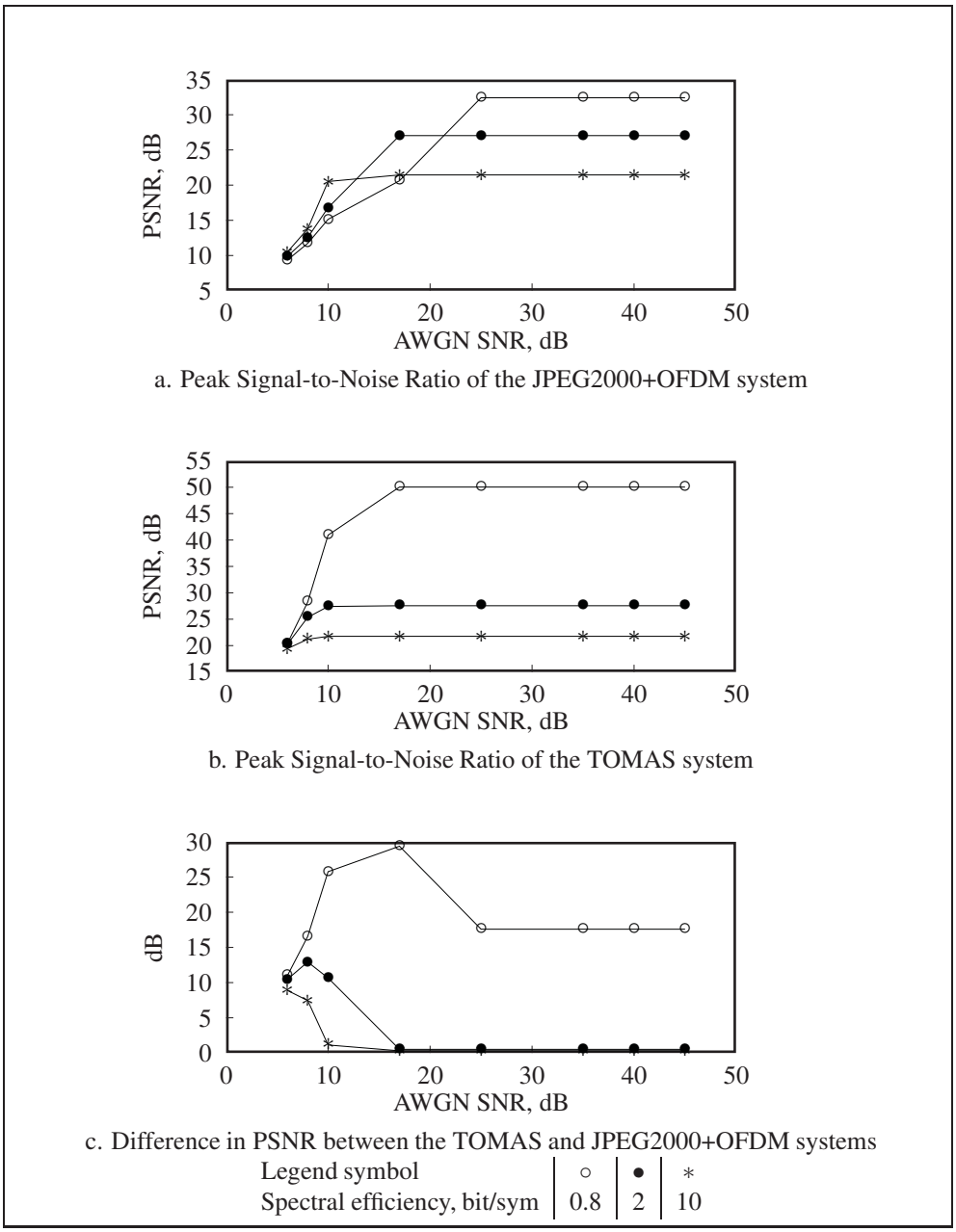

Figure 6.14 Comparison of system performances using the PSNR criterion and the image Aerial. Fading rate = 2 Hz.

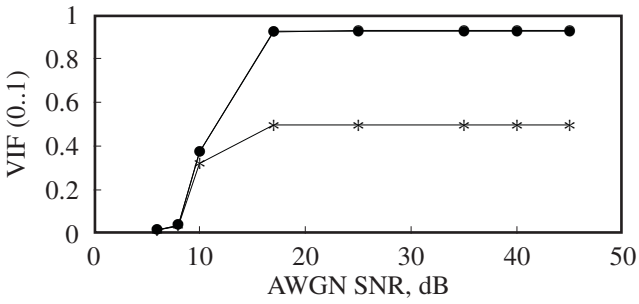

a. Visual Information Fidelity Measure of the JPEG2000+OFDM system

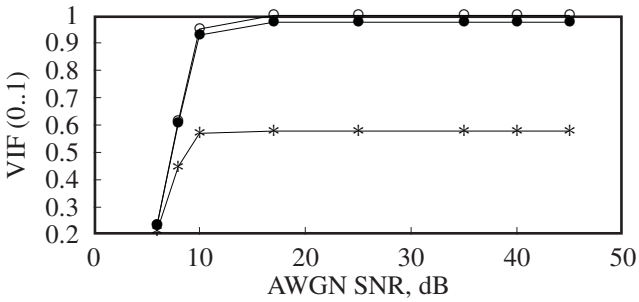

b. Visual Information Fidelity Measure of the TOMAS system

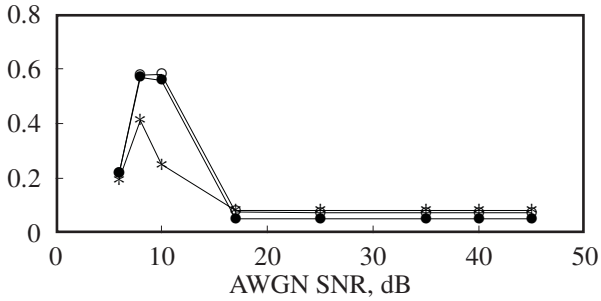

c. Difference in VIF between the TOMAS and JPEG2000+OFDM systems

Legend symbol	○	●	∗
Spectral efficiency, bit/sym	0.8	2	10

Figure 6.15 Comparison of system performances using the VIF criterion and the image Aerial. Fading rate = 2 Hz.

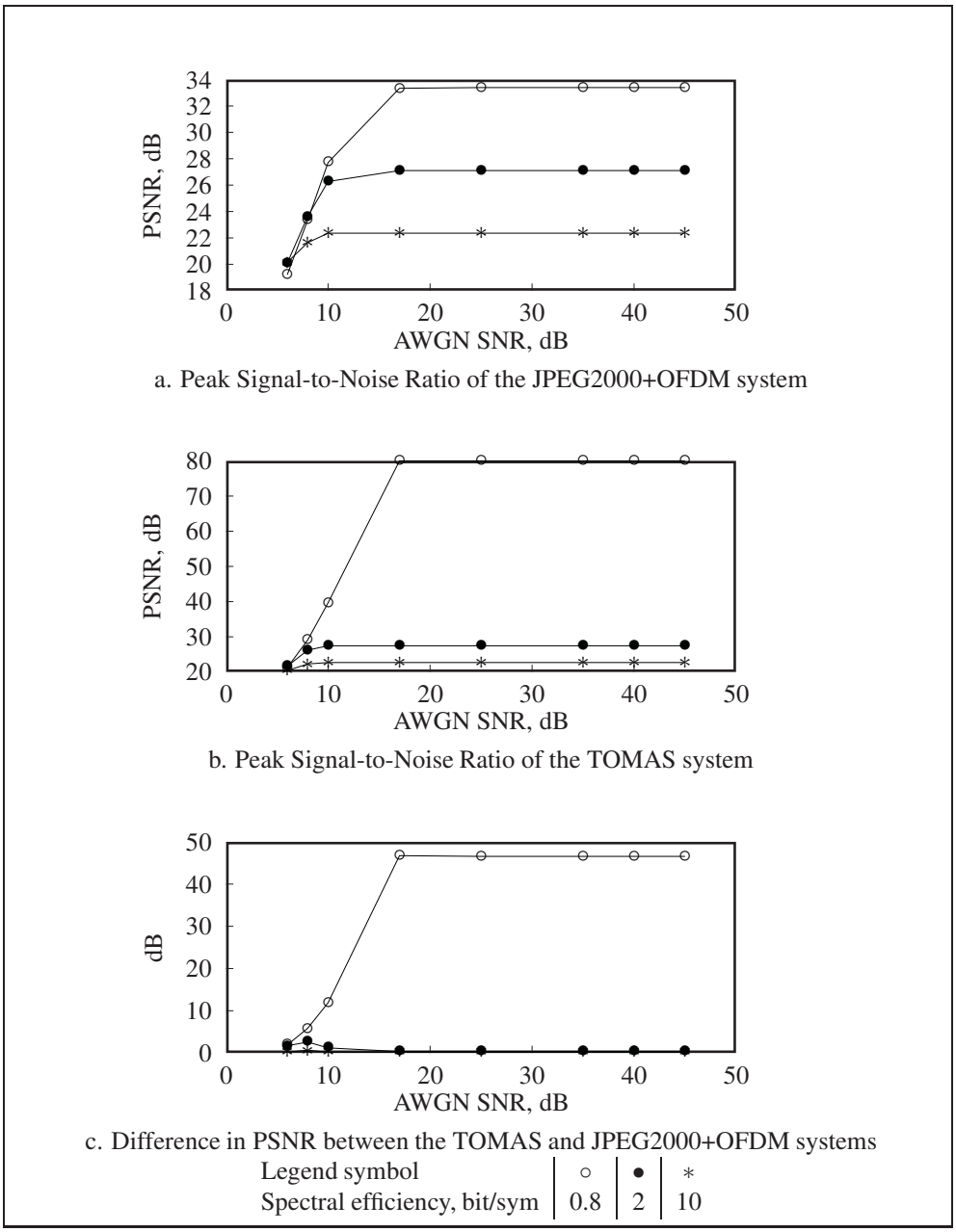

Figure 6.16 Comparison of system performances using the PSNR criterion and the image Aerial2. Fading rate = 2 Hz.

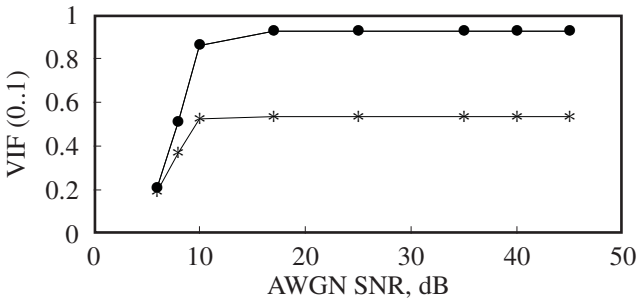

a. Visual Information Fidelity Measure of the JPEG2000+OFDM system

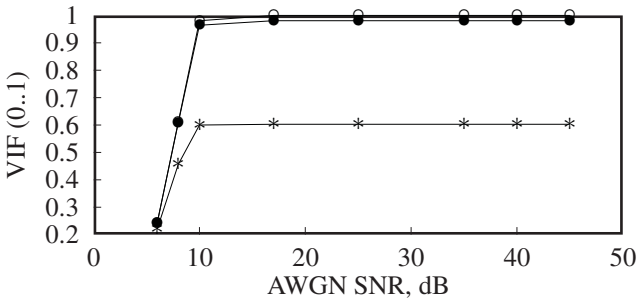

b. Visual Information Fidelity Measure of the TOMAS system

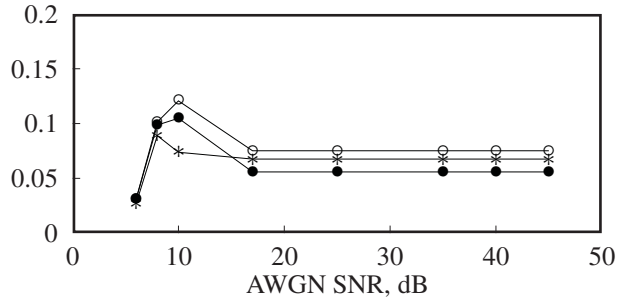

c. Difference in VIF between the TOMAS and JPEG2000+OFDM systems

Legend symbol	○	●	∗
Spectral efficiency, bit/sym	0.8	2	10

Figure 6.17 Comparison of system performances using the VIF criterion and the image Aerial2. Fading rate = 2 Hz.

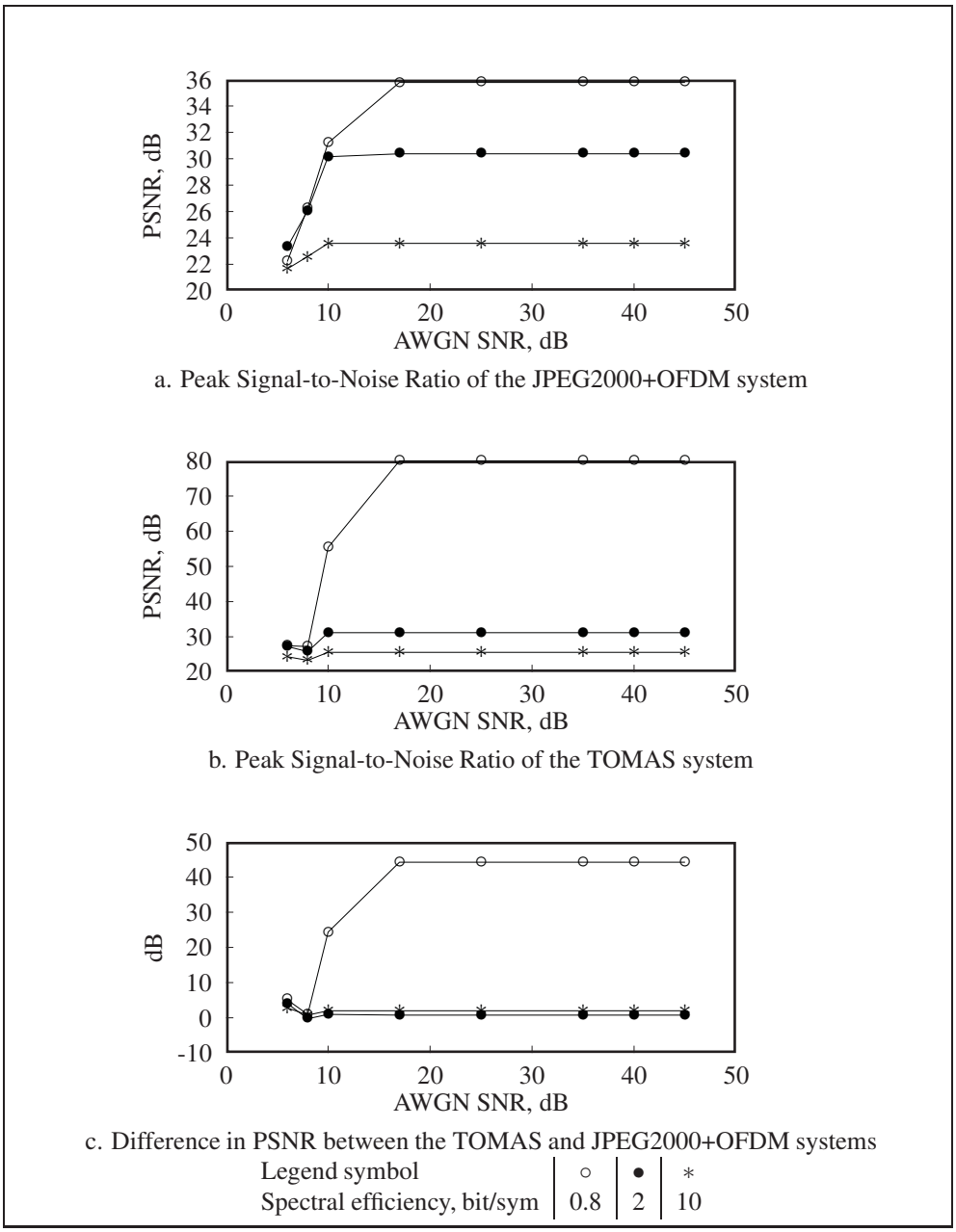

Figure 6.18 Comparison of system performances using the PSNR criterion and the image Lena128. Fading rate = 37 Hz.

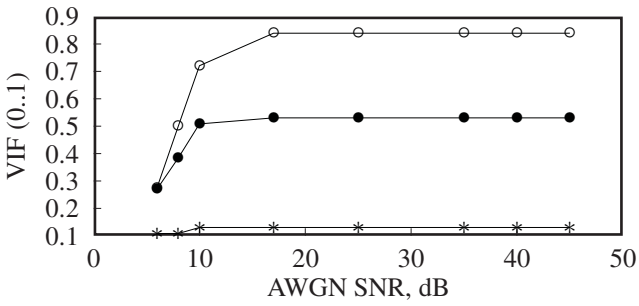

a. Visual Information Fidelity Measure of the JPEG2000+OFDM system

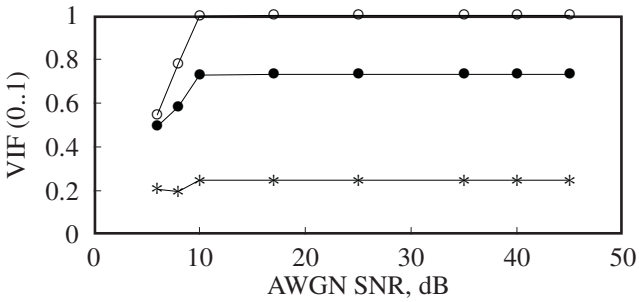

b. Visual Information Fidelity Measure of the TOMAS system

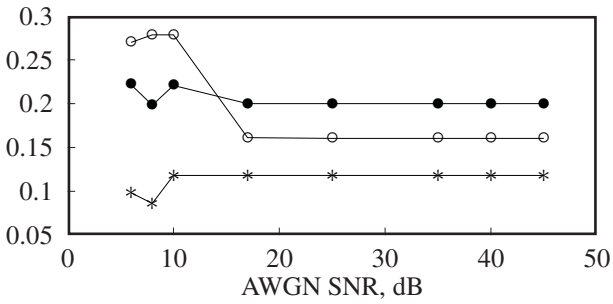

c. Difference in VIF between the TOMAS and JPEG2000+OFDM systems

Legend symbol	○	●	∗
Spectral efficiency, bit/sym	0.8	2	10

Figure 6.19 Comparison of system performances using the VIF criterion and the image Lena128. Fading rate = 37 Hz.

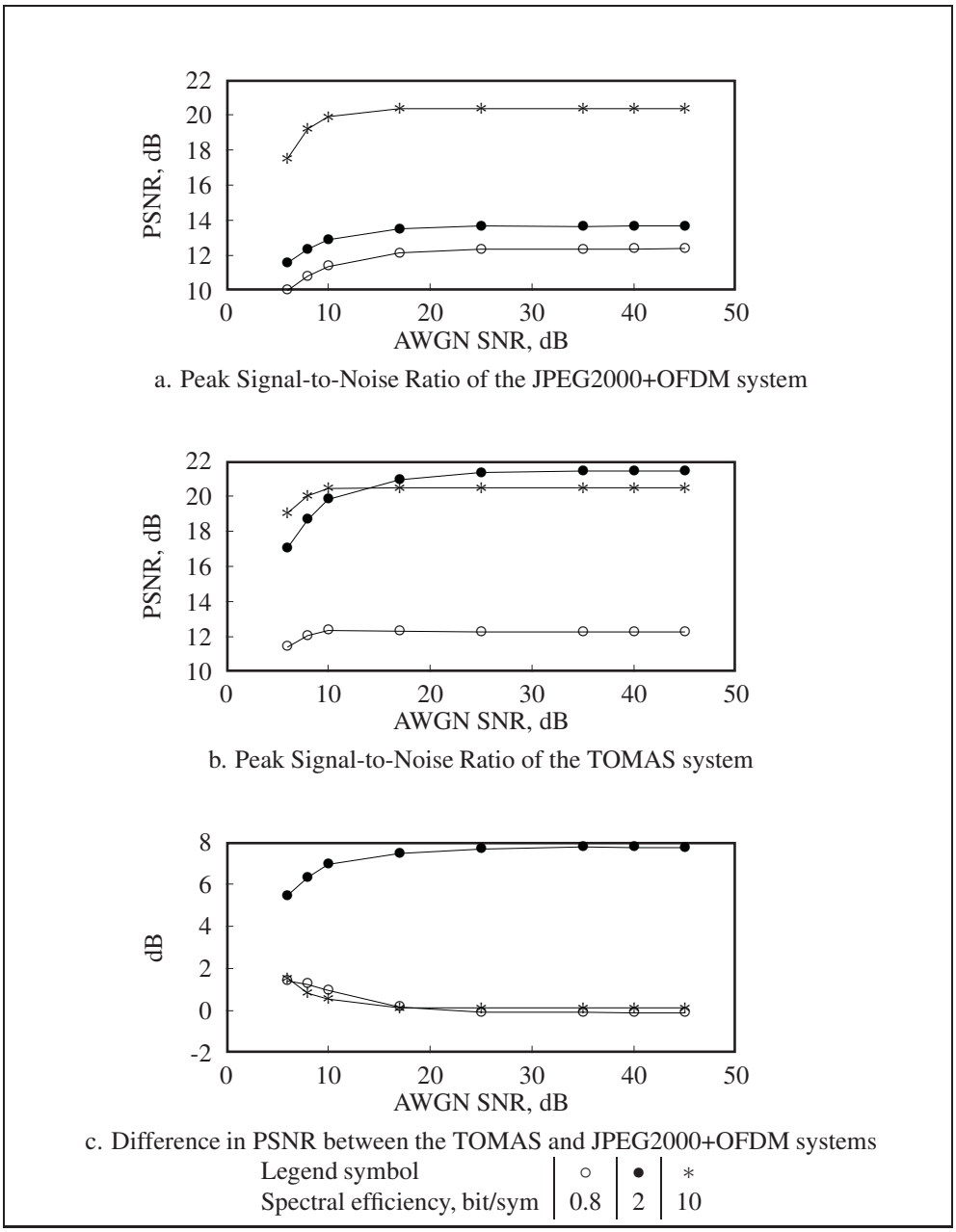

Figure 6.20 Comparison of system performances using the PSNR criterion and the image Mandrill. Fading rate = 37 Hz.

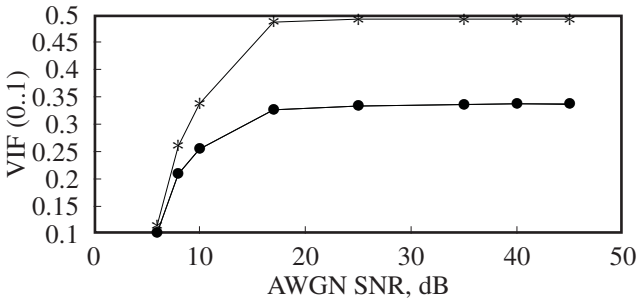

a. Visual Information Fidelity Measure of the JPEG2000+OFDM system

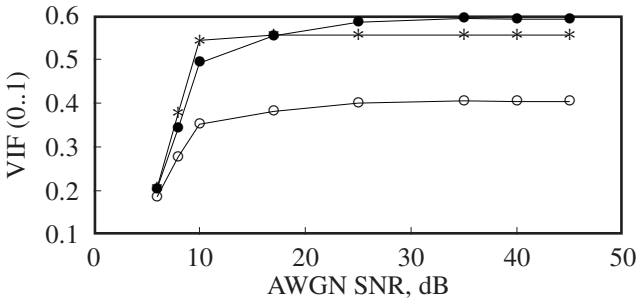

b. Visual Information Fidelity Measure of the TOMAS system

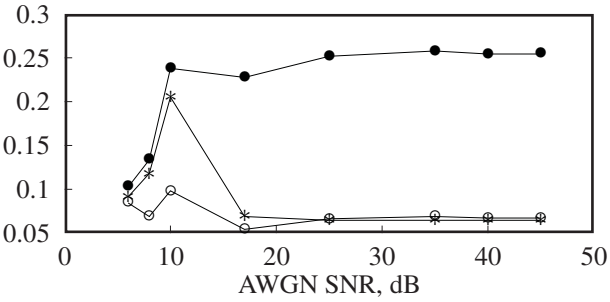

c. Difference in VIF between the TOMAS and JPEG2000+OFDM systems

Legend symbol	○	●	∗
Spectral efficiency, bit/sym	0.8	2	10

Figure 6.21 Comparison of system performances using the VIF criterion and the image Mandrill. Fading rate = 37 Hz.

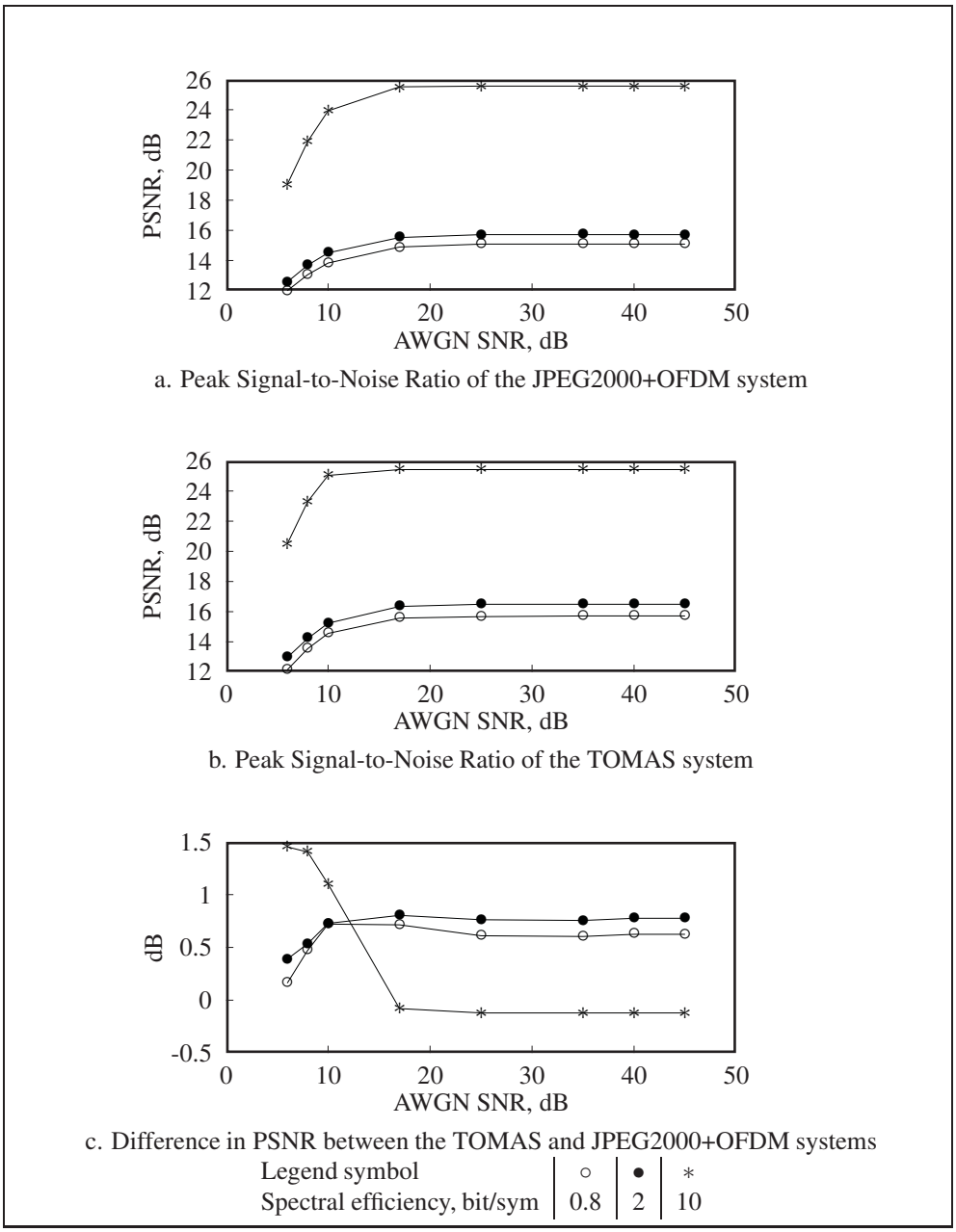

Figure 6.22 Comparison of system performances using the PSNR criterion and the image Peppers. Fading rate = 37 Hz.

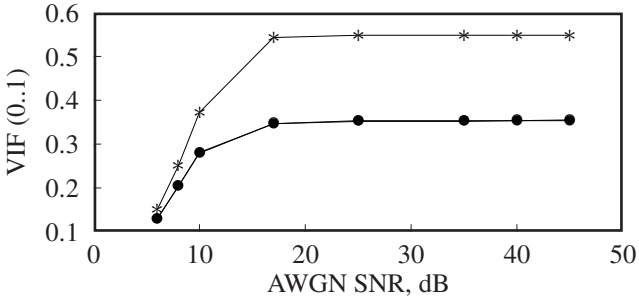

a. Visual Information Fidelity Measure of the JPEG2000+OFDM system

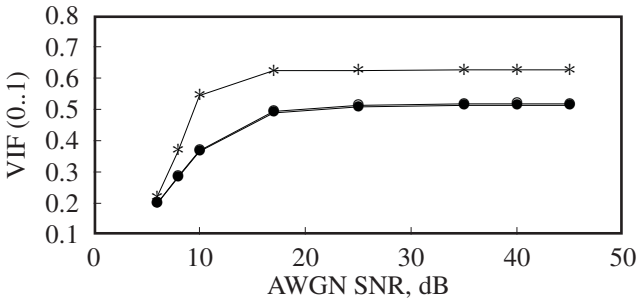

b. Visual Information Fidelity Measure of the TOMAS system

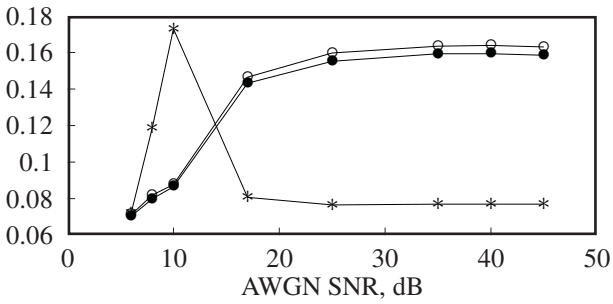

c. Difference in VIF between the TOMAS and JPEG2000+OFDM systems

Legend symbol	○	●	∗
Spectral efficiency, bit/sym	0.8	2	10

Figure 6.23 Comparison of system performances using the VIF criterion and the image Peppers. Fading rate = 37 Hz.

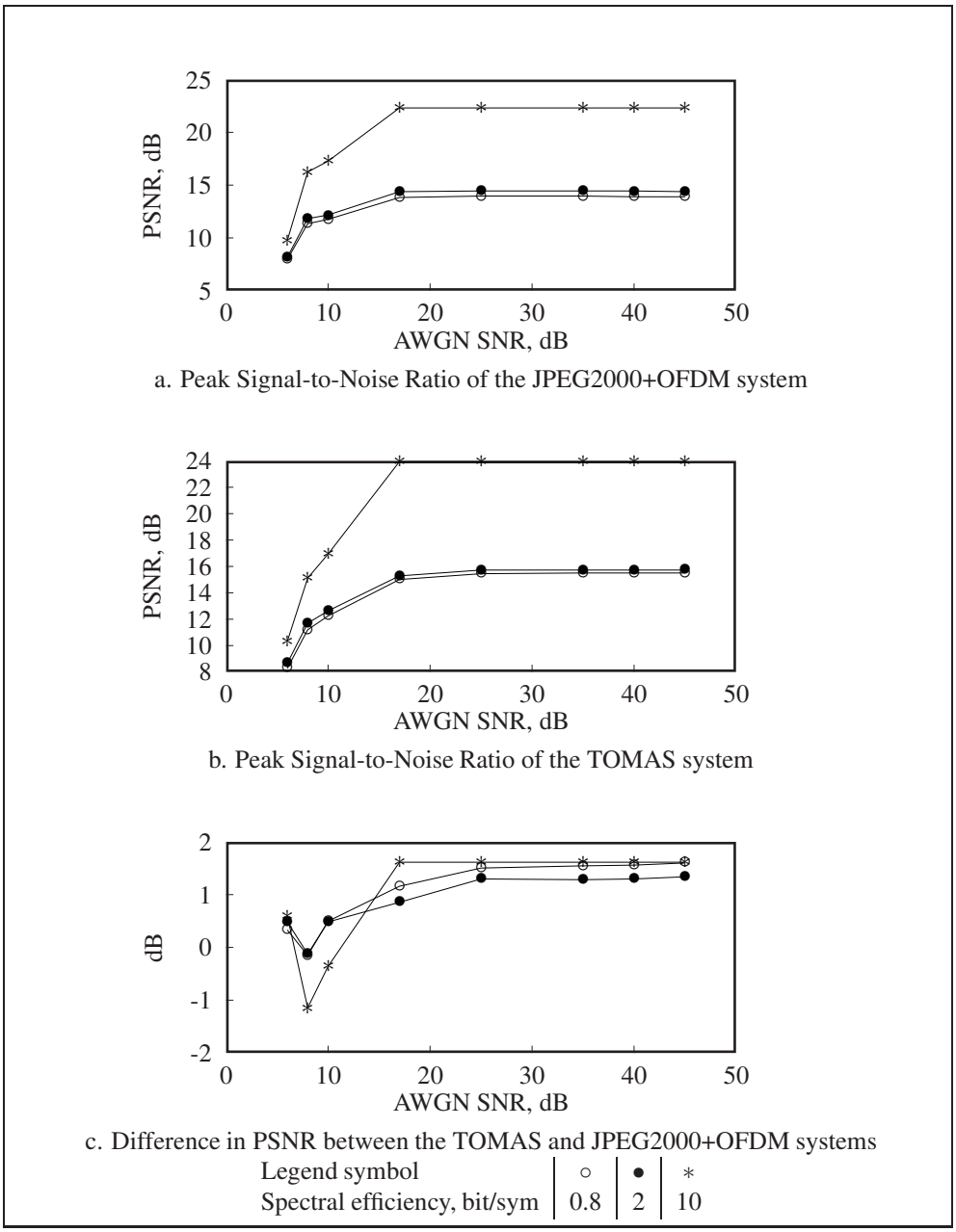

Figure 6.24 Comparison of system performances using the PSNR criterion and the image F16. Fading rate = 37 Hz.

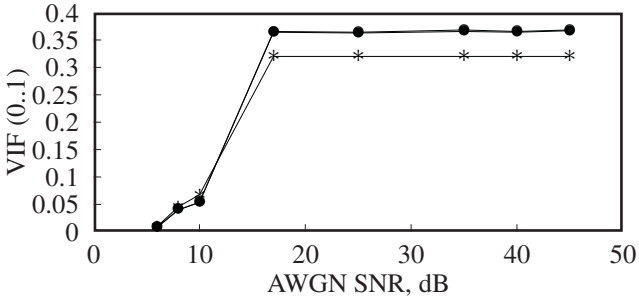

a. Visual Information Fidelity Measure of the JPEG2000+OFDM system

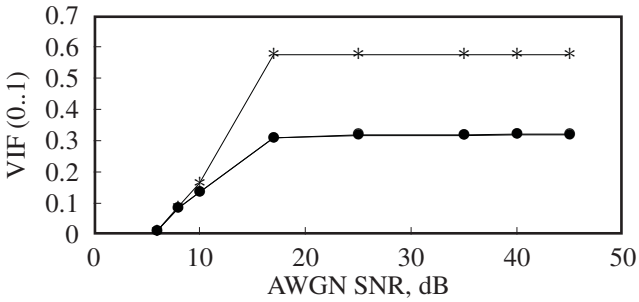

b. Visual Information Fidelity Measure of the TOMAS system

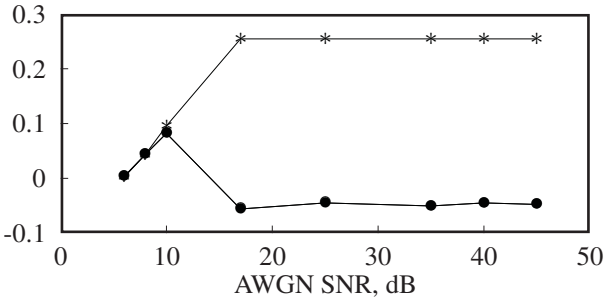

c. Difference in VIF between the TOMAS and JPEG2000+OFDM systems

Legend symbol	○	●	∗
Spectral efficiency, bit/sym	0.8	2	10

Figure 6.25 Comparison of system performances using the VIF criterion and the image F16. Fading rate = 37 Hz.

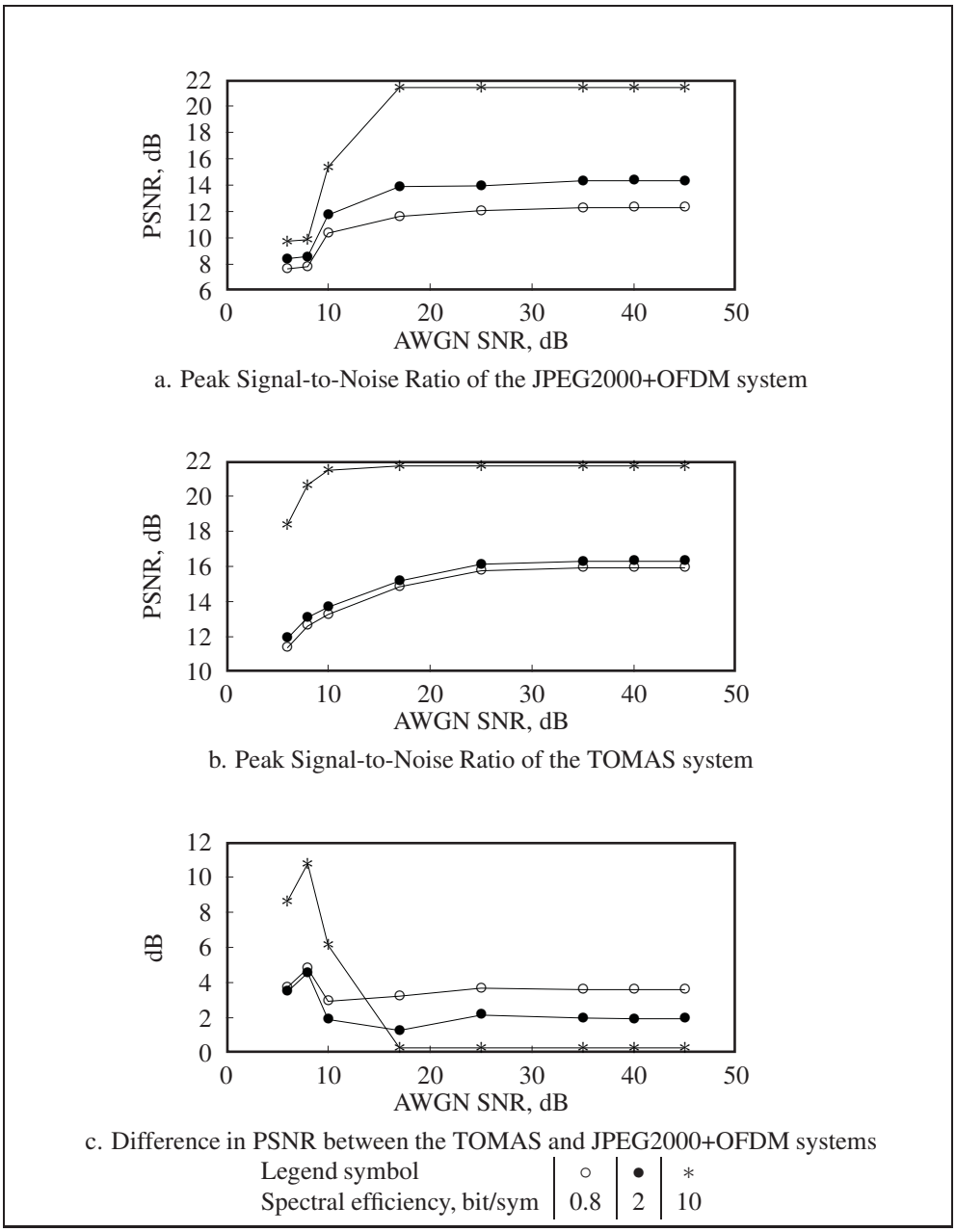

Figure 6.26 Comparison of system performances using the PSNR criterion and the image Aerial. Fading rate = 37 Hz.

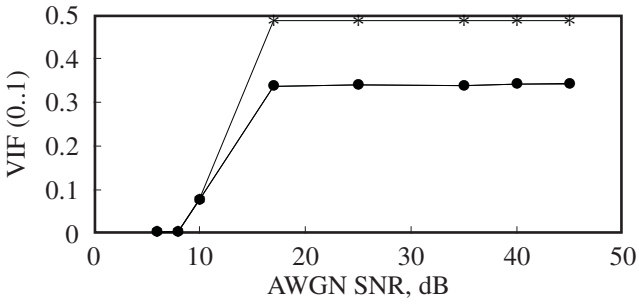

a. Visual Information Fidelity Measure of the JPEG2000+OFDM system

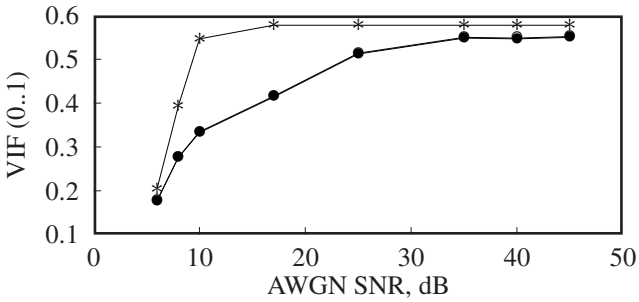

b. Visual Information Fidelity Measure of the TOMAS system

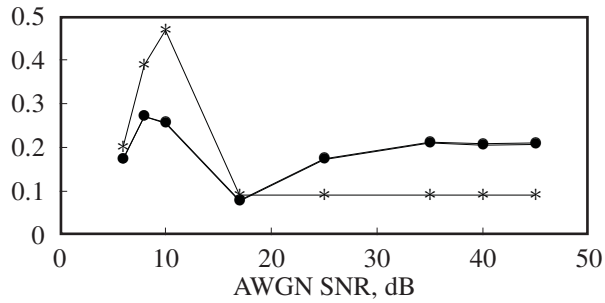

c. Difference in VIF between the TOMAS and JPEG2000+OFDM systems

Legend symbol	○	●	∗
Spectral efficiency, bit/sym	0.8	2	10

Figure 6.27 Comparison of system performances using the VIF criterion and the image Aerial. Fading rate = 37 Hz.

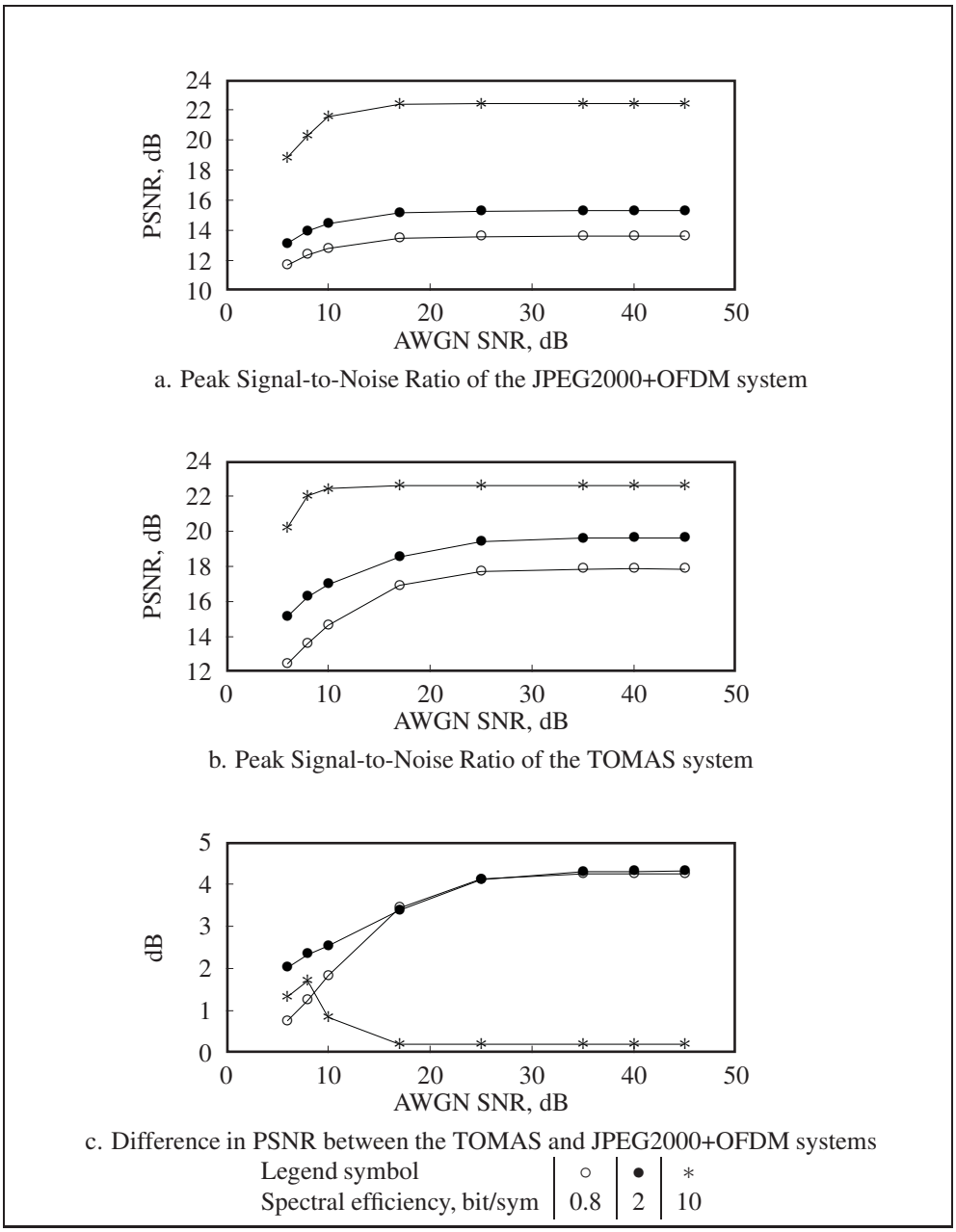

Figure 6.28 Comparison of system performances using the PSNR criterion and the image Aerial2. Fading rate = 37 Hz.

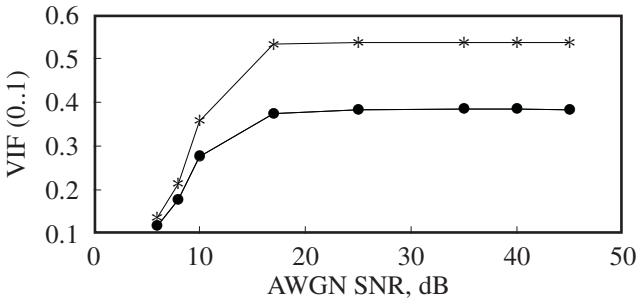

a. Visual Information Fidelity Measure of the JPEG2000+OFDM system

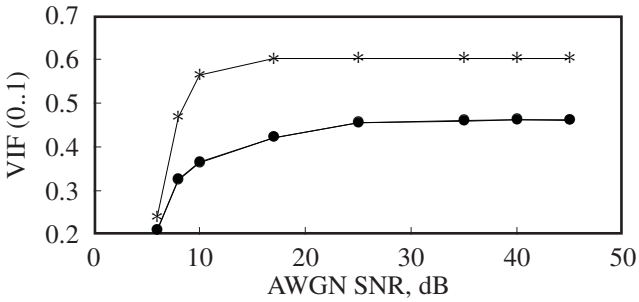

b. Visual Information Fidelity Measure of the TOMAS system

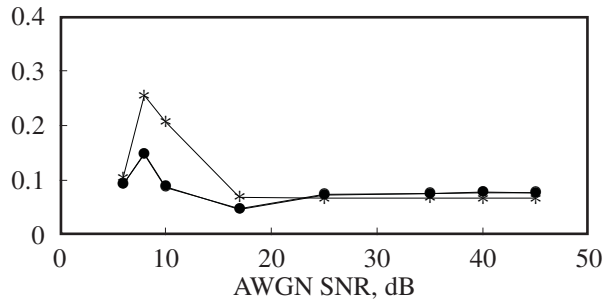

c. Difference in VIF between the TOMAS and JPEG2000+OFDM systems

Legend symbol	○	●	∗
Spectral efficiency, bit/sym	0.8	2	10

Figure 6.29 Comparison of system performances using the VIF criterion and the image Aerial2. Fading rate = 37 Hz.

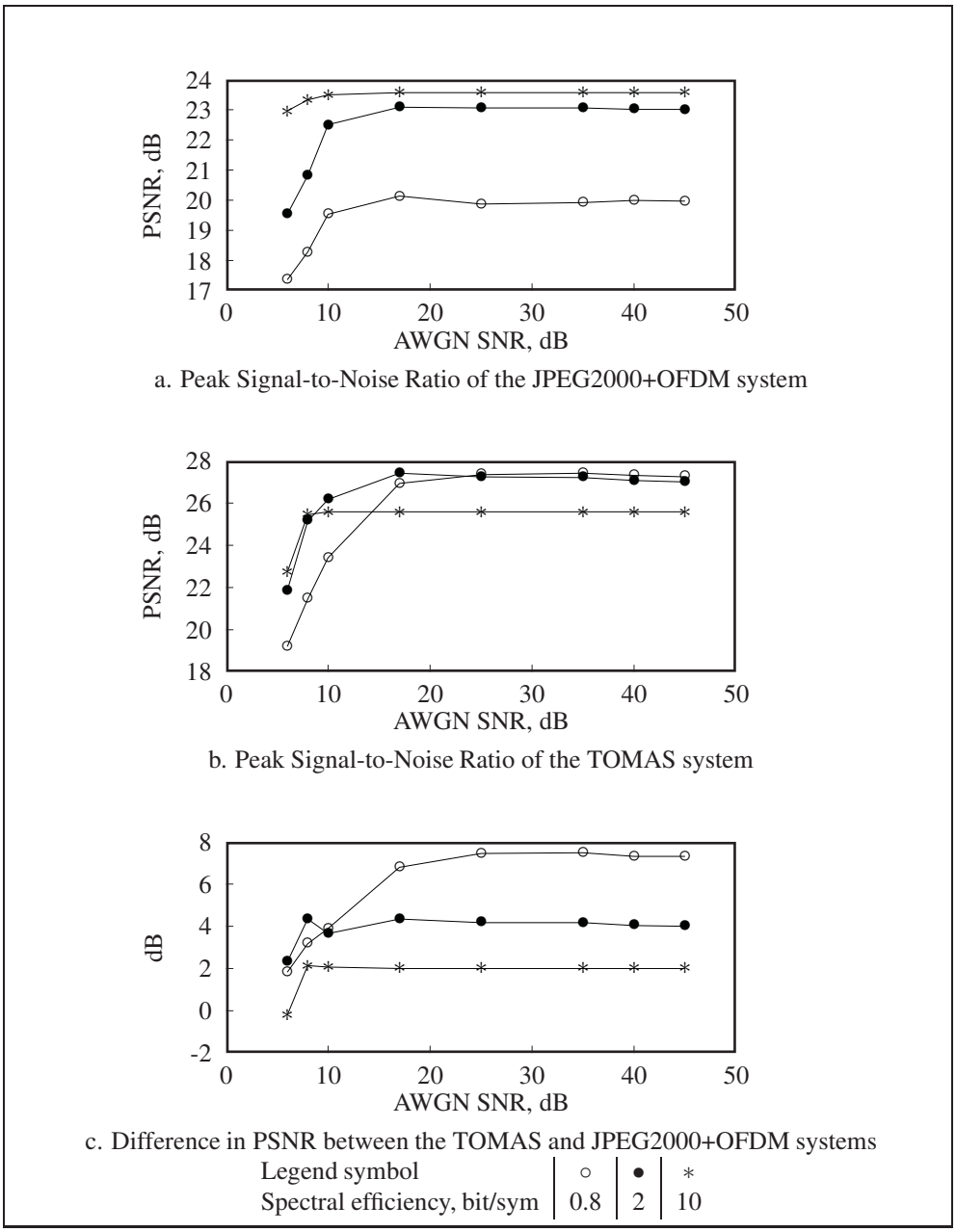

Figure 6.30 Comparison of system performances using the PSNR criterion and the image Lena128. Fading rate = 225 Hz.

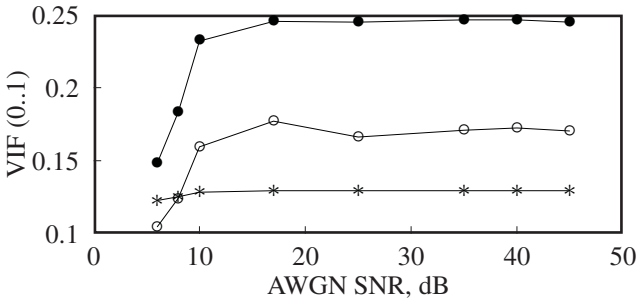

a. Visual Information Fidelity Measure of the JPEG2000+OFDM system

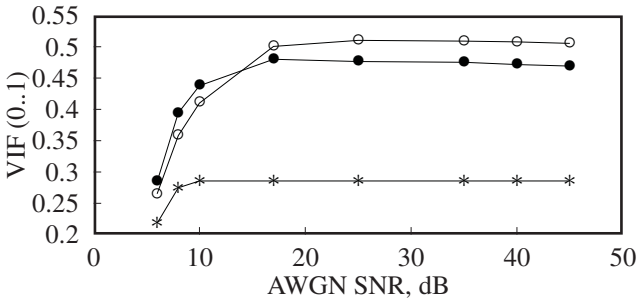

b. Visual Information Fidelity Measure of the TOMAS system

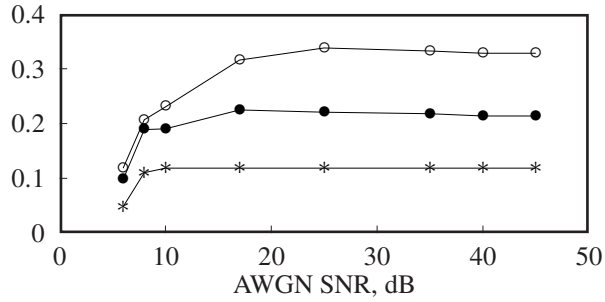

c. Difference in VIF between the TOMAS and JPEG2000+OFDM systems

Legend symbol	○	●	∗
Spectral efficiency, bit/sym	0.8	2	10

Figure 6.31 Comparison of system performances using the VIF criterion and the image Lena128. Fading rate = 225 Hz.

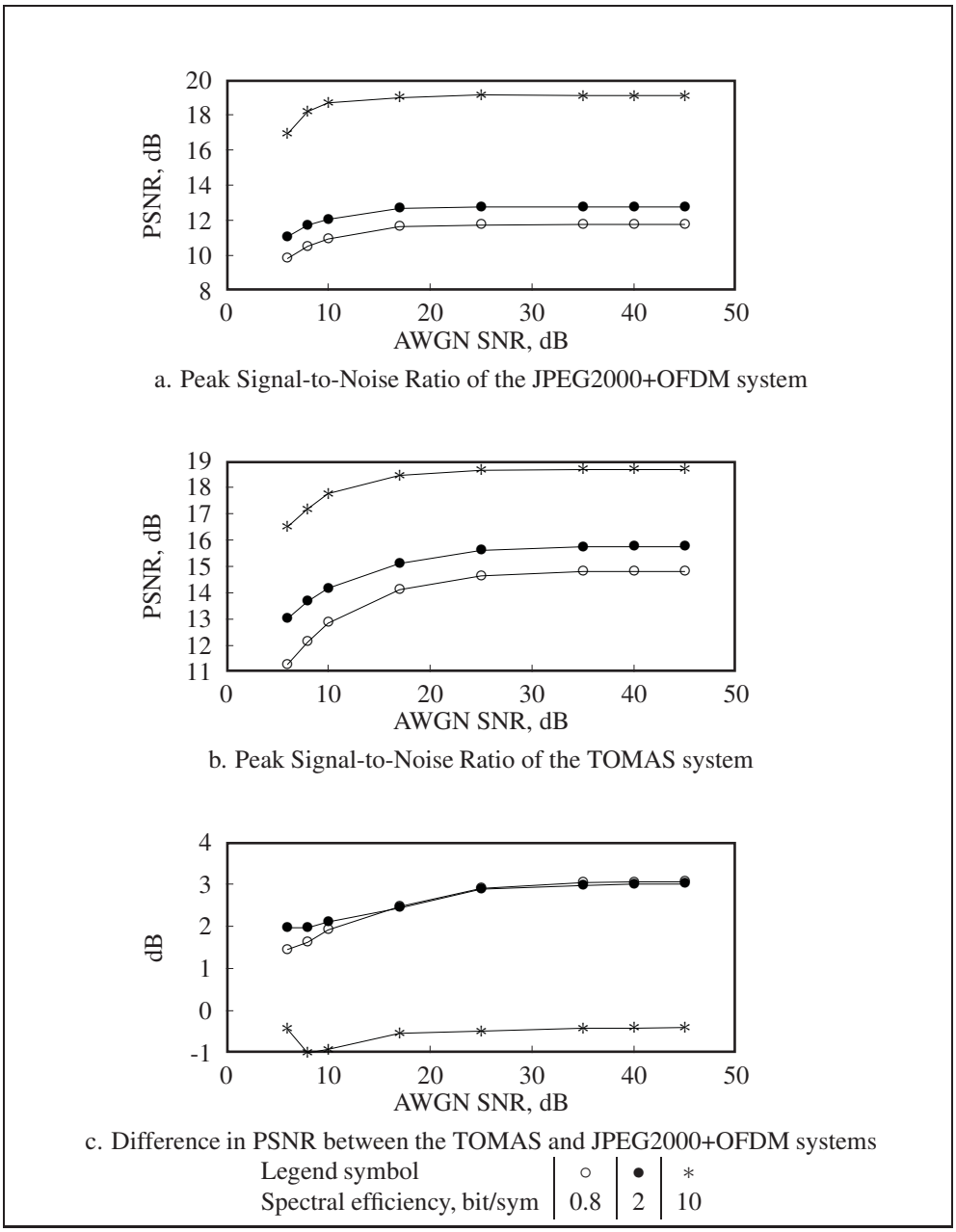

Figure 6.32 Comparison of system performances using the PSNR criterion and the image Mandrill. Fading rate = 225 Hz.

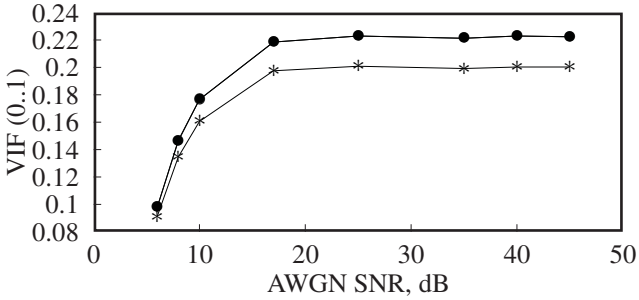

a. Visual Information Fidelity Measure of the JPEG2000+OFDM system

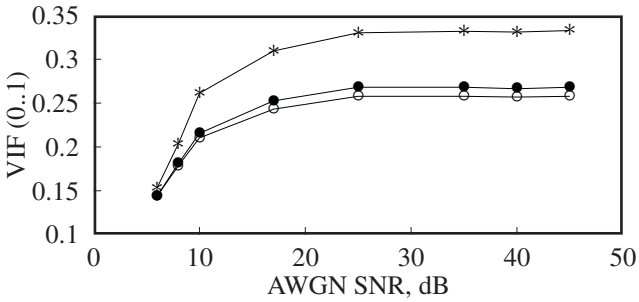

b. Visual Information Fidelity Measure of the TOMAS system

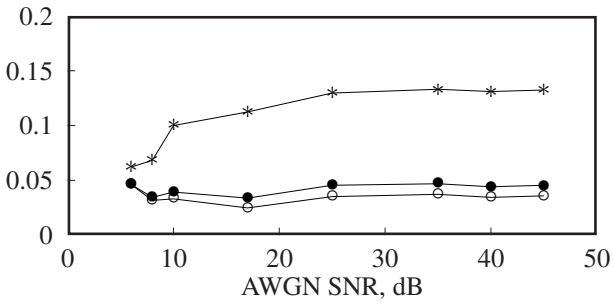

c. Difference in VIF between the TOMAS and JPEG2000+OFDM systems

Legend symbol	○	●	∗
Spectral efficiency, bit/sym	0.8	2	10

Figure 6.33 Comparison of system performances using the VIF criterion and the image Mandrill. Fading rate = 225 Hz.

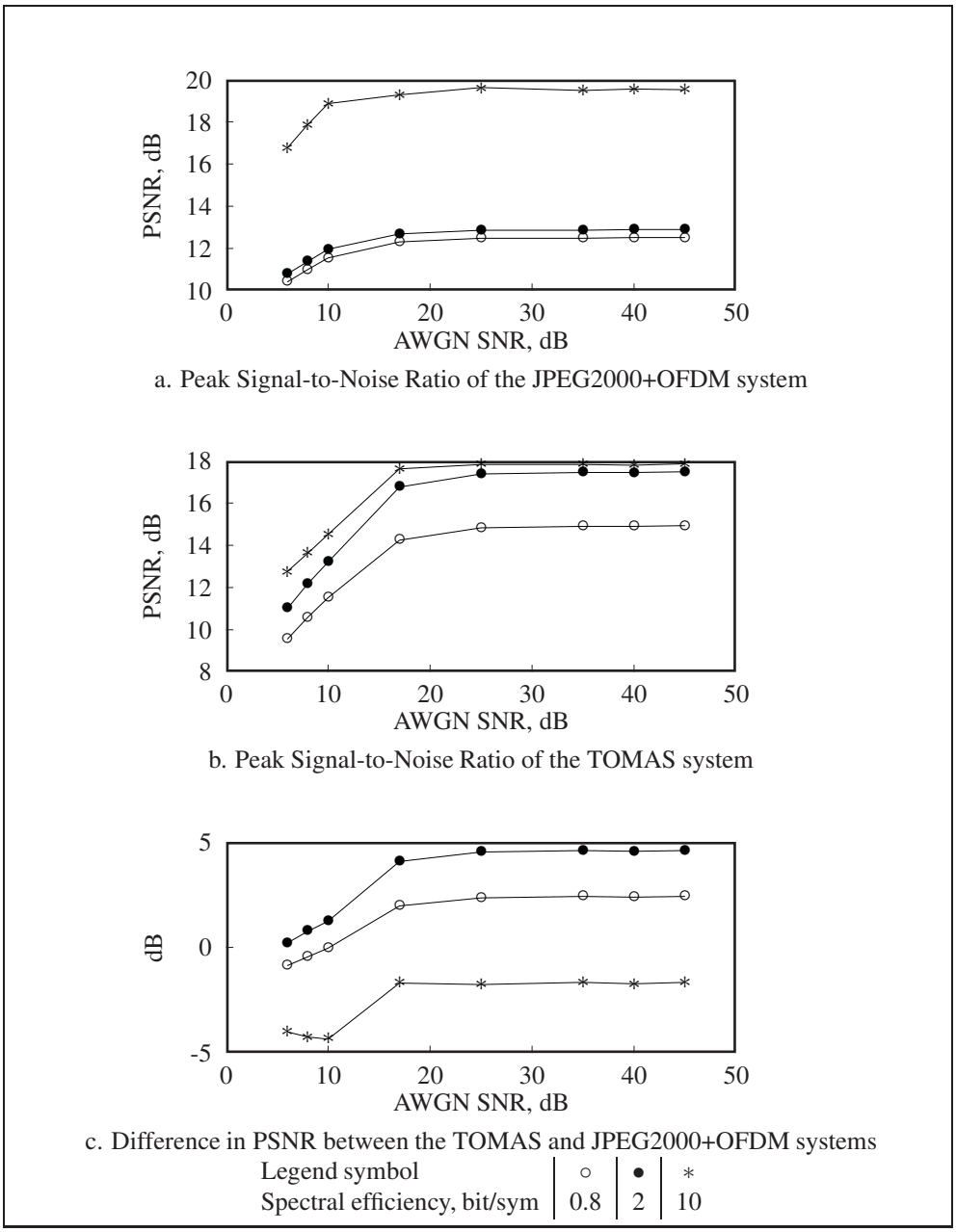

Figure 6.34 Comparison of system performances using the PSNR criterion and the image Peppers. Fading rate = 225 Hz.

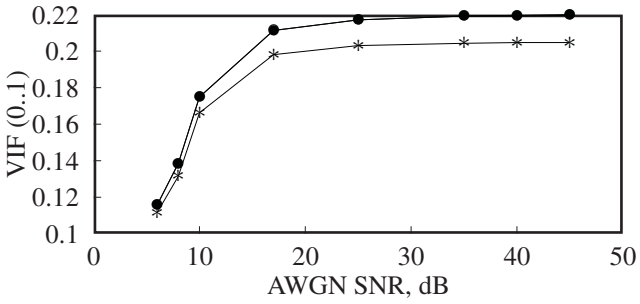

a. Visual Information Fidelity Measure of the JPEG2000+OFDM system

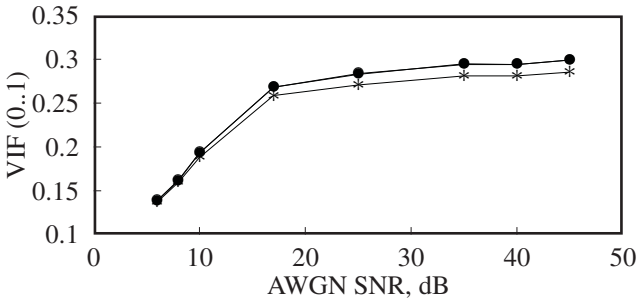

b. Visual Information Fidelity Measure of the TOMAS system

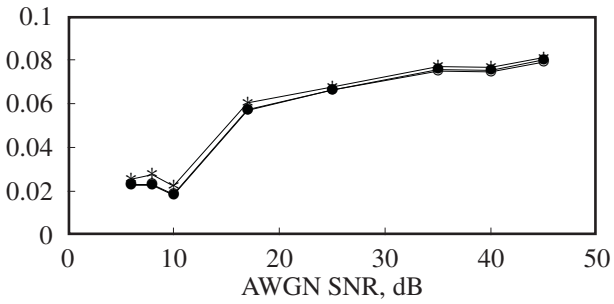

c. Difference in VIF between the TOMAS and JPEG2000+OFDM systems

Legend symbol	○	●	∗
Spectral efficiency, bit/sym	0.8	2	10

Figure 6.35 Comparison of system performances using the VIF criterion and the image Peppers. Fading rate = 225 Hz.

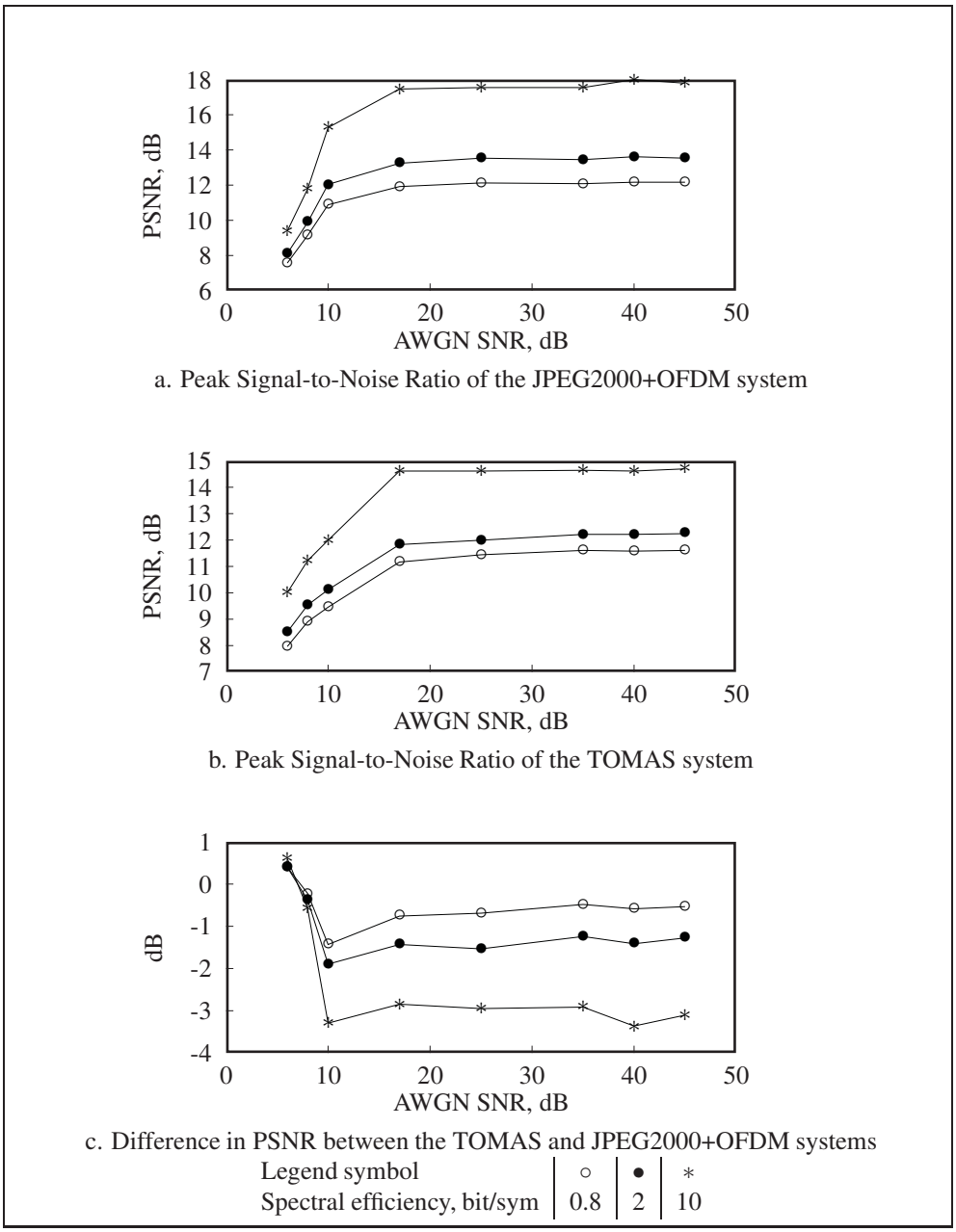

Figure 6.36 Comparison of system performances using the PSNR criterion and the image F16. Fading rate = 225 Hz.

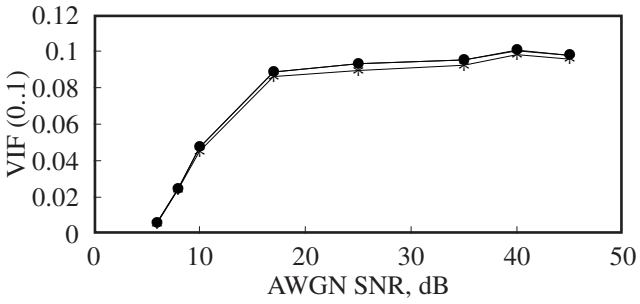

a. Visual Information Fidelity Measure of the JPEG2000+OFDM system

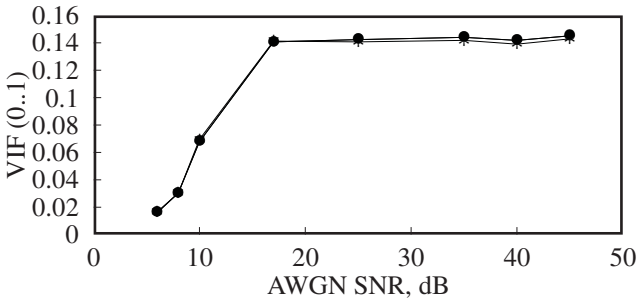

b. Visual Information Fidelity Measure of the TOMAS system

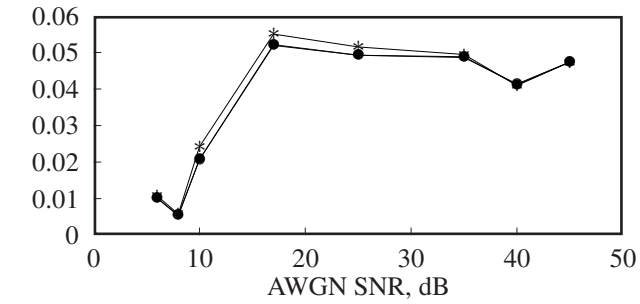

c. Difference in VIF between the TOMAS and JPEG2000+OFDM systems

Legend symbol	○	●	∗
Spectral efficiency, bit/sym	0.8	2	10

Figure 6.37 Comparison of system performances using the VIF criterion and the image F16. Fading rate = 225 Hz.

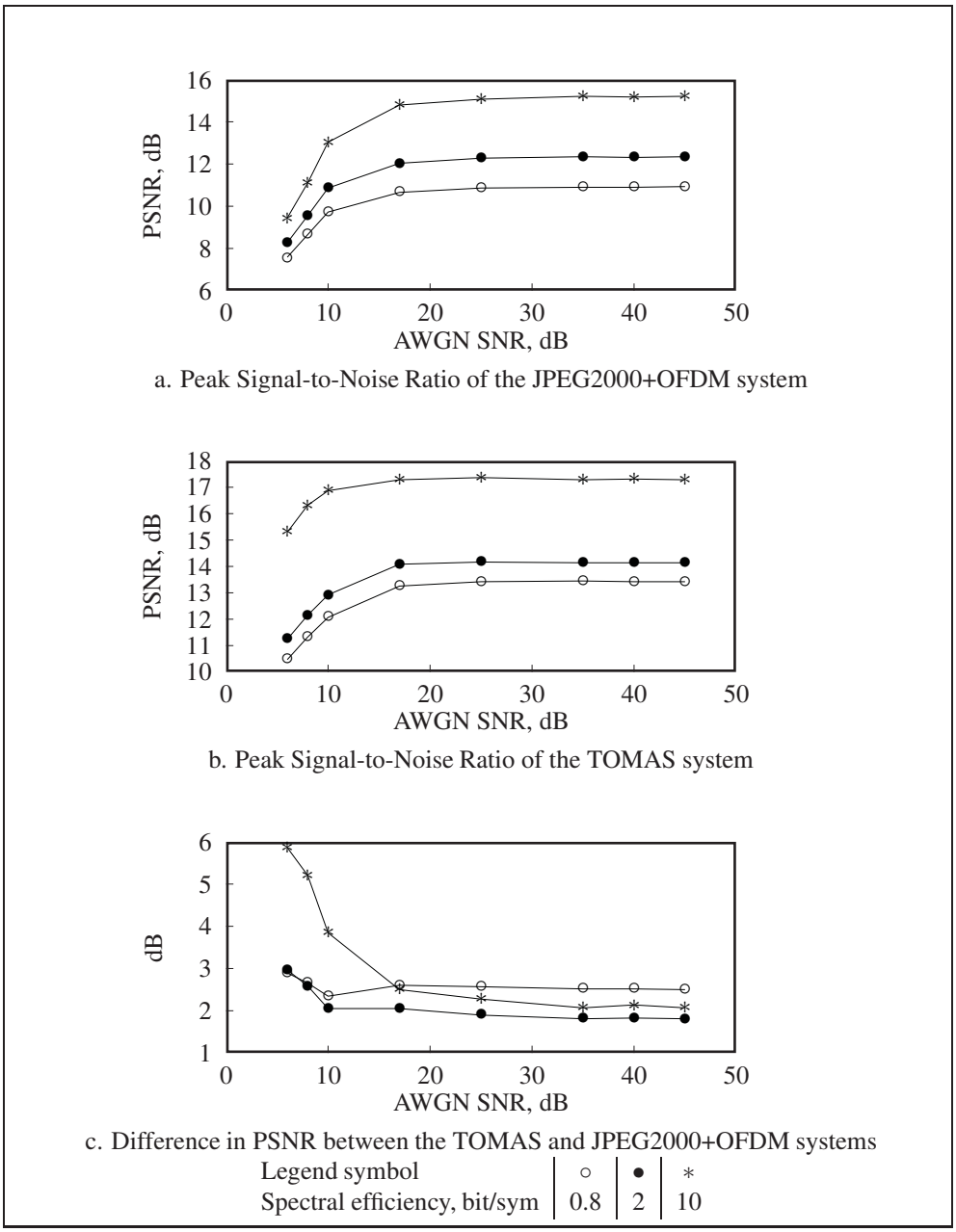

Figure 6.38 Comparison of system performances using the PSNR criterion and the image Aerial. Fading rate = 225 Hz.

The complexities of the algorithms are calculated theoretically for both systems. The results are presented in Table 6.4. The wireless TOMAS system does not employ any multiplications,

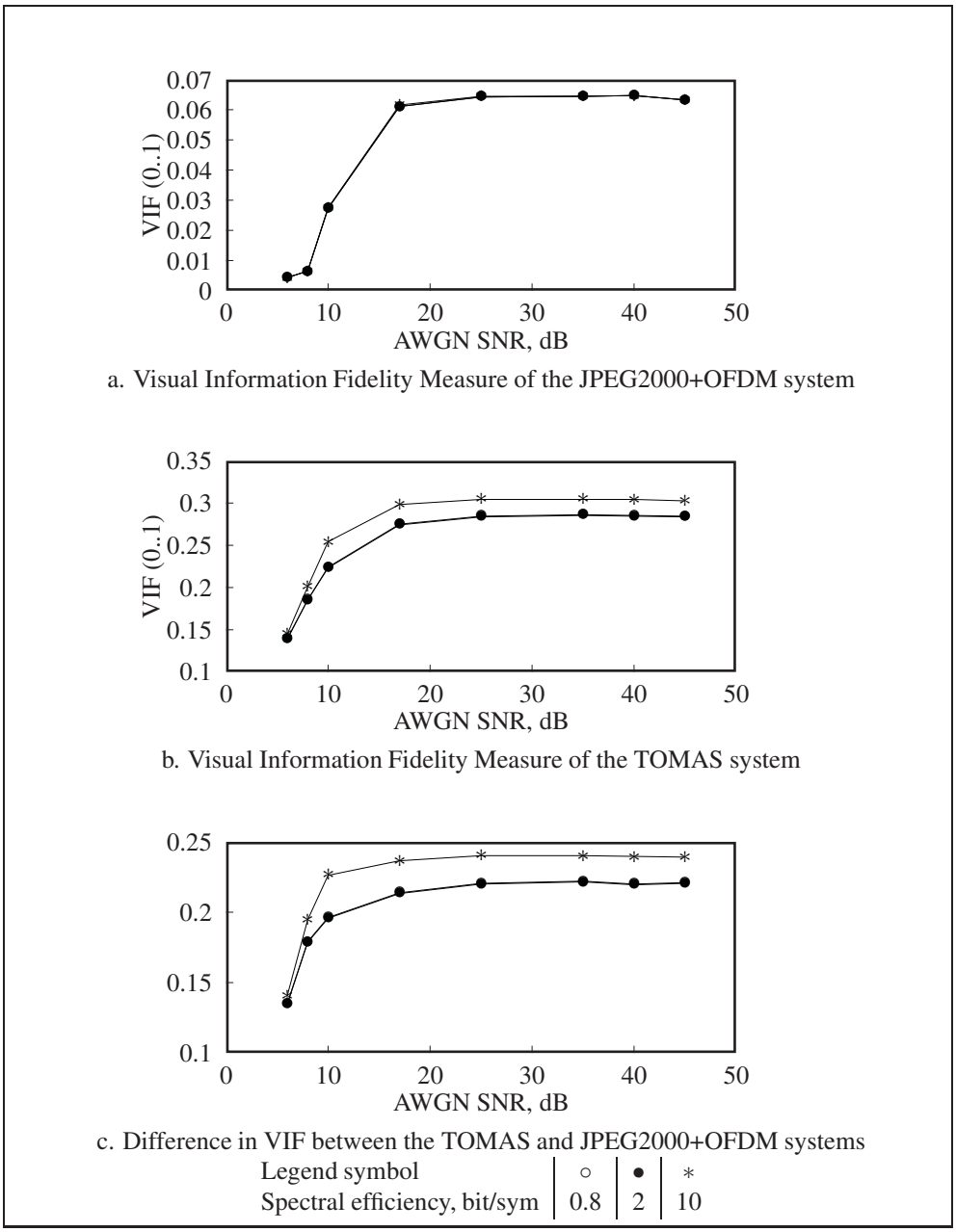

Figure 6.39 Comparison of system performances using the VIF criterion and the image Aerial. Fading rate = 225 Hz.

and it requires 3 times fewer additions than the JPEG2000+OFDM system does.

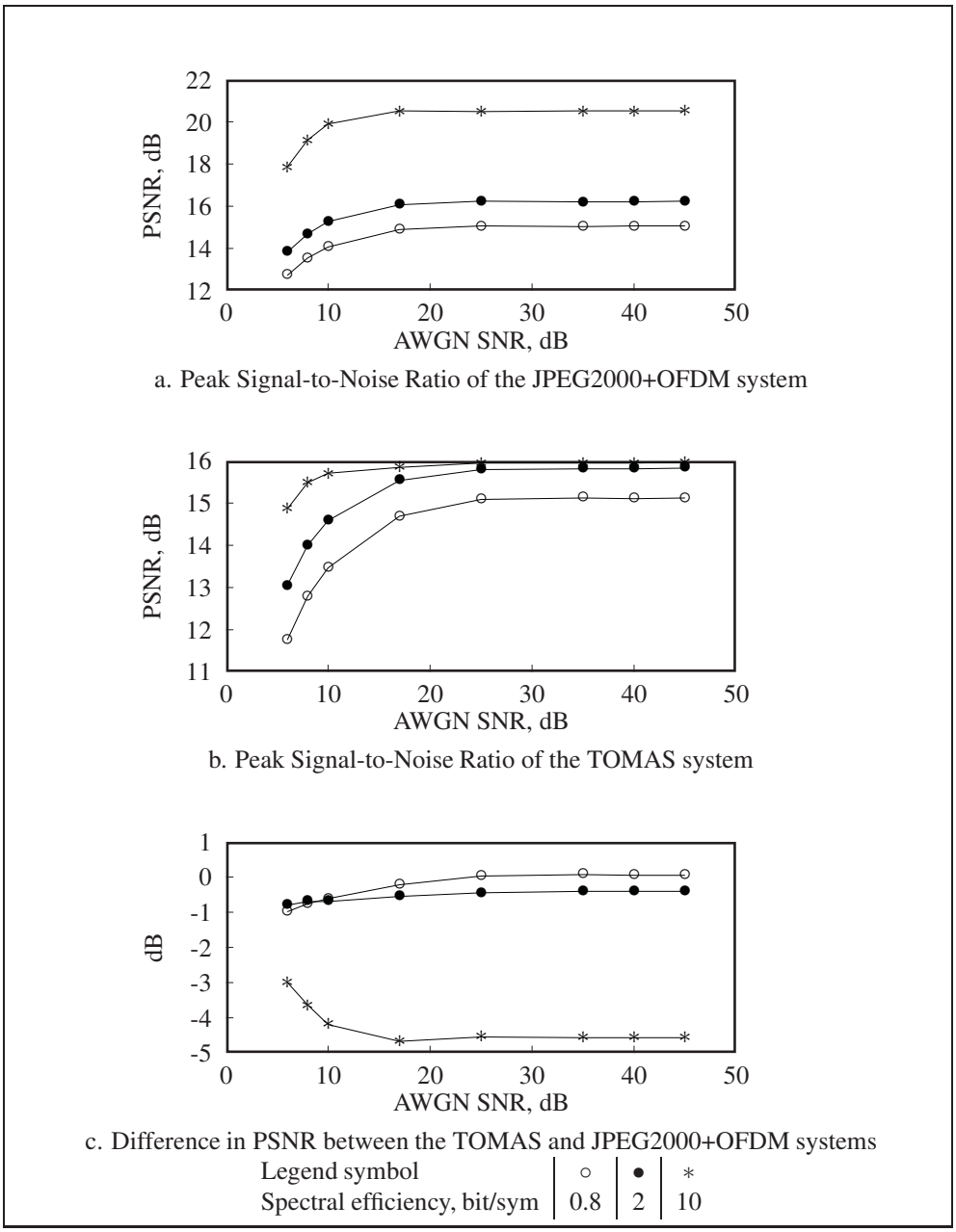

Figure 6.40 Comparison of system performances using the PSNR criterion and the image Aerial2. Fading rate = 225 Hz.

6.8 Conclusion

In this chapter we proposed evaluation of the data Transmission oriented on the Object, communication Media, Application, and state of communication Systems for the case of the wire-

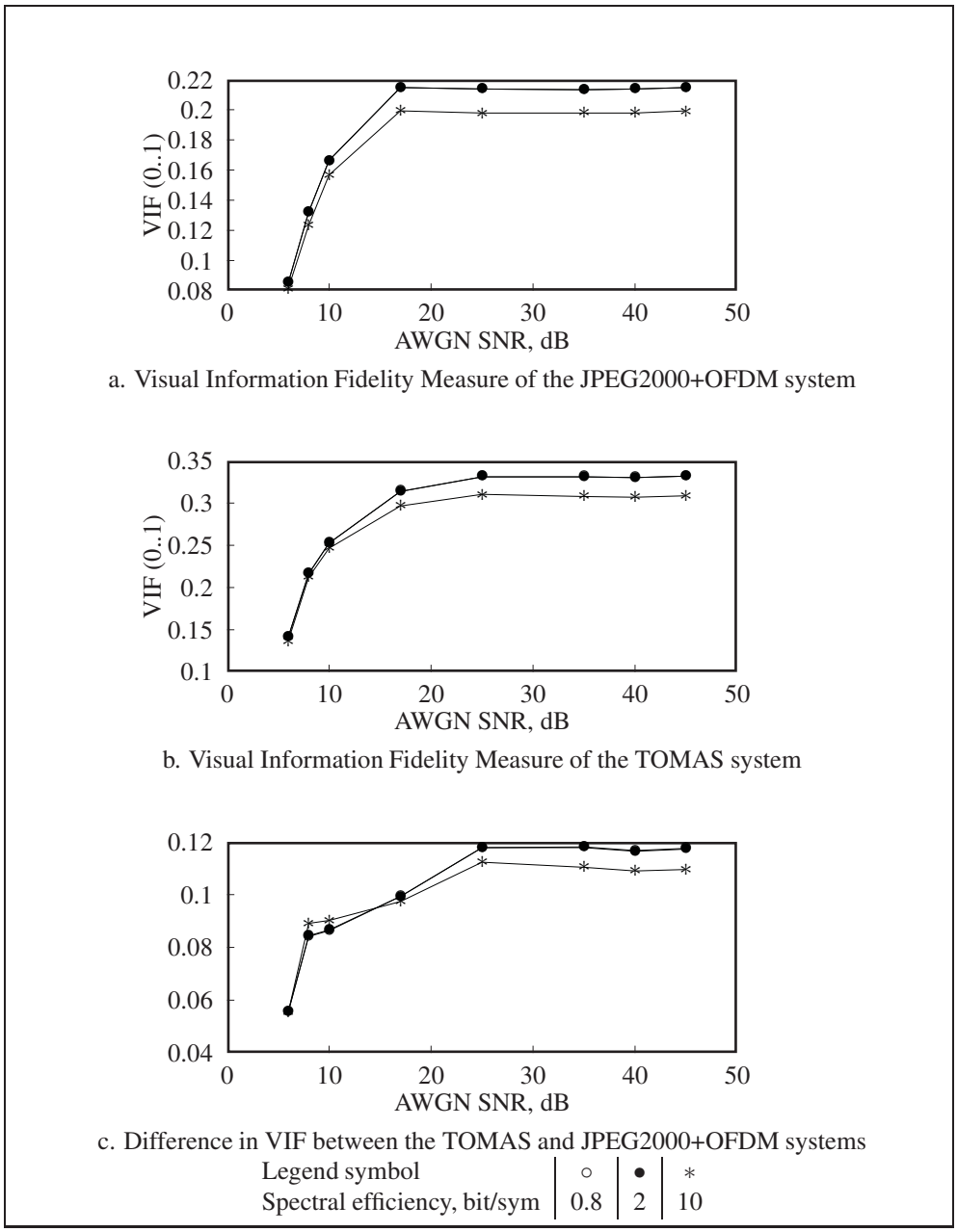

Figure 6.41 Comparison of system performances using the VIF criterion and the image Aerial2. Fading rate = 225 Hz.

less media (**Wireless TOMAS**). The benchmark system was a system that combines JPEG2000 image compression with Orthogonal Frequency Division Multiplexing (**JPEG2000 + OFDM**).

Table 6.4 Algorithm Complexity

Operations per bit	**JPEG2000+OFDM**	**TOMAS**
Real Multiplications	12.84	0
Real Additions	11.39	3.81

Both the wireless TOMAS and JPEG2000+OFDM systems as well as a wireless channel were simulated in a Matlab® environment. The grayscale still image was chosen as the data object. Given the particular scenario of image transmission over the wireless LOS channel, the wireless TOMAS system demonstrates superior performances compared to the JPEG2000 + OFDM system in restored image quality parameters over a wide range of wireless channel parameters, as is shown in Table 6.5. The wireless TOMAS system provides lossless progressive image transmission under the influence of moderate fading. Channel coding might mitigate the effects of severe fading in order to provide lossless transmission. The JPEG2000 + OFDM system is not able to provide lossless transmission at all. The wireless TOMAS system algorithm does not employ any multiplications, and it uses three times fewer real additions than the one of the JPEG2000 + OFDM system.

Table 6.5 Difference in restored image quality between the proposed system and JPEG2000+OFDM

Fading Rate	**Quality Parameter**	**Spectral efficiency, bit/sym**		
		0.8	**2**	**10**
Low (2 Hz)	PSNR, dB	lossless	1.41	2.00
	VIF	0.16	0.2	0.12
Moderate (37 Hz)	PSNR, dB	lossless	3.97	2.73
	VIF	0.28	0.22	0.12
High (225 Hz)	PSNR, dB	7.49	4.35	2.12
	VIF	0.34	0.22	0.12

CONCLUSION

In our research work, we addressed issues of Tactical Communication Systems, such as multiple data types, threats to communication sessions and operation environments. Our first objective was analyzing specifics of the data types, communication media, users and hardware the TCS consists of. The second objective was to propose some measures for evaluation of TCS performance. The third objective was to propose a structure of TCS that considers specifics of data types, communication media, users and hardware. And finally, we had to evaluate performance of the proposed system compared to a state-of-the-art system.

As a methodology to the TCS issues, we proposed a system architecture called TOMAS, which is data Transmission oriented on the Object, communication Media, Application, and state of communication Systems. We argued that efficient data transmission could be provided if communication systems involved in data transmission would take into consideration and monitor constantly the following four aspects: data object, communication media, application, and state of communication systems.

Analytical results as well as results of simulation in a Matlab® environment validate the idea of TOMAS.

Our research have made the following contributions to knowledge:

- Given a particular scenario of image transmission over a wireless LOS channel, the proposed system provides superior performances compared to the JPEG2000+ OFDM system in restored image quality parameters over a wide range of wireless channel parameters. The JPEG2000+ OFDM system is not able to provide lossless transmission at all.
- Despite a common opinion that channel coding is mandatory in wireless communications, we demonstrated that without any channel coding, the proposed system provides lossless

progressive image transmission under the influence of moderate fading. Channel coding might mitigate effects of severe fading.

- Despite a decrease of interest towards wavelets, they have a high potential in telecommunication. The fast algorithm, derived from wavelets, does not employ any multiplications, and it uses three times fewer real additions than the one of the JPEG2000+ OFDM system.
- Complex telecommunication networks, which operate with multimedia content over mixture of communication media types, could profit from use of TOMAS.

The proposed idea of TOMAS has been validated by presentation of the research results at the 10th Wireless Telecommunications Symposium (WTS 2011) in April, 2011, in New York City, New York, USA, Sabelkin and Gagnon (2011a). Also the research results have been published in the International Journal of Interdisciplinary Telecommunications and Networking (IJITN), Sabelkin and Gagnon (2011b), and in the Proceedings of the 7th International Conference on Wireless Advanced 2011 (WiAd 2011), June 2011, London, UK, Sabelkin and Gagnon (2011c). The TOMAS system employs a fast proprietary patent pending algorithm, Sabelkin (2011) and Sabelkin and Gagnon (2011c).

Future work will be concentrated on implementing the wireless TOMAS in the Software Defined Radio platform called the *Software Radio Dongle*™, which is developed by DTMSDR Technologies INC.

APPENDIX I

INVERSE WAVELET PACKET MATRIX $\mathbb{W}_4^{-1}$

Matrix $\mathbb{W}_4$:

$$\mathbb{W}_4 = \begin{pmatrix} m_{00} = \frac{1}{2} & m_{01} = \frac{1}{2} & m_{02} = \frac{1}{2} & m_{03} = \frac{1}{2} \\ m_{10} = \frac{1}{2} & m_{11} = \frac{1}{2} & m_{12} = -\frac{1}{2} & m_{13} = -\frac{1}{2} \\ m_{20} = \frac{1}{2} & m_{21} = -\frac{1}{2} & m_{22} = \frac{1}{2} & m_{23} = -\frac{1}{2} \\ m_{30} = \frac{1}{2} & m_{31} = -\frac{1}{2} & m_{32} = -\frac{1}{2} & m_{33} = \frac{1}{2} \end{pmatrix}. \tag{AI.1}$$

Inverse Matrix $\mathbb{W}_4^{-1}$:

$$\mathbb{W}_4^{-1} = \frac{1}{det(\mathbb{W}_4)} \begin{pmatrix} n_{00} & n_{01} & n_{02} & n_{03} \\ n_{10} & n_{11} & n_{12} & n_{13} \\ n_{20} & n_{21} & n_{22} & n_{23} \\ n_{30} & n_{31} & n_{32} & n_{33} \end{pmatrix}, \tag{AI.2}$$

where

$$\begin{aligned} n_{00} &= m_{12}m_{23}m_{31} - m_{13}m_{22}m_{31} + m_{13}m_{21}m_{32} - \\ &- m_{11}m_{23}m_{32} - m_{12}m_{21}m_{33} + m_{11}m_{22}m_{33} = \\ &= \frac{1}{-2\cdot(-2)\cdot(-2)} - \frac{1}{-2\cdot 2\cdot(-2)} + \frac{1}{-2\cdot(-2)\cdot(-2)} - \\ &- \frac{1}{2\cdot(-2)\cdot(-2)} - \frac{1}{-2\cdot(-2)\cdot 2} + \frac{1}{2\cdot 2\cdot 2} = \\ &= \frac{1}{8}(-1-1-1-1-1+1) = -\frac{4}{8} = -\frac{1}{2}; \end{aligned} \tag{AI.3}$$

$$
\begin{aligned}
n_{01} &= m_{03}m_{22}m_{31} - m_{02}m_{23}m_{31} - m_{03}m_{21}m_{32} + \\
&+ m_{01}m_{23}m_{32} + m_{02}m_{21}m_{33} - m_{01}m_{22}m_{33} = \\
&= \frac{1}{2\cdot 2\cdot(-2)} - \frac{1}{2\cdot(-2)\cdot(-2)} - \frac{1}{2\cdot(-2)\cdot(-2)} + \\
&+ \frac{1}{2\cdot(-2)\cdot(-2)} + \frac{1}{2\cdot(-2)\cdot 2} - \frac{1}{2\cdot 2\cdot 2} = \\
&= \frac{1}{8}(-1-1-1+1-1-1) = -\frac{4}{8} = -\frac{1}{2}; \qquad \text{(AI.4)}
\end{aligned}
$$

$$
\begin{aligned}
n_{02} &= m_{02}m_{13}m_{31} - m_{03}m_{12}m_{31} + m_{03}m_{11}m_{32} - \\
&- m_{01}m_{13}m_{32} - m_{02}m_{11}m_{33} + m_{01}m_{12}m_{33} = \\
&= \frac{1}{2\cdot(-2)\cdot(-2)} - \frac{1}{2\cdot(-2)\cdot(-2)} + \frac{1}{2\cdot 2\cdot(-2)} - \\
&- \frac{1}{2\cdot(-2)\cdot(-2)} - \frac{1}{2\cdot 2\cdot 2} + \frac{1}{2\cdot(-2)\cdot 2} = \\
&= \frac{1}{8}(1-1-1-1-1-1) = -\frac{4}{8} = -\frac{1}{2}; \qquad \text{(AI.5)}
\end{aligned}
$$

$$
\begin{aligned}
n_{03} &= m_{03}m_{12}m_{21} - m_{02}m_{13}m_{21} - m_{03}m_{11}m_{22} + \\
&+ m_{01}m_{13}m_{22} + m_{02}m_{11}m_{23} - m_{01}m_{12}m_{23} = \\
&= \frac{1}{2\cdot(-2)\cdot(-2)} - \frac{1}{2\cdot(-2)\cdot(-2)} - \frac{1}{2\cdot 2\cdot 2} + \\
&+ \frac{1}{2\cdot(-2)\cdot 2} + \frac{1}{2\cdot 2\cdot(-2)} - \frac{1}{2\cdot(-2)\cdot(-2)} = \\
&= \frac{1}{8}(1-1-1-1-1-1) = -\frac{4}{8} = -\frac{1}{2}; \qquad \text{(AI.6)}
\end{aligned}
$$

$$
\begin{aligned}
n_{10} &= m_{13}m_{22}m_{30} - m_{12}m_{23}m_{30} - m_{13}m_{20}m_{32} + \\
&+ m_{10}m_{23}m_{32} + m_{12}m_{20}m_{33} - m_{10}m_{22}m_{33} = \\
&= \frac{1}{-2\cdot 2\cdot 2} - \frac{1}{-2\cdot(-2)\cdot 2} - \frac{1}{-2\cdot 2\cdot(-2)} + \\
&+ \frac{1}{2\cdot(-2)\cdot(-2)} + \frac{1}{-2\cdot 2\cdot 2} - \frac{1}{2\cdot 2\cdot 2} = \\
&= \frac{1}{8}(-1-1-1+1-1-1) = -\frac{4}{8} = -\frac{1}{2};
\end{aligned}
\tag{AI.7}
$$

$$
\begin{aligned}
n_{11} &= m_{02}m_{23}m_{30} - m_{03}m_{22}m_{30} + m_{03}m_{20}m_{32} - \\
&- m_{00}m_{23}m_{32} - m_{02}m_{20}m_{33} + m_{00}m_{22}m_{33} = \\
&= \frac{1}{2\cdot(-2)\cdot 2} - \frac{1}{2\cdot 2\cdot 2} + \frac{1}{2\cdot 2\cdot(-2)} - \\
&- \frac{1}{2\cdot(-2)\cdot(-2)} - \frac{1}{2\cdot 2\cdot 2} + \frac{1}{-2\cdot 2\cdot 2} = \\
&= \frac{1}{8}(-1-1-1-1-1+1) = -\frac{4}{8} = -\frac{1}{2};
\end{aligned}
\tag{AI.8}
$$

$$
\begin{aligned}
n_{12} &= m_{03}m_{12}m_{30} - m_{02}m_{13}m_{30} - m_{03}m_{10}m_{32} + \\
&+ m_{00}m_{13}m_{32} + m_{02}m_{10}m_{33} - m_{00}m_{12}m_{33} = \\
&= \frac{1}{2\cdot(-2)\cdot 2} - \frac{1}{2\cdot(-2)\cdot 2} - \frac{1}{2\cdot 2\cdot(-2)} + \\
&+ \frac{1}{2\cdot(-2)\cdot(-2)} + \frac{1}{2\cdot 2\cdot 2} - \frac{1}{2\cdot(-2)\cdot 2} = \\
&= \frac{1}{8}(-1+1+1+1+1+1) = \frac{4}{8} = \frac{1}{2};
\end{aligned}
\tag{AI.9}
$$

$$
\begin{aligned}
n_{13} &= m_{02}m_{13}m_{20} - m_{03}m_{12}m_{20} + m_{03}m_{10}m_{22} - \\
&- m_{00}m_{13}m_{22} - m_{02}m_{10}m_{23} + m_{00}m_{12}m_{23} = \\
&= \frac{1}{2\cdot(-2)\cdot 2} - \frac{1}{2\cdot(-2)\cdot 2} + \frac{1}{2\cdot 2\cdot 2} - \\
&- \frac{1}{2\cdot(-2)\cdot 2} - \frac{1}{2\cdot 2\cdot(-2)} + \frac{1}{2\cdot(-2)\cdot(-2)} = \\
&= \frac{1}{8}(-1+1+1+1+1+1) = \frac{4}{8} = \frac{1}{2}; \qquad \text{(AI.10)}
\end{aligned}
$$

$$
\begin{aligned}
n_{20} &= m_{11}m_{23}m_{30} - m_{13}m_{21}m_{30} + m_{13}m_{20}m_{31} - \\
&- m_{10}m_{23}m_{31} - m_{11}m_{20}m_{33} + m_{10}m_{21}m_{33} = \\
&= \frac{1}{2\cdot(-2)\cdot 2} - \frac{1}{-2\cdot(-2)\cdot 2} + \frac{1}{-2\cdot 2\cdot(-2)} - \\
&- \frac{1}{2\cdot(-2)\cdot(-2)} - \frac{1}{2\cdot 2\cdot 2)} + \frac{1}{2\cdot(-2)\cdot 2} = \\
&= \frac{1}{8}(-1-1+1-1-1-1) = -\frac{4}{8} = -\frac{1}{2}; \qquad \text{(AI.11)}
\end{aligned}
$$

$$
\begin{aligned}
n_{21} &= m_{03}m_{21}m_{30} - m_{01}m_{23}m_{30} - m_{03}m_{20}m_{31} + \\
&+ m_{00}m_{23}m_{31} + m_{01}m_{20}m_{33} - m_{00}m_{21}m_{33} = \\
&= \frac{1}{2\cdot(-2)\cdot 2} - \frac{1}{2\cdot(-2)\cdot 2} - \frac{1}{2\cdot 2\cdot(-2)} + \\
&+ \frac{1}{2\cdot(-2)\cdot(-2)} + \frac{1}{2\cdot 2\cdot 2} - \frac{1}{2\cdot(-2)\cdot 2} = \\
&= \frac{1}{8}(-1+1+1+1+1+1) = \frac{4}{8} = \frac{1}{2}; \qquad \text{(AI.12)}
\end{aligned}
$$

$$
\begin{aligned}
n_{22} &= m_{01}m_{13}m_{30} - m_{03}m_{11}m_{30} + m_{03}m_{10}m_{31} - \\
&- m_{00}m_{13}m_{31} - m_{01}m_{10}m_{33} + m_{00}m_{11}m_{33} = \\
&= \frac{1}{2\cdot(-2)\cdot 2} - \frac{1}{2\cdot 2\cdot 2} + \frac{1}{2\cdot 2\cdot(-2)} - \\
&- \frac{1}{2\cdot(-2)\cdot(-2)} - \frac{1}{2\cdot 2\cdot 2} + \frac{1}{2\cdot 2\cdot 2} = \\
&= \frac{1}{8}(-1-1-1-1-1+1) = -\frac{4}{8} = -\frac{1}{2}; \qquad \text{(AI.13)}
\end{aligned}
$$

$$
\begin{aligned}
n_{23} &= m_{03}m_{11}m_{20} - m_{01}m_{13}m_{20} - m_{03}m_{10}m_{21} + \\
&+ m_{00}m_{13}m_{21} + m_{01}m_{10}m_{23} - m_{00}m_{11}m_{23} = \\
&= \frac{1}{2\cdot 2\cdot 2} - \frac{1}{2\cdot(-2)\cdot 2} - \frac{1}{2\cdot 2\cdot(-2)} + \\
&+ \frac{1}{2\cdot(-2)\cdot(-2)} + \frac{1}{2\cdot 2\cdot(-2)} - \frac{1}{2\cdot 2\cdot(-2)} = \\
&= \frac{1}{8}(1+1+1+1-1+1) = \frac{4}{8} = \frac{1}{2}; \qquad \text{(AI.14)}
\end{aligned}
$$

$$
\begin{aligned}
n_{30} &= m_{12}m_{21}m_{30} - m_{11}m_{22}m_{30} - m_{12}m_{20}m_{31} + \\
&+ m_{10}m_{22}m_{31} + m_{11}m_{20}m_{32} - m_{10}m_{21}m_{32} = \\
&= \frac{1}{-2\cdot(-2)\cdot 2} - \frac{1}{2\cdot 2\cdot 2} - \frac{1}{-2\cdot 2\cdot(-2)} + \\
&+ \frac{1}{2\cdot 2\cdot(-2)} + \frac{1}{2\cdot 2\cdot(-2)} - \frac{1}{2\cdot(-2)\cdot(-2)} = \\
&= \frac{1}{8}(1-1-1-1-1-1) = -\frac{4}{8} = -\frac{1}{2}; \qquad \text{(AI.15)}
\end{aligned}
$$

$$
\begin{aligned}
n_{31} &= m_{01}m_{22}m_{30} - m_{02}m_{21}m_{30} + m_{02}m_{20}m_{31} - \\
&- m_{00}m_{22}m_{31} - m_{01}m_{20}m_{32} + m_{00}m_{21}m_{32} = \\
&= \frac{1}{2\cdot 2\cdot 2} - \frac{1}{2\cdot(-2)\cdot 2} + \frac{1}{2\cdot 2\cdot(-2)} - \\
&- \frac{1}{2\cdot 2\cdot(-2)} - \frac{1}{2\cdot 2\cdot(-2)} + \frac{1}{2\cdot(-2)\cdot(-2)} = \\
&= \frac{1}{8}(1+1-1+1+1+1) = \frac{4}{8} = \frac{1}{2}; \qquad \text{(AI.16)}
\end{aligned}
$$

$$
\begin{aligned}
n_{32} &= m_{02}m_{11}m_{30} - m_{01}m_{12}m_{30} - m_{02}m_{10}m_{31} + \\
&+ m_{00}m_{12}m_{31} + m_{01}m_{10}m_{32} - m_{00}m_{11}m_{32} = \\
&= \frac{1}{2\cdot 2\cdot 2} - \frac{1}{2\cdot(-2)\cdot 2} - \frac{1}{2\cdot 2\cdot(-2)} + \\
&+ \frac{1}{2\cdot(-2)\cdot(-2)} + \frac{1}{2\cdot 2\cdot(-2)} - \frac{1}{2\cdot 2\cdot(-2)} = \\
&= \frac{1}{8}(1+1+1+1-1+1) = \frac{4}{8} = \frac{1}{2}; \qquad \text{(AI.17)}
\end{aligned}
$$

$$
\begin{aligned}
n_{33} &= m_{01}m_{12}m_{20} - m_{02}m_{11}m_{20} + m_{02}m_{10}m_{21} - \\
&- m_{00}m_{12}m_{21} - m_{01}m_{10}m_{22} + m_{00}m_{11}m_{22} = \\
&= \frac{1}{2\cdot(-2)\cdot 2} - \frac{1}{2\cdot 2\cdot 2} + \frac{1}{2\cdot 2\cdot(-2)} - \\
&- \frac{1}{2\cdot(-2)\cdot(-2)} - \frac{1}{2\cdot 2\cdot 2} + \frac{1}{2\cdot 2\cdot 2} = \\
&= \frac{1}{8}(-1-1-1-1-1+1) = -\frac{4}{8} = -\frac{1}{2}; \qquad \text{(AI.18)}
\end{aligned}
$$

$$
\begin{aligned}
det(\mathbb{W}_4) &= m_{03}m_{12}m_{21}m_{30} - m_{02}m_{13}m_{21}m_{30} - m_{03}m_{11}m_{22}m_{30} + \\
&+ m_{01}m_{13}m_{22}m_{30} + m_{02}m_{11}m_{23}m_{30} - m_{01}m_{12}m_{23}m_{30} - \\
&- m_{03}m_{12}m_{20}m_{31} + m_{02}m_{13}m_{20}m_{31} + m_{03}m_{10}m_{22}m_{31} - \\
&- m_{00}m_{13}m_{22}m_{31} - m_{02}m_{10}m_{23}m_{31} + m_{00}m_{12}m_{23}m_{31} + \\
&+ m_{03}m_{11}m_{20}m_{32} - m_{01}m_{13}m_{20}m_{32} - m_{03}m_{10}m_{21}m_{32} + \\
&+ m_{00}m_{13}m_{21}m_{32} + m_{01}m_{10}m_{23}m_{32} - m_{00}m_{11}m_{23}m_{32} - \\
&- m_{02}m_{11}m_{20}m_{33} + m_{01}m_{12}m_{20}m_{33} + m_{02}m_{10}m_{21}m_{33} - \\
&- m_{00}m_{12}m_{21}m_{33} - m_{01}m_{10}m_{22}m_{33} + m_{00}m_{11}m_{22}m_{33} = \\
&= \frac{1}{2\cdot(-2)\cdot(-2)\cdot 2} - \frac{1}{2\cdot(-2)\cdot(-2)\cdot 2} - \frac{1}{2\cdot 2\cdot 2\cdot 2} + \\
&+ \frac{1}{2\cdot(-2)\cdot 2\cdot 2} + \frac{1}{2\cdot 2\cdot(-2)\cdot 2} - \frac{1}{2\cdot(-2)\cdot(-2)\cdot 2} - \\
&- \frac{1}{2\cdot(-2)\cdot 2\cdot(-2)} + \frac{1}{2\cdot(-2)\cdot 2\cdot(-2)} + \frac{1}{2\cdot 2\cdot 2\cdot(-2)} - \\
&- \frac{1}{2\cdot(-2)\cdot 2\cdot(-2)} - \frac{1}{2\cdot 2\cdot(-2)\cdot(-2)} + \frac{1}{2\cdot(-2)\cdot(-2)\cdot(-2)} + \\
&+ \frac{1}{2\cdot 2\cdot 2\cdot(-2)} - \frac{1}{2\cdot(-2)\cdot 2\cdot(-2)} - \frac{1}{2\cdot 2\cdot(-2)\cdot(-2)} + \\
&+ \frac{1}{2\cdot(-2)\cdot(-2)\cdot(-2)} + \frac{1}{2\cdot 2\cdot(-2)\cdot(-2)} - \frac{1}{2\cdot 2\cdot(-2)\cdot(-2)} - \\
&- \frac{1}{2\cdot 2\cdot 2\cdot 2} + \frac{1}{2\cdot(-2)\cdot 2\cdot 2} + \frac{1}{2\cdot 2\cdot(-2)\cdot 2} - \\
&- \frac{1}{2\cdot(-2)\cdot(-2)\cdot 2} - \frac{1}{2\cdot 2\cdot 2\cdot 2} + \frac{1}{2\cdot(-2)\cdot(-2)\cdot 2} = \\
&= \frac{1}{2^4} - \frac{1}{2^4} - \frac{1}{2^4} - \frac{1}{2^4} - \frac{1}{2^4} - \frac{1}{2^4} - \frac{1}{2^4} + \frac{1}{2^4} - \frac{1}{2^4} - \frac{1}{2^4} - \frac{1}{2^4} - \frac{1}{2^4} - \\
&- \frac{1}{2^4} - \frac{1}{2^4} - \frac{1}{2^4} - \frac{1}{2^4} + \frac{1}{2^4} - \frac{1}{2^4} - \frac{1}{2^4} - \frac{1}{2^4} - \frac{1}{2^4} - \frac{1}{2^4} - \frac{1}{2^4} + \frac{1}{2^4} = \\
&= -\frac{1}{2^4}(24-8) = -\frac{16}{16} = -1; \qquad \text{(AI.19)}
\end{aligned}
$$

$$\mathbb{W}_4^{-1} = \frac{1}{-1}\begin{pmatrix} n_{00}=-\frac{1}{2} & n_{01}=-\frac{1}{2} & n_{02}=-\frac{1}{2} & n_{03}=-\frac{1}{2} \\ n_{10}=-\frac{1}{2} & n_{11}=-\frac{1}{2} & n_{12}=\frac{1}{2} & n_{13}=\frac{1}{2} \\ n_{20}=-\frac{1}{2} & n_{21}=\frac{1}{2} & n_{22}=-\frac{1}{2} & n_{23}=\frac{1}{2} \\ n_{30}=-\frac{1}{2} & n_{31}=\frac{1}{2} & n_{32}=\frac{1}{2} & n_{33}=-\frac{1}{2} \end{pmatrix} =$$

$$= \begin{pmatrix} \frac{1}{2} & \frac{1}{2} & \frac{1}{2} & \frac{1}{2} \\ \frac{1}{2} & \frac{1}{2} & -\frac{1}{2} & -\frac{1}{2} \\ \frac{1}{2} & -\frac{1}{2} & \frac{1}{2} & -\frac{1}{2} \\ \frac{1}{2} & -\frac{1}{2} & -\frac{1}{2} & \frac{1}{2} \end{pmatrix} = \mathbb{W}_4. \qquad \text{(AI.20)}$$

Hence, $\mathbb{W}_4 = \mathbb{W}_4^{-1}$.

APPENDIX II

COMPLEXITY OF ARITHMETIC OPERATIONS ON COMPLEX NUMBERS

Complexity of arithmetic operations on two complex numbers

Definitions:

Additive identity ("zero"): $0+0i$;

Multiplicative identity ("one"): $1+0i$.

Assume that $A=a+bi$ and $B=c+di$ are complex numbers. The following operations can be performed on them:

Additive Inverse $\ominus$: $-A=-(a+bi)=(-a)+(-b)i$;

Multiplicative Inverse $\oslash$: $A^{-1}=\frac{1}{A}=\left(\frac{a}{a^2+b^2}\right)+\left(\frac{-b}{a^2+b^2}\right)i$;

Addition: $A+B=(a+bi)+(c+di)=(a+c)+(b+d)i$;

Subtraction: $A-B=(a+bi)-(c+di)=(a-c)+(b-d)i$;

Multiplication: $A\cdot B=(a+bi)\cdot(c+di)=a\cdot c+b\cdot c\cdot i+a\cdot d\cdot i+b\cdot d\cdot i^2=(ac-bd)+(bc+ad)i$;

Division: $\frac{A}{B}=\frac{a+bi}{c+di}=\left(\frac{ac+bd}{c^2+d^2}\right)+\left(\frac{bc-ad}{c^2+d^2}\right)i$.

The complexity of arithmetic operations on two complex numbers, or complex-complex operation complexity, is defined by the number of real operations, such as additions, multiplications, multiplicative and additive inverses, as is shown in Table-A II-1.

Table-A II-1 Complexity of arithmetic operations on complex numbers

Complex Operation	$\oplus$	$\otimes$	$\ominus$	$\oslash$
Additive Inverse $\ominus$	-	-	2	-
Multiplicative Inverse $\oslash$	1	4	1	1
Addition $\oplus$	2	-	-	-
Subtraction	2	-	2	-
Multiplication $\otimes$	2	4	1	-
Division	3	8	1	1

Complexity of arithmetic operations on real and complex numbers

Assume that $A = a + 0i$ is a real number and $B = c + di$ is a complex number. In this case the complex number algebra is represented by the following operations:

Addition: $A + B = (a + 0i) + (c + di) = (a + c) + di$;

Subtraction: $A - B = (a + 0i) - (c + di) = (a - c) + di$;

Multiplication: $A \cdot B = (a + 0i) \cdot (c + di) = a \cdot c + 0 \cdot c \cdot i + a \cdot d \cdot i + 0 \cdot d \cdot i^2 = a \cdot c + a \cdot di$;

Division: $\frac{A}{B} = \frac{a+0i}{c+di} = \left(\frac{a \cdot c + 0 \cdot d}{c^2 + d^2}\right) + \left(\frac{a \cdot d - 0 \cdot c}{c^2 + d^2}\right) i = a \cdot \left(\frac{c}{c^2 + d^2}\right) + a \cdot \left(\frac{-d}{c^2 + d^2}\right) i.$

The complexity of arithmetic operations on real and complex numbers, or real-complex operation complexity, is defined by the number of real operations, such as additions, multiplications, multiplicative and additive inverses, as is shown in Table-A II-2.

Table-A II-2 Complexity of arithmetic operations on a pair of real-complex numbers

Real-Complex Operation	$\oplus$	$\otimes$	$\ominus$	$\oslash$
Addition $\oplus$	1	-	-	-
Subtraction	1	-	1	-
Multiplication $\otimes$	-	2	-	-
Division	1	6	1	1

BIBLIOGRAPHY

Adhikary, T.K. and Reddy, V.U. 1998. « Complex wavelet packets for multicarrier modulation ». In *International Conference on Acoustics, Speech, and Signal Processing*, vol. 3, p. 1821–1824.

Berrou, C., Glavieux, A., and Thitimajshima, P. 1993. « Near shannon limit error-correcting coding and decoding: Turbo-codes. » In *International Conference on Communications*, p. 1064–1070.

Boeglen, H. and Chatellier, C. 2006. « On the robustness of a joint source-channel coding scheme for image transmission over non frequency selective Rayleigh fading channels ». In *Information and Communication Technologies ICTTA*, vol. 2, p. 2320–2324.

Burr, A. 2001. *Modulation and coding for wireless communications*. Pearson education, Prentice Hall.

Chang, Meng-Chun, Lay, Kuen-Tsair, and Chen, Jiunn-Tsair. 2001. « Dynamic water-filling for wavelet communications ». In *53rd IEEE Vehicular Technology Conference VTC*, vol. 2, p. 1254–1258.

Chang, R. W. 1966. *Orthogonal Frequency Division Multiplexing*. United States Patent and Trademark Office (USPTO), Patent 3 488 445.

Choi, Sunghyun and Kim, Sang Wu. 1999. « Multipath channels ». *Webster (ed.), Wiley Encyclopedia of Electrical and Electronics Engineering Online. John Wiley and Sons, Inc.*

Ciolino, S., Ghavarni, M., and Aghvami, A.H. 2004. « An ultra-wideband pulse shape modulation system based on wavelet packets ». In *IEEE Seminar on Ultra Wideband Communications Technologies and System Design*, p. 99–102.

Clark Jr., G. C. and Cain, J. B. 1981. *Error-Correction Coding for Digital Communications*. New York: Plenum.

Coifman, R.R. and Wickerhauser, M.V. 1992. « Entropy-based algorithms for best basis selection ». *IEEE Transactions on Information Theory*, vol. 38, no. 2, p. 713–718.

Daly, D., Heneghan, C., Fagan, A., and Vetterli, M. 2002. « Optimal wavelet packet modulation under finite complexity constraint ». In *International Conference on Acoustics, Speech, and Signal Processing*, vol. 3, p. 2789–2792.

Daneshagaran, F. and Mondin, M. 1994. « Bandwidth efficient modulation with wavelets ». *Electronics Letters*, vol. 30, no. 15, p. 1200–1202.

Daubechies, I. 1989. « Wavelets: a tool for time-frequency analysis ». In *Sixth Multidimensional Signal Processing Workshop*, p. 98.

Daubechies, I. 1990. « The wavelet transform, time-frequency localization and signal analysis ». *IEEE Transactions on Information Theory*, vol. 36, no. 5, p. 961–1005.

Dixon, R. C. 1975. *Spread Spectrum Systems*. New York: Wiley.

Donoho, D.L. 1995. « De-noising by soft-thresholding ». *IEEE Transactions on Information Theory*, vol. 41, no. 3, p. 613–627.

Donoho, D.L. and Johnstone, I.M. 1994. « Ideal de-noising in an orthonormal basis chosen from a library of bases ». *C.R.A.S. Paris*, vol. 1, no. 319, p. 1317–1322.

Dovis, F., Mondin, M., and Daneshgaran, F. 1999. « Performance of wavelet waveforms over linear and nonlinear channels ». In *Wireless Communications and Networking Conference*, p. 1148–1152.

Engels, Marc. 2002. *Wireless OFDM systems: How to make them work?* Kluwer Academic publishers.

Fahmy, M.F., Amin, O.M.H., Hassan, Y.M.Y., and El-Raheem, G.M.A. 2004. « A fast wavelet packet based blind signal separation ». In *21st National Radio Science Conference*, vol. B11, p. 1–8.

Gao, Xinying, Zhang, Haixia, and Yuan, Dongfeng. 2004. « Unequal error protected image transmission over multilevel coded wavelet packet multicarrier modulation system ». In *International Symposium on Information Theory*, p. 390.

IEEE. 1993. *American national standard, Canadian standard graphic symbols for electrical and electronics diagrams (including reference designation letters)*. Institute of Electrical and Electronics Engineers IEEE, 315-1975.

IEEE. 2004. *Standard for Local and metropolitan area networks. Part 16: Air Interface for Fixed Broadband Wireless Access Systems*. Institute of Electrical and Electronics Engineers IEEE, 802.16-2004.

ISO/IEC. 1994. *Information technology - Open Systems Interconnection - Basic Reference Model - Conventions for the definition of OSI services*. International Organization for Standardization and the International Electrotechnical Commission ISO/IEC, 10731. Online. <http://www.iso.org/iso/>. Consulted May 10, 2008.

Jakes, W. C. 1974. *Microwave Mobile Communications*. New York: Wiley.

JPEG. 1994. *JPEG image coding system*. Joint Photographic Experts Group. International Organization for Standardization and the International Electrotechnical Commission ISO/IEC, 10918-1. Online. <http://www.jpeg.org/jpeg/index.html>. Consulted May 10, 2008.

JPEG. 2000. *JPEG 2000 image coding system*. Joint Photographic Experts Group. International Organization for Standardization and the International Electrotechnical Commission ISO/IEC, 15444-11. Online. <http://www.jpeg.org/jpeg2000/index.html>. Consulted May 10, 2008.

Kjeldsen, E., Dill, J.C., and Lindsey, A.R. 2003. « Exploiting the synergies of circular simplex turbo block coding and wavelet packet modulation ». In *Military Communications Conference*, vol. 2, p. 1202–1207.

Lee, M.J., Temple, M.A., Claypoole, Jr., R.L., and Raines, R.A. 2002. « Transform domain communications and interference avoidance using wavelet packet decomposition ». In *Wireless Communications and Networking Conference*, vol. 1, p. 255–259.

Lee, William C. Y. 1989. *Mobile cellular telecommunications systems*. McGraw-Hill.

Lee, William C. Y. 1997. *Mobile communication engineering: Theory and Applications*, 2 edition. McGraw-Hill.

Liew, B.A., Berber, S.M., and Sandhu, G.S. 2005. « Performance of a multiple access orthogonal wavelet division multiplexing system ». In *Third International Conference on Information Technology and Applications*, vol. 2, p. 350–353.

Lindsey, A.R. 1996. « Improved spread-spectrum communication with a wavelet packet based transceiver ». In *IEEE-SP International Symposium on Time-Frequency and Time-Scale Analysis*, p. 417–420.

Lindsey, A.R. 1997. « Wavelet packet modulation for orthogonally multiplexed communication ». *IEEE Transactions on Signal Processing, IEEE Transactions on Acoustics, Speech, and Signal Processing*, vol. 45, no. 5, p. 1336–1339.

Lindsey, A.R. and Dill, J.C. 1995. « Wavelet packet modulation: a generalized method for orthogonally multiplexed communications ». In *Twenty-Seventh Southeastern Symposium on System Theory*, p. 392–396.

Mallat, S.G. 1989a. « Multifrequency channel decompositions of images and wavelet models ». *IEEE Transactions on Acoustics, Speech, and Signal Processing [see also IEEE Transactions on Signal Processing]*, vol. 37, no. 12, p. 2091–2110.

Mallat, S.G. 1989b. « A theory for multiresolution signal decomposition: the wavelet representation ». *IEEE Transactions on Pattern Analysis and Machine Intelligence*, vol. 11, no. 7, p. 674–693.

Morais, Douglas H. 2004. *Fixed Broadband Wireless Communications. Principles and Practical Applications*. Prentice Hall.

Newlin, H.M. 1998. « Developments in the use of wavelets in communication systems ». In *Military Communications Conference*, vol. 1, p. 343–349.

Nguyen, V. D., Kyamakya, K., and Gelle, G. 2004. « SER of uncoded OFDM systems with insufficient guard interval length and on time-varying channels ». In *Vehicular Technology Conference VTC*.

Nitzberg, R. 1991. *Adaptive Signal Processing for Radar*. Norwood, MA: Artech House.

Okamoto, E., Iwanami, Y., and Ikegami, T. 2003. « Multimode transmission using wavelet packet modulation and OFDM ». In *58th Vehicular Technology Conference*, vol. 3, p. 1458–1462.

O'Shaughnessy, Douglas. 1999. *Speech Communications: Human and Machine*, 2 edition. Wiley-IEEE Press.

Peterson, W. W. and Weldon, Jr., E. J. 1971. *Error-Correcting Codes*. Cambridge, MA: MIT Press.

Ponomarenko, N., Zriakhov, M., Lukin, V., Astola, J., and Egiazarian, K. September 2006. « Estimation of accesible quality in noisy image compression ». In *EUSIPCO, Florence, Italy*, p. 4.

Pratt, William K. 1978. *Digital Image Processing*. John Wiley and Sons.

Price, R. and Green, P. E. 1958. « A communication technique for multipath channel ». In *Proceedings IRE*, p. 555–570.

Proakis, J. C. and Salehi, M. 2007. *Digital Communications, 5th Edition*. New York: McGraw-Hill Science/Engineering/Math.

Qureshi, S. H. 1985. « Adaptive equalization ». In *Proceedings IEEE*, vol. 37(9), p. 1340–1387. IEEE.

Ramzan, N. and Izquierdo, E. 2006. « Scalable video transmission using double binary turbo code ». In *IEEE International Conference on Image Processing*, p. 1309–1312.

Rappaport, Theodore S. 2002. *Wireless Communications: principles and practice*. Prentice Hall PTR.

Rice, R. F. 1974. *Channel Coding and Data Compression System Consideration for Efficient Communication of Planetary Imaging Data*. « Technical report of the Jet Propulsion Laboratory », 33-695. Pasadena, CA.

Ryan, W. E. and Lin, S. 2009. *Channel codes: classical and modern*. Cambridge University Press.

Sabelkin, M. 2000. « Threshold choice in algorithm of image compression based on 2D discrete wavelet transform ». *Aerospace Technique and Technology Journal*, vol. 21, p. 186–191.

Sabelkin, M. 2001. « Wavelet coefficient thresholding for radar image compression ». In *First International Workshop on Mathematical Modelling of Physical Processes in Inhomogeneous Media*, p. 47–49.

Sabelkin, M. 2011. *Method and Apparatus for Data Transmission Oriented on the Object, Communication Media, Agents, and State of Communication Systems*. United States Patent and Trademark Office (USPTO), Applicaton Number 13/090,608.

Sabelkin, M. and Gagnon, F. April 2011a. « Combined source-channel transform for image transmission over wireless channel ». In *10th Wireless Telecommunications Symposium (WTS 2011)*, p. 4.

Sabelkin, M. and Gagnon, F. 2011b. « Data transmission oriented on the object, communication media, application, and state of communication systems ». *International Journal of Interdisciplinary Telecommunications and Networking (IJITN)*, vol. 3, no. 2, p. 51–65.

Sabelkin, M. and Gagnon, F. June 2011c. « Fast transform for multi-carrier wireless communications ». In *7th International Conference on Wireless Advanced 2011 (WiAd 2011)*, p. 6.

Sabelkin, M. and Lukin, V. 1999. « Image compression method based on 2D discrete wavelet transform ». *Aerospace Technique and Technology Journal*, vol. 12, p. 100–102.

Sabelkin, M. and Piscorzh, V. 1998. « Method of image coding ». In *International Symposium on Information Theory and its Applications*, p. 663–665.

Sabelkin, M. and Ponomarenko, N. 2001. « MM-band radar image wavelet compression with prefiltering ». In *International Symposium on Physics and Engineering of Millimeter and Submillimeter Waves*, p. 280–282.

Sheikh, H.R. and Bovik, A.C. February 2006. « Image information and visual quality ». *IEEE Transactions on Image Processing*, vol. 15, no. 2, p. 430–444.

Soyjaudah, K.M.S and Fowdur, T.P. 2006. « An integrated unequal error protection scheme for the transmission of compressed images with ARQ ». In *International Conference on Networking, International Conference on Systems and International Conference on Mobile Communications and Learning Technologies ICN/ICONS/MCL*, p. 103.

Strang, G. and Nguyen, T. 1996. *Wavelets and filter banks*. Wellesley-Cambridge Press.

Suzuki, N., Fujimoto, M., Shibata, T., Itoh, N., and Nishikawa, K. 1999. « Maximum likelihood decoding for wavelet packet modulation ». In *50th IEEE Vehicular Technology Conference VTC*, vol. 5, p. 2895–2898.

Thomos, N., Boulgouris, N.V., and Strintzis, M.G. 2005. « Wireless image transmission using turbo codes and optimal unequal error protection ». *IEEE Transactions on Image Processing*, vol. 14, no. 11, p. 1890–1901.

TIA/EIA. 1995. *Interim Standard-95. Mobile station-base station compatibility standard for dual-mode wideband spread spectrum cellular system*. Telecommunications Industry Association and Electronic Industries Alliance TIA/EIA, Interim Standard 95 (IS-95).

To, Kin-Fai, Wong, K.T., and Wong, Kon Max. 2000. « Analysis of amplifier nonlinearities on wavelet packet division multiplexing ». In *IEEE International Conference on Acoustics, Speech, and Signal Processing*, vol. 5, p. 2813–2816.

Torrieri, D. 2011. *Principles of Spread-Spectrum Communication Systems, 2nd edition*. Springer.

USC-SIPI. 2006. The usc-sipi image database: Version 5. Signal and Image Processing Institute of the University of Southern California (USC-SIPI). Online. <http://sipi.usc.edu/database/>. Consulted May 10, 2008.

Van Bouwel, C., Potemans, J., Schepers, S., Nauwelaers, B., and Van de Capelle, A. 2000. « Wavelet packet based multicarrier modulation ». In *Symposium on Communications and Vehicular Technology*, p. 131–138.

Viterbi, A. J. and Omura, J. K. 1979. *Principles of Digital Communication and Coding*. New York: McGraw-Hill.

Wang, Charles C., Nguyen, Tien M., and Goo, Gary W. 1999. « Military communication ». *Wiley Encyclopedia of Electrical and Electronics Engineering Online*.

Wang, Sashuang, Dai, Jufeng, Hou, Chunping, and Liu, Xueqing. 2006. « Progressive image transmission over wavelet packet based OFDM ». In *Canadian Conference on Electrical and Computer Engineering*, p. 950–953.

Weihua, Li, Rong, Wang, Yahong, Zhao, and Weiling, Wu. 2001. « Bi-orthogonal wavelet packet based multicarrier modulation ». In *International Conferences on Info-tech and Info-net*, vol. 2, p. 464–467.

Xiaofan, Ying, Zhenyong, Chu, yong, Wang, and Kechu, Yi. 2004. « A scheme of M-ary multi-carrier spread spectrum based on wavelet packet ». In *18th International Conference on Advanced Information Networking and Applications*, vol. 2, p. 219–222.

Xingxin, Gao, Mingquan, Lu, and Zhenming, Feng. 2002. « Optimal wavelet packet based multicarrier modulation over multipath wireless channels ». In *International Conference on Communications, Circuits and Systems and West Sino Expositions*, vol. 1, p. 313–317.

Yang, Weimin, Bi, Guangguo, and Yum, T.-S.P. 1997. « A multirate wireless transmission system using wavelet packet modulation ». In *47th Vehicular Technology Conference VTC*, vol. 1, p. 368–372.

You, Mingli and Ilow, Jacek. 2004a. « Adaptive multiwavelet packet modulation for channels with time-frequency localized interference ». In *6th Circuits and Systems Symposium on Emerging Technologies: Frontiers of Mobile and Wireless Communication*, vol. 2, p. 441–444.

You, Mingli and Ilow, Jacek. 2004b. « An application of multi-wavelet packets in digital communications ». In *2nd Annual Conference on Communication Networks and Services Research*, p. 10–18.

You, Mingli and Ilow, Jacek. 2004c. « A multi-wavelet packet modulation in wireless communications ». In *Canadian Conference on Electrical and Computer Engineering*, vol. 4, p. 2367–2370.

Yu, Xiangbin and Bi, Guangguo. 2004. « Performance of turbo-coded MC-CDMA system based on complex wavelet packet in Rayleigh fading channel ». In *International Conference on Communications, Circuits and Systems*, vol. 1, p. 52–56.

Zhang, Hongbing, Fan, H.H., and Lindsey, A. 2001. « A wavelet packet based model for time-varying wireless communication channels ». In *3rd IEEE Workshop on Signal Processing Advances in Wireless Communications*, p. 50–53.

Zhang, Xiaodong and Bi, Guangguo. 2001. « OFDM scheme based on complex orthogonal wavelet packet ». In *12th IEEE International Symposium on Personal, Indoor and Mobile Radio Communications*, vol. 2, p. 99–104.

Zhang, Yifeng and Dill, J. 1999. « An anti-jamming algorithm using wavelet packet modulated spread spectrum ». In *Military Communications Conference*, vol. 2, p. 846–850.